

MICROWAVE CIRCULATOR DESIGN

SECOND
EDITION



Douglas K.
Linkhart

Microwave Circulator Design

Second Edition

For a listing of recent titles in the
Artech House Microwave Library,
turn to the back of this book.

Microwave Circulator Design

Second Edition

Douglas K. Linkhart



**ARTECH
HOUSE**

BOSTON | LONDON
artechhouse.com

Library of Congress Cataloging-in-Publication Data

A catalog record for this book is available from the U.S. Library of Congress.

British Library Cataloguing in Publication Data

A catalogue record for this book is available from the British Library.

ISBN-13: 978-1-60807-583-6

Cover design by Vicki Kane

**© 2014 ARTECH HOUSE
685 Canton Street
Norwood, MA 02062**

All rights reserved. Printed and bound in the United States of America. No part of this book may be reproduced or utilized in any form or by any means, electronic or mechanical, including photocopying, recording, or by any information storage and retrieval system, without permission in writing from the publisher.

All terms mentioned in this book that are known to be trademarks or service marks have been appropriately capitalized. Artech House cannot attest to the accuracy of this information. Use of a term in this book should not be regarded as affecting the validity of any trademark or service mark.

10 9 8 7 6 5 4 3 2 1

Contents

Preface	<i>xi</i>
Acknowledgments	<i>xv</i>
1 Theory of Operation	1
1.1 Units, Conversions, and Symbols	1
1.2 The Physical Basis of Ferrimagnetism	4
1.3 Ferrimagnetic Resonance	11
1.4 Microwave Propagation in Ferrites	15
1.5 Other Technologies	29
1.5.1 Semiconductor Circulators	29
1.5.2 Nanotechnology Circulators	30
1.5.3 Thin Ferrite Films	31
1.5.4 Active Circulators	32
2 Circulator Specification	35
2.1 The Parameters	35
2.2 Reflections and Segmentation	48
2.3 Junction Circulators	52

2.3.1	Single-Ferrite (Non-Composite) Junction Circulators	54
2.3.2	Composite-Ferrite Junction Circulators	56
2.4	Lumped-Constant Circulators	56
2.5	Differential Phase Shift Circulators	58
2.6	Switching Circulators	60
2.7	Okada Circulators	61
2.8	Field-Displacement Isolators	61
2.9	Resonance Isolators	64
3	Applications of Circulators	69
3.1	Load Isolation	69
3.2	Duplexing	71
3.3	Multiplexing	76
3.4	Parametric Amplifiers	77
3.5	Phase Shifting	81
4	Material Selection	87
4.1	Ferrites	87
4.1.1	Ferrite Classes	87
4.1.2	Ferrite Manufacturing	88
4.1.3	Design Considerations	90
4.1.4	Test Methods	91
4.1.5	Specifications	93
4.1.6	Temperature Effects	93
4.1.7	Ferrite Selection	96
4.2	Magnet Selection	100
4.3	Magnetic Compensating Material Selection	102
4.4	Dielectric Selection	103
4.5	Metals Selection	104

5	Electrical Design	107
5.1	Junction Circulators	107
5.1.1	Basic Principles	107
5.1.2	Historical Papers	111
5.1.3	Above-Resonance Approximations	125
5.1.4	Below-Resonance Approximations	130
5.1.5	Network Synthesis	132
5.1.6	Center Conductor Geometries	143
5.1.7	Waveguide Junction Geometries	149
5.1.8	Stripline Circulator Synthesis Algorithm	153
5.1.9	Microstrip Circulator Synthesis Algorithm	157
5.1.10	Waveguide Junction Circulator Synthesis Algorithm	161
5.1.11	Okada Circulators	163
5.1.12	Circulators Having Composite Ferrites	165
5.2	Lumped-Constant Circulators	167
5.3	Differential Phase Shift Circulators	171
5.4	Resonance Isolators	177
5.5	Dummy Loads for Isolators	179
5.6	Temperature Effects	181
5.7	Intermodulation Distortion	186
5.8	RF Power Effects	187
5.8.1	Steady-State Thermal Effects	187
5.8.2	Transient Thermal Effects	191
5.8.3	Voltage Breakdown	193
5.8.4	Spin-Wave Instability	198
6	Magnetic Design	205
6.1	Magnet Sizing	205
6.1.1	Ferrite Demagnetization Factors	207
6.1.2	Leakage Flux Approximation	213
6.1.3	Approximate Design of Magnetic Circuits	214

6.1.4	Simulation of Magnetic Circuits	217
6.2	Shielding	219
6.3	Temperature Compensation	221
6.4	Completing the Circuit	223
6.5	Special Cases	225
6.5.1	Switching Circulators	225
6.5.2	Self-Biased Circulators	228
6.5.3	Considerations for Microstrip Circulators	228
7	Mechanical Design	231
7.1	Thermal Considerations	231
7.1.1	Stripline Power Handling	231
7.1.2	Power Dissipation in Ferrites	233
7.1.3	Cooling of Ferrites	234
7.2	Venting	235
7.3	Coaxial Junction Circulators	237
7.3.1	Packaging Techniques	237
7.3.2	Dimensional Tolerances	242
7.3.3	Controlling Cavity Resonances	244
7.3.4	Transitions	249
7.3.5	RFI Control	253
7.3.6	Dissimilar Metals	253
7.3.7	Finishes	253
7.4	Lumped-Constant Circulators	254
7.5	Waveguide Circulators	256
7.6	Resonance Isolators	258
8	Assembly and Testing	261
8.1	Assembly Techniques	261
8.2	Testing	268
8.2.1	Finding the Operating Point	268

8.2.2	Taking Data	271
8.2.3	RF Power Testing	272
8.2.4	Intermodulation Testing	272
8.2.5	Multipaction Testing	273
8.2.6	Magnetic Moment Measurement	275
8.2.7	Measurement Uncertainty and Gauge Studies	276
9	Tuning	281
9.1	Interaction Between Magnetic and Electrical Adjustments	281
9.2	Magnetic Adjustment	281
9.2.1	Above-Resonance Magnetic Adjustment	282
9.2.2	Below-Resonance Magnetic Adjustment	283
9.2.3	Magnet Charging, Calibration, and Stabilization	283
9.3	Electrical Adjustment	285
9.4	Eigenvalue Evaluation	295
10	Design Examples	301
10.1	Introduction to Examples	301
10.2	Above-Resonance Stripline Junction Circulator	302
10.3	Below-Resonance Stripline Junction Circulator	311
10.4	Waveguide Junction Circulator	319
10.5	Microstrip Circulator	324
10.6	Differential Phase Shift Circulator	329
10.7	Lumped-Constant Circulator	333
List of Symbols		339
Frequently Used Equations		347
About the Author		351
Index		353

Preface

Much has changed in the 25 years since I wrote the first edition of this book. The first IBM personal computers were introduced in the 1980s, and we used Tandy Radio Shack (TRS) computers in that era. The TRS-80 Model 4 computer had a Z80 8-bit 4-MHz CPU, 128 kB of RAM, and a floppy disk drive for storing up to 180 kB of data per disk. Today we have 64-bit desktop computers with CPUs that run at several gigahertz, many gigabytes of RAM, and hard disks that store terabytes of data. This computing power has enabled electromagnetic simulations that were impractical 25 years ago and has empowered engineers in other ways.

I prepared the manuscript for the first edition using a typewriter and I inked the illustrations on vellum. Changes to the text were made by cutting out sections of paper and pasting in new paper. Research meant road trips to big-city and university libraries, where I searched card files and read microfilms. Communication with Artech House meant phone calls and overnight shipments of paper. The manuscript for the second edition is composed of Microsoft Word documents, and I generated the new illustrations using Microsoft Excel and AutoCAD. The Internet is a powerful research tool, eliminating research road trips, card files, and microfilm. E-mail allowed nearly instant transfer of manuscript sections. A portable computer allowed me to write at home, in the park, at the beach, in my car (not while driving), on planes, and in hotel rooms.

Many circulator design engineers now integrate electromagnetic simulation tools into the design process. There are several good tools for circulators on the market now; among them are CST Microwave Studio, COMSOL, and Ansys® HFSS™. I chose to use HFSS to perform the simulations for this book. Simulation software is not available to all readers, so I have presented

circulator design procedures in which electromagnetic simulations are optional, not required. Simulation software can provide first-pass design success if accurate material properties are available and dimensional tolerances can be tightly controlled.

There is no question that computer technology has advanced significantly in the past score and five years. Circulator technology has also made some strides, although not in such a spectacular way. I have expanded this book with information about the use of computers in the design process, and added more circulator design information, but the circulator theory, equations, and design concepts are not new. You will find that this book will reduce the time you spend seeking relevant mathematical tools and procedures.

The objective of this book is to present theory, information, and design procedures that will enable microwave engineers and technicians to design and build circulators successfully. We begin in Chapter 1 with a discussion of the various units used in the circulator design computations, then we cover the theory of operation, but only to a depth sufficient to form a foundation for the rest of the text. The unique anisotropic properties of ferrites, described in this chapter, make circulators possible.

Those who prefer not to read through the theory of operation can skip to Chapter 2, which describes how to specify a circulator. Typically, the specification process comes before design and construction, so this chapter is placed near the front of the book. The beginner can become involved in circulator specification before learning about microwave magnetics. This chapter has proven to be a useful guide for people who specify circulators, even if they are not involved in the circulator design process.

Chapter 3 is about applications of circulators. The information presented here may give the engineer new ideas about how to solve problems using circulators. Knowledge of circulator applications will also help the designer do a better job.

Material selection criteria are presented in Chapter 4. The correct selection of materials, particularly ferrites, is very important in circulator design.

Chapters 5, 6, and 7 cover electrical, magnetic, and mechanical design, respectively. The order in which design procedures are presented in this book is the order in which they are typically applied in practice. Thus, the reader can begin the design process before he or she finishes the book. It is important to keep in mind that all of the design aspects, the electrical, magnetic, and mechanical ones, are best considered together and not in isolation. When working on one design aspect, the implications of the other aspects should be considered. Also, circulator design should be iterative in nature. After preliminary electrical, magnetic, and mechanical design is completed, revisit

each one of these to optimize the design in light of decisions made with regard to the other design aspects. If the circulator is designed by a team, then collaboration is important to arrive at the best design compromise.

The next two chapters are devoted to assembly and testing (Chapter 8) and tuning (Chapter 9), the benchwork involved in making a circulator work. If only engineering prototypes or a very small quantity of circulators are to be delivered, then little thought about the material in these two chapters is needed before it is time for assembly. If higher-volume manufacturing is anticipated, then assembly, testing, and tuning should be considered during the entire design process. The goal is to minimize the costs of these processes and maximize circulator performance and manufacturing yield.

New in this edition of the book, Chapter 10 contains design examples, which demonstrate how the material in this book could be applied to real-world design tasks. The circulators in the design examples are not fully engineered devices, but rather first passes at electrical design.

Field-displacement isolators and resonance isolators are not circulators at all, but their design parallels circulator design in many respects, so I have included some information about them (see Sections 2.7 and 2.8).

I hope that this book continues to fill the need for comprehensive circulator design information and procedures. Please explore the book and discover all that it has to offer you and your circulator designs.

Acknowledgments

I am indebted to many early workers in the microwave industry for their research efforts. Thanks are also due my coworkers and customers, past and present, with whom I have had discussions about circulators or related topics.

I wish to thank my friends at UTE Microwave: Len Nilson, Jeffrey Gross, and Andrew Owens, for providing electrical testing services for the design examples in Chapter 10. I should point out here that the poorly-performing carelessly-built design-example circulators that I personally designed and built are *not* products of UTE Microwave. UTE makes high-quality circulators, unlike my design examples.

Jeff Gross and Andy Owens sacrificed part of their weekend to test my circulators, and were outstanding hosts during my visit to New Jersey. Andy continued to work under adverse conditions: while testing a circulator one evening, the electrical power went out, forcing us to work by emergency light. We plugged the VNA into a UPS and continued testing. This was the first time I had ever used a VNA that was running on battery power.

Thanks to the folks at Ansys for providing HFSS for use in running the circulator simulations that I used for this book. HFSS is an outstanding product, and is widely used in our industry.

Finally, I would like to thank Jennifer Linkhart, my daughter, for producing the photographs in this book, and Christopher Linkhart, my son, for helping with the assembly of a design-example circulator.

1

Theory of Operation

1.1 Units, Conversions, and Symbols

There are several systems of standard units in use today. These include the centimeter-gram-second (CGS), meter-kilogram-second (MKS), international system (SI), and English systems. The SI system is now the most widely used.

When a book is written using an accepted standard system of units, it is often difficult for an American engineer to use. This is because many of us measure lengths in inches and angles in degrees (and probably will for some time). Ferrite and magnet manufacturers use CGS units, so a book written entirely in SI units would require us to perform still more conversions.

Table 1.1 shows the units that are used in this book. In many of the equations presented, particularly those that are part of derivations, the units are unimportant. In other equations, any units may be used as long as we are consistent. If we stick to the units shown in the table, difficulty in calculation should not arise.

The units in Table 1.1 are mostly SI units, with the exceptions of those for magnetic field intensity and magnetic induction, which are CGS units. Data for ferrite and magnet materials are normally presented in CGS format. Thermal conductivity is also not an SI unit, because the $\text{W}/\text{in}^\circ\text{C}$ unit is much more practical. The length, area, and angle units can be changed to inches, square inches, and degrees in many equations. Care should be exercised so as not to mix units from different systems in the same equation.

Some useful conversion factors are listed in Table 1.2. It may be necessary to change units in some instances.

Table 1.1
Units Used in This Book

Quantity	Unit	System	Other Units
Angle	rad	SI	deg
Length	m	SI	in
Area	m^2	SI	in^2
Time	s	SI	
Frequency	Hz	SI	
Velocity	m/s	SI	
Mass	kg	SI	g
Force	N	SI	
Torque	Nm	SI	
Energy	J	SI	
Power	W	SI	
Temperature	$^\circ\text{C}$	SI	
Thermal conductivity	$\text{W/in}^\circ\text{C}$	US	
Electric charge	C	SI	
Voltage (EMF)	V	SI	
Permittivity	F/m	SI	
Electric current	A	SI	
Magnetic field intensity	Oe	CGS	
Magnetic induction	G	CGS	
Permeability	H/m	SI	
Capacitance	F	SI	
Inductance	H	SI	
Resistance	Ω	SI	
Conductance	S	SI	
Conductivity	S/m	SI	
Impedance	Ω	SI	
Admittance	S	SI	
Susceptance	S	SI	
Isolation	dB		
Insertion loss	dB		
Return loss	dB		

Table 1.1
Units Used in This Book (*Cont.*)

Abbreviations Used in this Table			
Abbreviation	Unit	Abbreviation	Unit
A	Ampere	J	Joule
° C	Degree Celsius	kg	Kilogram
C	Coulomb	m	Meter
dB	Decibel	N	Newton
deg	Cegree	Oe	Oersted
F	Farad	rad	Radian
g	Gram	s	Second
G	Gauss	S	Siemen
H	Henry	SI	International system
Hz	Hertz	W	Watt
in	Inch	Ω	Ohm

Table 1.2
Conversion Factors

Quantity	To convert	Into	Multiply by
Angle	rad	Degrees	5.730×10^1
Length	m	in	3.937×10^1
Area	m^2	in^2	1.550×10^3
Temperature	° F	° C	$5.556 \times 10^{-1} *$
Thermal conductivity	g cal/s cm ² °C/cm	W/in°C	1.06×10^1
Thermal conductivity	BTU/hr ft ² °F/ft	W/in°C	4.4×10^{-2}
Magnetic field intensity	A/m	Oe	1.257×10^{-2}
Magnetic induction	T (tesla)	G	1.000×10^4
Magnetomotance	Ampere turns	Gilberts	1.257×10^0

* First subtract 32, then multiply by factor shown.

To the uninitiated, the symbols for the ferrite material magnetization and saturation magnetization can be confusing. In the MKS system, magnetic induction, magnetic field intensity, and magnetization are related by

$$B = \mu_0 H + \mu_0 M$$

The equivalent of this equation in the CGS system is somewhat different:

$$B = H + 4\pi M$$

Usually, the factor 4π is included with the magnetization so that $4\pi M$ in the CGS system is equivalent to $\mu_0 M$ in the MKS system. Thus, the ferrite magnetization in the CGS system is denoted $4\pi M$ and the saturation magnetization is $4\pi M_S$. The subscript simply means saturation.

The gyromagnetic ratio, γ , is presented in the text as a constant relating the ferrimagnetic resonance radian frequency and the dc magnetic field. This constant is given the value of 2.80 MHz/Oe. The frequency here (MHz) is clearly not a radian frequency. The value of the gyromagnetic ratio in radian frequency/Oersted units is 17.6 Mrad/s/Oe. The reason for giving the constant a value in MHz/Oe is that the factor of 2π in any frequencies in the same equation with the gyromagnetic ratio can be eliminated to simplify calculation. Therefore, radian frequencies (ω or ω_0) that appear in the same equation with γ are not really radian frequencies, but frequencies in MHz.

The permittivity symbol, ϵ , represents either absolute or relative permittivity depending on the context. In general, it represents relative permittivity in equations that are used in the circulator design process and absolute permittivity in derivations. A complete list of symbols appears at the end of the text.

1.2 The Physical Basis of Ferrimagnetism

Nearly all microwave circulators contain ferrimagnetic materials; therefore, it is important that we understand the theory behind the magnetic properties of these materials to better understand circulator operation.

Ferrimagnetic materials were known some 3,000 years ago in the form of lodestones (magnetites). The first artificial ferrimagnets, or ferrites, as we shall refer to them from now on, were made in 1909 by Hilpert [1]. At the time, the composition of the ferrites could not be controlled reliably, so it was not until some time later that practical ferrites were successfully produced.

In 2009, the Institute of Electrical and Electronics Engineers (IEEE) honored the Tokyo Institute of Technology and TDK Corporation with the Milestone award [2] for “Development of Ferrite Materials and their Applications, 1930–1945.” In 1930, T. Takei and Y. Kato of Tokyo Institute of Technology developed ferrite, and TDK was founded in 1935 to produce ferrite cores.

In the 1940s, J. L. Snoek developed ferrites [3] at the Philips Gloeilampenfabriken research laboratories in The Netherlands. These ferrites were originally intended for use at low frequencies, but it was soon discovered that the materials had many possibilities for use at microwave frequencies. A different class of ferrites, the garnets, was first produced [3] in the 1950s by the French physicist Louis Néel and by workers at Bell Laboratories. Hexagonal ferrites, yet another class of ferrites, were also produced by Philips in the 1950s [4].

There are three main classes of ferrites: the spinels, the garnets, and the hexagonal ferrites, also known as hexaferrites. The names of the ferrite classes describe the crystal structures of the materials. The spinels have the same crystal structure as the mineral spinel, and the garnets have the structure of the mineral andradite (common garnet or black garnet). The hexagonal ferrites, which have hexagonal crystal structures, are used primarily for ceramic magnets and devices that operate at millimeter wavelengths.

By definition, all ferrites contain iron. Iron has a large magnetic moment due to irregularities in filling electron states [5] and resulting incomplete electron spin cancelation, as described later in this section. Other elements, such as cobalt, nickel, and some rare earths, also have relatively large magnetic moments.

The ferrites are ionic crystals. That is, the atoms in the crystal are bonded together by ionic bonds—the ions either lose or accept electrons when they become bonded. A lowering of potential energy occurs when ions of opposite charge approach each other, and it is such a lowering of energy that the atoms seek. Because a crystal structure also leads to a lowered energy level, the ferrite molecules do not commonly exist separately but become arranged in the crystal. A ferrite can be thought of as one giant molecule.

Single crystal ferrites can be produced for some special applications, but most ferrites are polycrystalline. A polycrystal has a nonuniform orientation of the crystal lattice.

Ions in the ferrite have magnetic moments that lead to paramagnetism, which is the ability of the ions to be acted upon individually, with no mutual interaction, by a magnetic field. The magnetic moment of an ion is equal to the sum of two different moments: one due to the electron spin, and the other due to the orbital motion of the electrons.

The magnetic moments of the ions can be calculated [6] from the quantum numbers, but there is no reason to do so here. Atoms that have only filled shells have no net magnetic moment, because the electron spins and the electron orbital effects cancel each other. Only when there are unpaired electron spins or a net orbital angular momentum can there be paramagnetism. The net magnetic moment due to electron spins depends on the number of spins in each direction. If all the spins are up, the net moment is equal to the sum of the moments due to each spin. If all the spins are down, the net moment would be determined in the same manner. If some of the spins are up and others down, the difference in the number of spins in each direction would determine the net magnetic moment (equal quantities of spins in each direction would cause complete cancellation).

Hund's rule states that electrons entering a subshell containing more than one orbital will be spread out over the available orbitals with their spins in the same direction. Figure 1.1 illustrates the determination of the net moment from the spins.

The mineral spinel has the formula $(\text{MgAl}_2\text{O}_4)_8$. The microwave spinels (ferrites) have a similar general formula, $(\text{MOFe}_2\text{O}_3)_8$, where M represents a divalent metal such as iron, manganese, magnesium, nickel, zinc, cadmium, cobalt, copper, or a mixture of these. The metallic ions are small in comparison to the oxygen ions, so the crystal structure is determined primarily by the locations of the oxygen ions. The metallic ions fit in between the oxygen ions.



IF 5 ELECTRONS ARE PRESENT,
ALL 5 CAN HAVE SPINS IN THE
SAME DIRECTION: EITHER UP OR
DOWN. THE MAXIMUM SPIN ANGU-
LAR MOMENTUM A d SHELL CAN
HAVE IS 5.



IF 10 ELECTRONS ARE PRESENT,
THERE ARE 5 WITH SPIN UP AND
5 WITH SPIN DOWN. THE NET
SPIN MOMENTUM IS ZERO.

HUND'S RULE: ELECTRONS ENTERING A SUBSHELL CONTAINING MORE THAN ONE ORBITAL WILL BE SPREAD OUT OVER THE AVAILABLE ORBITALS WITH THEIR SPINS IN THE SAME DIRECTION.

Figure 1.1 Determination of net spin angular momentum from electron spins.

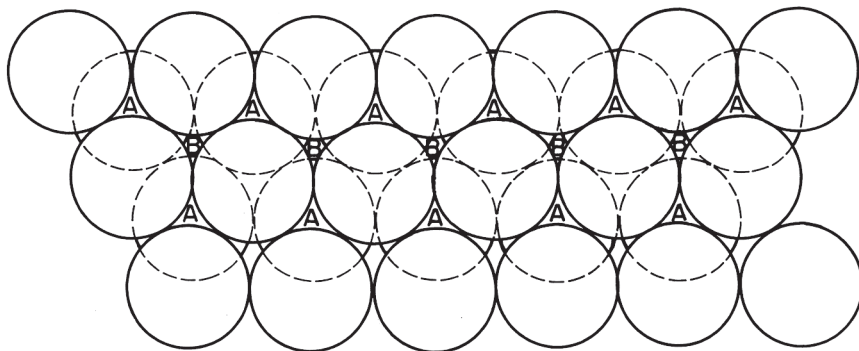


Figure 1.2 Hexagonal close-packed (FCC) lattice: A = tetrahedral sites; B = octahedral sites.

The ions are arranged in a *face-centered cubic* (FCC) lattice. Figure 1.2 shows the orientation of the ions if viewed in the direction of a body diagonal of the spinel crystal ((111) crystal plane). If we consider only two layers, then there is no difference between an FCC lattice and a hexagonal close packed (HCP) one. The difference between FCC and HCP structures is the stacking sequence, which would be obvious if there were three or more layers shown.

There are two possible sites for the metallic ions in this FCC lattice [7]. These sites are shown in Figure 1.2. The A sites have as the four nearest neighbors the oxygen ions. These sites are said to have tetrahedral coordination because of the shape formed by the oxygen ions. Six nearest neighbor oxygen ions surround the metallic ions at the B sites. These sites have octahedral coordination.

There are also two types of octants in the spinel structure, shown in Figures 1.3 and 1.4. The spinel crystal would be made up of four of each of these octants. In Figure 1.4, three of the oxygen ions shown with the octahedral site are actually part of adjacent octants. The unit crystal contains 56 atoms: 32 oxygen atoms and 24 metallic atoms. Each unit cell also contains 8 occupied tetrahedral sites and 16 occupied octahedral sites. The balance of the 64 tetrahedral and 32 octahedral sites are unoccupied. Note that the oxygen ions are shared by more than one site; the tetrahedron and octahedrons are not really isolated, as shown in Figures 1.3 and 1.4. Metallic ions with valences of +3 occupy all of the occupied tetrahedral sites and half of the occupied octahedral sites. The remaining occupied octahedral sites are filled by +2 valence metallic ions.

The ferrimagnetic properties of the spinels result from the orientation of the net magnetic moments of the metallic ions. The moments of the ions at

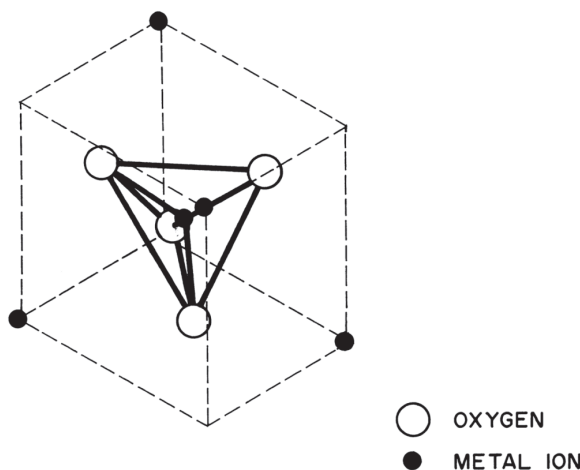


Figure 1.3 One octant of spinel crystal structure including tetrahedral site.

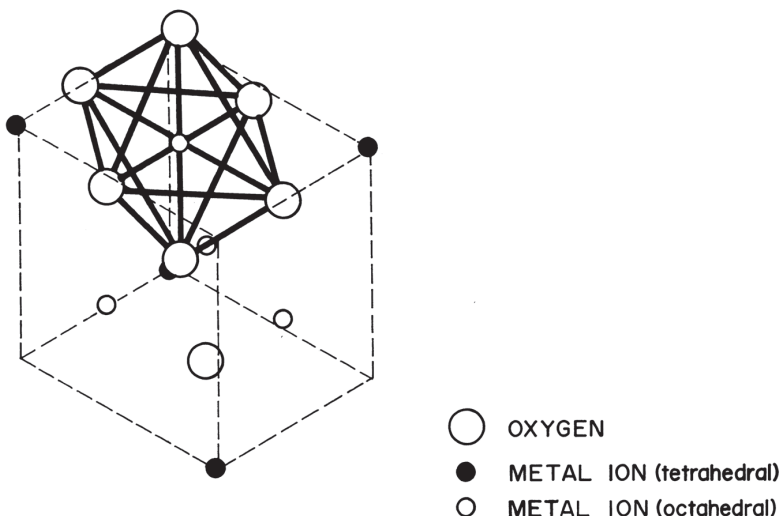


Figure 1.4 One octant of spinel crystal structure including octahedral site.

the tetrahedral sites cancel the moments of eight of the ions at octahedral sites. The remaining eight octahedral ions give the ferrite a net magnetic moment.

Ferrimagnetism should not be confused with ferromagnetism. Ferromagnetism is the spontaneous alignment of all the atomic magnetic moments. Antiferromagnetism is the complete cancellation of all the magnetic moments

in the solid. Ferrimagnetism, then, is a hybrid of ferromagnetism and antiferromagnetism—there is an incomplete cancellation of the atomic magnetic moments.

Garnets, which have the general formula $5\text{Fe}_2\text{O}_33\text{M}_2\text{O}_3$, have crystal structures that are different from those of the spinels in two respects. First, in the garnet structure there are three types of sites for metallic ions, instead of the two site types in the spinel structure. Garnets have tetrahedral, octahedral, and dodecahedral sites. Second, all 64 sites in the garnet structure are filled with metallic ions.

The M in the garnet formula represents yttrium or some other rare earth. Some of the iron in the garnet can be replaced by aluminum to vary the net magnetic moment.

Hexagonal ferrites are an extended family of materials used not only for some microwave and millimeter-wavelength applications, but also for ceramic permanent magnets. Figure 1.5 shows how the composition can be varied to form different types of hexagonal ferrites [8]. Me in the figure represents a divalent metal, such as iron, manganese, magnesium, nickel, zinc, cobalt, or copper. The barium can be substituted by strontium, calcium, or lead. Several key compositions or “types” of hexagonal ferrites are shown in Figure 1.5: M-, U-, W-, X-, Y-, and Z-types. By varying the type and the metal ions used, many different hexagonal ferrite compounds have been synthesized.

We can represent the various structures of hexagonal ferrites as stacks of basic block units, called S, R, and T blocks. The S block resembles the spinel structure, and contains two tetrahedral and four octahedral sites. The R block contains five octahedral sites, and the T block contains two tetrahedral sites and six octahedral sites. An M-type hexagonal ferrite, for example, consists of two S blocks and two R blocks.

Hexagonal ferrites can have considerable magnetic anisotropy compared to spinels and garnets. In some hexagonal ferrites, the crystallographic c-axis is the easy axis of magnetization, and in other hexagonal ferrites, it is the hard axis. We call these ferrites uniaxial and planar materials, respectively.

The M-type ferrites have uniaxial anisotropy and are used for ceramic permanent magnets. They can also be used for self-biased (or partially self-biased) circulators. We cover details of self-biased circulators in Section 6.5.2 of this book. Y-type ferrites have planar anisotropy and cannot be used as permanent magnets, but they can be useful for other microwave devices [9]. W- and Z-type ferrites can be either planar or uniaxial materials, depending on their composition. For example, if they contain a large amount of cobalt, then they have planar anisotropy.

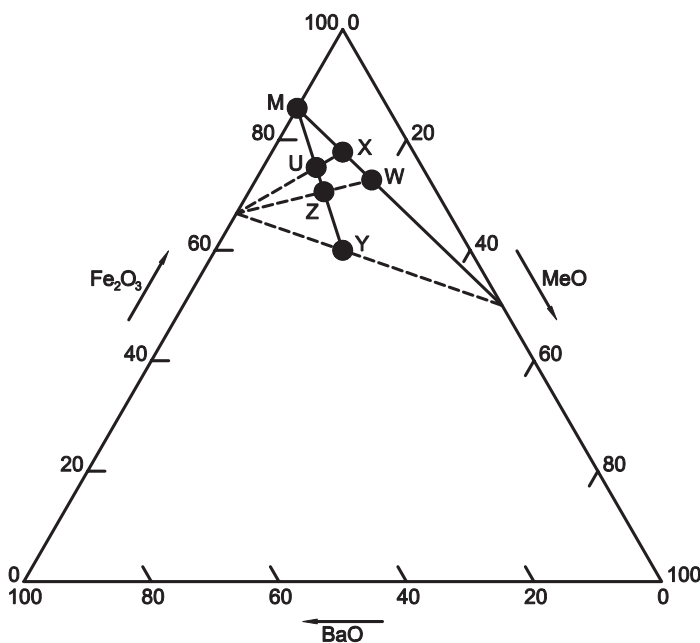


Figure 1.5 Composition of hexagonal ferrites.

An interesting difference between the classes of ferrites is the size of the cations (typically metallic ions) that they can accept [8]. Spinel s can accept a wide variety of small cations. Garnets can accept larger cations in their dodecahedral sites, but hexagonal ferrites can accept even larger ions by replacing some oxygen atoms with large ions.

While the crystal structure of a ferrite significantly affects its properties, on a larger dimensional scale, the microstructure of the material also impacts its properties. Ferrite material manufacturers work to control the microstructure of the ferrites they produce. This is because magnetic, electrical, and mechanical properties depend strongly on the microstructure [5]. Grain-size effects in polycrystalline ferrites, as well as the shape and orientation of grains, affect microwave losses in ferrites [10, 11].

A very important electrical property of ferrites is low conductivity. The molecules of ferrites can be engineered so that there are no mechanisms of conduction. A complete absence of conduction electrons in the crystal structure will ensure that the ferrite material has high resistivity.

High resistivity is important in microwave applications of ferrites because it reduces eddy current losses. Before there were ferrites, there were iron powder

materials. The key to reducing the eddy current losses in these materials is to reduce the size of the iron particles and disperse them in an insulating material. The smallest possible particle of iron is an iron atom. Therefore, the development of ferrites was based on forming materials from iron atoms using chemical techniques.

Ferrite materials having high resistivity will not necessarily have low dielectric loss [12]. Electric dipole relaxation theory [6] explains that at microwave frequencies, the polarization of the dipole may not follow the swing of the RF electric field. This leads to dielectric losses in the form of changes in the complex permittivity of the material. As described in Chapter 4, the dielectric loss tangent is a parameter to consider when selecting a ferrite material.

1.3 Ferrimagnetic Resonance

We can more easily comprehend the concept of ferrimagnetic resonance if we first consider a bicycle wheel. If we hold a bicycle wheel by one end of the axle and spin the wheel, as shown in Figure 1.6, the axle will remain in a

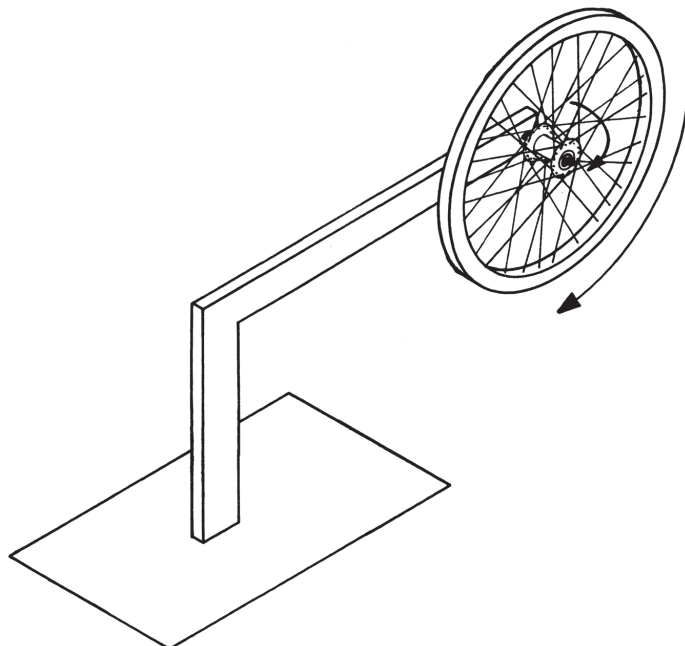


Figure 1.6 Precession of a bicycle wheel.

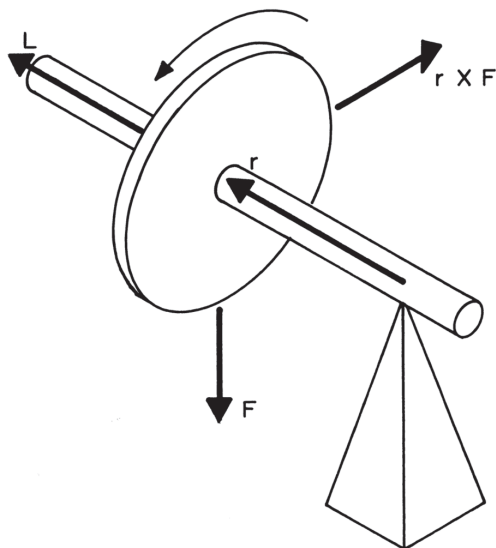


Figure 1.7 Vector analysis of a gyroscope.

plane parallel to the ground and twist in the direction indicated. This gyroscopic effect can be explained mathematically with reference to the vectors in Figure 1.7.

Because the angular momentum of this gyroscope system must be conserved [13], we have

$$\frac{d\mathbf{L}}{dt} = \mathbf{N} \quad (1.1)$$

where \mathbf{L} is the total angular momentum, and \mathbf{N} is the total external torque applied. The torque applied to the system in Figure 1.7 by gravity is $(\mathbf{r} \times \mathbf{F})$ and is directed perpendicular to \mathbf{L} and \mathbf{r} . Insofar as $d\mathbf{L}/dt$ is in the same direction as the torque, by (1.1), \mathbf{L} will precess in the direction of $(\mathbf{r} \times \mathbf{F})$. Note that the new direction of \mathbf{L} after the infinitesimal time increment dt is simply

$$\mathbf{L}(\text{new}) = \mathbf{L}(\text{old}) + \frac{d\mathbf{L}}{dt} \cdot dt \quad (1.2)$$

This simple gyroscopic mechanical model of ferrimagnetic resonance has withstood the test of time and, together with other mathematics, provides

reasonable results for circulator analysis and simulation. However, it may not account for many features of ferrimagnetism, particularly nonlinear effects. Development of new theories of ferrimagnetism is beyond the scope of this book.

We now depart from bicycle mechanics by replacing our bicycle wheel with a spinning electron in the ferrite material, depicted in Figure 1.8.

The spinning orbital electrons of the ions in a ferrite material, which have net magnetic moments (\mathbf{m}), can be acted upon by a magnetic field in much the same way that the bicycle wheel is acted upon by gravity. The torque acting on the electron is given by

$$\mathbf{N} = \mathbf{m} \times (H_{dc} + H_{RF}) \quad (1.3)$$

where H_{dc} is an applied direct magnetic field, H_{RF} is a radio-frequency magnetic field applied to the ferrite, and \mathbf{m} is the net magnetic moment of the electron.

The torques acting on the electrons cause them to precess, or wobble. If no RF magnetic field is applied to the ferrite, the electron spin axes will become aligned with the dc magnetic field in a short time. This is because

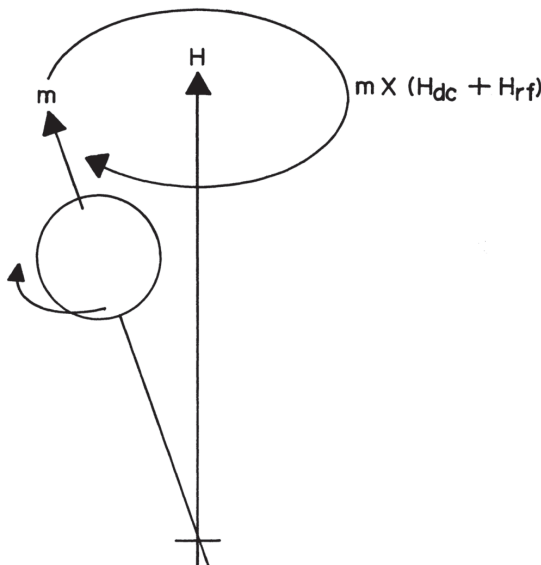


Figure 1.8 Spinning electron in the presence of a magnetic field.

there is no longer any torque acting on the electron when its spin axis is aligned with the magnetic field.

When an RF magnetic field is applied to the ferrite in addition to a dc field, the electrons precess about the direction of the dc field. This precession was shown [14] by Landau and Lifshitz in 1935.

If we substitute the torque given by (1.3) for \mathbf{N} in (1.1), and use $d\mathbf{m}/(gd\mathbf{t})$ as the first derivative of the electronic momentum, we have

$$\frac{d\mathbf{m}}{gd\mathbf{t}} = \mathbf{m} \times (H_{dc} + H_{RF}) \quad (1.4)$$

where g is a constant—the Landé splitting factor, or g factor, as it has come to be known. Ideally, the g factor is equal to 2, but because of orbital interactions (the electrons are not really independent particles), this factor differs slightly from 2. The exact value of the g factor depends on the specific ferrite material. When we depart from theory and deal with real-world materials, we replace g with an effective value, g_{eff} . Section 4.1.4 describes how the g_{eff} value for a particular ferrite material is determined.

Because the electrons precess in a circular fashion, $d\mathbf{m}/dt$ can be replaced by $\mathbf{m}\omega$, where ω is the radian frequency of the precession. We can replace \mathbf{m} with $-eh/4\pi m_0 c$ and \mathbf{m}/g with $-h/4\pi$ to derive

$$\omega = \frac{e(H_{dc} + H_{RF})}{m_0 c} \quad (1.5)$$

where e is the unit electron charge, m_0 is the mass of the electron, and c is the velocity of light; $\mathbf{m} = -eh/4\pi m_0 c$ is the Bohr magneton, the natural unit of magnetic moment; \mathbf{m}/g is the angular momentum. The electron spin number is $-1/2$, so the angular momentum is $-1/2h/2\pi = -h/4\pi$.

We now have an expression for the frequency with which the electrons precess about the dc magnetic field. If the frequency of the applied RF magnetic field is equal to the precessional frequency, the direction of the electron spin magnetic moment will depart greatly from the direction of the dc field. This is the ferrimagnetic resonance effect, discovered in 1946 by Griffiths. A theory of ferrimagnetic resonance, or gyromagnetic resonance as it is also called, was developed by Kittel in 1948.

At resonance, the only torque acting on the electrons is that due to the dc magnetic field, because the electrons are precessing at the frequency of the RF magnetic field. Therefore, at resonance, (1.5) becomes

$$\omega_0 = \frac{eH_{dc}}{m_0 c} \quad (1.6)$$

where ω_0 is the radian frequency of the ferrimagnetic resonance. In MKS units, the factor $e/m_0 c$ in (1.6) becomes $\mu_0 e/m_0$, where μ_0 is the permeability of free space ($4\pi \times 10^{-7}$ H/m). This factor is called the gyromagnetic ratio, γ . We can rewrite (1.6) as

$$\omega_0 = \gamma H_{dc} \quad (1.7)$$

For practical application, when the value of the g factor differs from 2, we use the g_{eff} value for the particular material. In these cases, we replace γ with $\gamma_{eff} = 2.80 \cdot g_{eff}/2$.

The gyromagnetic ratio *ideally* has the value of 2.80 MHz/Oe and is useful for determining the ferrimagnetic resonance frequency if the dc magnetic field is known or for determining the magnetic field required to cause resonance at a specific frequency.

It is important to note that the dc magnetic field here is the field acting on the electrons, which may differ from the magnetic field applied externally to the ferrite material because of the ferrite sample demagnetization factors. These factors vary depending on the shape of the ferrite.

In the preceding discussion we have turned our attention to the effect of the magnetic fields on a single electron, but all the electrons in the ferrite sample in these magnetic fields precess in the same manner. Insofar as the RF magnetic field (and the dc field also, perhaps) may vary at different positions in the ferrite sample, we have made the assumption that the ferrite is small compared to a wavelength so that the magnetic fields in the ferrite are uniform.

The ferrimagnetic resonance is of great importance in the theory of microwave circulators. In some types of circulators, the resonance is used directly to perform the circulation (or isolation) function, while in other types of circulators, the magnetic operating point of the circulator is chosen to be near the ferrimagnetic resonance in order to take advantage of the nonreciprocal properties of the ferrites in the vicinity of resonance.

1.4 Microwave Propagation in Ferrites

Michael Faraday discovered [15] in 1845 that a piece of glass becomes optically active when placed in a strong magnetic field. The Faraday effect occurs as shown in Figure 1.9. Plane-polarized light incident upon the glass in a direction

parallel to the applied magnetic field becomes polarized in a different plane. The glass rotates the plane of polarization of the light. The amount of rotation is directly proportional to the applied magnetic field and to the distance the light travels through the glass.

A similar effect, also called Faraday rotation, occurs when microwaves of a specific polarization are incident upon ferrite material that is subjected to a magnetic field parallel to the direction of propagation of the microwaves. One of the first microwave circulators was the Faraday rotation circulator. This circulator is illustrated in Figure 1.10. The arrows indicate the direction of the electric vectors in the waveguides. The center section of the circulator is a circular waveguide, and a transition to a rectangular waveguide is located at each end. The rectangular guide at port 2 is rotated through 45 degrees with respect to the guide at port 1. Two other rectangular waveguides emerge radially from the circular waveguide at ports 3 and 4. The axes of these two guides are parallel to the electric vectors in the guides at ports 1 and 2. The circular waveguide operates in the H_{11} mode and the rectangular guides operate in the H_{10} mode.

A signal entering the device at port 1 is rotated by 45 degrees in the ferrite rod and appears at port 2. Because of the locations of the waveguides at ports 3 and 4, the mode of operation of these guides, and the direction of the electric vector of the signal entering at port 1, little or no signal is coupled to ports 3 and 4. For the same reasons, signals incident on port 3 are coupled

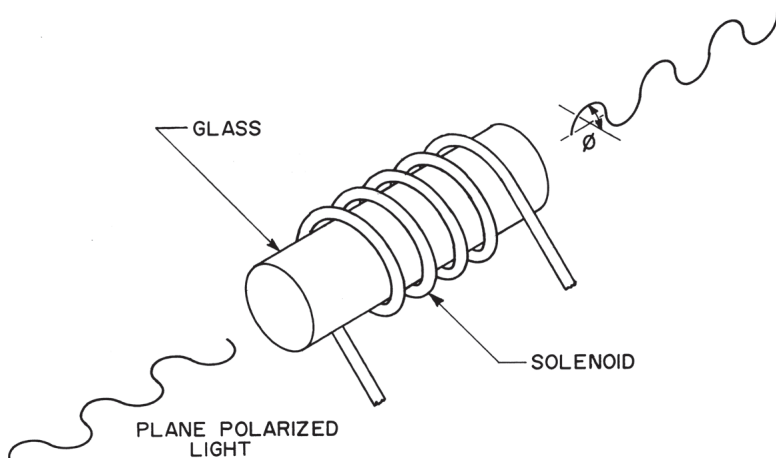


Figure 1.9 The Faraday effect.

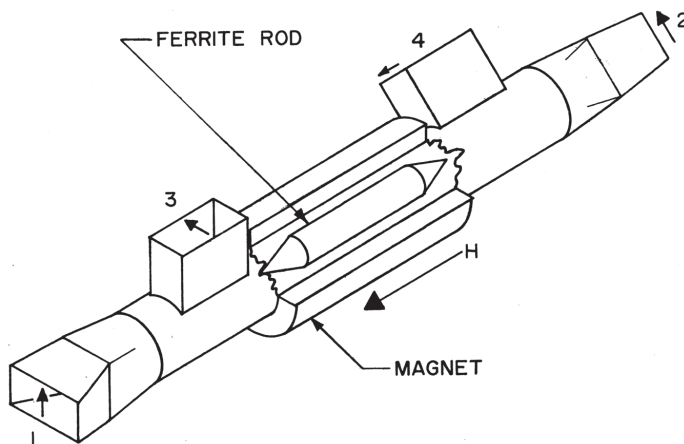


Figure 1.10 The Faraday rotation circulator.

only to port 4 and signals entering port 4 appear only at 1. Thus, the circulator is a four-port device with the signal path 1-2-3-4-1-...

Although Faraday rotation circulators are seldom (if ever) used in modern systems, the theory of operation interestingly follows from that of the optical Faraday effect.

In 1949, Polder [16] opened the door to extensive research involving microwave ferrites when he mathematically described the permeability of ferrites as a function of magnetization, microwave frequency, and properties of the ferrite material.

A tensor is an abstract object representing a generalization of the vector concept. If we have a product of two vectors, \mathbf{AB} , also called a dyad, we can form a new vector, \mathbf{D} , from the dyad \mathbf{AB} and another vector \mathbf{C} by applying the dot product:

$$\mathbf{D} = (\mathbf{AB}) \cdot \mathbf{C} = \mathbf{A}(\mathbf{B} \cdot \mathbf{C})$$

The dyad has properties that are different from those of either a vector or a scalar. It can be described as an operator, a linear vector operator in particular. \mathbf{D} is a linear function of vector \mathbf{C} .

A linear vector operator is also called a tensor. The name *tensor* was first applied when linear vector functions were used in writing elastic deformations and the corresponding stress and strain relations.

Although tensors may be composed of any number of vectorial factors and dimensions, the most commonly occurring tensors are of rank 2 (the product of two vectors) and are in three-dimensional space. These tensors have nine components, which we can write in much the same way we write vector components:

$$\begin{aligned} \mathbf{T} = & T_{xx}\hat{x}\hat{x} + T_{xy}\hat{x}\hat{y} + T_{xz}\hat{x}\hat{z} \\ & + T_{yx}\hat{y}\hat{x} + T_{yy}\hat{y}\hat{y} + T_{yz}\hat{y}\hat{z} \\ & + T_{zx}\hat{z}\hat{x} + T_{zy}\hat{z}\hat{y} + T_{zz}\hat{z}\hat{z} \end{aligned}$$

where \mathbf{T} represents the general tensor. We can also write the components in matrix form:

$$\mathbf{T} = \begin{pmatrix} T_{xx} & T_{xy} & T_{xz} \\ T_{yx} & T_{yy} & T_{yz} \\ T_{zx} & T_{zy} & T_{zz} \end{pmatrix}$$

The permeability of magnetized ferrite material is described by a tensor.

Tensors have special characteristics that enable them to undergo certain types of transformations under changes of coordinate system. There are also operations that can be performed on tensors such as transposition and diagonalization. A complete treatment of tensor algebra is beyond the scope of this book.

The physical significance of the tensor permeability is that the \mathbf{B} and \mathbf{H} vectors may point in different directions.

We begin our derivation of the Polder tensor with the Gilbert equation of motion of the magnetization, which bears some resemblance to (1.4) except that it includes a damping factor, α :

$$\frac{d\mathbf{M}}{dt} = \gamma(\mathbf{M} \times \mathbf{H}) + \frac{\alpha\mathbf{M}}{\mathbf{M}} \times \frac{d\mathbf{M}}{dt} \quad (1.8)$$

The damping factor is given by

$$\alpha = \frac{\Delta H \gamma}{2\omega_0} \quad (1.9)$$

where ΔH is the resonance line width of the ferrite material. \mathbf{H} and \mathbf{M} in (1.8) are defined as

$$\mathbf{H} = \hat{z}H_{dc} + \mathbf{h}e^{j\omega t} \quad (1.10)$$

$$\mathbf{M} = \hat{z}M_0 + \mathbf{m}e^{j\omega t} \quad (1.11)$$

Here, M_0 is the ferrite magnetization and \mathbf{h} and \mathbf{m} are the microwave magnetic field and magnetization components, respectively. If we substitute (1.10) and (1.11) into (1.8), we derive

$$j\omega\mathbf{m} = \gamma M_0(\hat{z} \times \mathbf{h}) + (\omega_0 + j\omega\alpha)(\hat{z} \times \mathbf{m}) \quad (1.12)$$

We now decompose (1.12) into x , y , and z components:

$$j\omega m_x = -(\omega_0 + j\omega\alpha)m_y - \gamma M_0 h_y \quad (1.13)$$

$$j\omega m_y = \gamma M_0 h_x + (\omega_0 + j\omega\alpha)m_x \quad (1.14)$$

$$j\omega m_z = 0 \quad (1.15)$$

We solve for m_x and m_y and write

$$m_x = -\frac{(\omega_0 + j\omega\alpha)\gamma M_0}{(\omega_0 + j\omega\alpha)^2 - \omega^2} h_x - \frac{j\omega\gamma M_0}{(\omega_0 + j\omega\alpha)^2 - \omega^2} h_y \quad (1.16)$$

$$m_y = \frac{j\omega\gamma M_0}{(\omega_0 + j\omega\alpha)^2 - \omega^2} h_x - \frac{(\omega_0 + j\omega\alpha)\gamma M_0}{(\omega_0 + j\omega\alpha)^2 - \omega^2} h_y \quad (1.17)$$

To simplify these expressions, we use the substitutions:

$$\chi = -\frac{(\omega_0 + j\omega\alpha)\gamma M_0}{(\omega_0 + j\omega\alpha)^2 - \omega^2} \quad (1.18)$$

$$\kappa = \frac{\omega\gamma M_0}{(\omega_0 + j\omega\alpha)^2 - \omega^2} \quad (1.19)$$

The simplification of (1.15), (1.16), and (1.17) gives us

$$m_x = \chi h_x - j\kappa h_y \quad (1.20)$$

$$m_y = j\kappa h_x + \chi h_y \quad (1.21)$$

$$m_z = 0 \quad (1.22)$$

These equations can be rewritten in matrix form:

$$\begin{pmatrix} m_x \\ m_y \\ m_z \end{pmatrix} = \begin{pmatrix} \chi & -j\kappa & 0 \\ j\kappa & \chi & 0 \\ 0 & 0 & 0 \end{pmatrix} \begin{pmatrix} h_x \\ h_y \\ h_z \end{pmatrix} \quad (1.23)$$

An intermediate result in our derivation of the Polder tensor is the susceptibility tensor, which is actually a factor in (1.23):

$$\chi = \begin{pmatrix} \chi & -j\kappa & 0 \\ j\kappa & \chi & 0 \\ 0 & 0 & 0 \end{pmatrix} \quad (1.24)$$

χ and κ are complex variables, $\chi = \chi' + j\chi''$ and $\kappa = \kappa' + j\kappa''$. The real and imaginary components, derived from (1.18) and (1.19), are given by

$$\chi' = \frac{\gamma M_0 \omega_0 [\omega_0^2 - \omega^2(1 - \alpha^2)]}{[\omega_0^2 - \omega^2(1 + \alpha^2)]^2 + 4\omega^2\omega_0^2\alpha^2} \quad (1.25)$$

$$\chi'' = \frac{\gamma M_0 \omega \alpha [\omega_0^2 + \omega^2(1 + \alpha^2)]}{[\omega_0^2 - \omega^2(1 + \alpha^2)]^2 + 4\omega^2\omega_0^2\alpha^2} \quad (1.26)$$

$$\kappa' = \frac{\gamma M_0 \omega [\omega_0^2 - \omega^2(1 + \alpha^2)]}{[\omega_0^2 - \omega^2(1 + \alpha^2)]^2 + 4\omega^2\omega_0^2\alpha^2} \quad (1.27)$$

$$\kappa'' = \frac{2\gamma M_0 \omega_0 \omega^2 \alpha}{[\omega_0^2 - \omega^2(1 + \alpha^2)]^2 + 4\omega^2\omega_0^2\alpha^2} \quad (1.28)$$

Because the permeability $\mu = 1 + \kappa$, we can make slight modifications to the susceptibility tensor (1.24) to arrive at the Polder permeability tensor:

$$\boldsymbol{\mu} = \begin{pmatrix} \mu & -j\kappa & 0 \\ j\kappa & \mu & 0 \\ 0 & 0 & 1 \end{pmatrix} \quad (1.29)$$

In most cases, α^2 is much less than unity, so the $\omega^2(1 - \alpha^2)$ and $\omega^2(1 + \alpha^2)$ terms in (1.25) to (1.28) can be changed to simply ω^2 . The elements of the permeability tensor now are

$$\mu' = 1 + \frac{\gamma M_0 \omega_0 (\omega_0^2 - \omega^2)}{(\omega_0^2 - \omega^2)^2 + 4\omega^2 \omega_0^2 \alpha^2} \quad (1.30)$$

$$\mu'' = \frac{\gamma M_0 \omega \alpha (\omega_0^2 + \omega^2)}{(\omega_0^2 - \omega^2)^2 + 4\omega^2 \omega_0^2 \alpha^2} \quad (1.31)$$

$$\kappa' = \frac{\gamma M_0 \omega (\omega_0^2 - \omega^2)}{(\omega_0^2 - \omega^2)^2 + 4\omega^2 \omega_0^2 \alpha^2} \quad (1.32)$$

$$\kappa'' = \frac{2\gamma M_0 \omega_0 \omega^2 \alpha}{(\omega_0^2 - \omega^2)^2 + 4\omega^2 \omega_0^2 \alpha^2} \quad (1.33)$$

Figures 1.11 and 1.12 show the real (κ' and μ') and imaginary (κ'' and μ'') components of κ and μ , respectively, as functions of normalized frequency. For the calculations used to produce these figures, $\omega_0 = 1400$ MHz, $M_0 = 1000$ G, and $\alpha = 0.01$.

Now that we have equations for the permeability of the ferrite material, we can move on to find propagation constants for microwaves incident on ferrites. We assume that a wave makes an angle θ with the z axis, which is also the axis of the applied dc magnetic field, and an angle ϕ with the x axis, as shown in Figure 1.13.

From Maxwell's equations, it can be shown that

$$\mathbf{b} = \frac{\mathbf{\Gamma}^2}{\epsilon(j\omega)^2} [h_x - (\sin \theta \cos \phi h_x + \sin \theta \sin \phi h_y + \cos \theta h_z) \sin \theta \cos \phi] \quad (1.34)$$

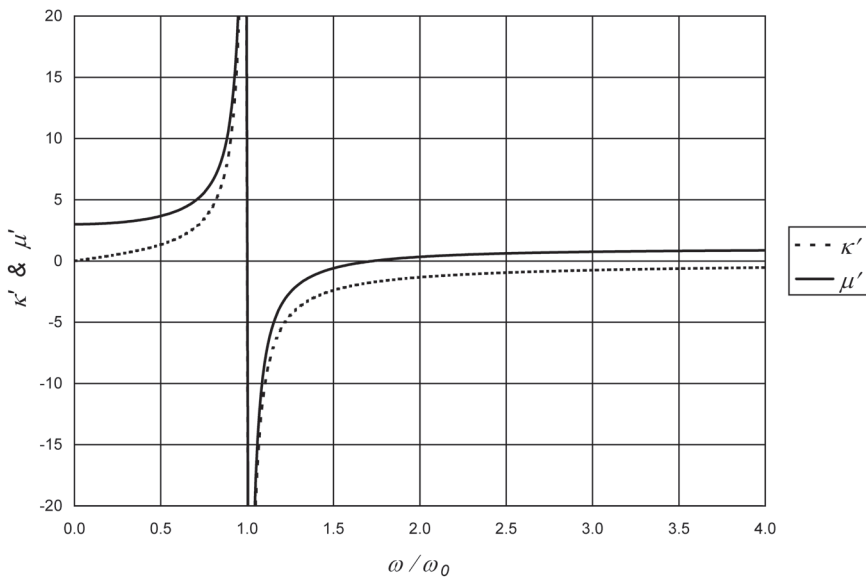


Figure 1.11 Real components of the Polder permeability tensor as functions of normalized frequency. $\omega_0 = 1400$ MHz, $M_0 = 1000$ G, and $\alpha = 0.01$.

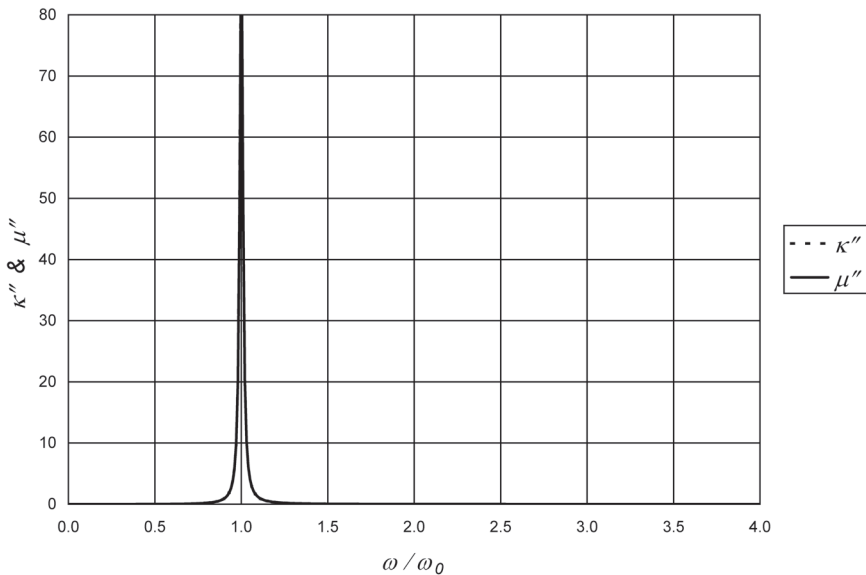


Figure 1.12 Imaginary components of the Polder permeability tensor as functions of normalized frequency. $\omega_0 = 1400$ MHz, $M_0 = 1000$ G, and $\alpha = 0.01$.

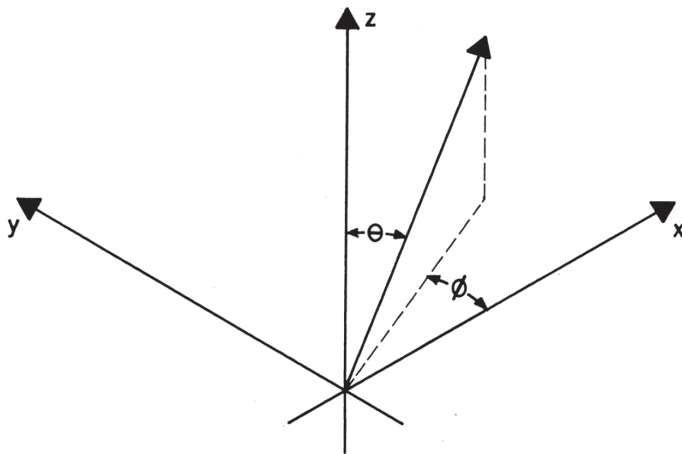


Figure 1.13 Direction of wave propagation in ferrite.

where Γ is the propagation constant, and ϵ is the permittivity. We can also equate \mathbf{b} , the magnetic induction, to the permeability tensor:

$$\mathbf{b} = \mu_0 \begin{pmatrix} \mu & -j\kappa & 0 \\ j\kappa & \mu & 0 \\ 0 & 0 & 1 \end{pmatrix} \begin{pmatrix} h_x \\ h_y \\ h_z \end{pmatrix} \quad (1.35)$$

Equating the right sides of (1.34) and (1.35), we solve for Γ , given by

$$\Gamma_{\pm} = j\omega\sqrt{\mu_0\epsilon} \sqrt{\frac{(\mu^2 - \mu - \kappa^2) \sin^2\theta + 2\mu \mp \sqrt{(\mu^2 - \mu - \kappa^2)^2 \sin^4\theta + 4\kappa^2 \cos^2\theta}}{2[(\mu - 1) \sin^2\theta + 1]}} \quad (1.36)$$

where Γ_+ and Γ_- are the propagation constants for waves that travel in the z direction. The plus and minus indicate different polarizations of the elliptically polarized waves. These waves propagate with different velocities through the ferrite. The propagation constants do not depend on the angle the waves make with the x axis.

The propagation constant describes the propagation of an electromagnetic wave in a particular medium. For a homogeneous, isotropic medium (magnetized ferrites are not isotropic), the propagation constant is given by

$$\Gamma = \pm j\omega\sqrt{\mu_0\mu\varepsilon}\sqrt{1 - \frac{j\sigma}{\omega\varepsilon}}$$

where ε is the absolute permittivity for the medium, and σ is the conductivity.

Γ is a complex quantity that can be broken down into an attenuation term (α) and a phase term (β):

$$\Gamma = \alpha + j\beta$$

By binomial theorem expansion, we can separate the attenuation and phase terms. The first few terms of the expansion give us:

$$\alpha = \frac{\sigma}{2}\sqrt{\frac{\mu_0\mu}{\varepsilon}}$$

$$j\beta = j\omega\sqrt{\mu_0\mu\varepsilon} \left(1 + \frac{1}{8}\sqrt{\frac{\sigma}{\omega\varepsilon}}\right)$$

The attenuation term (α) is a measure of the change in amplitude of the electric or magnetic field intensity per unit length in the path of propagation. The phase term (β) is a measure of the change in phase of the electric or magnetic field vectors per unit length.

If the conductivity of the medium is very low, the phase term reduces to

$$j\beta = j\omega\sqrt{\mu_0\mu\varepsilon}$$

and the attenuation term becomes negligible. Thus, we can approximate the propagation constant with the phase term or vice versa if the attenuation term is small.

The units for the attenuation and phase terms are nepers per unit length and radians per unit length, respectively.

To show the usefulness of the propagation constants in more detail, we will consider some special cases: the transverse-field case, where the dc magnetic field is perpendicular to the direction of propagation; the longitudinal field case, where the dc magnetic field is parallel to the direction of propagation; the case of Faraday rotation; and the case of resonance absorption.

When the direction of propagation is transverse to the applied dc magnetic field, $\theta = \pi/2$ and (1.36) reduces to

$$\Gamma_+ = j\omega\sqrt{\mu_0\epsilon} \sqrt{\frac{\mu^2 - \kappa^2}{\mu}} \quad (1.37)$$

$$\Gamma_- = j\omega\sqrt{\mu_0\epsilon} \quad (1.38)$$

The quotient $(\mu^2 - \kappa^2)/\mu$ in (1.37) is the effective permeability of the ferrite in the transverse-field case. Figures 1.14 and 1.15 show the real (μ_{eff}') and imaginary (μ_{eff}'') components of the effective permeability (μ_{eff}), respectively, as functions of normalized frequency. For the calculations used to produce these figures, $\omega_0 = 1400$ MHz, $M_0 = 1000$ G, and $\alpha = 0.01$. It is interesting to note that in this transverse-field case h_x and h_y have the relation:

$$h_y = -j\frac{\kappa}{\mu} h_x \quad (1.39)$$

and that b is linearly polarized transverse to the z axis.

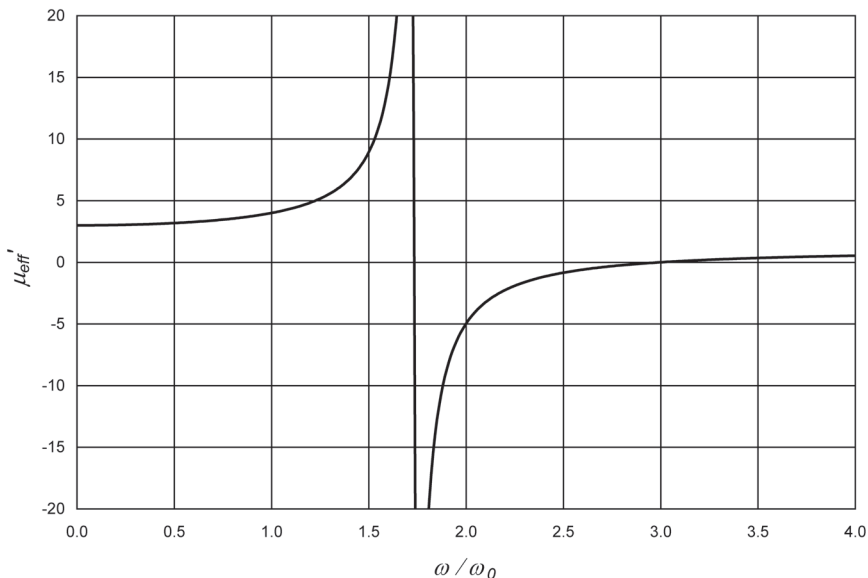


Figure 1.14 Real component of transverse-field effective ferrite permeability as a function of normalized frequency. $\omega_0 = 1400$ MHz, $M_0 = 1000$ G, and $\alpha = 0.01$.

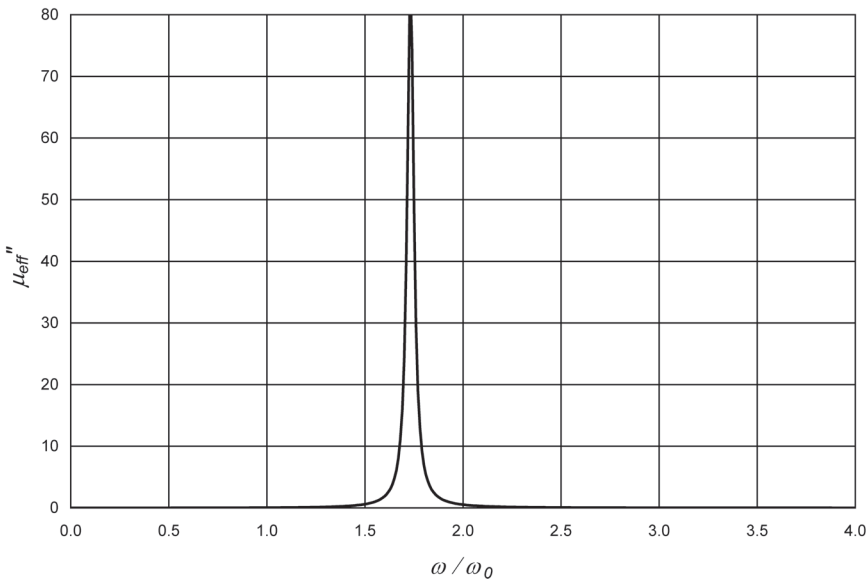


Figure 1.15 Imaginary component of transverse-field effective permeability as a function of normalized frequency. $\omega_0 = 1400$ MHz, $M_0 = 1000$ G, and $\alpha = 0.01$.

The transverse case applies to junction circulators, and the factor κ/μ in (1.39) has been used [17] in various theoretical studies to indicate specific ferrite magnetic operating points. Figure 1.16 shows the real (κ/μ') component of κ/μ as a function of normalized frequency. For the calculations used to produce this figure, $\omega_0 = 1400$ MHz, $M_0 = 1000$ G, and $\alpha = 0.01$.

In a junction circulator, the dc magnetic field is applied to the ferrite so that the direction of RF propagation is transverse to the dc magnetic field. Two elliptically polarized waves with propagation constants given by (1.37) and (1.38) are present in the ferrite. If the ferrites are in the form of disks, the two waves rotate in the disks in opposite directions. They are periodically in and out of phase, depending on the position around the disk perimeter (assuming the disks have the dc magnetic field applied parallel to their axes). If we provide a means of coupling RF energy into and out of these nodes and antinodes, we have a junction circulator. The operation of the junction circulator is described in more detail in Section 5.1.

In the longitudinal field case $\theta = 0$ and (1.36) reduces to

$$\Gamma_{\pm} = j\omega\sqrt{\mu_0(\mu \mp \kappa)\epsilon} \quad (1.40)$$

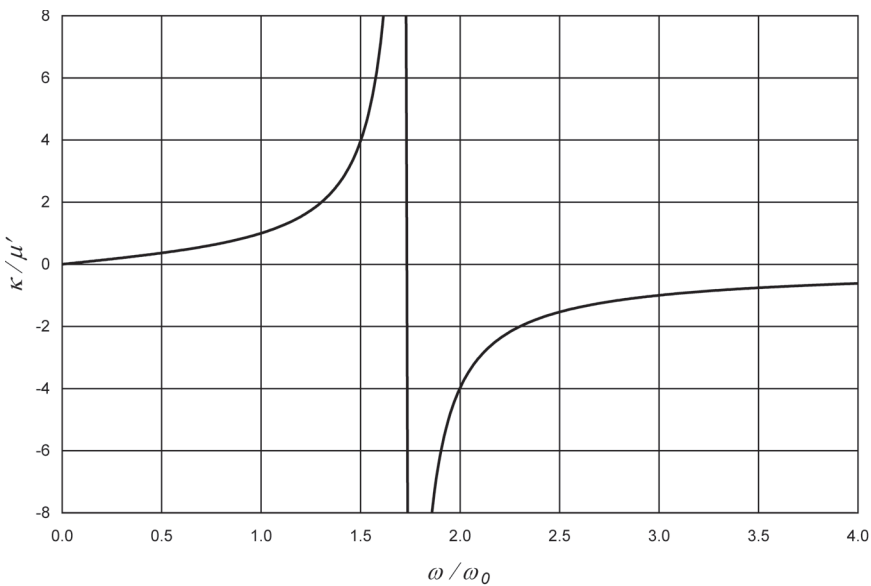


Figure 1.16 Real (κ/μ') component of κ/μ as a function of normalized frequency. $\omega_0 = 1400$ MHz, $M_0 = 1000$ G, and $\alpha = 0.01$.

Certain assumptions can be made to simplify the expressions for $\mu - \kappa$ and $\mu + \kappa$. In the magnetic region where the ferrite is unsaturated, that is, $\omega \gg \omega_0$ and $\alpha^2 \gg 1$, appropriate simplifications can be applied to (1.30) to (1.33). Terms involving α^2 in (1.25) to (1.28) can be dropped except when the ferrite is being used in a resonance device or the microwave frequency is very close to the ferrimagnetic resonance frequency. For devices that operate far from resonance in the frequency domain, it is possible that $\alpha \ll 1$. If this is the case, terms involving α may be dropped.

The amount of rotation caused by a longitudinally magnetized ferrite in a Faraday rotation device is given by

$$\phi = \left(\frac{\beta_+ - \beta_-}{2} \right) L \quad (1.41)$$

where L is the length of the ferrite. Equation (1.41) contains the average of the rotations caused by two elliptically polarized waves. These two waves have phase constants given by β_+ and β_- . For the typical case of a low value of applied dc magnetic field, β_+ and β_- can be approximated by Γ_+ and Γ_- . This is due to the low value of the attenuation-constant component of Γ .

In order to capitalize on the ferrimagnetic resonance absorption effect, we must again consider two counter-rotating elliptically polarized waves. The wave that rotates in the same direction as the precession of the electron spin moments will suffer high attenuation if the microwave frequency is at or near the ferrimagnetic resonance frequency. The other rotating wave will not suffer this attenuation.

Our treatment of the theory of microwave propagation in ferrites will not be complete until we discuss spin waves. If a microwave magnetic field is applied to a ferrite that is also biased by a dc magnetic field, the magnetization vector of the ferrite will be aligned with the dc magnetic field at very low RF signal levels. As the RF signal level is increased, the magnetization vector may begin to move away from alignment with the dc field. It is impossible, however, for the magnetization in the direction of the dc field to drop to zero or reverse polarity because of spin-wave effects.

As the critical microwave magnetic field, H_C , is reached, the change in angle of the magnetization vector excites spin waves. There is a spatial periodicity to the amount the magnetization vector deviates from the equilibrium direction due to nonuniformity of the magnetic fields, thermal excitation of the ferrite atoms (at 0 K it might be possible to eliminate spin-wave effects), and boundary effects caused by the dimensions of the ferrite sample. This spatial periodicity is the period of the spin wave. The name *spin wave* is derived from the electron spin axis direction, which is in the direction of the magnetization vector at equilibrium, and the sinusoidal wave nature that the spin waves possess.

Spin waves, mutually coupled and propagating in all directions in the ferrite, cause a broadening and reduction in amplitude of the ferrimagnetic resonance. Spin waves having half the frequency of the waves that cause the broadening of the main ferrimagnetic resonance are responsible for a subsidiary resonance.

The spin waves are most troublesome in the design of high-power, below-resonance devices. These devices usually operate in the region between ferrimagnetic resonance and the subsidiary resonance, so that a broadening of either resonance leads to increased insertion loss at high power.

The theoretical information presented in this chapter is mainly for qualitative purposes at this point. The mathematical complexity of the equations, together with the fact that none of the equations will yield high-performance circulator designs without the addition of other factors, prevents their quantitative use.

The information does, however, form a theoretical base for further development in later chapters, particularly Chapter 5.

1.5 Other Technologies

This book focuses on the design of microwave circulators containing bulk ferrimagnetic materials (ferrites), as nearly all circulators utilize these materials. There are several other technologies on which circulators can be based, which we will briefly describe in this section. Typically these technologies are not as practical as ferrimagnetism, but an understanding of emerging and alternative technologies may be helpful to the circulator designer.

1.5.1 Semiconductor Circulators

The first alternative technology that we will present is that of semiconductor circulators. Investigations of the Faraday effect in semiconductor materials date back to the 1950s [18, 19], the same decade in which the first ferrite-based Faraday rotators appeared. Analogous to the tensor permeability of magnetized ferrite, the solid-state plasma of a semiconductor in the presence of a magnetic field results in a tensor *permittivity* [20]. In ferrites, nonreciprocal action is explained by coupling of microwave energy with electron spins, whereas in semiconductors, microwave energy couples with electron orbital motion. The electron precession resonance in semiconductors is called the cyclotron resonance.

Table 1.3 shows some representative semiconductor circulator experimental results.

Table 1.3
Representative Semiconductor Circulator Experimental Results

Year:	1969	2001	2004
Reference:	[21]	[22]	[23]
Author(s):	Suzuki	Yong, Sloan, & Davis	Ng, Davis, & Sloan
Medium:	Waveguide	Finline	Waveguide
Semiconductor:	InSb	InSb	InSb
Temperature:	+25° C	-196° C	-196° C
Magnetic bias:	≈10 kG	7.3 kG	8.8 kG
Frequency range:	18 – 26 GHz*	34 – 38 GHz	55 – 65 GHz
Isolation:	20 dB	≈15 dB	≈13 dB
Insertion loss:	3 dB	≈1 dB	≈3 dB

* Single frequency in the stated range.

Ferrite circulators have limited bandwidths at millimeter wavelengths because the saturation magnetization ($4\pi M_s$) of available ferrite materials is limited to about 5000G. On the other hand, semiconductor circulators do not have the same upper frequency materials limitation. Also, the cyclotron resonance frequency of a semiconductor circulator is typically much higher than the ferrimagnetic resonance frequency would be for a ferrite circulator.

To minimize insertion loss in a semiconductor circulator, the electron collision frequency must be low. Collision frequency is inversely proportional to electron mobility, so high mobility is desirable. Indium Antimonide (InSb) has been the chosen material for semiconductor circulators because of its high electron mobility. Because the collision frequency is temperature dependent, operation at low temperatures is desirable. This is why much of the experimental data in the literature correspond to circulators that operate at low temperatures, such as -196° C (liquid nitrogen boiling point). In addition, the cyclotron resonance frequency must be much greater than the collision frequency. Because the cyclotron resonance frequency is proportional to the magnetic bias field, it can be increased by increasing the magnetic bias field.

While semiconductor circulators might offer good performance at millimeter wavelength and higher frequencies, their performance at lower frequencies is poor compared to that of ferrite circulators. The high magnetic bias field requirements require relatively large and massive magnetic circuits. At lower frequencies, or in applications where very low insertion loss is required, the semiconductors must be operated at very low temperatures. Higher-frequency semiconductor circulators may not have the same demand for cooling.

1.5.2 Nanotechnology Circulators

Nanotechnology is a relatively new field of scientific research, although it is based on older principles. Nanotechnology refers to engineering at the molecular scale, involving dimensions roughly less than 100 nm.

Experimental isolators have been made using 70-nm ferromagnetic nanowires in a polycarbonate dielectric [24], forming a 1-D (one-dimensional) composite nanostructure [25]. Circulators having a 0-D (zero-dimensional) composite consisting of 200-nm hexagonal ferrite nanoparticles suspended in photoresist have been demonstrated [26].

Although some nanotechnology circulators and isolators have relatively high insertion loss, nanotechnology promises to enable development of materials and devices having unique properties.

1.5.3 Thin Ferrite Films

With the widespread use of monolithic microwave integrated circuits (MMICs) came the demand for circulators that are compatible with them [27]. These circulators may take the form of miniaturized devices that can be placed adjacent to MMICs or circulators that can be deposited directly onto MMIC substrates.

Using the same procedure as that used for the design of other microstrip circulators, we can design circulators that utilize ferrite films. Various techniques have been used for the manufacture of thin ferrite films, including liquid phase epitaxy (LPE), sputtering, vacuum evaporation, chemical vapor deposition (CVD), spin spray plating (SSP), arc plasma, molecular beam epitaxy (MBE), and pulsed laser deposition (PLD) [5].

LPE involves heating a mixture of the ferrite and a flux [28]. The substrate, which serves as a seed, is then placed in the mixture and the ferrite film grows onto the substrate surface. Crystal lattice matching and coefficient of thermal expansion (CTE) must be considered when selecting a substrate. Gadolinium gallium garnet (GGG) is frequently used as a substrate for garnet films because of its good combination of properties. LPE ferrite films are typically of high quality and film thicknesses can be > 0.008 inches. Some processes, such as CVD and MBE, produce very thin films, ranging from roughly 0.4–100 microinches thick, which are too thin for practical microwave circulator applications.

The SSP process is a low-temperature one that can be applied to a wide range of substrates, but the films produced are relatively thin. Also, the films tend to be lossy because of contaminants.

PLD uses laser ablation to remove ferrite material from a target and deposit the material onto the substrate. This process also produces relatively thin films, up to about 100 microinches thick, and uses temperatures that may not be compatible with the MMIC substrate.

Thicker films can be produced by screen printing, followed by sintering, although the sintering temperatures are generally not compatible with MMIC (semiconductor) substrates.

One method of integrating a ferrite-film circulator with an MMIC is to grow the film on GGG using LPE, then bond the ferrite to the MMIC substrate using a low-temperature material, such as solder or epoxy [29, 30]. The GGG is then removed by grinding, and the ferrite film is metalized and the circulator circuit pattern is produced using photolithography. Another integration option is to grind bulk ferrite very thin, rather than manufacture ferrite film directly, then epoxy the ferrite to the MMIC substrate [31].

The thickness limitations of ferrite films result in inferior circulator electrical performance in comparison to other bulk-ferrite circulators. This is because the necessarily narrow microstrip transmission lines tend to be lossy, and the ferrite thickness is often not optimum.

1.5.4 Active Circulators

Amplifiers can be used to perform circulator and isolator functions. Most amplifiers have inherently nonreciprocal gain. That is, they have gain in the forward direction and much lower gain, or even loss, in the reverse direction. An amplifier can serve as an isolator by simply connecting the amplifier between the components to be isolated. An attenuator could be added before or after the amplifier to reduce gain and increase reverse isolation.

Figure 1.17 shows a partial schematic of an active circulator that uses operational amplifiers [32]. Dc power connections and decoupling capacitors are not shown in the figure. The resistor values are

$$R_1 = 2Z_0 \quad (1.42)$$

$$R_2 = 2Z_0 + 2\sqrt{5}Z_0 \quad (1.43)$$

where Z_0 is the characteristic impedance.

The advantages of active circulators and isolators are that they can operate over very wide bandwidths and can operate at very low frequencies, down to and including dc. Unfortunately, active circulators and isolators require dc

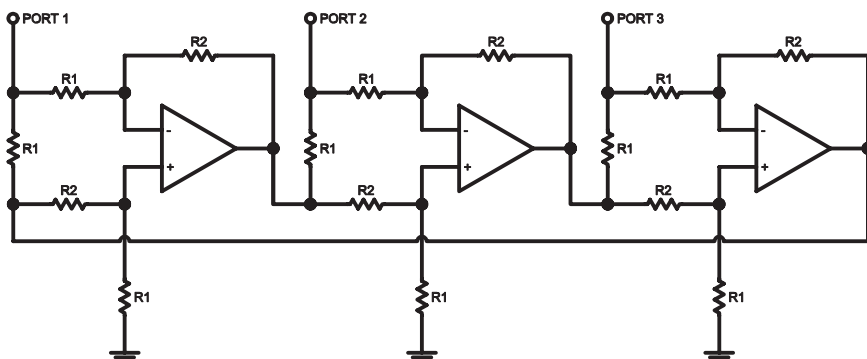


Figure 1.17 Active circulator schematic.

power, their power handling is limited by the amplifier(s) used, and they may introduce distortion and noise.

References

- [1] Waldron R. A., *Ferrites: An Introduction for Microwave Engineers*, London: Van Nostrand, 1962.
- [2] “Milestones: Development of Ferrite Materials and their Applications, 1930–1945,” http://www.ieeeghn.org/wiki/index.php/Milestones:Development_of_Ferrite_Materials_and_Their_Applications,_1930-1945. Last accessed Nov. 13, 2013.
- [3] Keffer, F., “The Magnetic Properties of Materials,” *Materials*, San Francisco: W. H. Freeman, 1967.
- [4] Goldman, A., *Modern Ferrite Technology*, 2nd Ed., New York: Springer Science + Business Media, 2006, p. 217.
- [5] Valenzuela, R., *Magnetic Ceramics*, Cambridge: Cambridge University Press, 1994.
- [6] Wert, C. A., and R. M. Thomson, *Physics of Solids*, New York: McGraw-Hill, 1970.
- [7] Soohoo, R. F., *Microwave Magnetics*, New York: Harper and Row, 1985.
- [8] Von Aulock, W. H., *Handbook of Microwave Ferrite Materials*, New York: Academic Press, 1965.
- [9] Braden, R. A., I. Gordon, and R. L. Harvey, “Microwave Properties of Planar Hexagonal Ferrites,” *IEEE Transactions on Magnetics*, March 1966, pp. 43–47.
- [10] Patton, C. E., “A Review of Microwave Relaxation in Polycrystalline Ferrites,” *IEEE Transactions on Magnetics*, September 1972, pp. 433–439.
- [11] Inui, T., and N. Ogasawara, “Grain-Size Effects on Microwave Ferrite Magnetic Properties,” *IEEE Transactions on Magnetics*, November 1977, pp. 1729–1744.
- [12] Baden-Fuller, A. J., *Ferrites at Microwave Frequencies*, London: Peter Peregrinus, 1987.
- [13] Symon, K. R., *Mechanics*, Reading, MA: Addison-Wesley, 1971.
- [14] Riches, E. E., *Ferrites: A Review of Materials and Applications*, London: Mills and Boon, 1972.
- [15] Jenkins, F. A., and H. E. White, *Fundamentals of Optics*, New York: McGraw-Hill, 1976.
- [16] Polder, D., “On the Theory of Ferromagnetic Resonance,” *Phil. Mag.*, Vol. 40, 1949, pp. 99–115.
- [17] Bosma, H., “On Stripline Y-Circulation at UHF,” *IEEE Transactions on Microwave Theory and Techniques*, January 1964, pp. 61–73.

- [18] Rau, R., and M. E. Caspari, "Faraday Effect in Germanium at Room Temperature," *Physical Review*, October 1955, pp. 632–639.
- [19] Hayes, R. E., M. Kanda, G. Masclet, W. G. May, "The Application of Semiconductors to Quasi-Optical and Waveguide Isolators for Use at Millimeter Wavelengths," Electrical Engineering Department, University of Colorado, July 1969.
- [20] Barlow, H. E. M., and R. Koike, "Microwave Propagation in a Waveguide Containing a Semiconductor to which Is Applied a Steady Transverse Magnetic Field," *Proceedings of the IEE*, December 1963, pp. 2177–2181.
- [21] Suzuki, K., "Room Temperature Solid-State Plasma Nonreciprocal Microwave Devices," *IEEE Transactions on Electron Devices*, December 1969, pp. 1018–1021.
- [22] Yong, C. K., R. Sloan, and L. E. Davis, "A Ka-Band Indium-Antimonide Junction Circulator," *IEEE Transactions on Microwave Theory and Techniques*, June 2001, pp. 1101–1106.
- [23] Ng, Z. M., L. E. Davis, and R. Sloan, "Measurements of V-Band N-Type InSb Junction Circulators," *IEEE Transactions on Microwave Theory and Techniques*, February 2004, pp. 482–488.
- [24] Spiegel, J., J. de la Torre, L. Piraux, I. Huynen, "Isolator Concept based on Ferromagnetic Nanowired Substrates," *IEEE Microwave Symposium Digest*, 2009, pp. 29–32.
- [25] Kittel, C., *Introduction to Solid State Physics*, Hoboken, NJ: John Wiley & Sons, 2005.
- [26] Boyajian, T., D. Vincent, S. Neveu, M. LeBerre, J. J. Rousseau, "Coplanar Circulator Made from Composite Magnetic Material," *IEEE Microwave Symposium Digest*, 2011.
- [27] Webb, D. C., "Status of Ferrite Technology in the United States," *IEEE Microwave Symposium Digest*, 1993, pp. 203–206.
- [28] Harris, V. G., "Modern Microwave Ferrites," *IEEE Transactions on Magnetics*, March 2012, pp. 1075–1104.
- [29] Oliver, S. A., P. M. Zavracky, N. E. McGruer, R. Schmidt, "A Monolithic Single-Crystal Yttrium Iron Garnet/Silicon X-Band Circulator," *IEEE Microwave and Guided Wave Letters*, August 1997, pp. 239–241.
- [30] How, H., S. A. Oliver, S. W. McKnight, P. M. Zavracky, N. E. McGruer, "Theory and Experiment of Thin-Film Junction Circulator," *IEEE Transactions on Microwave Theory and Techniques*, November 1998, pp. 1645–1653.
- [31] Shi, P., "MmW Monolithic Y-Junction Circulator on Single-Crystal Sc-Doped Ba-Hexaferrite," *IEEE Microwave Symposium Digest*, 2000, pp. 909–912.
- [32] Wenzel, C., "Low Frequency Circulator/Isolator uses no Ferrite or Magnet," *RFDesign*, July 1991.

2

Circulator Specification

2.1 The Parameters

Engineers assigned the task of designing a ferrite circulator or isolator need to know how to specify these devices. If specifications are supplied to the designer, he or she must know whether they are reasonable—whether the device can be built. The design engineer also must know how to generate specifications for circulators in order to market his or her designs.

Although this book is aimed primarily at design engineers, others may learn how to specify isolators and circulators by reading this chapter.

Circulator specification is complicated by the large variety of devices on the market. Several different types of circulators—junction, lumped-constant, differential phase shift, field displacement, resonance, and others, available in coaxial and waveguide versions that cover many frequency bands—crowd the market.

Incorrect circulator specification can lead to inconvenience at best and disaster at worst. If a particular circulator design will not perform the desired function, it is necessary to try a different design or eliminate the circulator entirely. Most circulators [1] are used to protect high-power RF sources. In this application, a circulator failure could easily destroy the power source, possibly costing thousands of dollars and lost time. Circulator failures in national defense systems could have much more serious consequences.

The first commercial microwave circulators appeared in the early 1950s [2]. Faraday rotation circulators (see Figure 1.10 in the previous chapter) were among the first to appear. These were later replaced by resonance isolators and differential phase shift circulators, which have higher power-handling

characteristics and are simpler in construction. Field-displacement devices soon joined the ranks, as did junction circulators in the early 1960s. In 1964, Yoshihiro Konishi [3] brought the lumped-element circulator to the attention of the microwave industry.

A circulator is defined as a device with ports (coaxial connectors or waveguide flanges) arranged such that energy entering a port is coupled to an adjacent port, but not coupled to the other ports. This circulator definition is depicted in Figure 2.1. A circulator can have any number of ports, but only circulators with three or more ports involve the nonreciprocal behavior of ferrites. A one-port circulator would be analogous to a short circuit. A two-port circulator would perform the same function as a section of transmission line.

It is interesting to note that if there are reflections from the port to which a signal is coupled, these reflections are in turn coupled to the next adjacent port. Thus, a signal entering port 1 in Figure 2.1 that encounters a short circuit at port 2 will be coupled to port 3. If there is also a short circuit at port 3, the signal, having gone full circle, reappears at port 1.

An isolator is a two-port device that transfers energy from input to output with little attenuation and from output to input with high attenuation. The isolator, shown in Figure 2.2, can be derived from a three-port circulator by simply placing a matched load (reflectionless termination) on one port. Junction isolators are made in this manner. Field displacement isolators and resonance isolators are strictly two-port devices and do not have third ports.

The theory of operation of circulators has been described using a water-pipe analogy [4], but because we have already discussed theory of operation in Chapter 1, we will dispense with the water piping. The theory of operation of all circulators and isolators is as described in Chapter 1. The specific

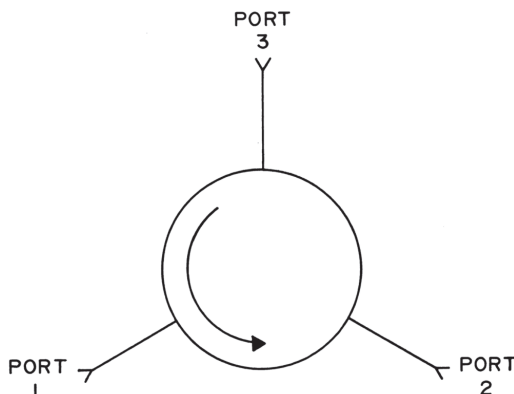


Figure 2.1 The circulator.

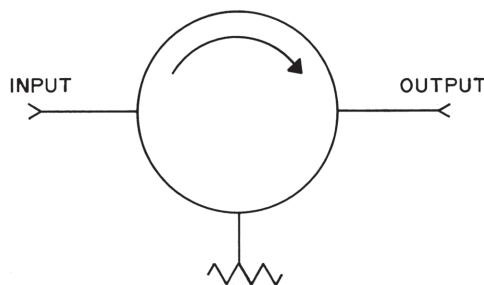


Figure 2.2 The isolator.

applications of the theory are described in the sections on the particular types of circulators and isolators that appear later in this chapter.

The important circulator (and isolator) parameters are:

1. Frequency range or center frequency and bandwidth;
2. Isolation;
3. Insertion loss and other transmission characteristics, such as insertion phase, group delay, and phase and amplitude matching or tracking;
4. Voltage standing wave ratio (VSWR) or return loss;
5. Power handling: incident power and reverse power or a maximum VSWR specification for the load that is to be connected to the device output;
6. Linearity or intermodulation distortion;
7. Temperature range (operating and storage);
8. Size and weight;
9. Shielding (electromagnetic and magnetic);
10. Other environmental factors: shock, vibration, humidity, and altitude/pressure;
11. Number of ports and configuration;
12. Type of transmission medium (coaxial line, waveguide, or microstrip);
13. Reliability;
14. Materials and finishes;
15. Method of cooling for high-power circulators;
16. Venting.

The frequency range of a circulator, usually designated by two frequencies, a lower limit and an upper limit, is defined as the range of frequencies over which all the electrical specifications apply. This frequency range is not the 3-dB bandwidth often used for other microwave components. The center frequency, f_0 , is related to the lower and upper frequency limits, f_1 and f_2 , by

$$f_0 = \frac{f_1 + f_2}{2} \quad (2.1)$$

The bandwidth is given by

$$BW = f_2 - f_1 \quad (2.2)$$

and the percentage bandwidth is defined as

$$\% BW = \frac{BW \cdot 100\%}{f_0} \quad (2.3)$$

Isolation is the ratio of a signal power applied to the output to that measured at the input, after passing through the isolator in the reverse direction. This ratio is typically expressed in decibels. The isolation of a circulator is measured with the third port (and other ports if there are more than three) terminated in a matched load. Isolation is a function of the VSWR at the third port and the VSWR of the test termination. The VSWR of the test termination, or *matched load* as it is also called, should be low enough so that it will not cause a significant measurement error. If the reflection coefficient of the test termination is an order of magnitude lower than the value of reflection coefficient that would result in the specified isolation figure, the termination will not cause a significant error in measurement.

The VSWR and reflection coefficient are related by

$$VSWR = \frac{1 + \rho}{1 - \rho} \quad (2.4)$$

The isolation of a circulator and the *return loss* (RL) at the third port have a direct correspondence. That is, if the third port has a return loss of 20 dB and it is terminated in a reflectionless termination, the isolation will be measured as 20 dB (assuming insertion loss is negligible). Return loss has a simple relationship to the reflection coefficient:

$$RL = -20 \cdot \log_{10} \rho \quad (2.5)$$

Figure 2.3 shows a simple test setup for measuring isolation, VSWR, and insertion loss of circulators and isolators. A wide range of test equipment is used by microwave component manufacturers, from antique signal generators and slotted lines to automatic vector network analyzers. We will make no comment as to which test installation is the best, only that Figure 2.3 shows a middle-of-the-road setup and the equipment details are left to the test technician.

Establishment of the required electrical performance, especially isolation, leads us to discussion about reflections and how they are affected by circulators. This discussion, along with some associated mathematical tools for analysis, appears in Section 2.2.

If more isolation is required than the amount that can be furnished by one circulator, circulators can be cascaded to achieve the desired performance. This technique is often accomplished within the same mechanical package; however, it also increases insertion loss.

Insertion loss is the ratio of output signal to input signal with the signal applied to the input, expressed in decibels. It is measured in the same manner as isolation, and the third port is terminated with a matched load for this test as well. Some specifications [5] call for insertion loss to be measured in all the forward transmission paths (ports 1–2, 2–3, and 3–1 in Figure 2.1), but this is not always necessary because we are usually concerned only with having low insertion loss in one path. Higher insertion loss in the other paths is often desirable.

It might seem obvious that circulators designed to handle high power levels will have low insertion loss to minimize the amount of power dissipated

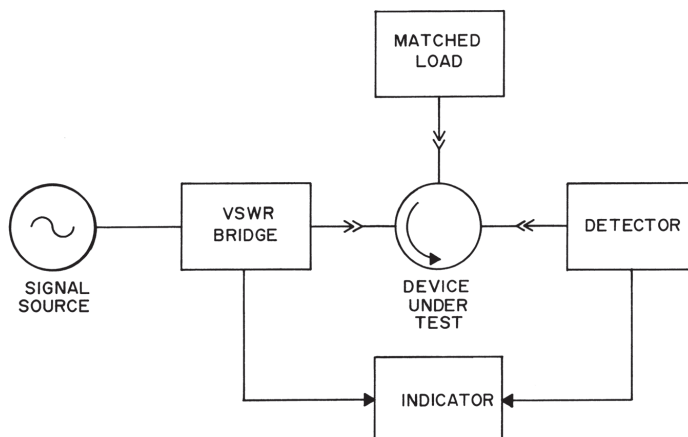


Figure 2.3 Typical circulator test setup.

in the circulator in the form of heat, but in many cases the insertion loss of high-power circulators is higher than the loss of low-power units. This paradox will be explained further when we discuss power handling.

Factors such as conductor losses of the transmission medium, dielectric losses, and magnetic losses in the ferrite set lower limits on the insertion loss specifications of practical circulators. The expected insertion losses of several different types of circulators are given later in this chapter.

In systems where there are multiple RF paths that are ultimately combined, such as in a power amplifier that has amplifier stages connected in parallel, or in a phased-array radar, insertion phase is also an important parameter. Usually the absolute insertion phase of a circulator is unimportant, but sometimes a group of circulators must match in insertion phase within specified limits. More often, if there is a capability in the system to adjust phase offset for each path/circulator, then a group of circulators need only track in phase. Circulators that track in phase may not be phase matched, but any variations in phase with temperature or frequency must match the phase variations of other circulators within specified limits. In some systems, it is desirable to have circulators that match or track in insertion loss magnitude as well.

Less common transmission characteristic specifications for circulators include group delay and deviation from linear phase (DLP). Group delay is essentially the time delay through the circulator, which is the derivative of phase with respect to frequency:

$$\tau = -\frac{d\phi}{d\omega} \quad (2.6)$$

DLP can be computed by fitting a straight line to insertion phase versus frequency data, then finding the deviation from the straight line at each frequency. DLP can also be interpreted as group-delay flatness.

Insertion phase and insertion loss performance levels of groups of circulators to be used in phased array systems are sometimes specified in statistical terms of averages and standard deviations. Antenna array performance can be determined, in part, from these statistical measures [6].

VSWR can also be measured using the setup shown in Figure 2.3. The VSWRs at all ports are usually taken. For a symmetrical circulator, the return losses at the input and output equal the isolation due to one terminated port. If several circulator junctions are cascaded to achieve higher isolation, the isolation will certainly be higher than the return losses.

By combining (2.4) and (2.5), we can derive a useful expression relating return loss and VSWR:

$$VSWR = \frac{1 + 10^{(RL/-20)}}{1 - 10^{(RL/-20)}} \quad (2.7)$$

Specifications for VSWR depend on the device bandwidth and design. Approximate figures are given in the sections on each type of circulator.

Circulator power handling depends on several parameters:

1. Power handling of coaxial connectors, waveguide, or another medium;
2. Power handling of the basic circulator;
3. Power threshold of ferrites;
4. The operating environment: altitude or space (high vacuum);
5. Load VSWR or reverse power.

Power handling limits can be exceeded in two modes: peak power and average power. Excessive peak power leads to corona and arcing due to the high voltages that can be present. Circulators destined for operation in space or other high-vacuum applications could be susceptible to multipaction, another voltage breakdown mechanism discussed in more detail in Section 5.8.3. Average power failure is typically due to overheating.

Table 2.1 lists continuous-wave (CW) power handling [7] for rectangular waveguides commonly encountered in circulator design. It is unlikely that the CW rating of any of the waveguides would be exceeded by a CW signal, but the CW ratings are useful for determining the ratings under pulsed conditions. For pulse widths much greater than 1 μ s or pulse repetition rates greater than 2 kHz, the CW power handling figures can be used for the peak power handling. With narrow pulses or low repetition rates, the peak power rating will be higher. Pulse widths on the order of 3 ns, for example, can increase the peak power handling by a factor of 8–9.

The mechanism for peak power breakdown in a waveguide is the production of free electrons and collisions of the accelerated free electrons with gas molecules, leading to the production of more free electrons. Eventually, enough electrons are present to cause arcing or breakdown. It takes time for the quantity of free electrons to build up, which is why short pulses and low repetition rates are not as troublesome as long pulses and high repetition rates.

The breakdown voltages of the waveguides can be increased if the mean free paths of the electrons can be shortened. This can be done by pressurizing the waveguide. Also, substitution of other dielectric gases for air can be helpful in preventing breakdown.

Table 2.1
Rectangular Waveguide Power Handling [7]

Waveguide Type	Frequency Range	CW Power Handling
WR 42	18.0–26.5 GHz	160 kW
WR 51	15.0–22.0	300
WR 62	12.4–18.0	440
WR 75	10.0–15.0	600
WR 90	8.2–12.4	730
WR 112	7.05–10.0	1.2 MW
WR 137	5.85–8.2	1.9
WR 159	4.9–7.05	2.7
WR 187	3.95–5.85	3.2
WR 229	3.3–4.9	5.3
WR 284	2.6–3.95	7.3
WR 340	2.2–3.3	12
WR 430	1.7–2.6	18
WR 510	1.45–2.2	25
WR 650	1.12–1.7	40
WR 770	960–1450 MHz	58
WR 1150	640–960	130
WR 1800	410–625	310
WR 2300	320–490	510

The maximum VSWR to be present at the connections to the circulator should also be considered. The voltage is increased by a factor of $1 + \rho$:

$$V \propto 1 + \rho \quad (2.8)$$

The peak power ratings of coaxial connectors can be determined [8] from the 60 Hz dielectric withstand voltage using

$$P = \frac{V_{dw}^2}{Z_0(1 + \rho)^2 \sqrt{F} A} \quad (2.9)$$

where V_{dw} is the connector dielectric withstand voltage, Z_0 is the characteristic impedance, F is the frequency in GHz, and A is an altitude derating factor. Tables 2.2 and 2.3 list dielectric withstand voltages for some common connectors and A values, respectively.

Table 2.2
Connector Dielectric Withstanding Voltage [9]

Connector Type	Dielectric Withstanding Voltage (kV)	Mating
SMA	1.0	1/4-36 thread
BNC	1.5	Bayonet
TNC	1.5	7/16-28 thread
N	2.5	5/8-24 thread
SC	3.0	11/16-24 thread
HN	5.0	3/4-20 thread
LC	10.0	1 1/4-18 thread

Table 2.3
Altitude Derating Factors [8]

Altitude (ft)	Derating Factor (A)
0	1
10,000	2
20,000	5
30,000	7
40,000	10
50,000	12
60,000	15
70,000	20
80,000	22

The average or CW power handling of coaxial connectors is usually equal to the average power capability of the associated cable. Figure 2.4 shows the average power handling versus frequency for some selected flexible cables and rigid EIA-type coaxial transmission lines.

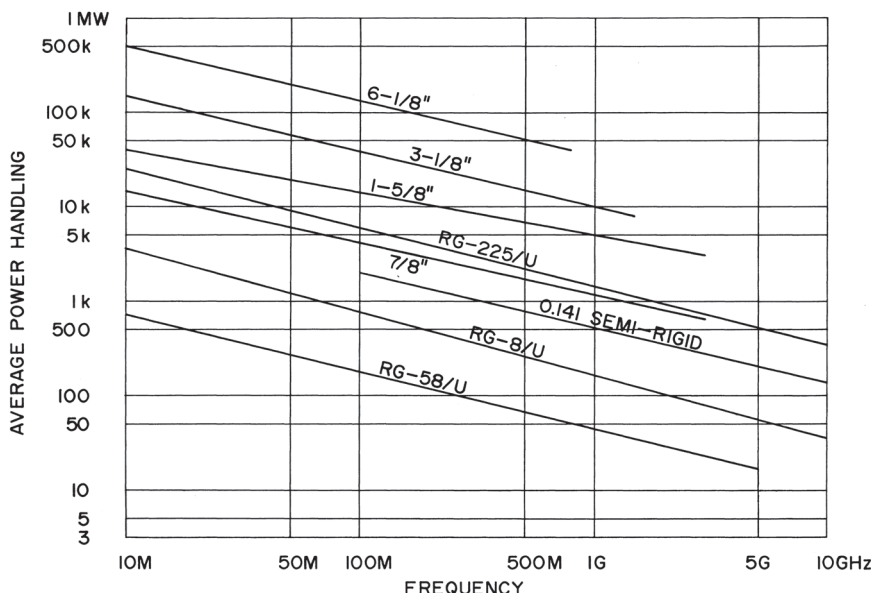


Figure 2.4 Average power handling of selected coaxial transmission lines.

The power handling of a circulator cannot exceed the capacity of the waveguides or connectors that interface with it, but in many cases the basic circulator will limit the power handling. Waveguides have higher power handling than coaxial transmission lines, but at low frequencies they become very large. The choice between waveguide and coaxial transmission line will normally be dictated to the circulator designer, but in some instances it may be advantageous to make transitions between the two media to improve power handling, electrical performance, or to make the transition part of the circulator (e.g., waveguide input and coaxial output).

An introduction to the three possible magnetic operating regions for circulators and isolators will make the following discussion of power threshold clearer. The magnetic operating regions, shown later in Figure 4.3 of Chapter 4, refer to the magnitude of the applied dc magnetic field relative to the amount of field required for ferrimagnetic resonance. Below resonance means simply that the amount of dc magnetic field is below that required for resonance, and above resonance means the field is above the resonance field magnitude. Thus, the three magnetic operating regions are below resonance, resonance, and above resonance. The resonance region is used only for resonant devices such as resonance isolators. Circulators, in general, fall into either the below- or above-resonance category.

The power threshold of the ferrites is of concern when the specifications indicate that a below-resonance design must be used. When a certain critical power level is reached, the excitation of spin waves begins as described in Chapter 1. When this happens, the insertion loss of the circulator increases, hence we have nonlinearity. This nonlinearity causes the generation of harmonics and other mixing products if two or more signals are present.

Circulators for communications systems may have either third-order intermodulation levels or third-order intercept points specified. Figure 2.5 shows the relationship of these two parameters. The third-order mixing products that are typically most troublesome are $2f_1-f_2$ and $2f_2-f_1$, where f_1 and f_2 are the fundamental signals. Fundamental signals plotted on a graph showing circulator output power as a function of input power, as in Figure 2.5, will increase linearly in 1:1 correspondence with input power. The third-order products have a 3:1 slope. As input power increases, the circulator will eventually compress or limit. If the linear fundamental line is extended, it will intersect the third-order line at the third-order intercept (TOI). TOI is not a measurable parameter, but we can calculate it if we know the power level of the third-order products corresponding to a lower input power:

$$\text{TOI} = IP_3 = \frac{IM_3}{3 - 1} + P_{\text{output}} \quad (2.10)$$

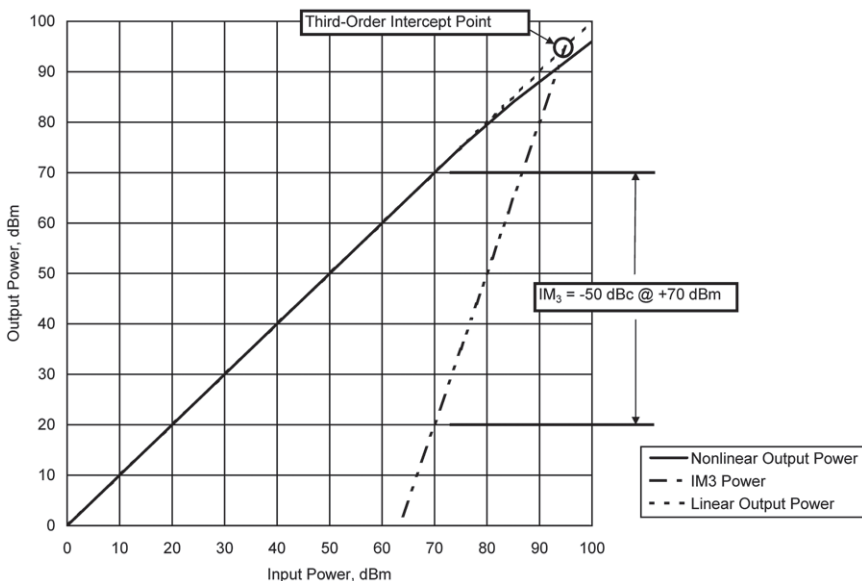


Figure 2.5 Third-order intermodulation distortion products.

where P_{output} and TOI are in dBm, and IM_3 is in dB or dBc.

A third-order intercept point of +95 dBm has been suggested [1] as attainable for circulators operating at frequencies up to about 4 GHz. There are various factors that affect the intermodulation distortion of circulators, which are discussed in Section 5.7. Above-resonance circulators may have IM_3 levels of –80 to –60 dBc at moderate power levels [10]. Below-resonance circulators are often not as linear as their above-resonance counterparts, so IM_3 levels could be 10–20 dB worse. Reasonably linear performance can be obtained [11] at power levels up to 30 kW at 2 GHz. For octave-bandwidth circulators, 2 kW at 2 GHz and 200 W at 16 GHz are typical figures.

Increased power threshold and linearity can be obtained by changing the ferrite material and geometry. Broad-bandwidth and high power threshold are contradictory terms, as are low loss and high power threshold. Ironically, at higher power levels where you would think low loss would be a necessity, we must use ferrite materials that have greater spin-wave line widths with higher magnetic losses. Broad bandwidth and high power threshold are contradictory because broad bandwidth indicates the use of the below-resonance operating region, where the excitation of spin waves at high power levels causes nonlinearity. The compromises involved in ferrite material selection are discussed further in Section 4.1.

The storage temperature range of circulators can readily be extended to cover -55° to $+125^{\circ}$ C. Some circulators are exposed to higher-temperature manufacturing processes during installation. Usually this does not cause degradation of performance if the circulator is stabilized by temperature cycling up to its maximum expected process or storage temperature, whichever is higher. The operating temperature range may not be as broad. Below-resonance circulators for low frequencies (below 1 GHz) contain ferrite materials that have low Curie temperatures and thus have narrow operating temperature ranges (e.g., 0° to $+50^{\circ}$ C). Curie temperature is the temperature above which the ferrite material has effectively no magnetic properties. At higher frequencies and for above resonance units, the temperature range can be increased to -55° to $+85^{\circ}$ C or even $+125^{\circ}$ C, depending on the required electrical performance. Circulators with tighter electrical specifications or broader bandwidths necessarily have reduced operating temperature ranges. More information pertaining to temperature effects is presented in Section 5.6.

The size and weight of circulators is usually dictated by the design type. However, certain things can be done to reduce the circulator weight, such as selecting lightweight materials. Size can sometimes be reduced by incorporating dielectrics with higher relative permittivities.

Most circulators have inherently good electromagnetic (*radio frequency interference* (RFI) and *electromagnetic interference* (EMI)) shielding. Leakage on the order of -30 dB is typical, and leakage of -80 to -100 dB is possible if attention is given to the reduction of radiation. The shielding capabilities of the circulator connectors should be considered. Some connectors have holes in the outer conductor, such as those used for epoxy captivation of the center conductor, which can leak. Some connectors rely on the quality of machining and surface finish of the mating surfaces for shielding integrity. If the mating surface of these connectors is nicked or otherwise damaged, then shielding can degrade significantly. There are different test methods for RF leakage, ranging from simple “sniff” tests to extensive MIL-STD-461 or EIA-364-66 testing, so the test method should be specified in addition to the permissible leakage level.

Almost any degree of magnetic shielding can be achieved. Because circulators contain strong permanent magnets, concern stems from the effect of the internal magnetic field on other nearby components. For spaceflight applications, it is desirable to minimize the net magnetic dipole moment of the circulator. This is because the magnetic moment of the circulator could react with Earth’s magnetic field, exerting a torque on the spacecraft. Performance of a circulator may degrade if it is brought either near or in contact with ferrous materials. Magnetic shielding may be specified as a minimum

distance the circulator must be kept from ferrous material, as a maximum flux density at a given distance from the circulator, or as the maximum magnetic dipole moment.

Various other environmental factors can be specified for circulators such as vibration, shock, and humidity. The specifications depend on the environment in which the circulator is intended to be used. Military Specification MIL-DTL-28791C [5] states that circulators are to be tested for shock, vibration, and moisture resistance per MIL-STD-202 methods 213, 204, and 106, respectively. For circulators that operate in Earth's atmosphere, the altitude is an important specification, because it can impact power handling. Circulators destined for space flight usually will be required to operate in high vacuum. Rockets, missiles, and other projectiles can experience a wide range of pressures and rapid changes in pressure.

We can configure circulators and isolators with any number of ports, and package them in a wide variety of orientations and combinations. To specify the number of ports, configuration, and packaging for a device, we need to consider the particular application.

The reliability of circulators and isolators is quite high—a circulator operating in a benign environment could have a *mean time between failures* (MTBF) of 10^7 hours. Table 2.4 lists MTBF figures for circulators operating in various environments, calculated from data given in MIL-HDBK-217F [12]. The figures in Table 2.4 apply for circulators used at power levels less than or equal to 100W. For higher-power units, the MTBF values should be halved. Use of parts-count reliability estimates for circulators is ill advised.

For critical applications, materials and finishes of circulators may be specified. For space applications, all materials used in circulators should have low outgassing properties: total mass loss (TML) less than 1% and collected volatile condensable materials (CVCM) less than 0.1% when tested per ASTM E595. MIL-DTL-28791C [5] contains specific requirements for circulator (and isolator) materials and finishes.

For circulators that must handle significant RF power, the method of cooling should be specified. Typical cooling methods include radiation, conduction, natural convection, forced air, and liquid cooling. The chosen method(s) will depend on the heat energy that must be dissipated, the size of the circulator, its environment, the ability of the surface to which it will be mounted to absorb heat, and the availability of forced air or liquid coolant.

Venting is sometimes required for circulators that are subjected to rapid ambient pressure changes, such as are experienced during rocket or missile ascent or descent. Circulators that operate in a spaceflight environment may require vent holes to ensure that air is removed from the device to prevent

Table 2.4
Circulator Reliability [12]

Environment	Mean Time Between Failures (Hours)
Ground, benign, including missile silo	10,000,000
Fixed	5,000,000
Mobile, including manpack	1,250,000
Naval, sheltered, including submarine	2,000,000
Unsheltered, including undersea and hydrofoil	833,300
Airborne, cargo, inhabited, including trainer and bomber	2,000,000
Fighter, inhabited, including attack	1,250,000
Cargo, uninhabited, including trainer and bomber	1,428,600
Fighter, uninhabited, including attack	909,100
Rotary-winged (helicopter)	588,200
Space flight	20,000,000
Missile flight, including free flight and air-breathing	1,111,100
Missile launch, including undersea launch	416,700
Cannon launch	22,200

partial-pressure voltage breakdown. More information regarding venting is presented in Chapter 7.

ESA/SCC Generic Specification 3202 [13] covers general requirements for circulators and isolators destined for space applications.

2.2 Reflections and Segmentation

The determination of the required amount of isolation depends on the particular application of the device. Here, we will first discuss the isolation needed for a circulator used to protect an RF power source from a potential high-VSWR condition. Then we will present some mathematical constructs that we may use to analyze the performance of a circulator in its associated system. We use these analyses to help establish circulator electrical specifications.

The pertinent data to determine the required isolation are maximum VSWR to be presented by the load to the circulator output; the circulator VSWR; and the maximum VSWR that can safely be presented to the RF source. We start by converting the VSWR figures to voltage reflection coefficients, because we can easily add two signals together when we work with these coefficients. We use the conversion:

$$\rho = \frac{VSWR - 1}{VSWR + 1} \quad (2.11)$$

We represent the load reflection coefficient by ρ_L , the circulator reflection coefficient by ρ_C , and the source coefficient (of the signal reflected from the circulator, and the load beyond, back to the source) by ρ_S . First, the reflected signal from the load adds to the signal reflected at the circulator output port. The worst case is when the two signals are in-phase and the voltage reflection coefficients add directly. Next, this new signal traveling through the circulator toward the source is attenuated by the isolation of the circulator, denoted by I . Finally, the signal interacts with the signal reflected from the circulator input port. We again use the worst-case in-phase scenario. This final signal must be below ρ_S , which relates to the maximum VSWR that can safely be presented to the source. The various signals in this analysis are shown in Figure 2.6.

The equation for this analysis is

$$\rho_S > (\rho_L + \rho_C) 10^{(I/-20)} + \rho_C \quad (2.12)$$

Solving for I , the required isolation, we derive

$$I = -20 \cdot \log_{10} \left(\frac{\rho_S - \rho_C}{\rho_L + \rho_C} \right) \quad (2.13)$$

Figure 2.7 is a plot of the required isolation for various values of circulator VSWR versus the maximum allowable VSWR presented to the source.

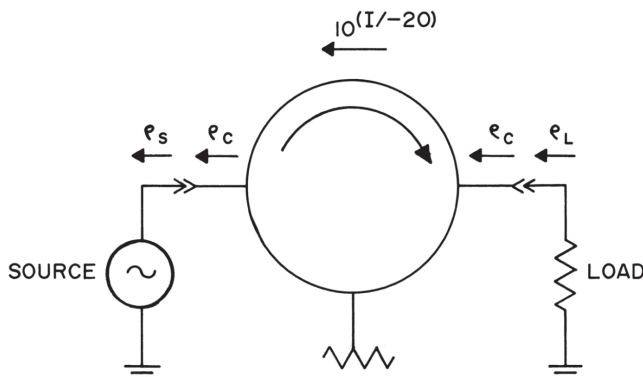


Figure 2.6 Circulator analysis to determine required isolation.

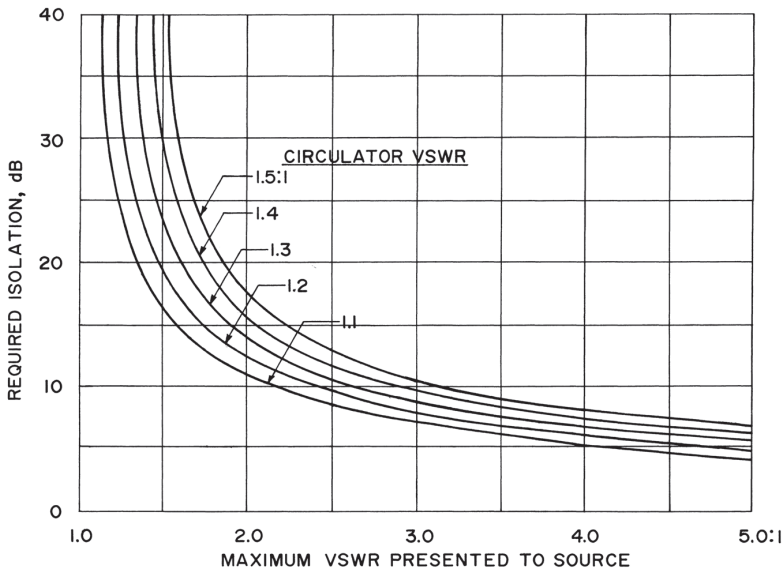


Figure 2.7 Required isolation to achieve a given source VSWR with an infinite VSWR presented to circulator output.

Insertion loss has been neglected in (2.12) and (2.13), as it can be in most practical situations where we are considering the effect of reflections.

Insofar as the voltage reflection coefficient can never exceed unity, if the load reflection coefficient is 1, the denominator in (2.13) becomes 1.

The preceding scheme of adding voltage reflection coefficients is approximate, but provides reasonably accurate results and is simple and easy to understand. Equation (2.12) tends to overstate the result, which provides for conservative design. An alternative scheme [14], which is based on VSWR products, sometimes provides more accurate results and is preferred by some:

$$VSWR_S = \frac{1 + 10^{\left[\frac{\log_{10}(VSWR_L \cdot VSWR_C - 1) - I}{20} \right]}}{1 - 10^{\left[\frac{\log_{10}(VSWR_L \cdot VSWR_C - 1) - I}{20} \right]}} VSWR_C \quad (2.14)$$

In this equation, $VSWR_L$, $VSWR_C$, and $VSWR_S$ represent the load VSWR, circulator VSWR, and the maximum VSWR presented to the source, respectively. Circulator insertion loss is neglected here as it was in (2.12) and (2.13). With a little rearrangement, we find that

$$I = -20 \cdot \log_{10} \left[\frac{(VSWR_L \cdot VSWR_C + 1) \left(\frac{VSWR_S}{VSWR_C} - 1 \right)}{(VSWR_L \cdot VSWR_C - 1) \left(\frac{VSWR_S}{VSWR_C} + 1 \right)} \right] \quad (2.15)$$

In the preceding discussion, we have presented equations and a graph (Figure 2.7) that are useful for determining the maximum (worst-case) VSWR presented by a circulator to its RF source. The determination is made with a load having known VSWR virtually connected to the circulator output. This sort of analysis is known as *segmentation* [15]. In the analysis, the circulator and the load are discrete segments, which are mathematically combined.

If we have available to us the S-parameters for a circulator or isolator, and the S-parameters for the load to be connected to it, then we can perform more rigorous segmentation analysis [16]:

$$\mathbf{S}_{11}' = \mathbf{S}_{11} + \frac{\mathbf{S}_{12}\mathbf{S}_{21}\Gamma_L}{1 - \mathbf{S}_{22}\Gamma_L} \quad (2.16)$$

where \mathbf{S}_{11} , \mathbf{S}_{12} , \mathbf{S}_{21} , and \mathbf{S}_{22} are the complex S-parameters for the circulator or isolator, Γ_L is the complex load reflection coefficient, and \mathbf{S}_{11}' is the complex circulator or isolator input reflection coefficient with the load segment included. Solving for the required isolation, we have, using scalar values,

$$I = -20 \cdot \log_{10} (\mathbf{S}_{12}) = -20 \cdot \log_{10} \left[\frac{(\mathbf{S}_{11}' - \mathbf{S}_{11})(1 - \mathbf{S}_{22}\Gamma_L)}{\mathbf{S}_{21}\Gamma_L} \right] \quad (2.17)$$

Using S-parameter segmentation, we can readily cascade a circulator or isolator (S) with another device (T) [17]:

$$\mathbf{S}_{11}' = \mathbf{S}_{11} + \frac{\mathbf{S}_{12}\mathbf{S}_{21}\mathbf{T}_{11}}{1 - \mathbf{S}_{22}\mathbf{T}_{11}} \quad (2.18)$$

$$\mathbf{S}_{12}' = \frac{\mathbf{S}_{12}\mathbf{T}_{12}}{1 - \mathbf{S}_{22}\mathbf{T}_{11}} \quad (2.19)$$

$$\mathbf{S}_{21}' = \frac{\mathbf{S}_{21}\mathbf{T}_{21}}{1 - \mathbf{S}_{22}\mathbf{T}_{11}} \quad (2.20)$$

$$\mathbf{S}_{22}' = \mathbf{T}_{22} + \frac{\mathbf{S}_{22}\mathbf{T}_{12}\mathbf{T}_{21}}{1 - \mathbf{S}_{22}\mathbf{T}_{11}} \quad (2.21)$$

In (2.18–2.21), \mathbf{S}_{11}' , \mathbf{S}_{12}' , \mathbf{S}_{21}' , and \mathbf{S}_{22}' are the S-parameters of the two cascaded segments together.

When a short circuit or other reflective device is connected to one port of a circulator as shown in Figure 3.17, we are interested in the insertion loss of the path from input to output. It seems that the loss would be about twice the single-path value, but the insertion loss can deviate considerably from this value. It has been suggested [18] that the “loss varies between one and three times the single path loss.” With knowledge of the circulator S-parameters and the reflection coefficient of the device connected to port 3 of the circulator, we compute the insertion loss using

$$\mathbf{S}_{12}' = \mathbf{S}_{12} + \frac{\mathbf{S}_{13}\mathbf{S}_{32}\Gamma_3}{1 - \mathbf{S}_{33}\Gamma_3} \quad (2.22)$$

2.3 Junction Circulators

The most common circulators are the junction type, available in stripline, microstrip, and waveguide varieties. Stripline circulators are available in both coaxial (connectorized) and drop-in (tabbed) varieties. Some typical junction circulators are shown in Figures 2.8–2.12.

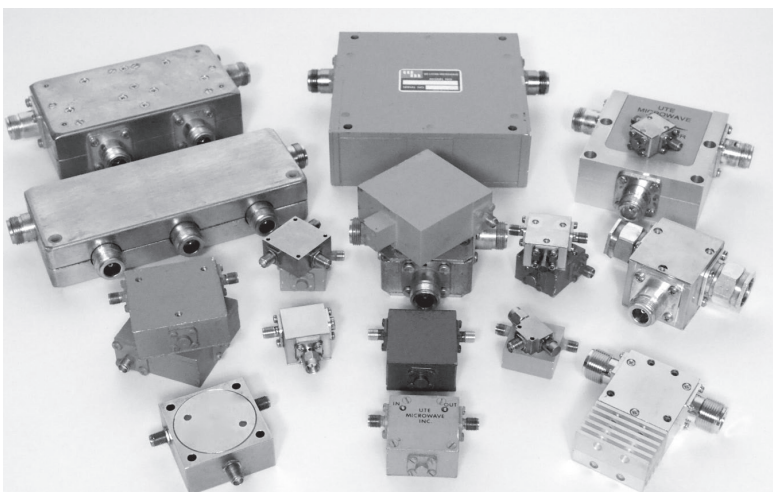


Figure 2.8 Coaxial stripline junction circulators and isolators.

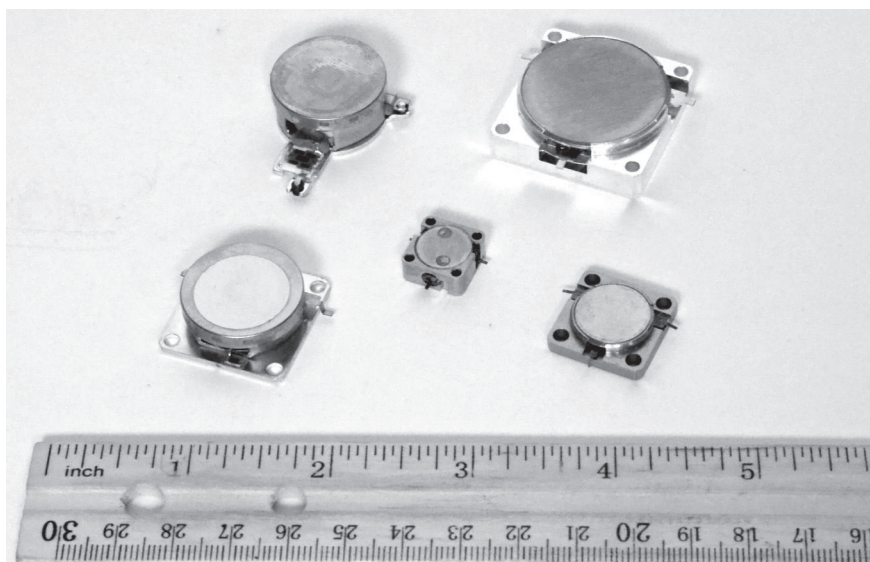


Figure 2.9 Drop-in stripline junction circulators and isolators.

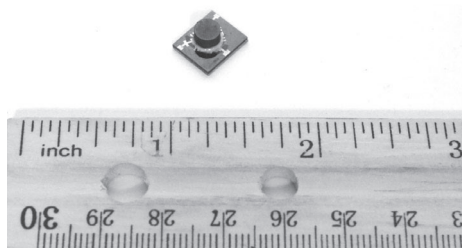


Figure 2.10 Microstrip junction circulator.

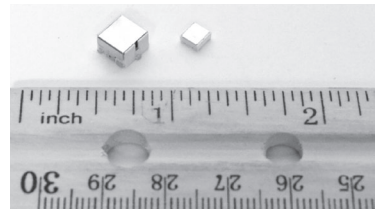


Figure 2.11 Surface-mount isolators.

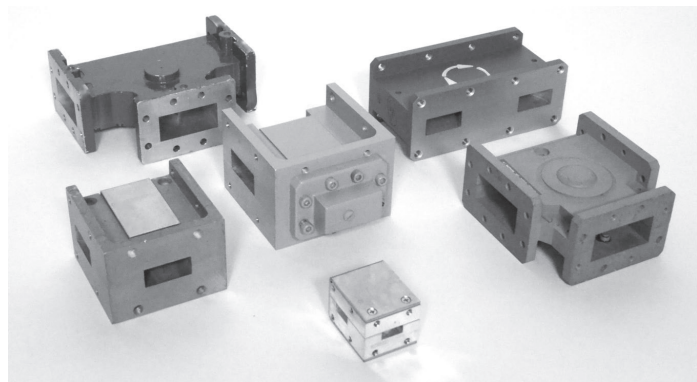


Figure 2.12 Waveguide junction circulators and isolator.

2.3.1 Single-Ferrite (Non-Composite) Junction Circulators

Coaxial (stripline) circulators are constructed as shown in Figure 2.13. The center conductor is sandwiched between two ferrite disks or triangles. Both ferrite disks or triangles in this structure are of the same material, in contrast with the ferrites in composite-ferrite junction circulators, which are discussed in Section 2.3.2. These ferrites are then placed between ground planes and magnetically biased by permanent magnets outside the ground planes. Microstrip circulators are similar, but the conductor is usually a metalization applied to the single ferrite disk or rectangle. The connections to the external circuitry are made with tabs, metal ribbons, or wire bonds. The ground plane is simply metalization on the ferrite, often with a metal disk or rectangle as well, and a magnet is soldered or glued to the ground plane. Alternatively, the magnet may be attached to a dielectric disk between it and the circuit pattern. Screw clamps, soldering, or epoxy hold the circulators in place.

Waveguide junction circulators consist of sections of waveguides that form an *H*-plane junction. The ferrite disks or triangles are located against the walls of the waveguides in the *H* plane. The biasing magnets are positioned outside the waveguide. Waveguide junction circulators are also less commonly implemented in the form of *E*-plane junctions.

More information about junction circulators is presented in Section 5.1.

Most common rectangular waveguide bands can be covered by waveguide junction circulators. Typically, insertion loss is 0.2 dB or less and VSWR

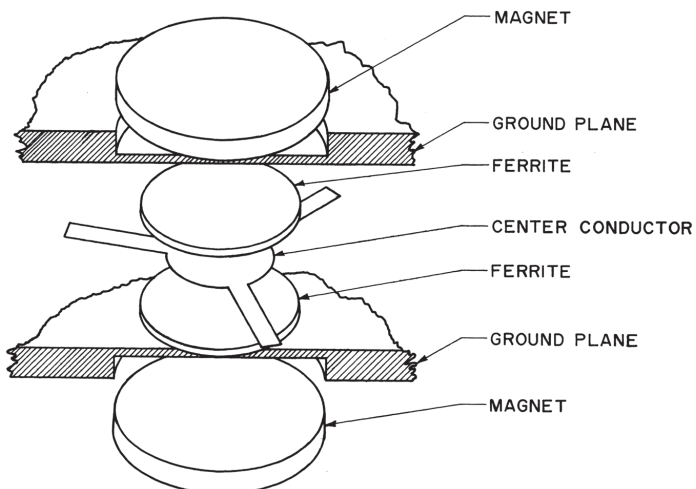


Figure 2.13 Stripline circulator construction.

is on the order of 1.2:1. Octave bandwidths can be accommodated by double-ridged waveguide junction circulators with somewhat reduced performance.

Coaxial and microstrip circulators operate in one of two magnetic bias regions: above resonance or below resonance. The majority of waveguide units operate below resonance. Above resonance coax junctions can cover bandwidths up to about 40% with less than 0.5 dB insertion loss and 1.3:1 VSWR. Improved performance can be obtained over more narrow bandwidths, but for identical frequency ranges, waveguide junctions will have lower loss.

Below resonance, bandwidths of more than 75% can be achieved. Octave-bandwidth units are fairly easy to construct, and may have less than 0.4 dB loss and 1.2:1 VSWR. The below-resonance designs are only used for frequencies above about 500 MHz because the required ferrite saturation magnetization becomes vanishingly small below this frequency. Devices for frequencies below 1 GHz suffer lesser performance than higher-frequency units because of the ferrite material limitations. The performance of both above- and below-resonance circulators will be discussed in more detail in Chapter 5.

Above-resonance circulators have almost no lower frequency limit but practical considerations of cost and size set a lower limit in the neighborhood of 100 MHz. At higher frequencies, above-resonance operation demands very high magnetic fields. The practical upper frequency limit for above-resonance circulators is between 2.5 and 3.0 GHz.

The peak power handling capability of above-resonance circulators is limited by such factors as the ground-plane spacing and connector capacity for coaxial devices and by the waveguide power capacity for waveguide devices. As presented in Section 5.8, there are many design aspects that should be considered to maximize the power handling of a circulator. Increasing the ground-plane spacing of a coaxial unit will not only increase the power handling, but could change the junction impedance to a less than optimum value for broad-bandwidth performance. For this reason, coaxial circulators with very high peak power ratings must have narrow bandwidths.

The upper limit of peak power handling for below-resonance circulators is set by the onset of spin-wave propagation and the resulting increase in insertion loss.

Average power-handling capacity of above-resonance circulators is usually higher than that of below-resonance circulators of the same frequency range because the ferrites used have higher Curie temperatures. In addition, high average powers can aggravate the nonlinear behavior of below-resonance units.

Cooling is a very important consideration for circulators that will handle high average powers. Power lost in the circulator junction due to insertion

loss must be dissipated in the form of heat. If the circulator in question must pass the RF power in two paths, as it would if there were a short circuit at the circulator output, the amount of dissipation will double. The type of cooling to be employed depends on the amount of heat that must be removed from the ferrite junction. Insofar as the power density in the ferrites must be held to a maximum value, the size of the ferrites will also have some influence on the type of cooling to be used. Cooling methods commonly used, in order of increasing efficiency, are radiation, conduction, natural convection, forced air, and liquid cooling. Of course, the surface area of the device, including any heat sink structures, will affect the efficiency of radiation cooling and cooling methods that involve heat transfer to surrounding air.

Junction circulators are the smallest and lightest next to lumped-constant circulators. Above-resonance devices are smaller than below-resonance units for a given frequency range. The sizing of ferrite junctions will be discussed in more detail in Chapter 5.

2.3.2 Composite-Ferrite Junction Circulators

Circulators that utilize more than one type of ferrite material in their construction were developed to increase bandwidth. These circulators are typically constructed as shown in Figure 5.39 and designed as described in Section 5.1.12.

These circulators typically operate below resonance and can cover bandwidths of 100% (3:1 bandwidth) or more. At 100% bandwidth, insertion loss may be less than 1.0 dB and VSWR better than 2:1.

2.4 Lumped-Constant Circulators

The smallest circulators for the VHF and UHF bands are of the lumped-constant (also called lumped-element) design. The construction of this type of circulator is illustrated in Figure 2.14, and some examples are shown in Figure 2.15. The lumped-element circulator consists of a ferrite disk with three coils wound on it so that the RF magnetic fields are oriented at 120° with respect to each other. The ferrite disk and center conductor (coil) are shown in Figure 2.14. More details regarding the construction of lumped-element circulators are presented in Chapter 5. Most lumped-constant circulators are for use with coaxial transmission lines.

Lumped-constant circulators are most often used for frequencies below 1 GHz. Above this frequency, junction circulators are not much larger and offer lower insertion loss and simpler construction. There is practically no lower

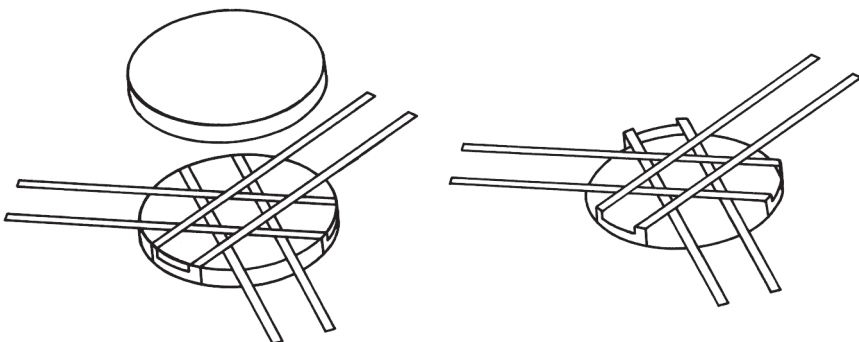


Figure 2.14 Lumped-element circulator construction. Center conductor with ferrites (left) and without ferrites (right).

frequency limit for the operation of lumped-constant circulators; devices have been built for use at frequencies below 10 MHz.

We can readily accommodate bandwidths of 15% to 20% at 0.6 dB insertion loss and 1.2:1 VSWR points. With proper impedance-matching circuit design, bandwidths of about 50% can be realized while maintaining 1.2:1 VSWR.

The power handling of lumped-constant circulators is not as high as that for junction circulators. The ferrites used are smaller and the losses are higher, so the power dissipation in the ferrites is higher. In the VHF range, 1 kW of average power can be handled with forced-air cooling. The peak power capability of lumped units is low because of the necessarily small spacing between portions of the center conductor mesh connected to adjacent ports.

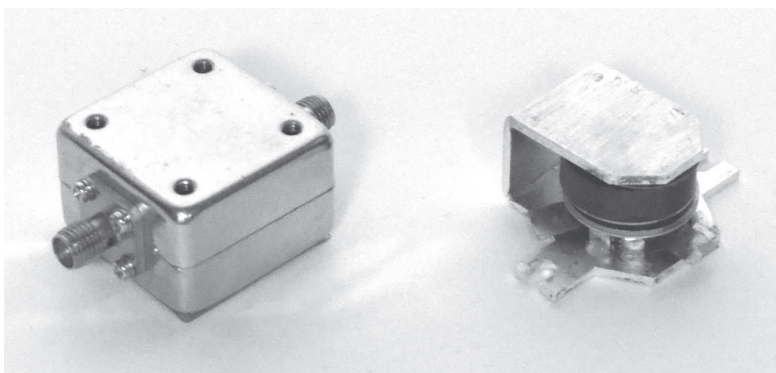


Figure 2.15 Lumped-constant circulators.

Because lumped-constant circulators usually operate in the above-resonance region, there is little concern about harmonic generation or intermodulation products unless the power level is high.

To generate harmonics or intermodulation products, we must have a nonlinear component of some type. If there is no nonlinear component, there is no harmonic generation. Below-resonance circulators can become nonlinear if they are operated at a power level sufficient to cause spin-wave excitation. The spin waves cause increased insertion loss at high powers as described in Chapter 1. Above-resonance circulators, on the other hand, are not subject to increases in insertion loss due to spin-wave excitation. Above-resonance circulators behave as linear components.

It is interesting to note two items. First, any component can be shown to be nonlinear if a sufficiently high power level is applied to it. There are, of course, large differences in the amount of nonlinearity exhibited by “linear” and “nonlinear” components. Second, ferrite devices are manufactured that capitalize on nonlinear properties of ferrites, such as limiters and frequency multipliers.

The operating temperature range is influenced not only by the ferrite material used but also by the lumped components (capacitors and inductors) used in the matching circuits between the ferrite and the ports. Careful capacitor selection can compensate for variations in the matching circuits and can also help reduce the effects of changes in the ferrite properties with temperature.

Lumped-constant circulators are generally not well suited for applications where they will be exposed to high levels of mechanical shock or vibration due to the instability of the lumped-element matching circuits.

2.5 Differential Phase Shift Circulators

The differential phase shift, or transverse-field, circulator has the advantage of very high power handling capacity, even at high frequencies. These circulators are manufactured only in waveguide configurations. A typical unit is shown in Figure 2.16.

We will explain the operation of the differential phase shift circulator with the aid of Figure 2.17. Two sections of waveguide (EG and FH) connect two hybrid junctions. The junctions are magic tees or quadrature directional couplers. The two sections of waveguide are loaded with ferrite, and the ferrites are biased by an external dc magnetic field. The ferrites are located such that a signal traversing the waveguide in one direction undergoes a phase

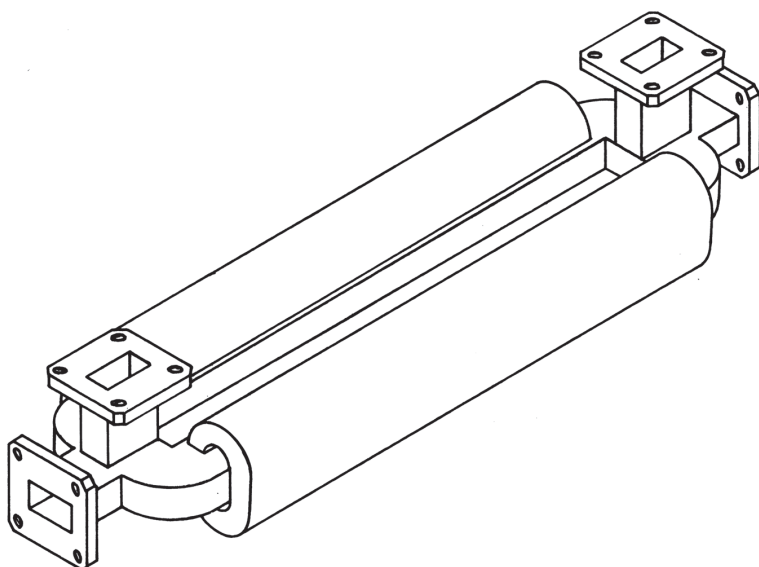


Figure 2.16 A typical differential phase shift circulator.

shift different from a signal traveling in the opposite direction. The name differential phase shift comes from this different phase shift behavior of the waveguide sections.

A signal entering the circulator at port A is split by the hybrid and presented to the two waveguide sections at E and F. The two signals are phase shifted and arrive at G and H. Because of the phase relationship of the two signals, a summation occurs at one port of the output hybrid, D for example. At port C, the signals cancel each other, so no power is delivered to this port. A signal entering port D is split and phase shifted different amounts than is the signal that originated at port A. The sum port for a signal entering port

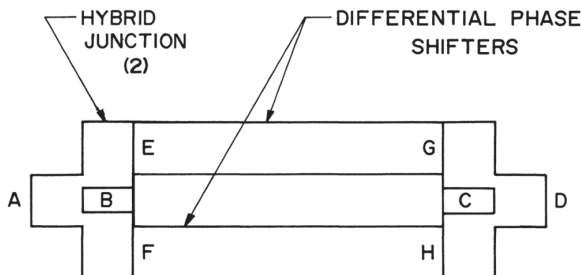


Figure 2.17 The operation of the differential phase shift circulator.

D is port B. In a similar manner, a signal incident on port B is coupled to C, and port C is coupled to A.

More information about differential phase shift circulators is presented in Section 5.3.

Differential phase shift circulators can be built to cover the common waveguide bands, and octave-bandwidth performance has been achieved with double-ridged waveguide units. For rectangular waveguide, the bandwidth is often somewhat narrower than the waveguide bandwidth, as performance over the broader band is not good.

Most differential phase shift circulators have insertion loss between 0.5 and 1.0 dB. Many have lower loss, but usually the loss is slightly higher than that of a junction circulator.

Despite the higher loss, differential phase shift circulators can handle very high power levels because the power can be spread out over a large area of ferrite. The peak power capability is nearly as high as the capacity of the waveguide itself. If a differential phase shift circulator does not have sufficient power handling capability for an application, do not use a circulator.

The disadvantages of the differential phase shift circulator are its relatively large size and correspondingly heavy weight, and the effort that must be expended to construct it. These circulators are more complicated than junction circulators, and as such are more difficult to assemble and adjust.

2.6 Switching Circulators

The direction of circulation of a switching circulator can be controlled electronically. The switching function can be performed using either a latching approach or a nonlatching one. In a latching circulator, a current pulse through a wire passing through the ferrite is used to set the ferrite in its retentive state, in one polarity or the other, depending on the desired direction of circulation. In a nonlatching circulator, continuous current must be applied to maintain circulator performance. Often a nonlatching circulator incorporates external coils to provide the magnetic bias [19].

In addition to the specifications that apply to other types of circulators, switching circulators will have a switching speed requirement. The design of the driver for a switching circulator, particularly one that has fast switching, is an integral part of the circulator design. Sometimes the driver circuitry is integrated with the circulator. A switching circulator and its driver will have dc power requirements.

2.7 Okada Circulators

Okada circulators were developed to increase the average power capability of waveguide junction circulators. The topology of the Okada circulator is shown in Figures 5.37 and 5.38. The concept is to spread the RF power over some number of cells, each containing ferrites, so that the power density in each ferrite is lower than it would be in a simple waveguide junction circulator. The Okada structure facilitates cooling of the ferrites through the use of septums, also known as struts, or pipes for liquid coolant.

The electrical performance of an Okada circulator can be similar to that of a conventional waveguide junction circulator. If the power level is very high, bandwidth may be traded off to improve cooling of the ferrites.

2.8 Field-Displacement Isolators

Field-displacement isolators and resonance isolators are actually not circulators at all, but they are closely related devices, so we include some information about them.

Very wide bandwidths can be accommodated with coaxial (stripline) field-displacement isolators, also referred to as *peripheral-mode* isolators: two octaves and wider. Waveguide units do not, of course, have this bandwidth. This design cannot be used to build circulators because the RF energy incident on the output port is dissipated in an internal resistive element.

The construction of a waveguide field-displacement isolator is shown in Figure 2.18, and Figure 2.19 illustrates a microstrip unit. Examples of coaxial field-displacement isolators are shown in Figure 2.20.

The ferrite material in a field-displacement isolator is positioned so that the concentrations of energy near the ferrite for signals traveling in forward and reverse directions are very different. In a waveguide device, this position is near a wall. Coaxial devices are implemented using a wide, asymmetrical strip transmission line in contact with ferrite. The energy concentrations are different on opposite sides of the line.

Both coaxial and waveguide field-displacement isolators may utilize resistance cards, one example of which is a Mylar film metalized with a resistive coating. The film in a waveguide isolator is placed near the ferrite so that it absorbs the energy concentrated in the area. The RF energy incident on the isolator output is absorbed in the resistance card. Energy entering the input does not become concentrated near the resistive material and is transmitted

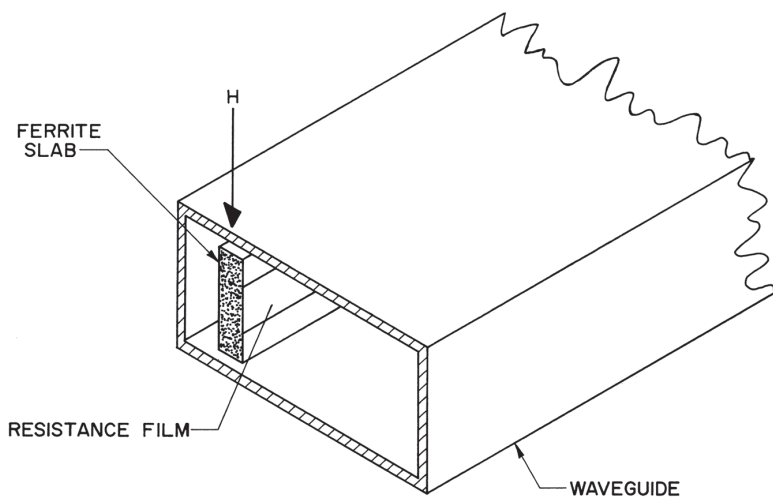


Figure 2.18 Waveguide field-displacement isolator.

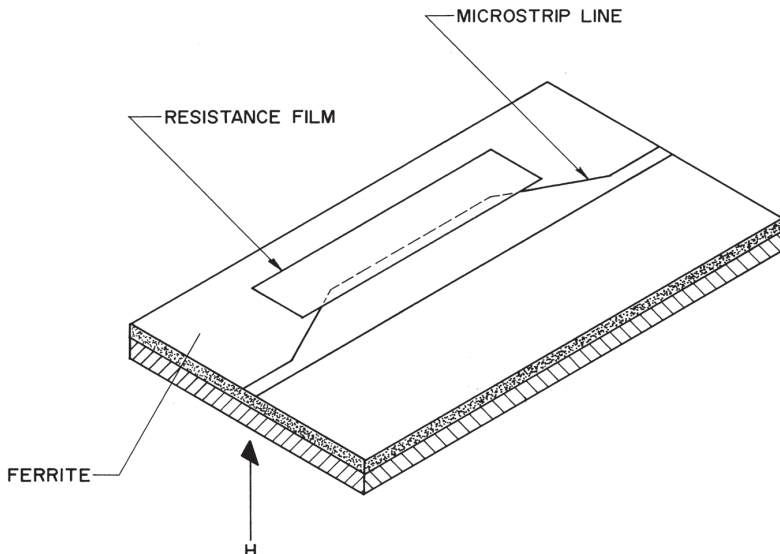


Figure 2.19 Microstrip field-displacement isolator.

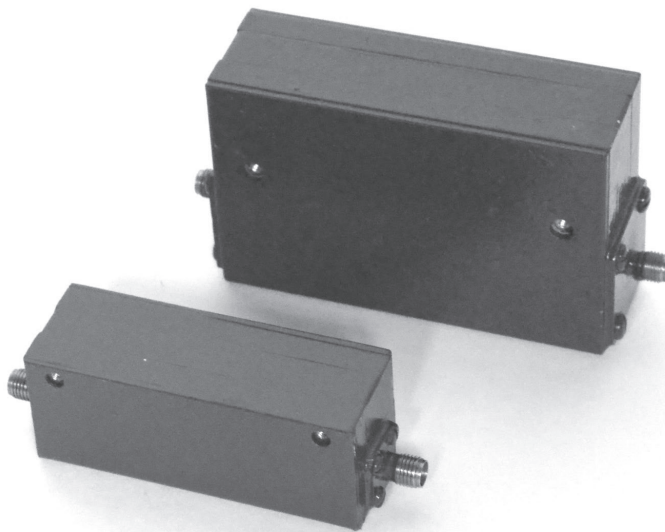


Figure 2.20 Field-displacement (peripheral-mode) isolators.

with low attenuation to the output. For reverse power absorption in a coaxial isolator, the resistance card is placed over one edge of the strip transmission line. In some isolators, slabs of absorber material are used rather than a resistance card. The energy is concentrated at this edge for reverse-directed signals, and elsewhere for signals traveling in the forward direction.

Most practical field-displacement isolators covering broad bandwidths have insertion losses near 1.0 dB, or more than 1.0 dB for devices covering two octaves or more. It is possible to reduce the insertion loss to 0.2 dB or less if the bandwidth is narrow. It is difficult to obtain low insertion loss, because the RF energy cannot be kept out of the resistive material entirely over a broad range of frequencies.

The power handling of field-displacement isolators is limited because all the reverse power must be dissipated in the resistive film or absorber slabs. Isolators with average power ratings of several hundred watts have been marketed.

Insofar as a wavelength-related variation of electrical energy is the basis of operation of field-displacement isolators, the operating frequencies are in the microwave range only. Units for lower frequencies would be prohibitively large.

2.9 Resonance Isolators

Another type of two-port ferrite device is the resonance isolator. Like the field-displacement isolator, this isolator does not have an accessible third port. The advantages of the resonance isolator are simplicity and a long, thin shape that can sometimes be fit into a tight place more easily.

Typical coaxial and waveguide resonance isolators are shown in Figures 2.21 and 2.22, respectively. The construction of a waveguide unit, shown in Figure 2.23, is very similar to its coaxial counterpart. There are several variations on the positioning and orientation of the ferrite, which will be discussed in more detail later.

The ferrite slabs in the waveguide are biased by a dc magnetic field supplied by an external magnet. The magnitude of the field is such that the ferrites are at ferrimagnetic resonance. The ferrites are positioned such that the electromagnetic field coupled into them is circularly polarized, and resonance absorption takes place for one direction of circular rotation as described in Chapter 1. A signal entering the isolator input propagates through the waveguide with little attenuation to the output. RF power traveling in the reverse direction suffers resonance absorption in the ferrites, so it does not appear at the input.

The reason for the difference in attenuations of the forward and reverse signals lies in the sense of circular polarization of the two waves in the ferrite. Forward waves traveling through the waveguide excite circularly polarized waves in the ferrite, while reverse waves excite circularly polarized waves with the opposite sense of polarization (the electric vectors of the two waves rotate in opposite directions). The rotation of the reverse circularly polarized mode

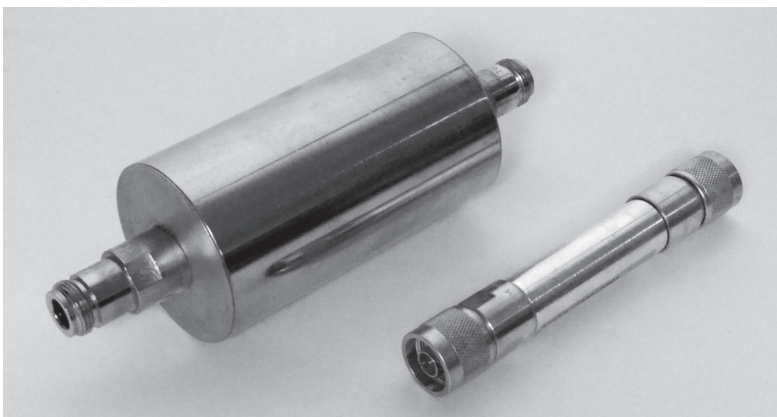


Figure 2.21 Coaxial resonance isolators.

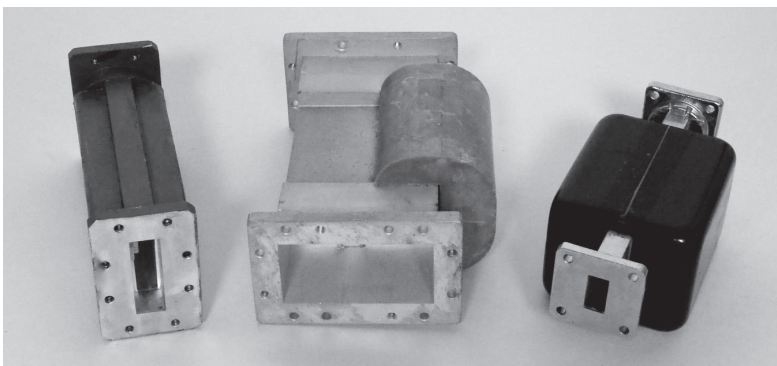


Figure 2.22 Waveguide resonance isolators.

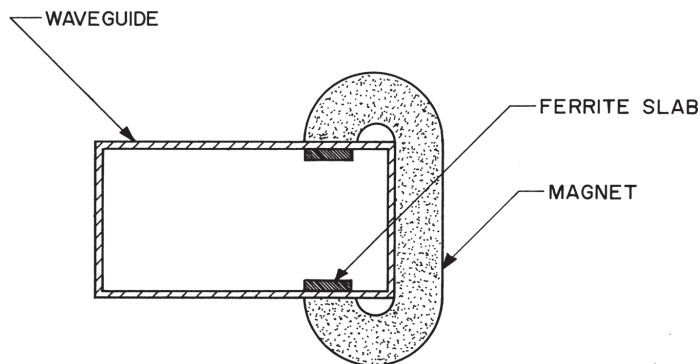


Figure 2.23 Waveguide resonance isolator construction.

coincides with the direction of electron precession, so the electromagnetic energy in the reverse wave is coupled into the precession. We say the reverse wave undergoes resonance absorption. Because the electrons can only precess in one direction for a particular polarity of applied dc magnetic field, and the rotation of the forward circularly polarized mode does not coincide with the direction of electron precession, the forward wave does not exhibit resonance absorption. More information regarding resonance isolators and how circular polarization is achieved is presented in Section 5.4.

Figure 2.24 is a cross-sectional view of a coaxial resonance isolator. The operation is the same as that of the waveguide isolator.

Coaxial resonance isolators can be built to cover bandwidths of two octaves, with approximately 1.0 dB loss and 10 dB isolation. We can obtain

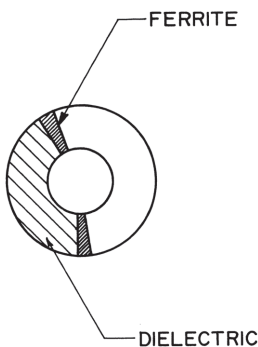


Figure 2.24 Coaxial resonance isolator construction.

improved performance over narrower bands, and waveguide devices fall into this category.

The power-handling capacity of the coaxial variety of resonance isolator is on the order of several hundred watts of average power and 20–30 kW peak power, provided that the reverse power is much lower. The ferrites in the waveguide isolator are easier to keep cool because the broad sides of the slabs are in contact with the waveguide walls. Therefore, the waveguide units have higher power capacities of tens of kilowatts average power.

References

- [1] Collado R. O., and J. McCrea, “Learn to Specify High-Power Ferrite Circulators,” *Microwaves & RF*, November 1987, pp. 107–114, and December 1987, pp. 91–97.
- [2] Soohoo, R. F., *Microwave Magnetics*, New York: Harper and Row, 1985.
- [3] Konishi, Y., “Lumped Element Y Circulator,” *IEEE Transactions on Microwave Theory and Techniques*, November 1965, pp. 852–864.
- [4] *Microwave Ferrimagnetic Circulator and Isolator Catalog*, Kensington, MD: Cirqtel, 1987.
- [5] Military Specification MIL-DTL-28791C, U.S. Department of Defense, March 2011.
- [6] Wang, H. S. C., “Performance of Phased-Array Antennas with Mechanical Errors,” *IEEE Transactions on Aerospace and Electronic Systems*, April 1992, pp. 535–545.
- [7] *Military Handbook MIL-HDBK-216*, U.S. Department of Defense, April 1967.
- [8] Gartzke, D. O., “Determination of RF Peak and Average Power for Coaxial Connectors,” Port Salerno, FL: Solitron/Microwave, 1982.

- [9] *General Connector Catalog*, Oak Brook, IL: Amphenol, 1983.
- [10] *Circulator and Isolator Primer*, San Jose, CA: Raditek International, 2004.
- [11] Sekhon, W. S., R. G. Sanders, and C. Nugent, "Understanding Coaxial Circulators and Isolators," *Microwave Systems News*, June 1979.
- [12] *Military Handbook MIL-HDBK-217F*, U.S. Department of Defense, December 1991.
- [13] ESA/SCC Generic Specification 3202, April 1999.
- [14] *Catalog M31*, Tampa: TRAK Microwave Corp., 1991.
- [15] Gupta, K. C., and M. D. Abouzahra, *Analysis and Design of Planar Microwave Components*, Piscataway, NJ: IEEE Press, 1994.
- [16] Vendelin, G. D., *Design of Amplifiers and Oscillators by the S-Parameter Method*, New York: John Wiley and Sons, 1982.
- [17] Medley, M. W., *Microwave and RF Circuits: Analysis, Synthesis, and Design*, Norwood, MA: Artech House, 1993.
- [18] Helszajn, J., G. P. Riblet, and J. R. Mather, "Insertion Loss of 3-Port Circulator with One Port Terminated in Variable Short Circuit," *IEEE Transactions on Microwave Theory and Techniques*, November 1975, pp. 926–927.
- [19] Helszajn, J., *Waveguide Junction Circulators: Theory and Practice*, New York: John Wiley and Sons, 1998.

3

Applications of Circulators

3.1 Load Isolation

The principal application of the circulator is in providing isolation. When used as an isolator, the circulator has one port terminated in a matched load as described in Section 2.1. A two-port isolator is, of course, already in the proper configuration for providing isolation.

When we speak of isolation, we are speaking of a property whereby there is low transmission loss in one direction and relatively high loss in the other (reverse) direction. This isolation can be achieved using one device or many in series, and may be large in magnitude or small. For our present discussion, we will consider neither the magnitude of the isolation nor how it is obtained. We will represent the isolator by the symbol in Figure 2.2.

There are six important types [1, 2] of vacuum tubes used to generate or amplify microwaves. These are the klystrons, magnetrons, traveling wave tubes (TWTs), backward wave oscillators (BWOs), crossed field amplifiers (CFAs), and gyrotrons. At low microwave frequencies, gridded tubes, such as triodes, tetrodes, and klystrodes,— also known as inductive output tubes (IOTs)—find some applications. Solid-state devices in the form of diodes or transistors serve as oscillators or amplifiers as well. Generally the vacuum tubes are capable of higher power and higher frequency than solid-state devices, although it is not always clear which class of devices is the better choice.

All types of microwave oscillators can be subject to frequency shifting due to variations in load impedance (load pulling). If we install an isolator between the oscillator and the load, as shown in Figure 3.1, the oscillator can still deliver power to the load, but reflections from the load are attenuated in the isolator

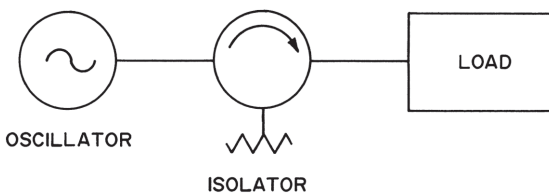


Figure 3.1 Oscillator isolation.

before they can return to the oscillator. Thus, the oscillator sees an essentially constant impedance. An isolator can take the place of a buffer amplifier in many applications, reducing power consumption and, in some cases, cost.

Amplifiers are not always unconditionally stable [3]. If an amplifier does not see the correct load impedance, it could break into oscillation at one or several frequencies, near or far away from the desired signal frequency. Not only are these oscillations undesirable, they could be damaging to an expensive amplifier. Isolators find application in isolating amplifiers from the loads they drive, even if these loads happen to be successive amplifiers in a chain, as shown in Figure 3.2.

Where an oscillator or amplifier drives a higher-power device, there is a possibility that the device could reflect back the signal from the amplifier or oscillator at a much higher amplitude, causing severe damage. Here again, an isolator rated to withstand the highest expected reflected signal level will protect the source.

In a receiver, an isolator may be placed in line with the antenna, as shown in Figure 3.3. The isolator may serve to prevent radiation of the local oscillator signal or to provide a good match for the transmission line coming from the antenna. The input VSWR of a low-noise amplifier (LNA) can be high because the input impedance for optimum low-noise performance may differ substantially from the transmission line characteristic impedance. Because of this, it may be desirable to use an isolator to improve the impedance match. However, this would be at the expense of noise figure due to isolator insertion loss and standing waves between the isolator and LNA.

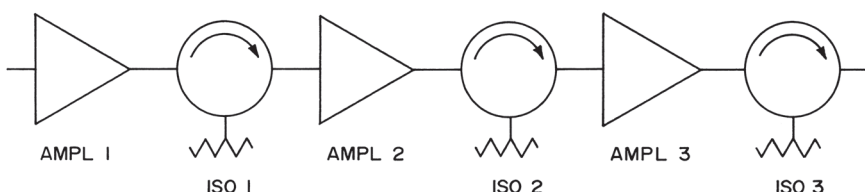


Figure 3.2 Amplifier isolation.

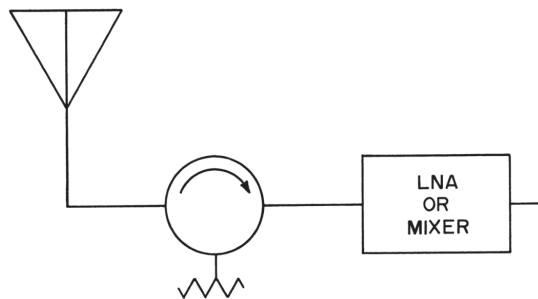


Figure 3.3 Receiver application.

3.2 Duplexing

A duplexer [4] is a device that switches an antenna to either a transmitter or a receiver, so that the same antenna can be used for both. There are several types of duplexers, including gas-discharge devices, solid-state switches, hybrid junctions, and ferrite units.

A ferrite duplexer in its simplest form is a circulator, connected as in Figure 3.4. The transmitted signal is coupled to the antenna, with reflections only from the antenna due to impedance mismatch coupled to the receiver. Signals incident on the antenna are coupled to the receiver. This scheme has the advantages of circuit simplicity, no need for mechanical or electrical switching, and high reliability. Also, transmission and reception can occur simultaneously.

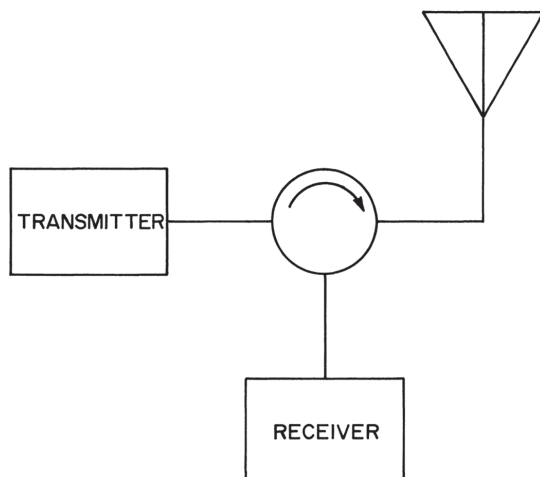


Figure 3.4 A simple ferrite duplexer.

Where only a circulator is used for duplexing, the signal leaking from the transmitter to the receiver, or TR isolation, is attenuated by the return loss of the antenna seen by the circulator. Therefore, a poor antenna VSWR (low return loss) results in poor TR isolation. To improve the isolation, we can add a limiter or switch to the receiver port of the circulator, as shown in Figure 3.5. The limiter could be a solid-state device, a tube type of limiter, or a ferrite limiter. Both the tube and solid-state limiters have the disadvantages of spike leakage and finite recovery time. A switch could be triggered by a high level of return signal from the antenna or by a separate signal from a control circuit.

Although ferrite limiters and switches are beyond the scope of this book, we will briefly describe their operation here to improve our understanding of duplexer theory.

The limiters rely on the nonlinear properties of ferrites. When the RF power exceeds a certain threshold, the insertion loss of the limiter rapidly increases. This nonlinearity is undesirable for the construction of circulators but finds use in limiters. Spin waves are responsible for the nonlinearity of ferrite limiters.

There are several methods [5] of constructing ferrite limiters. One is to place a ferrite sphere, magnetically biased at resonance, between two orthogonal stripline resonators. This orthogonal stripline limiter is shown in Figure 3.6. The input signal is coupled to the sphere by one resonator, and the output is

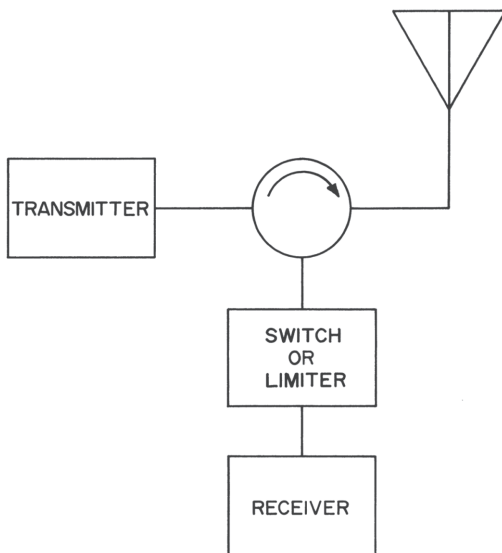


Figure 3.5 A ferrite duplexer with improved transmit-receive isolation.

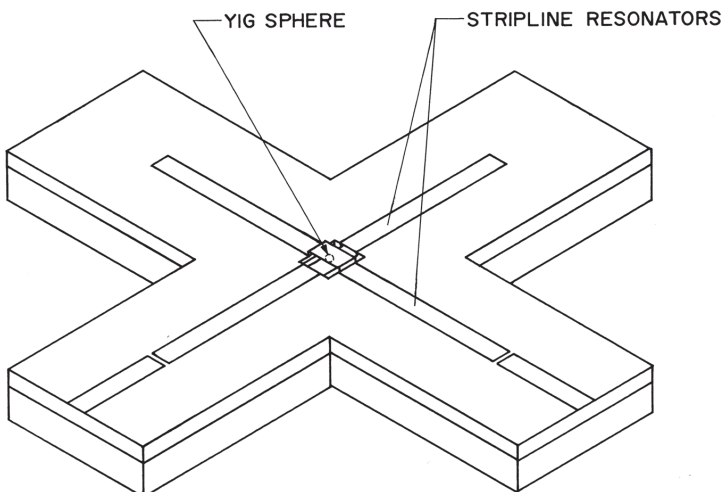


Figure 3.6 Orthogonal stripline limiter.

taken from the other. When the input signal level is high enough, the ferrite magnetic spin moment precesses sufficiently to prevent coupling the signal to the output resonator. Single-crystal yttrium-iron garnet (YIG) ferrite material is suitable for low-power limiters, as well as some higher-power ones, because of its narrow resonance line width, low critical power threshold, and moderate saturation magnetization. These material properties are discussed in more detail in Chapter 4. The details of materials selection for limiter applications are beyond the scope of this book.

Other types of ferrite limiters include the cavity limiter, shown in Figure 3.7, where the ferrite sphere is located inside a resonant cavity; the comb limiter, shown in Figure 3.8, where a ferrite sphere is used to couple two or more quarter-wavelength resonators in a waveguide; and the subsidiary-resonance limiter, shown in Figure 3.9, in which a ferrite slab in a waveguide, operated in the region of the subsidiary resonance that occurs when the power threshold is exceeded, provides limiting.

Ferrite switching can be accomplished by reversing the magnetic field applied to a circulator, which reverses the direction of circulation, so that a signal incident on the input is no longer coupled to the output. Ferrite materials that retain their magnetization after the magnetizing field is removed find application in switches. These materials are called square-loop ferrites because of the square shape of the hysteresis loop. They are highly specialized materials because they have the necessary microwave properties as well as appropriate retentivity. With these materials, all that is needed to change the state of the

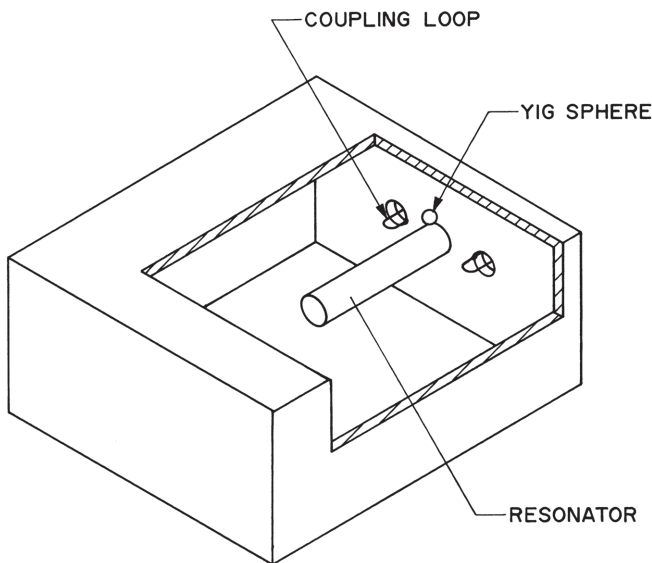


Figure 3.7 Cavity limiter.

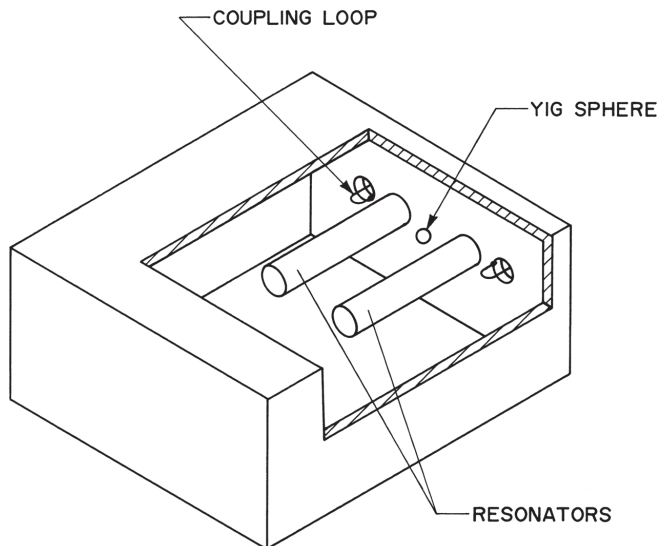


Figure 3.8 Comb limiter.

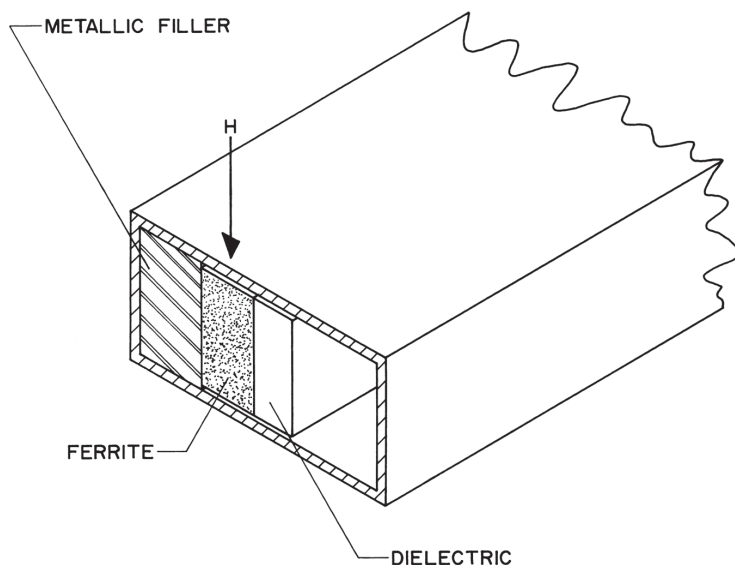


Figure 3.9 Subsidiary-resonance limiter.

switch is a low-energy current pulse. More information regarding the magnetic switching characteristics of switching circulators is provided in Section 6.5.1.

We can synthesize a reciprocal ferrite switch [6] by connecting the circulator junctions, as shown in Figure 3.10. In the on state, the input is coupled to the output and vice versa, so power may be transmitted in either direction. In the off state, both input and output appear reflective.

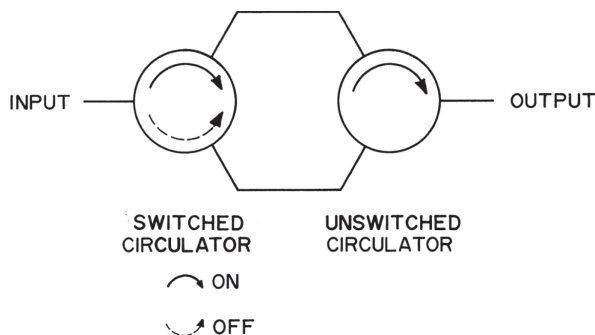


Figure 3.10 The reciprocal ferrite switch.

3.3 Multiplexing

A multiplexer [7] is a device composed of interconnected filters that can split a single channel carrying many frequencies into two or more channels carrying narrower bands of frequencies. The inverse process can also be carried out by a multiplexer; that is, by combining two or more channels carrying different bands of frequencies into a single broadband channel.

A diplexer is a two-channel multiplexer. It is typically made from a low-pass filter and a high-pass filter, whereas a multiplexer having three or more channels is typically constructed using bandpass filters. A diplexer and a multiplexer, both based on circulators, are shown in Figures 3.11 and 3.12, respectively.

Diplexers and duplexers are frequently confused. One reason for this is the similarity in the names. Another is the fact that a diplexer could be used as a duplexer if the transmit and receive frequencies were different. A duplexer, however, is not a frequency-selective device like a diplexer.

We can build a multiplexer without a circulator by simply interconnecting the filters, but the filters must be specially designed to avoid interaction between them. If we use a circulator, we can build the multiplexer with almost any type of filter. In some cases, the filters are part of the equipment connected to the multiplexer, so the multiplexer consists of only a circulator.

A typical application of a multiplexer is to connect more than one transmitter or more than one receiver to a common antenna, which eliminates the necessity of having more than one antenna.

The between-channel isolation of a multiplexer depends on the filter rejection at the frequency of interest. Multiplexers that combine channels close together in frequency necessarily contain filters having very sharp skirts (rapid increase in rejection with frequency outside the passband).

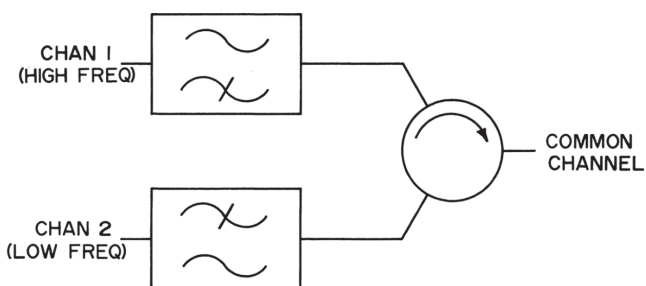


Figure 3.11 Diplexer.

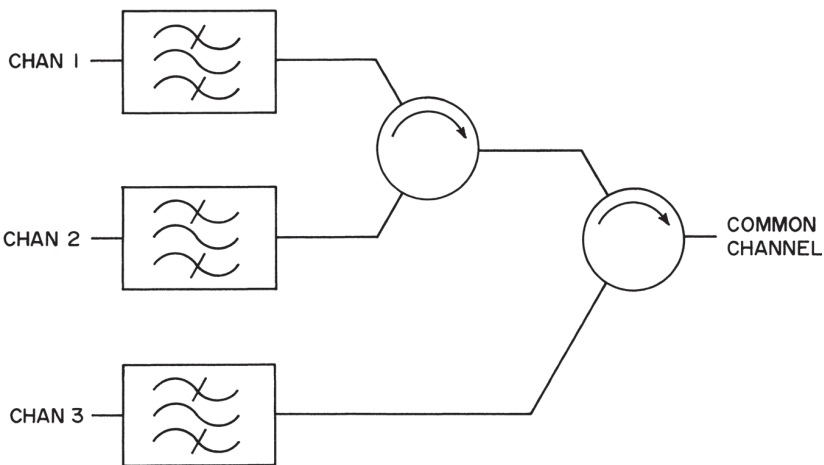


Figure 3.12 A three-channel multiplexer.

To minimize multiplexer insertion loss, we need to be careful how we connect the circulator, because a signal entering the common port of the multiplexer may be reflected off a number of filters and pass through a number of circulator junctions before arriving at its intended channel. Insofar as higher frequencies are attenuated more than lower frequencies in a coaxial medium, it would be wise to arrange the multiplexer so that higher frequencies do not have to travel as far as lower frequencies. If a particular channel must have lower insertion loss than other channels, it should be positioned first in line.

3.4 Parametric Amplifiers

Although not as widely used as they once were, parametric amplifiers are an interesting application of circulators. A parametric amplifier achieves signal gain, with or without frequency conversion, using a nonlinear, time-varying reactance [8]. Because the diode used to provide this time-varying reactance, a varactor diode, is primarily reactive in nature, it contributes very little noise [9], enabling the construction of a low-noise amplifier. Many *parametric amplifiers*, or PARAMPS, are built around circulators, so it is important for the ferrite device designer to know a little about these amplifiers and how they function.

The basic configuration of one type of parametric amplifier is shown in Figure 3.13. This PARAMP is called a nondegenerate one-port. The term nondegenerate refers to the relation of the pump frequency to the signal frequency. A degenerate PARAMP uses a pump frequency of twice the signal

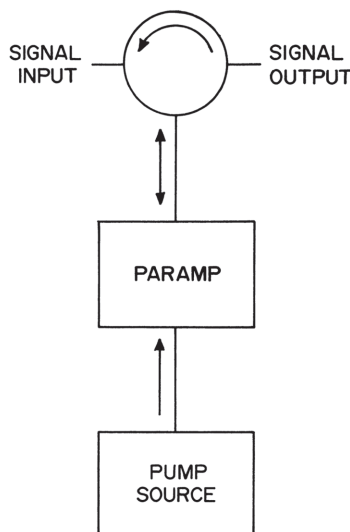


Figure 3.13 The parametric amplifier.

frequency. The pump source provides the energy that varies the reactance in the PARAMP to provide amplification. A PARAMP does not require dc power for operation, as the power added to the input signal in the amplifier comes from the pump source.

There are various types of PARAMPs, including two-port, the one-port already mentioned, multiple pumps, degenerate, and nondegenerate. The one-port PARAMP with circulator is the most widely used type because of its good performance and circuit simplicity.

We can represent the PARAMP block in Figure 3.13 by the schematic of Figure 3.14. This circuit contains three resonators: one tuned to the signal frequency, one for the pump, and an idler, tuned to the difference between the signal and pump frequencies. The pump source drives the varactor diode so that its capacitance changes periodically at the pump frequency. The input signal, entering the PARAMP proper by way of the circulator, is also incident on the varactor. The pump and signal frequencies mix in the nonlinear varactor, and the desired mixing product is picked out by the resonant idler. The idler current remixes with the pump current in the varactor to produce a strengthened version of the input signal. This signal, which is in-phase with the original input signal, is reflected back toward the circulator where it is coupled to the amplifier output.

The power flowing out of the pump source is delivered to both the signal port and the idler. Because the power flows out through the same port where

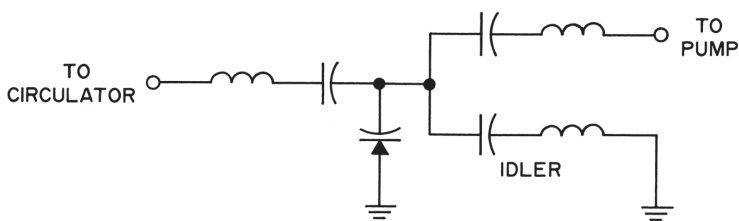


Figure 3.14 PARAMP schematic.

the input signal enters, we need a circulator to separate the input and output ports of the amplifier.

Parametric amplifiers usually operate at relatively low power levels, so circulator power handling is generally not a consideration. However, low insertion loss is desirable because PARAMP designers often need to achieve low noise figures. Provisions for mounting the amplifier diode and other circuitry may be included in the circulator design.

Parametric amplifiers that have no separate pump source can be built. An avalanche diode can be used to oscillate at one frequency, supplying the pump signal used to drive an integrated PARAMP. The PARAMP then uses a varactor diode to provide amplification at a frequency different from the oscillator frequency.

Another type of amplifier, very similar to the parametric amplifier, is the one-port negative-resistance amplifier. This amplifier also must utilize a circulator to separate the input and output ports of the amplifier. The basic circuit for the negative-resistance amplifier is shown in Figure 3.15.

Some of the most popular diodes for negative-resistance amplifiers include the impact ionization avalanche transit time (IMPATT), trapped

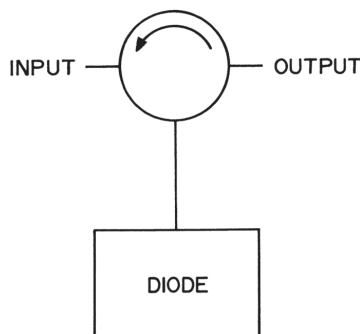


Figure 3.15 The basic negative-resistance amplifier.

plasma avalanche triggered transit (TRAPATT), and barrier injected transit time (BARITT).

Insofar as the negative-resistance amplifier depends on the reflective properties of the diode (the input signal is incident on the diode and the output signal is what is reflected from the diode), the gain of these amplifiers is given by

$$\text{Gain} = \rho^2 = \left(\frac{Z_d - Z_0}{Z_d + Z_0} \right)^2 \quad (3.1)$$

where Z_d is the impedance of the diode. We see that impedance matching is very important to achieve optimum performance from a negative-resistance amplifier. In some applications, the impedance matching circuit may be included as part of the circulator.

Greater isolation between output and input for both the PARAMP and the reflective (negative-resistance) amplifier can be obtained with the configuration shown in Figure 3.16. We can include both circulator junctions in a single package, producing a four-port circulator or circulator-isolator combination.

The BARITT diodes offer lower noise performance than the IMPATT diodes, but the IMPATTs provide better power output. We can obtain high peak power capability and better efficiency from TRAPATT diodes, with greater difficulty in impedance matching.

Yet another type of amplifier that may use a circulator to separate input and output signals is the *maser*. The maser (microwave amplification by stimulated emission of radiation) is a predecessor [10] of the *laser*, which is now very much a part of our everyday lives. The maser is less common.

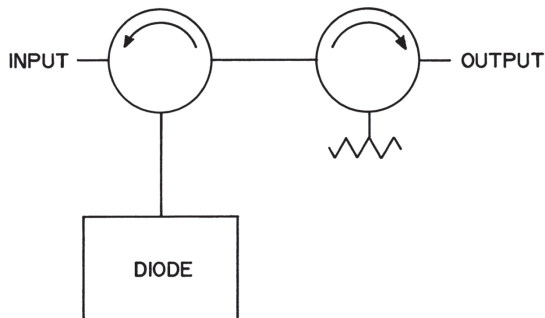


Figure 3.16 A negative-resistance amplifier configuration to obtain higher output-input isolation.

Masers amplify without the use of tubes, transistors, or diodes. Amplification is performed by raising the energy level of atoms or molecules in a solid or gas and then allowing the energy to be emitted. The energy level is raised by pumping with either a microwave signal or light.

One application of the maser is as a frequency standard. The energy-level transitions of the solid or gas cause emission of specific microwave frequencies that are very stable because they are frequency-dependent on the invariant atomic properties of the material.

A maser amplifier that makes use of a circulator functions in much the same manner as the previously described parametric and negative-resistance amplifiers.

3.5 Phase Shifting

Microwave circulators can be used in the construction of narrow-band phase shifters. The connection scheme is shown in Figure 3.17.

The reflective phase shifter block in Figure 3.17 may represent a varactor diode, a mechanical sliding short, or a section of transmission line shorted at various points along its length by PIN diodes. A fixed short circuit might also be placed here, and the magnetic field applied to the circulator junction could be varied to change the transmission phase shift.

The advantage of this type of phase shifter is simplicity; only a reflective phase shifter is needed instead of a transmission type. The circulator converts the one-port phaser to a two-port transmission device. Among the disadvantages is the frequency sensitivity. A constant phase shift cannot be maintained over a wide bandwidth with this design.

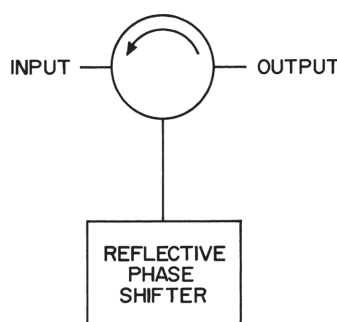


Figure 3.17 Phase shifter.

Several other types of ferrite phase shifters, not based on the circulator, exist. These include [11] toroidal waveguide, dual-mode, Reggia-Spencer, TEM, and Fox phase shifters.

The toroidal waveguide phase shifter, shown in Figure 3.18, uses rectangular ferrite toroids placed inside a section of waveguide with their axes coincidental with the waveguide axis. A wire is threaded through the centers of the toroids, and by application of a current pulse, a toroid can be magnetized with the desired magnitude and direction of magnetic field. Thus, the phase shift is changed by the current pulses. A phase shifter may contain one long toroid, and the magnetization is varied to change the phase shift, or several shorter toroids may be used, and the polarity of the magnetization is changed to switch phase shift sections.

The dual-mode phase shifter is akin to the Faraday rotation circulator. The end transitions are set up so that the energy is transmitted through the unit regardless of the direction of propagation, but different modes are used for the two phase states. The two modes use different polarizations in the phase-shifting ferrite rod: left-hand circular or right-hand circular. Figure 3.19 illustrates the scheme used in this device.

A Reggia-Spencer phase shifter consists of a ferrite rod or slab centered inside a section of waveguide, as shown in Figure 3.20. A solenoid around the waveguide provides the longitudinal magnetic field. The phase shift is varied by changing the magnetic bias.

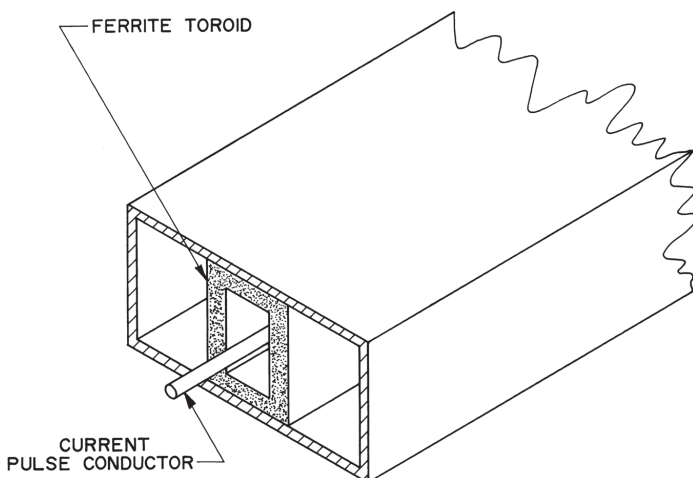


Figure 3.18 Toroidal waveguide phase shifter.

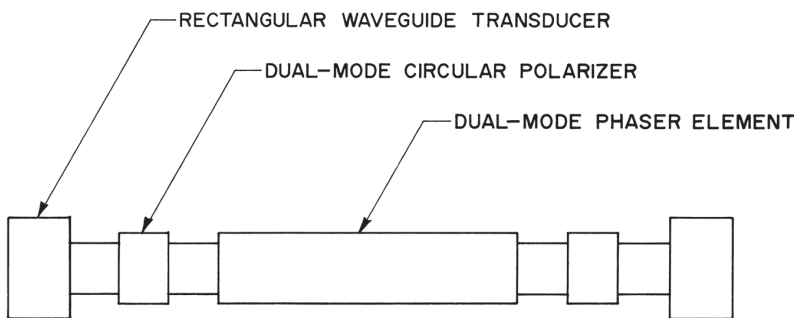


Figure 3.19 Dual-mode phase shifter scheme.

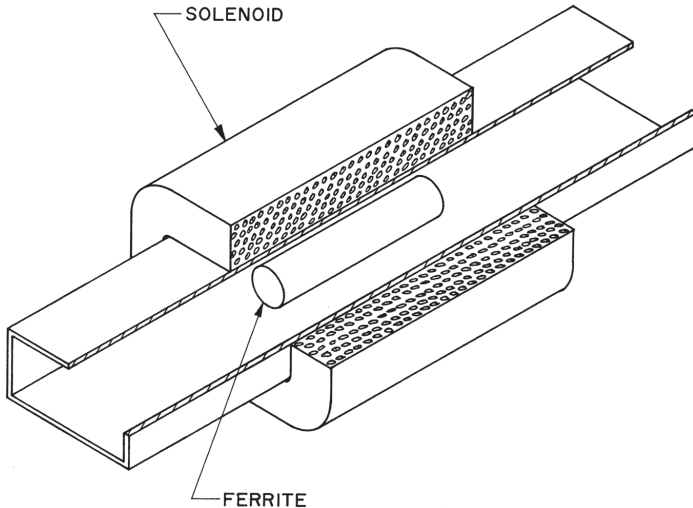


Figure 3.20 Reggia-Spencer phase shifter.

The TEM phase shifters are coaxial versions that can be built using ferrite toroids or slabs in contact with a strip transmission line. Both types are depicted in Figure 3.21. The construction of a toroidal TEM phaser is very similar to that of the toroidal waveguide unit.

The Fox phase shifter has transitions to achieve circular polarization in the center section. A half-wavelength ferrite plate is placed in this center section and is mechanically rotated to change the phase shift. This phase-shifting scheme is illustrated in Figure 3.22.

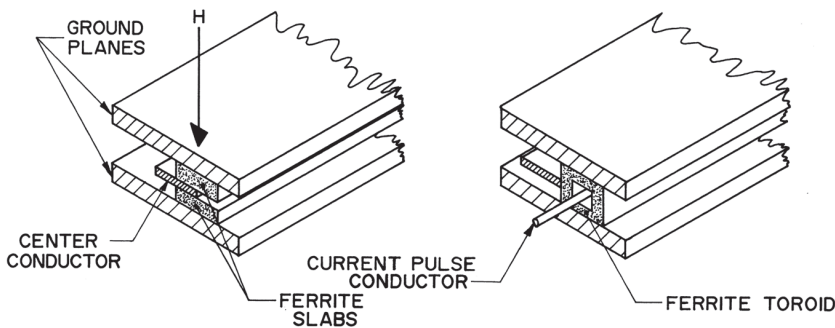


Figure 3.21 Stripline TEM phase shifters: slab type (left) and toroidal type (right).

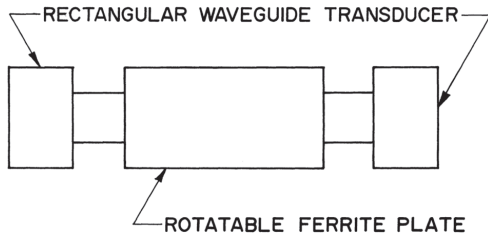


Figure 3.22 Fox phase shifter scheme.

References

- [1] Shrader, R. L., *Electronic Communication*, New York: McGraw-Hill, 1980.
- [2] Gilmour, A. A., *Klystrons, Traveling Wave Tubes, Magnetrons, Crossed-Field Amplifiers, and Gyrotrons*, Norwood, MA: Artech House, 2011.
- [3] Vendelin, G. D., *Design of Amplifiers and Oscillators by the S-Parameter Method*, New York: John Wiley and Sons, 1982.
- [4] Skolnik, M. I., *Introduction to Radar Systems*, 2nd Ed., New York: McGraw-Hill, 1980.
- [5] Arams, F. R., M. Grace, and S. Okwit, "Low-Level Garnet Limiters," *Proceedings of IRE*, August 1961, pp. 1308–1313.
- [6] Clavin, A., "Reciprocal and Nonreciprocal Switches Utilizing Ferrite Junction Circulators," *IEEE Transactions on Microwave Theory and Techniques*, May 1963, pp. 217–218.
- [7] Matthaei, G. L., L. Young, and E. M. T. Jones, *Microwave Filters, Impedance-Matching Networks, and Coupling Structures*, Dedham, MA: Artech House, 1980.

- [8] Fink, D. G., and D. Christiansen, *Electronics Engineers' Handbook*, New York: McGraw-Hill, 1982.
- [9] Liao, S. Y., *Microwave Devices and Circuits*, 3rd. Ed., Englewood Cliffs, NJ: Prentice Hall, 1990.
- [10] Seippel, R. G., *Optoelectronics*, Reston, VA: Reston Publishing, 1981.
- [11] Whicker, L. R., *Ferrite Control Components*, Vol. 2, Dedham, MA: Artech House, 1974.

4

Material Selection

4.1 Ferrites

The selection of ferrite material is perhaps the most critical aspect of circulator design. If the material is chosen incorrectly, the circulator will not perform as desired. In addition, if the material must be reordered from a vendor, a significant delay can result.

By the time the designer is ready to select materials, he or she will have some specifications for the circulator in question. The selection of ferrites depends on the operating frequency and bandwidth of the circulator as well as the RF power level, insertion loss desired, and the ambient temperature range. A good designer will also want to know what the material is and how it is made, so we will begin with a description of ferrites and how they are manufactured. We will then present some design considerations and information regarding the test methods used for ferrites, followed by some typical characteristics of ferrites. Finally, we will briefly cover temperature effects in ferrites and complete this section with criteria for ferrite material selection.

4.1.1 Ferrite Classes

Solid-state physicists like to name crystal structures after the minerals occurring in nature that have similar crystal structures. For this reason, two of the general classes of microwave ferrite materials are called garnets and spinels. The mineral andradite (common garnet or black garnet) has the formula [1] $\text{Ca}_3\text{Fe}_2\text{Si}_3\text{O}_{12}$. If the silicon is replaced [2] by iron and the calcium by a rare earth such as yttrium, we have a new compound: the *yttrium iron garnet* (YIG).

The iron ions in the YIG structure are arranged in such a manner that some of their spin moments cancel each other and other spin moments are not canceled. This incomplete cancellation of spin moments is the basis of ferrimagnetism [3].

By substituting aluminum for some of the iron ions in the YIG, the net magnetic moment can be varied. Other rare earths such as gadolinium, holmium, or dysprosium may be added to change other properties such as spin-wave line width.

The mineral spinel has the formula $MgAl_2O_4$. Microwave ferrites (spinel)s are similar in crystal structure, with a general formula of MFe_2O_4 . The M may represent any one or a combination of the following ions: Al, Co, Li, Mg, Mn, Ni, Ti, and Zn.

Hexagonal ferrites, or *hexaferrites* as they are sometimes called, have hexagonal crystal structures. As described in Chapter 1, there is a wide variety of hexagonal ferrites, and because of their potential to have considerable magnetic anisotropy, they are used for ceramic magnets as well as for microwave applications.

4.1.2 Ferrite Manufacturing

Ferrites can be manufactured using a number of different techniques [4]. For our purposes here, we will cover only bulk polycrystalline ferrite materials. Ferrites are manufactured using ceramic techniques. The exact procedures used vary among manufacturers and are usually secret. The raw materials used [5] include oxides, carbonates, oxalates, and nitrates.

The first step in the manufacturing of ferrites is to grind or mill the raw materials to the correct particle size and then mix them together in the correct proportions. The mixing is often carried out in the presence of water or methylated spirits (denatured alcohol) [2] to ensure homogeneity. The proportions of the raw materials can be very critical, so consideration must be given to the materials used for milling the raw ferrite materials. For example, if a steel ball milling drum and steel milling balls are used, steel will wear off the milling equipment and be deposited in the ferrite. This might be acceptable for a ferrite material if allowances are made, but would generally be unacceptable for a dielectric material, which would require a nonmetallic ball mill. Other techniques for mixing and reducing particle size include coprecipitation, precursor methods, sol-gel methods, spray drying, and freeze drying [4].

The mixture is then dried, if necessary, and “presintered” at a temperature somewhat lower than that used for final firing. The purpose of this firing

is to cause a partial reaction between the raw materials and to help control shrinkage in the final firing. After presintering, the material is remilled and mixed with a binder to make shaping the material easier. One example of a binder is distilled water [2].

The paste can be formed to the desired shape through processes such as extruding, pressing, and casting [5]. Ferrites having high anisotropy, such as hexagonal ferrites, are pressed in a magnetic field to properly orient the crystals. The shaped parts are heated gently at first to drive off the binder.

Next, the ferrites are fired at temperatures of between 1000° and 1500° C in a carefully controlled atmosphere. The firing process can last from four hours to seven days, depending on the particular material. Firing temperature can be critical. For example, for yttrium iron garnet (YIG), a deviation in firing temperature of as little as 10°C significantly impacts resonance linewidth (ΔH) [6].

The ferrites produced by this ceramic process are polycrystalline; that is, they have a nonuniform orientation of the crystal lattice. The properties of the polycrystals are an integration of the properties of a single crystal and are usually acceptable. In some applications, however, single crystals are desirable. These single crystals can be produced by other methods, but their size is limited and they are quite expensive.

Most manufacturing facilities and laboratories do not have the equipment to make ferrites, but many have the necessary machinery to cut and grind them. Ferrites can be purchased “as fired” (unmachined) in various shapes and sizes. These ferrites can be machined to the desired dimensions and surface finish. Being able to machine ferrites is convenient, even if they are purchased already machined, because changes in dimension are sometimes required to achieve optimum performance from circulators.

Ferrites are brittle, hard, and have low thermal conductivity, which makes them difficult to machine. Diamond wheels are usually required [7] to grind these materials, but in some situations silicon carbide wheels will suffice. Water should be used as a coolant during all grinding operations. The surfaces of ferrites can be ground using a surface grinder, and the same machine with a diamond cut-off wheel can be used to slice the ferrite edges. The fact that ferrites are magnetic makes it easy to hold them by using a magnetic chuck.

The ferrites should be thoroughly cleaned after machining, because any surface impurities can degrade electrical performance.

Machining introduces stresses in the ferrite material. These stresses may affect the magnetic properties of the ferrite via magnetostrictive effects [8]. For critical applications, thermal annealing can be used to relieve the mechanical stresses in the ferrite and restore normal magnetic properties.

4.1.3 Design Considerations

Dimensional tolerances of finished ferrite parts are very important. If the thickness of a disk used in a stripline configuration were too great, the result could be a fractured ferrite. If the thickness were too small, the space between the ground planes would not be fully filled with ferrite, and a degradation in electrical performance would result. A typical thickness tolerance, including parallelism, is ± 0.0005 inches. For the diameter of a disk or the altitude of a triangle, ± 0.005 inches might be a reasonable figure. For ferrites destined for use in millimeter- and shorter-wavelength circulators, this tolerance may need to be reduced. Smaller parts, of course, will require tighter tolerances. Smooth surface finishes are generally desirable, and a typical ferrite will have a finish of 16 microinches or better.

Another important consideration in the selection of ferrite materials is grain size. In below-resonance circulators, where the peak power threshold can cause higher insertion loss at higher peak power levels, reduced grain size can increase the threshold by an order of magnitude [9]. Normally, grain size is 10–20 μm . If the grain size is reduced, down to a practical limit of about one micron, the wavelength of the longer wavelength spin waves is equal to the grain size. When the spin-wave wavelength and the grain size are similar, the spin waves are effectively broken up and the peak power threshold increases. The disadvantage of smaller grain size is higher cost.

A question that the designer of a junction circulator must face is whether to use a triangular ferrite or a disk. Nearly equal electrical performance can be obtained from either one, although experiment has shown that lower loss might be achieved using a triangular geometry [10].

Depending on the manufacturing processes used, it could be less expensive to manufacture small disks than small triangles—they can be sliced from a rod. When considering larger ferrites, the disk part would not be cut from a rod, due to the immense proportions required of the rod and the cut-off blade. It could be more economical to slice a triangle from a rectangular bar or to grind the edges of a fired triangle than to grind the circumference of a large disk.

Some engineers think that the raw material cost is lower if a disk is used rather than a triangle (see Figure 4.1). While this may be true for a directly coupled circulator (one that has no impedance-matching transformers), if transformers are used, and they are implemented in the ferrite medium, rather than in a separate dielectric, a triangle may reduce raw material cost. For most ferrites, the raw material cost (especially for small parts) is a small fraction of the part cost. For small quantities and small parts, labor and manufacturing yield are larger terms than raw materials.

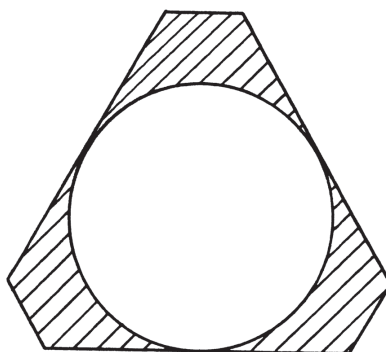


Figure 4.1 Ferrite disk superimposed on electrically equivalent triangle. Shaded area is “wasted” ferrite.

One must draw a dividing line between disk and triangle: At what dimension should you change over to a triangle from a disk? It may be more cost effective to use disks where small ferrites are required, and more cost effective to use triangles where large ferrites are required. Since “large” ferrites are not normally encountered in below-resonance designs, and above-resonance circulators are primarily for lower frequencies (meaning large ferrites), a good rule of thumb is to use disks for below resonance units and triangles for above-resonance units.

4.1.4 Test Methods

The saturation magnetization is often measured [11] by the vibrating sample method. In this method, the test sample is a ferrite sphere approximately 2 mm in diameter. The spherical shape was chosen because in a sphere the internal magnetic field is more uniform than for any other shape. The ferrite sphere is placed in a strong dc magnetic field and vibrated to produce an induced voltage in a pickup coil. This induced voltage is proportional to the volume of the ferrite sphere and its saturation magnetization. If the voltage is compared to the voltage induced by a known reference sphere, the saturation magnetization can be calculated. A standard test method for saturation magnetization is described in ASTM A894/A894M [12].

ASTM A883/A883M [13] is a standard test method for resonance linewidth and gyromagnetic ratio. The test for resonance line width is made with a spherical sample inside a cavity resonator. The cavity is excited with an X-band RF signal, and a dc magnetic field applied to the sample under

test is varied until maximum absorption occurs. If the RF frequency and the applied magnetic field are known, the effective gyromagnetic ratio, γ_{eff} , can be calculated from

$$\gamma_{\text{eff}} = \frac{\omega}{H} \quad (4.1)$$

Once γ_{eff} is known the g-effective value of the ferrite sample can be calculated from

$$g_{\text{eff}} = \gamma_{\text{eff}} \frac{2m_0c}{e} \quad (4.2)$$

where m_0 is the mass of an electron, c is the velocity of light, and e is the unit electron charge.

The dc magnetic field applied to the ferrite sphere is varied until the resonance absorption drops to half power on each side of resonance (-3 dB points). The difference in magnetic field between these two 3 dB points is called the resonance line width.

Not all manufacturers use the ASTM standard test method for these measurements, so it is important for the designer to keep in mind that published specifications may vary with the test methods used. ASTM A883/A883M was withdrawn in May 2006 due to lack of interest, but the test methods are still used.

Resonance line width (ΔH) is a useful measure of ferrite magnetic losses in the vicinity of ferrimagnetic resonance. For off-resonance operating points (below resonance and above resonance), *effective line width* (ΔH_{eff}) is more useful for purposes of circulator computations and simulations. ΔH_{eff} is generally lower than ΔH , as magnetic losses are lower away from resonance. Measurement of ΔH_{eff} can be more involved [14], and few ferrite materials manufacturers publish ΔH_{eff} values for their materials. Fortunately, it is possible to develop ΔH_{eff} values for a material type or specific material lot by comparing measured insertion loss data with simulation results and adjusting the ΔH_{eff} value used in the simulation until the loss data match.

The Curie temperature is determined by measuring the saturation magnetization as a function of temperature. The temperature where the saturation magnetization drops to zero is the Curie temperature. Only above this temperature is the ferrite material paramagnetic.

To measure spin-wave line width, the same ferrite sphere used for the other parameter measurements is placed at a point of maximum microwave

magnetic field in a resonant cavity. The dc magnetic field is applied in the same direction as the RF field. This is called parallel pumping. The RF signal applied to the cavity is pulsed, and an RF output signal from the cavity is monitored. The dc magnetic field is varied until the output pulse starts to deteriorate, indicating the onset of nonlinearity in the ferrite sample. The microwave magnetic field, H_{RF} , can be calculated from the RF power applied to the cavity and certain constants of the cavity. From H_{RF} , the spin-wave line width can be calculated:

$$\Delta H_k = \frac{H_{RF}\gamma_{\text{eff}} 4\pi M_S}{\omega} \quad (4.3)$$

ASTM A893/A893M [15] provides a test method for complex dielectric constant of ferrites. Exercise caution when specifying or comparing dielectric constants, as not all manufacturers use the same test methods.

4.1.5 Specifications

Table 4.1 lists typical characteristics of commercially available garnets, and Table 4.2, the characteristics of spinels. The most important parameters of ferrite materials are the saturation magnetization ($4\pi M_S$), line width (ΔH), Curie temperature (T_C), spin-wave line width (ΔH_k), and of lesser importance, the g-effective value, dielectric constant, and dielectric loss tangent.

Hexagonal ferrites differ from garnets and spinels in that they can have considerable magnetic anisotropy (H_a), up to at least 35 kOe. Typically ΔH values are also relatively high, often over 1 kOe. A large variety of hexagonal ferrites have been developed, but aside from their application as ceramic magnets, they have not been widely used for microwave circulators. Hexaferrites do find use in self-biased circulators and in some other high-frequency circulators. Because of the limited availability of microwave hexaferrites, and the wide variety of materials, we will not present a table of typical ferrite properties. We refer the reader to the manufacturer of the candidate hexaferrites for material specifications.

4.1.6 Temperature Effects

The ferrite material Curie temperature is a good indication of the material's temperature stability. For applications that require operation over a broad temperature range, it is important to consider the change in saturation magnetization with temperature. In many cases, high-power devices will also require

Table 4.1
Garnets

Composition	$4\pi M_s$ (G)	T_c (°C)	ΔH (Oe)	ΔH_k (Oe)	Composition	$4\pi M_s$ (G)	T_c (°C)	ΔH (Oe)	ΔH_k (Oe)
Y	1800	280	45	1.4	Y GdAl Co	800	250	85	13.0
						1000	240	60	7.0
Y Al	175	90	40	1.5		1800	280	85	10.0
	250	100	40	1.5					
	300	115	30	2.0	Y Gd Al Dy	500	225	95	8.6
	350	125	40	1.5		600	175	85	8.9
	400	135	45	1.4		700	240	80	9.1
	550	160	40	1.4		800	245	70	3.0
	700	185	40	1.5		900	270	185	12.0
	800	200	40	1.5		1100	270	150	11.0
	1000	210	40	1.4		1200	260	60	9.4
	1200	230	40	1.4		1400	270	110	8.0
	1400	250	70	2.7		1600	280	75	6.6
	1600	265	40	1.4	Y Gd Al Ho	550	180	100	8.5
Y Gd Al	210	110	65	2.2		700	240	90	7.9
	400	150	65	4.2		800	240	110	8.1
	550	185	65	3.6					
	700	200	60	4.0	Y Gd Ho	1000	280	120	8.9
	800	220	75	5.2		1200	280	95	8.1
	800	260	55	4.3		1600	280	70	5.4
	1000	250	75	3.6					
	1200	260	50	3.2	Ca V In	600	200	25	1.2
	1400	265	50	3.2		800	205	10	1.2
						1000	210	10	1.4
Y Gd	720	280	200	7.6		1200	220	10	1.2
	900	280	140	6.4		1400	230	10	1.3
	1000	280	100	5.8		1600	230	12	1.4
	1200	280	75	4.3		1850	240	15	1.3
	1400	280	95	4.1					
	1600	280	50	3.8	Y Ca Zr	1950	240	60	

Table 4.2
Spinsels

Composition	$4\pi M_s$ (G)	T_c (°C)	ΔH (Oe)	ΔH_k (Oe)	Composition	$4\pi M_s$ (G)	T_c (°C)	ΔH (Oe)	ΔH_k (Oe)
Mg Al	650	100	115		Ni Al	500	120	150	
	950	140	80			1000	400	320	
	1250	160	155			2100	560	460	6.1
	1700	225	120			2500	570	490	6.9
	2000	290	250	2.1					
	2420	310	180			1400	425	260	20.0
Mg Mn						1600	450	370	19.0
	1130	175	180	2.5		1800	500	775	25.0
	1400	210	260	2.0		1900	545	880	33.0
	1600	230	290	2.0					
	1900	280	350	2.0	Ni Co	3000	585	350	12.0
	2150	320	540	2.5					
	2400	300	300	3.0	Ni Zn	4000	500	270	
Mg Mn Al	2800	300	300	2.9		5000	375	160	
	750	90	120	5.2	Li Ti	1000	330	300	1.5
	1000	100	100	3.2		1200	390	375	1.5
	1300	140	135	2.6		2000	490	400	1.5
	1500	180	180	2.4		2200	500	450	1.5
	1750	225	225	2.3		2900	600	550	1.5
Mg Mn Zn	2500	275	520	3.0	Li Ti Zn	1000	170	90	2.1
	2800	225	540	2.3		1300	210	150	2.1
	3000	240	190	3.2		3000	375	150	2.1
					Li	3750	640	650	
					Li Zn	4100	570	550	
						4800	400	240	

temperature-stable materials because power losses are converted to heat. The Curie temperature is an indicator of temperature stability, as is the manner in which $4\pi M_s$ changes with temperature. Some materials have saturation magnetization characteristics that do not vary as much with temperature as do those of other materials. Figure 4.2 illustrates this concept graphically.

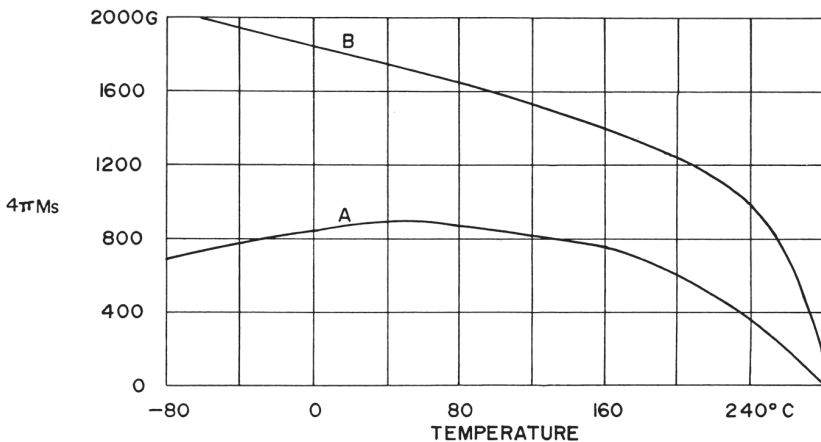


Figure 4.2 Curie temperature is not everything. Materials A and B have identical Curie temperatures, but A is much more temperature stable than B.

Section 5.6 presents some theory behind temperature effects in circulators, and Chapter 6 describes temperature compensation of the magnetic circuit, which also serves to improve circulator temperature stability.

4.1.7 Ferrite Selection

The selection of ferrite material is substantially independent of the microwave transmission medium (waveguide, stripline, coaxial line), so the medium will not be considered in the following discussion. Neither will the sizing of ferrite parts, which will be covered in the following chapter on electrical design (Chapter 5).

The selection of an appropriate saturation magnetization is mainly dependent upon the microwave frequency, and three modes of operation will be considered: resonance, below resonance, and above resonance. The terms *above resonance* and *below resonance* refer to the magnetic operating point relative to ferrimagnetic resonance (see Figure 4.3). The magnetic operating points must not be confused with the operating points in the frequency domain, because they are just opposite—the below resonance region is higher in frequency than ferrimagnetic resonance. Low field loss will first appear at the upper frequency limit in a below-resonance circulator, and ferrimagnetic resonance will show itself at the upper frequency edge of an above-resonance circulator.

To avoid low field losses in both the resonance mode and the below-resonance mode, the saturation magnetization should be chosen such that the ferrite is fully biased magnetically. To meet this condition, we need [16]

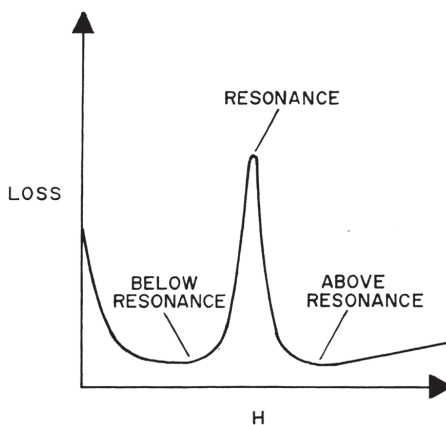


Figure 4.3 Magnetic operating points: below resonance, resonance, above resonance.
 H = magnetic intensity.

$$4\pi M_S < \frac{\omega}{\gamma} - H_a \quad (4.4)$$

where H_a is the anisotropy field associated with the particular material selected. Typically, H_a is on the order of 100 Oe. Figure 4.4 is a plot of $4\pi M_S$ versus microwave frequency for $H_a \approx 100$ Oe, calculated using (4.4). The maximum usable value of saturation magnetization varies linearly with frequency. For a resonance isolator, it is usually desirable to choose a high value of saturation magnetization to minimize the amount of magnetic field required. In the below-resonance mode, a lower value of saturation magnetization will increase [16] the peak power handling capability. The lower $4\pi M_S$ will also result in a narrower bandwidth for a given impedance-matching circuit complexity. One must decide which is more important—the bandwidth or the power handling. There are other methods of increasing the power handling that will be discussed later.

The saturation magnetization for above-resonance devices is not as critical as that for resonance and below-resonance devices. Because of the much higher magnetic fields, low field loss is not a concern. To achieve greater bandwidths, high values of $4\pi M_S$ should be selected. The mathematical relationship between saturation magnetization and bandwidth is presented in Section 5.1, but again, the choice of $4\pi M_S$ is not critical. At high frequencies, it may be necessary to select lower saturation magnetizations due to the extremely high magnetic fields required by higher saturation magnetizations and microwave frequencies.

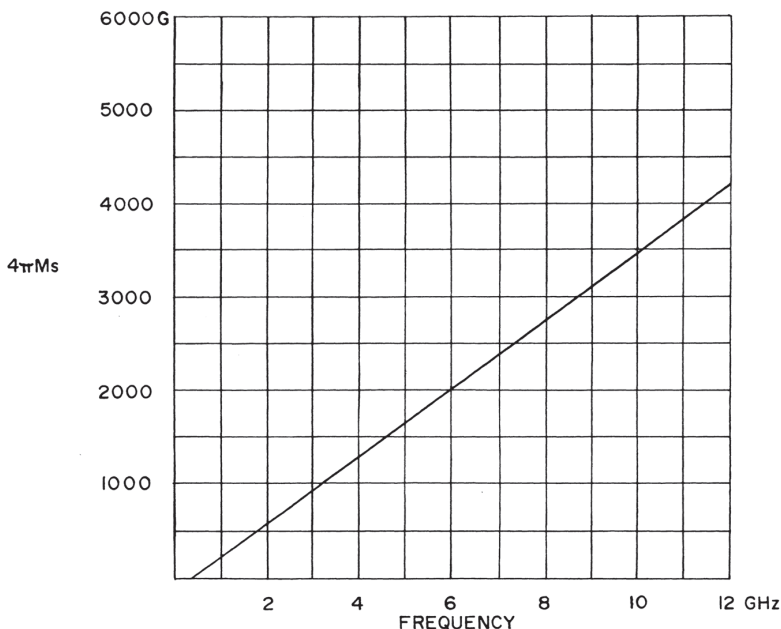


Figure 4.4 Maximum values of saturation magnetization for below-resonance operation.

The resonance line width for nonresonant devices (above- and below-resonance modes) should be as narrow as possible. This is especially important for the above-resonance mode. The narrow line width and moderate saturation magnetization of the calcium vanadium garnets make them a good choice for broadband above-resonance devices where temperature stability is not important. In applications where high $4\pi M_s$ and narrow line width are needed, the lithium ferrites are desirable. YIGs and YAIGs find usage where low $4\pi M_s$ and narrow line width are necessary. Excessive line width will result in increased insertion loss of a nonresonant device.

The shape of the ferrimagnetic resonance curve may be worthy of consideration in some cases. Some resonance curves are distinctly asymmetrical, making the material more suitable for operation on one side of resonance than the other. For example, some Lithium ferrites exhibit lower loss below resonance.

For a resonance isolator, we want to have a relatively broad resonance line width to achieve broadband operation. The bandwidth is proportional to the line width and the isolation (attenuation per unit length) is inversely proportional to the line width.

For an above-resonance circulator, we are not concerned with the nonlinear effects and subsidiary resonances that occur below resonance, so we select

a material with a low spin-wave line width to avoid magnetic losses associated with a doped material.

Magnetic losses are caused largely by the ferrimagnetic resonance. If the ferrimagnetic resonance line width is higher, the resonance is broader, and resonance losses can manifest themselves in the operating frequency range of the circulator. Increased line width can be caused either by pores and other inclusions in the ferrite that reduce its density (higher density ferrites generally have lower line widths) or higher anisotropy due to random orientation of grains in the ferrite. Higher concentrations of rare-earth doping in garnets lead to higher anisotropy and hence higher resonance line width. Therefore, it is essential to hold rare-earth impurity levels low if narrow line width and low magnetic loss are desired. Higher doping levels are used in high spin-wave line width materials because the rare-earth ions tend to “pin” the spin waves.

Below-resonance devices built with low spin-wave line width ferrites can exhibit high power thresholds on the order of 100W, or even lower in power. For a YAIG having a saturation magnetization of approximately 800G, the threshold [17] can be increased by a factor of 30 by changing to gadolinium-doped YAIGs. Y-Gd garnets would raise the threshold by a factor of 170. The tradeoff here is increased insertion loss. In the case of the Y-Gd-Al garnets, the loss increases by a factor of 10 (at low power) and by a factor of 40 for the Y-Gd garnets. These loss estimates are only approximate, as the exact increase in loss would depend (in part) on the proximity to ferrimagnetic resonance. The high power threshold is proportional to the square of the spin-wave line width and inversely proportional to the saturation magnetization. A rough estimate of the increase in magnetic losses due to the use of a material with higher spin-wave line width can be obtained by comparing the squares of the resonance line widths.

Ferrites that have high g-effective values will require less magnetic bias than ferrites that have values near the theoretical value of 2.00. The converse is true of ferrites having low g-effective values—they require larger biasing magnets.

The dielectric loss tangent should always be as low as possible, but it is more important to keep dielectric losses low when the ferrite is positioned in a region of high electric field.

The dielectric constants of the garnets and spinels are relatively constant. For garnets, the figure is 14–16, and for spinels, 12–13.

For self-biased circulators, which are circulators that do not require separate magnets, there is an additional consideration for the selection of an appropriate hexagonal ferrite. To ensure that the ferrite is magnetically saturated, the aspect ratio of the ferrite must be such that [18]

$$N_z < \frac{H_C}{4\pi M_S} \quad (4.5)$$

where N_z is a ferrite demagnetization factor, which is determined from the ferrite dimensions as described in Chapter 6, and H_C is the ferrite coercivity. This equation establishes an upper limit for the ratio R/d in terms of ferrite disk dimensions, for a particular ferrite material. Sadly, good circulator design often dictates the use of a large R/d ratio, and not all hexaferrites have high enough H_C to tolerate this.

It is not difficult to understand why there are not more self-biased circulators if we consider the additional ferrite shape constraint, the typically large resonance line width, and limited materials availability. We wish the designers of self-biased circulators good luck!

Hexagonal ferrites find use in resonance isolators. If the ferrite has the proper level of anisotropy field and sufficient coercivity, then bias magnets can be substantially reduced in size or eliminated.

4.2 Magnet Selection

After ferrite materials have been selected and a preliminary electrical and magnetic design is developed, the designer will have some knowledge of the magnetic field requirements for the circulator, as well as the size or weight limitations imposed upon the design. The magnitude of the magnetic field together with the maximum size and weight of the magnetic components are the key factors in the selection of magnets.

Magnets commonly used in circulators fall into one of four broad classes: ceramic (barium or strontium ferrite), alnico (aluminum-nickel-cobalt), samarium cobalt, and neodymium-iron-boron. Table 4.3 lists some of the more important characteristics of several magnet materials [19, 20].

When the first edition of this book was published, Nd-Fe-B magnets were a relatively new development [21]. The technology has matured, magnets with higher energy products are now available, and two general techniques are used to manufacture these magnets. One technique is called jet casting. In this process, molten neodymium alloy is sprayed onto a rotating drum, which rapidly cools the material and forms it into ribbons. The ribbons are then crushed and the particles undergo further processing depending on the grade of magnet. For MQ 1 (bonded) magnets, the particles are annealed and mixed with epoxy resin. This results in an inexpensive product that is

Table 4.3
Magnets

Material	Energy Product (MGOe)	Coercive Force (Oe)	Density (g/cc)	Max. Operating Temp. (°C)
Ceramic 1	1.0	1825	3.6	300
Ceramic 5	3.5	2200	4.9	300
Ceramic 8	4.3	2500	4.9	300
Alnico 5	5.5	640	7.3	540
Alnico 9	9.0	1300	7.3	540
Sm-Co (1:5) 16	16.0	7900	8.3	250
Sm-Co (1:5) 20	20.0	8300	8.3	250
Sm-Co (2:17) 32	32.0	10800	8.3	300
Nd-Fe-B MQ 1 (bonded)	8.0	5300	6.0	125
Nd-Fe-B MQ 3	32.0	10500	7.5	150
Nd-Fe-B 52	52.0	10600	7.5	50

easily machined. The energy product of MQ 1 is slightly higher than that of the ceramic magnets, and for a given application, the prices are similar. Hot pressing and further processing of the particles from the jet caster results in the anisotropic MQ 3. MQ 3, being anisotropic, has the disadvantage that it can only be magnetized in one direction. The other manufacturing technique involves powder metallurgy and sintering, and produces the highest-energy magnets available.

The energy product of a magnetic material is the maximum product of flux density (B) and magnetic intensity (H) taken from the material demagnetization curve. This provides a measure of the “strength” of the material, or the size of a magnet necessary to provide a particular magnetic field. The coercive force (H_C) is the demagnetizing force required to reduce the induction (flux density) in the material to zero. Magnets that have low coercive forces should be charged (magnetized) in the magnetic circuit to get the maximum energy from them, because removing them from the circuit usually causes a loss of magnetism. Alnico magnets fall into this category and are less desirable because of their low coercive forces.

The most cost-effective biasing fields are provided by the ceramic and bonded materials. Standard-sized shapes such as disks and rectangular bars should be used whenever possible to avoid costly machining. When machining

is necessary, one will find that the bonded materials, being epoxy-based rather than ceramic, are easier to machine. Triangles are normally not available as standard shapes, so their use should be avoided when possible.

For applications demanding high magnetic fields and minimum size and weight, the samarium cobalt and Nd-Fe-B materials are preferred. Nd-Fe-B magnets are more susceptible to oxidation (rusting) than other magnet materials. These magnets should be coated or plated for corrosion protection.

Another factor worthy of consideration is the maximum operating temperature of the magnet. The highest-energy Nd-Fe-B magnets have fairly low maximum operating temperatures of about 50° C. The other Nd-Fe-B materials also have relatively low maximum operating temperatures. Maximum temperatures at least 100° higher apply to the other materials in Table 4.3. Above these maximum operating temperatures, there is an irreversible loss of magnetic flux.

Reversible temperature effects in magnets can be advantageous. Because ferrite $4\pi M_s$ usually drops with increasing temperature, it is desirable to have reduced magnetic flux at higher temperatures. The ceramic magnets have the highest negative reversible temperature coefficient of about 0.2%/°C [20].

In applications where the magnets will not be charged in the magnetic circuit and a magnet charger is not available, magnets should be ordered from the vendor “fully oriented” and the direction (plane) of magnetization should be specified.

4.3 Magnetic Compensating Material Selection

To design a circulator with a wide operating temperature range, it is often necessary to temperature-compensate the magnetic circuit. Magnet manufacturers strive to produce magnets that provide a nearly constant flux regardless of temperature, but for most circulators we want a decrease in flux as temperature increases.

Special materials are available that will provide a reduction in magnetic flux as temperature increases. These materials can be either ferrites or nickel-steel alloys. The manufacturers of the materials provide data indicating the change in permeability versus temperature for a specific H (magnetizing force). Some typical data are presented in Figure 6.8 of Chapter 6.

Once the required magnetic flux density as a function of temperature is determined, either by calculation or testing, an appropriate compensating material can be selected by examining the manufacturer's data.

The metals are far easier to machine than the ferrites, but are not usually available in the small quantities needed for most circulator requirements. A minimum order from a steel mill can be quite a large quantity, but the ferrites, on the other hand, are available in small quantities.

4.4 Dielectric Selection

Many circulator designs will require the use of dielectric materials. Dielectrics provide insulation to prevent voltage breakdown and reduce the size of distributed capacitances (transmission lines) by increasing the electric flux density.

Dielectrics can be classified according to physical characteristics, dielectric constant, dielectric loss tangent, and dielectric strength.

The lowest loss dielectric is air, which has a relative dielectric constant of 1. Air does not have high dielectric strength, but the voltage breakdown characteristic can be improved by pressurization. Other gases, such as sulfur hexafluoride, are used where high dielectric strength is needed without sacrificing the low loss aspect of a gas dielectric.

Higher in loss and dielectric constant, we have silicone materials: greases, two-part liquids that cure to a rubberlike consistency, and self-curing silicone sealants available in various viscosities. These materials have a dielectric constant of about 2.7 and very good dielectric strength.

Rexolite and Teflon are two low-loss plastics that have dielectric constants of 2.5 and 2.1, respectively. Rexolite has a maximum temperature rating of only 100°C but has lower loss than Teflon, which is a much higher-temperature material.

Various printed-circuit laminates find use in circulators. These materials are available in a wide range of dielectric constants and thicknesses, and are usually copper-clad. Circulator construction can be simplified by using these laminates because the circuit can be etched onto the dielectric.

Composite dielectric materials consisting of high dielectric constant ceramics mixed with polystyrene are offered in various values of dielectric constant from 3 to 30. These materials, when cut into small blocks, are useful for tuning low-power circulators.

Ceramic dielectrics, made from oxides of aluminum, calcium, magnesium, and titanium, are usually marketed by ferrite manufacturers. Dielectric constants from 6 to over 100 are available, the dielectric loss tangent increasing with dielectric constant.

Ferrites can be purchased with ceramic dielectrics bonded to them. These assemblies make junction circulator construction simple, because the impedance transformers typically extend radially from the ferrite.

To select a dielectric material, it is wise to first determine the required dielectric constant. Physical size limitations placed on distributed capacitances or transmission lines require minimum values of dielectric constant. The upper limit of dielectric constant is set by the vanishingly small dimensions of the center conductor in a coaxial structure, the propagation of higher-order modes, the higher dielectric loss tangent, and the tighter dimensional tolerances required.

Once the required dielectric constant has been determined, the dielectric material can be selected by considering the expected voltage gradient in the dielectric and the dielectric loss tangents. The lowest-loss dielectric that has the required dielectric constant and dielectric strength should be chosen. Where further discrimination between materials is needed, the material that is easiest to form to the desired shape and size should be selected. The silicone materials (and air) are excellent in this respect.

4.5 Metals Selection

The metals commonly encountered in circulators are aluminum, brass, copper, silver, and steel. Characteristics to be considered in the selection of metals include cost, machinability, electrical conductivity, thermal conductivity, weight, and magnetic properties.

For a circulator housing, which usually provides ground planes, the metal selected should be inexpensive, easily machinable, lightweight, highly conductive, and nonmagnetic. Thermal conductivity is secondary in most cases. Aluminum is a good choice. The particular alloy chosen should be one that can easily be machined to a very smooth, flat surface. In applications where low insertion loss is specified, the housing can be plated with a more conductive metal, silver. The thickness of the plating should be such that most of the RF current flows in the silver. Five times the skin depth is a good rule of thumb for thickness. Water-cooled circulator housings may be made from copper, which has twice the thermal conductivity of aluminum.

Center conductors for coaxial circulators need to have very good electrical conductivity and easy machinability or etchability. In addition, the metal must be solderable for attachment to the RF connectors. Brass is a good choice because it is cheap, easily machinable, and available in many precise thicknesses as shim stock. Where the center conductor will be etched, copper is a

better choice. If insertion loss is a critical specification, the center conductor may be silver-plated. This plating does not have a large influence over loss in most applications, however.

Cold rolled steel is generally used for magnet pole pieces, magnetic shielding, and other magnetic circuit components. The steel will normally be plated for rust prevention.

Large waveguide circulators are typically constructed from commercially available waveguide tubing and flanges.

An important consideration when selecting metals is the potential for galvanic corrosion. If dissimilar metals are placed in contact with each other, steps must be taken to prevent corrosion. MIL-STD-889B [22] contains a table (Table I) listing the compatibility of metal combinations in various environments. This military standard also contains a list of recommended surface treatments for corrosion protection.

Metals that are far apart in the galvanic series should not be placed in contact with each other without surface protection, as severe corrosion of the more anodic metal will occur. If dissimilar metals must be placed in contact, choose metals that are close together in the galvanic series, and ensure that the surface area of the more anodic metal is much larger than the area of the more cathodic metal.

References

- [1] *Handbook of Chemistry and Physics*, Cleveland, OH: Chemical Rubber Publishing Co., 1939.
- [2] Clarricoats, P. J. B., *Microwave Ferrites*, New York: John Wiley and Sons, 1961.
- [3] Wert, C. A., and R. M. Thomson, *Physics of Solids*, New York: McGraw-Hill, 1970.
- [4] Valenzuela, R., *Magnetic Ceramics*, Cambridge: Cambridge University Press, 1994.
- [5] *Publication No. 50030040*, Adamstown, MD: Trans-Tech, 1984.
- [6] Von Aulock, W. H., *Handbook of Microwave Ferrite Materials*, New York: Academic Press, 1965.
- [7] *Tech-Briefs*, Adamstown, MD: Trans-Tech, 1973, p. 13.
- [8] *Application Note: Stabilization of Remanent Induction by Thermal Annealing*, Adamstown, MD: Trans-Tech, May 15, 2013.
- [9] *Tech-Briefs*, Adamstown, MD: Trans-Tech, 1973, p. 14.
- [10] Helszajn, J., and D. S. James, "Planar Triangular Resonators with Magnetic Walls," *IEEE Transactions on Microwave Theory and Techniques*, February 1978, pp. 95–100.

- [11] *Tech-Briefs*, Adamstown, MD: Trans-Tech, 1973, p. 20.
- [12] ASTM A894/A894M, *Standard Test Method for Saturation Magnetization or Induction of Nonmetallic Magnetic Materials*, West Conshohocken, PA: ASTM International, December 2011)
- [13] ASTM A883/A883M, *Standard Test Method for Ferrimagnetic Resonance Linewidth and Gyromagnetic Ratio of Nonmetallic Magnetic Materials*, West Conshohocken, PA: ASTM International, December 2001.
- [14] Mo, N., J. J. Green, B. A. Beitscher, C. E. Patton, "High Precision Metrology Based Microwave Effective Linewidth Measurement Technique," *Review of Scientific Instruments*, November 19, 2007.
- [15] ASTM A893/A893M, *Standard Test Method for Complex Dielectric Constant of Nonmetallic Magnetic Materials at Microwave Frequencies*, West Conshohocken, PA: ASTM International, June 2008.
- [16] Dydyk, M., "Take Two Steps toward Better Circulator Design," *Microwaves*, March 1979, pp. 53–62.
- [17] Green, J. J., and F. Sandy, "A Catalog of Low Power Loss Parameters and High Power Thresholds for Partially Magnetized Ferrites," *IEEE Transactions on Microwave Theory and Techniques*, June 1974, pp. 645–651.
- [18] O'Neil, B. K., and J. L. Young, "Experimental Investigation of a Self-Biased Microstrip Circulator," *IEEE Transactions on Microwave Theory and Techniques*, July 2009, pp. 1669–1674.
- [19] *Magnet Catalog P5A*, Hicksville, NY: Permag Corp., 1986.
- [20] Dexter Magnetic Technologies, <http://www.dextermag.com>. Last accessed Nov. 14, 2013.
- [21] Carlisle, B. H., "Neodymium Challenges Ferrite Magnets," *Machine Design*, January 9, 1986, pp. 24–30.
- [22] *Military Standard MIL-STD-889B*, July 1976.

5

Electrical Design

5.1 Junction Circulators

After we have an understanding of the basic theory of operation of the circulator (the tensor permeability of ferrite), and have written a set of specifications for the circulator to be designed, we proceed to select a ferrite material using the criteria outlined in Chapter 4. The next steps in the design process are the sizing of the ferrite parts, selection of the correct position of the ferrites in the circulator, and synthesis of impedance-matching networks. For coaxial circulators, appropriate center conductor geometries must be chosen. The magnetic design and mechanical design of the circulator are covered in Chapters 6 and 7.

5.1.1 Basic Principles

We begin this chapter with a discussion of the propagation of microwave energy in the circulator junction [1]. The junction circulator is based on two counter-rotating wave components or modes. As we know from Chapter 2, a circulator is a device with ports arranged such that energy entering a port is coupled to an adjacent port, but not coupled to the other ports. With this in mind, we can analyze the rotating modes shown in Figure 5.1. A three-port circulator is depicted in this figure, but the analysis could be extended for any number of ports. Usually, however, junction circulators with more than three ports are made by simply cascading three-port circulators.

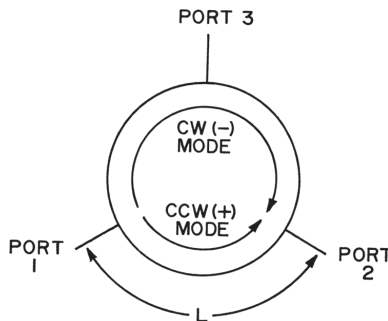


Figure 5.1 Rotating modes in a three-port circulator.

The two modes shown in Figure 5.1 must travel at different velocities for circulator action to occur. For coupling from port 1 to port 2, the clockwise (−) and counterclockwise (+) modes must differ in phase by $N2\pi$:

$$2\beta_- L - \beta_+ L = 2N\pi \quad (5.1)$$

where β is the phase constant of the positive or negative mode. Note that the negative wave must travel twice the distance the positive wave travels to reach port 2. N denotes any integer and L is the distance traversed by a wave. For port 3 to be decoupled or nulled, the two wave components arriving at this port must differ in phase by an odd multiple of π :

$$-\beta_- L + 2\beta_+ L = (2M - 1)\pi \quad (5.2)$$

where M is any integer. If we solve (5.1) and (5.2) simultaneously, we derive

$$\beta_- L = \frac{4N + 2M - 1}{3}\pi \quad (5.3)$$

$$\beta_+ L = \frac{2N + 4M - 2}{3}\pi \quad (5.4)$$

When (5.3) and (5.4) are satisfied, we have perfect circulation.

The two counter-rotating waves propagate in a ferrite disk with propagation constants given by (1.37) and (1.38) when the disk is biased with a dc magnetic field parallel to its axis (transverse to the direction of propagation). The waves form standing-wave patterns as shown in Figures 5.2 and 5.3 for disks and triangles, respectively. Any ferrite shape that has threefold symmetry could be used, but the two simplest shapes are the disk and the triangle. These shapes are the ones used in nearly all commercial circulators.

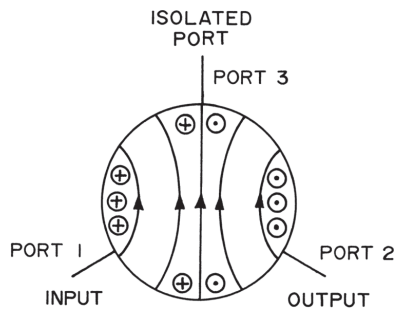


Figure 5.2 Ferrite disk standing-wave pattern. RF electric field lines are perpendicular to the disk plane, and the magnetic lines are parallel to the disk plane.

The standing-wave pattern for an unmagnetized ferrite disk is shown in Figure 5.4. Notice the difference between this pattern and the one for a magnetized disk in Figure 5.2: it is slightly rotated. In an unmagnetized disk (or triangle) the phase and amplitude of the signals appearing at ports 2 and 3 are equal and, ideally, the VSWR at port 1 is 2:1. The two rotating modes are said to be degenerate; the disk resonances due to them are at the same frequency. When a dc magnetic field is applied to the ferrite, the propagation constants of the positive and negative rotating modes are no longer equal, and the resonant frequencies for the two modes, ω_+ and ω_- , are different. The standing-wave pattern rotates, and the coupling to ports 2 and 3 from port 1 is not the same. The operating frequency of the circulator is between the disk resonant frequencies due to the two counter-rotating modes.

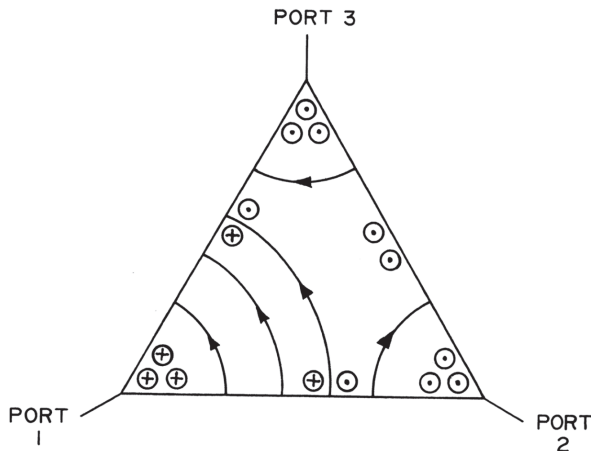


Figure 5.3 Ferrite triangle standing-wave pattern.

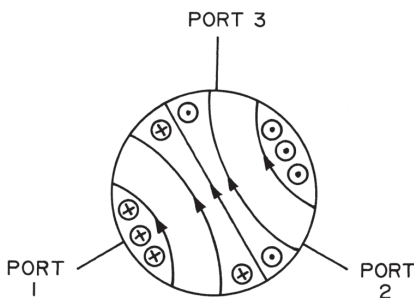


Figure 5.4 Unmagnetized ferrite disk standing-wave pattern.

The factor κ/μ from (1.39) not only relates orthogonal microwave magnetic field components, but describes the amount of frequency splitting between the two resonance frequencies for the counter-rotating modes. It also determines the amount of rotation of the standing-wave pattern and the anisotropy of the ferrite; κ and μ are elements of the Polder permeability tensor, defined by (1.30) to (1.33).

Depending on the type of circulator, the ferrite disks or triangles could be resonators, or the center conductor could include a resonator. Regardless of which object is the resonator, we need an algorithm for determining the size of these resonators from the circulator specifications. Engineers with experience in the design of circulators usually have repertoires of geometries in their memories upon which they can call when asked. Unfortunately, someone with no experience in circulator design has no idea where to start. We could print tables of ferrite dimensions in a book, but normally the needed information would have to be interpolated from the tables. Now, we need to know how to interpolate and arrive at a usable design. It is also helpful to learn the effects of changes in the various circulation parameters. For these reasons, and because most circulator manufacturers are unwilling to part with their valuable design data, we will not present tables.

A complicating factor in the presentation of specific circulator design information is that no universal equations exist that will, in all cases, produce working circulators. Much of circulator design [2] has “proceeded on an empirical basis.” This is not to say that we should not look at the equations that have been derived, because they do have value in that they can teach the relationships between the various circulator parameters. In addition, some concepts, such as the permeability tensor, are difficult if not impossible to visualize without the use of mathematics.

5.1.2 Historical Papers

To begin our development of resonator- or ferrite-sizing algorithms, we will briefly describe some papers by early workers in the circulator industry: Bosma [3], Fay and Comstock [4], Helszajn [5, 6, 7], Davies [8], Auld [9], Simon [10], and Green and Sandy [11]. We will present not all the mathematical details from these papers, only some results. All of these papers are required reading for the circulator expert.

The papers include approximations and assumptions to simplify the mathematics (which is one reason no universal, exact design equations exist), some of which include the following:

1. The ferrites are usually considered loss-less and magnetically saturated to avoid low-field losses.
2. Fringing at the edges of striplines is ignored.
3. The field intensities do not vary over the width of stripline conductors.
4. Striplines are purely in the TEM mode.
5. There is no z -coordinate variation of electromagnetic fields in the ferrites.
6. Coaxial center conductors are between two ferrites (the fields are the same on both sides of the conductor).
7. The electromagnetic fields fall off immediately at the ferrite and center conductor edges.

The paper by Bosma [3] is concerned with the stripline above-resonance circulator. He states that the magnetic bias applied to this type of circulator is more than four times greater than the field required for resonance in most cases. Bosma uses a scattering matrix approach to circulator synthesis. A scattering matrix is a matrix (3 by 3 in the case of a circulator) of reflection coefficients and transmission coefficients that describe the circulator junction. The matrix lends itself to devices that are symmetrical. The ferrite disks and center conductor are assumed to have the same diameters, and are arranged as shown in Figure 2.13. Figure 5.5 indicates the key dimensions of the stripline center conductor. These dimensions are related by

$$\sin \psi = \frac{W}{2R} \quad (5.5)$$

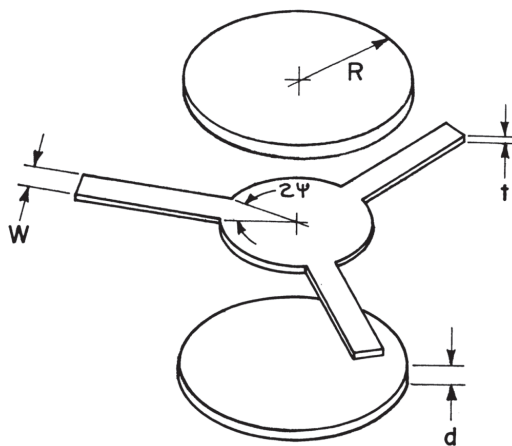


Figure 5.5 Stripline center conductor and ferrite dimensions.

The effective relative permeability of the magnetized ferrite, a factor in (1.37), is given by

$$\mu_{\text{eff}} = \frac{\mu^2 - \kappa^2}{\mu} \quad (5.6)$$

Bosma also introduces a wave number:

$$k^2 = \omega^2 \mu_0 \epsilon_0 \mu_{\text{eff}} \epsilon \quad (5.7)$$

He presents equations for the electric field, parallel to the z -axis (ferrite disk axis), and the magnetic fields, tangential and radial components, in the ferrites. These equations are related by a Green's function, and expressions for the relations between the fields in the striplines and the fields in the ferrites are derived. The Green's function can be thought of as a transfer impedance function for the electromagnetic fields in the ferrites.

The solutions of the electromagnetic field equations involve the Bessel function of the N th order. For most practical circulators, $N = 1$ and for resonance we have

$$J_1'(kR) = 0 \quad (5.8)$$

where J denotes the Bessel function, k is the wave number from (5.7), and R is the ferrite disk radius. If we evaluate (5.8), we find that $kR = 1.84$. This equation

is valid when the ferrites are not magnetized (i.e., when the rotating modes are degenerate). Because the resonance frequency from (5.8) is between the two resonance frequencies for the two counter-rotating modes when the disks are magnetized, it is an approximation of the operating frequency of the circulator.

Bosma explains that $\omega (\mu_0 \epsilon_0)^{1/2} = 2\pi/\lambda$ and derives from (5.7) and (5.8):

$$R = \frac{1.84\lambda}{2\pi\sqrt{\mu_{\text{eff}}\epsilon}} \quad (5.9)$$

where ϵ is the relative dielectric constant of the ferrite material. To obtain a simpler expression for μ_{eff} than (5.6), he assumes that $\omega_0^2 \gg \omega^2$ because the ferrites are biased far above resonance and $\omega_0^2 \gg \alpha^2$ because the resonance losses need not be considered, and by manipulation of the equations for μ and κ —(1.30) to (1.33)—derives

$$\mu_{\text{eff}} = \mu = \frac{H_{\text{dc}} + M_0}{H_{\text{dc}}} \quad (5.10)$$

$$\kappa = \frac{M_0}{H_{\text{dc}}^2} \quad (5.11)$$

The imaginary components of μ and κ do not need to be considered because the ferrites are biased far above resonance.

Substituting (5.10) into (5.9), we arrive at an expression for the ferrite disk radius as a function of wavelength, ferrite saturation magnetization, dielectric constant, and applied magnetic field:

$$R = \frac{1.84\lambda}{2\pi\sqrt{\epsilon}} \sqrt{\frac{H_{\text{dc}}}{H_{\text{dc}} + 4\pi M_S}} \quad (5.12)$$

Bosma suggests restrictions on stripline width to maintain the magnetic field in the ferrite as high as possible, a desired operating point for above-resonance circulators:

$$W < \frac{\lambda}{30} \quad (5.13)$$

$$W < 0.75R \quad (5.14)$$

W should not, however, be made too small, because losses and large stray fields will result.

Also presented in Bosma's paper is an equation for the circulator bandwidth:

$$\frac{f_2 - f_1}{f_0} = 2.90 \frac{\kappa}{\mu} \rho \quad (5.15)$$

where ρ is the maximum voltage reflection coefficient in the band, related to the circulator VSWR by (2.4). The bandwidth is proportional to the ratio κ/μ , which also describes the amount of splitting between the resonant frequencies due to the two counter-rotating modes. When the splitting is greater, there is not so much variation in bandwidth-reducing quantities. The implication of (5.15) to achieve large bandwidths is to operate the circulator very near to the ferrimagnetic resonance, which leads to high insertion loss.

Bosma defines the circulator input impedance as

$$Z = Z_0 - jZ_0 \frac{1.38}{\frac{\kappa}{\mu}} \frac{f - f_0}{f_0} \quad (5.16)$$

where f is the frequency where the impedance is to be evaluated, and Z_0 is the stripline characteristic impedance. We can see that this impedance behaves like a parallel resonant circuit: inductive for $f < f_0$ and capacitive for $f > f_0$. The paper states that the bandwidth of the circulator can be increased by adding series-resonant circuits at each of the three ports.

Fay and Comstock [4] describe the stripline circulator junction as being equivalent to a transmission cavity with one port isolated. They state that two counter-rotating modes are present in the magnetized ferrite disks, and the standing wave patterns are like the ones in Figures 5.2 and 5.4. The two rotating modes are said to have opposite reactive components of impedance, so that the net impedance at the operating frequency is real. The directions of circulation are opposite for below- and above-resonance operating points.

This paper also presents electromagnetic field equations for the biased ferrite. Equations (5.6) and (5.7) are asserted and the solutions of the field equations are given as

$$J_0(kR) - \frac{J_1(kR)}{kR} \left(1 + \frac{\kappa}{\mu} \right) = 0 \quad (5.17)$$

$$J_0(kR) - \frac{J_1(kR)}{kR} \left(1 - \frac{\kappa}{\mu} \right) = 0 \quad (5.18)$$

for the lowest order, $N = 1$ modes. The signs in front of the κ/μ terms correspond to the positive and negative rotating modes.

Fay and Comstock discuss the variation in mode splitting (κ/μ) with frequency relative to the ferrimagnetic resonance frequency (ω_0/ω).

Mode splitting refers to the amount of frequency splitting (difference in frequency) between the two resonance frequencies of the counter-rotating modes in the ferrite. The counter-rotating modes or waves have the same resonant frequencies when no dc magnetic field is applied to the ferrite, but when a magnetic bias is applied, the propagation constants of the two modes are no longer equal and the resonance frequencies become different. Insofar as the circulator operates between the two resonant frequencies, the circulator bandwidth is related to the amount of mode splitting. As described previously in this section, the operation of the junction circulator is based on the two counter-rotating wave components or modes.

Splitting is greatest at frequencies above ferrimagnetic resonance (below-resonance magnetic operating point). This indicates that greater bandwidths can be obtained using below-resonance circulators. Fay and Comstock also observe that the amount of splitting varies rapidly with saturation magnetization in the below-resonance region; hence the choice of $4\pi M_S$ is more critical for below-resonance circulators.

The Fay and Comstock paper also contains (5.8) as a solution of the field equations for the degenerate case. The wave admittance of the circulator at the center frequency of operation is

$$G_r = \frac{Y_{\text{eff}} \left| \frac{\kappa}{\mu} \right|}{\sin \psi} \quad (5.19)$$

where Y_{eff} is the intrinsic wave admittance:

$$Y_{\text{eff}} = \sqrt{\frac{\epsilon \epsilon_0}{\mu_0 \mu_{\text{eff}}}} \quad (5.20)$$

The paper describes the derivation of the loaded Q of the circulator junction from the energy stored in the ferrites and the amount of power coupled to the striplines. The result is

$$Q_L = 1.48 \frac{\omega R^2 \epsilon \epsilon_0}{G_r d} \quad (5.21)$$

where d in the denominator of this equation is the thickness of the ferrite disks. Fay and Comstock go on to develop expressions for the unloaded Q of the ferrite resonators that could be used to approximate the insertion loss of the circulator junction. For most below-resonance circulators, the unloaded Q is given by

$$Q_u = \frac{1}{\frac{\gamma^2 4\pi M_S \Delta H}{2\omega^2} + \tan \delta} \quad (5.22)$$

where $\tan \delta$ is the dielectric loss tangent of the ferrite material. The first term in the denominator of (5.22) represents the magnetic losses. The exact expression for the unloaded Q due to magnetic losses is $\mu_{\text{eff}}'/\mu_{\text{eff}}''$, which is difficult to evaluate without the approximations used.

The insertion loss of the circulator junction is approximately given by

$$\text{InsertionLoss}(dB) = -10 \log_{10} \left(1 - \frac{Q_L}{Q_u} \right) \quad (5.23)$$

This paper asserts that the rotating modes should each have 30° phase angles at the circulator center frequency. Because of this, the splitting of the modes is related to the loaded Q by

$$\frac{\omega_+ - \omega_-}{\omega} = \frac{\tan 30^\circ}{Q_L} = \frac{0.577}{Q_L} \quad (5.24)$$

Fay and Comstock describe the electrical equivalent circuit of the circulator input impedance as a parallel-resonant one. For narrow bandwidths, the circulator VSWR is related to the junction admittance and its phase angle as follows:

$$\text{VSWR} = \frac{Y_r^2}{G_r^2} = \sec^2 \theta \quad (5.25)$$

The circulator synthesis procedure suggested in this paper starts with the specified VSWR for the circulator, from which we find the admittance phase angle from (5.25). Next, we calculate the required Q_L from

$$Q_L = \frac{\tan \theta}{\frac{f_2 - f_1}{f_0}} \quad (5.26)$$

Once Q_L is known, we can find the required amount of counter-rotating mode frequency splitting using (5.24). Because the splitting is approximately proportional to κ/μ , we relate κ/μ to Q_L with a constant:

$$\frac{\kappa}{\mu} = \frac{0.71}{Q_L} \quad (5.27)$$

The required κ/μ can sometimes be realized in both the above- and below-resonance operating regions if the frequency is in the zone where the two regions overlap. The next step in the synthesis procedure would be to select the operating region and ferrite material based on the criteria presented in Chapters 2 and 4. Once the saturation magnetization of the ferrite is known, the disk radius is calculated using (5.6), (5.7), and (5.8). A simplification of (5.6) applies if the circulator is operated in the below-resonance region and the ferrite is just-saturated (internal magnetic field = 0):

$$\mu_{\text{eff}} = 1 - \kappa^2 = 1 - \frac{\gamma^2 M_0^2}{\omega^2} \quad (5.28)$$

Fay and Comstock suggest the use of a quarter-wavelength impedance transformer to match the circulator junction to the system characteristic impedance (typically 50Ω). From the known bandwidth and phase angle of the junction admittance—(5.25)—a characteristic impedance for the quarter-wavelength transformer can be determined, either by graphical means with a Smith chart or numerically. After the transformer impedance is known, the circulator junction conductance is found by transformation of the system characteristic admittance through the quarter-wavelength transformer. The last step in the circulator synthesis procedure is to calculate the ferrite disk thickness using (5.21).

The Fay and Comstock paper goes on to briefly discuss H -plane and E -plane waveguide junction circulators. The H -plane circulator is constructed from a symmetrical waveguide junction in the H -plane, with ferrite material placed in the center as shown in Figure 5.6. The ferrite is generally excited by the transverse RF H -field in the waveguide, because the rectangular waveguide usually operates in the TE_{10} mode and the ferrite is small in comparison to the width of the waveguide. The amount of coupling to the ferrite can be

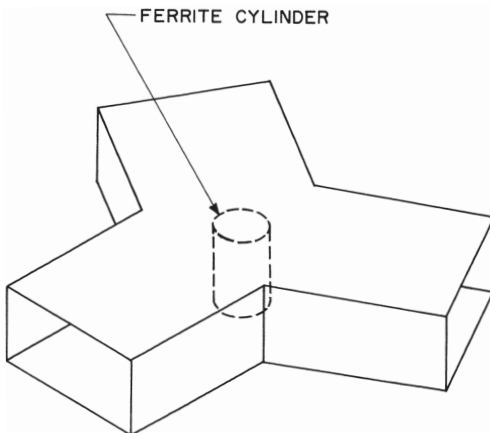


Figure 5.6 *H*-plane waveguide junction circulator construction.

limited by placing irises at each of the three waveguides where they enter the center section of the circulator. The center section then becomes the circulator junction and the air in this area must be included in the analysis. If the irises are not used, the boundaries of the center cavity are not clearly defined, which leads to some of the difficulties involved in the analysis of waveguide junction circulators. Reduced-height (low-impedance) waveguide is often used to construct these circulators.

E-plane circulators contain ferrites that are excited by the longitudinal RF *H*-fields. Usually, no ferrite is present in the center of the junction because it would not be active magnetically. This device is very different from the stripline junction circulator in that the striplines have no longitudinal RF *H*-fields.

Helszajn [5] describes an approximation of Q_L as a function of κ/μ in his paper, “Quarter-Wave Coupled Junction Circulators Using Weakly Magnetized Disk Resonators.” He claims that the approximation is valid for values of κ/μ to 0.3, which corresponds to a minimum achievable Q_L of about 2. The fact that the theory applies to weakly magnetized ferrites implies that it is only valid for below-resonance designs.

He states that Q_L is nearly independent of ψ , considering the conditions imposed. The approximation for Q_L is derived from the equations presented by Bosma, Fay, and Comstock, and includes a second-order polynomial correction factor to make the classic values of Q_L match other theoretical Q_L values calculated by other means. The approximation is

$$Q_L = 0.689 \frac{\mu}{\kappa} + \left(0.0463 - 2.6318 \frac{\kappa}{\mu} + 3.5513 \frac{\kappa^2}{\mu^2} \right) \quad (5.29)$$

Helszajn presents equations for the parameters of the complex gyrator equivalent circuit of the circulator:

$$G_r = \frac{Y_0(r - \sin^2\theta)}{r \cos^2\theta} \quad (5.30)$$

$$B' = \frac{\pi Y_0}{4} \frac{\sqrt{r - \sin^2\theta}}{r \cos\theta} (r - 1) \tan^2\theta \quad (5.31)$$

$$Q_L = \frac{\pi(r - 1) \sin\theta \tan\theta}{4 \sqrt{r - \sin^2\theta}} \quad (5.32)$$

where Y_0 is the system characteristic admittance (usually 0.02S), r is the circulator input VSWR, and θ is defined as follows:

$$\theta = \cos^{-1} \left\{ 0.707 \cos \left[\frac{\pi}{2} \left(1 + \frac{f_2 - f_1}{2f_0} \right) \right] \right\} \quad (5.33)$$

The paper presents the relations of Q_L , B , and G_r to the circulator junction parameters:

$$G_r = \frac{0.0192 \sqrt{\epsilon}}{\sqrt{\mu_{\text{eff}}} k R \sin \psi \ln \left(\frac{W+t+2d}{W+t} \right)} \frac{\kappa}{\mu} \quad (5.34)$$

$$B = \frac{0.0111 \sqrt{\epsilon}}{\sqrt{\mu_{\text{eff}}} \sin \psi \ln \left(\frac{W+t+2d}{W+t} \right)} \frac{J_1'(kR)}{J_1(kR)} \quad (5.35)$$

$$B' = \frac{0.0111 \sqrt{\epsilon}}{\sqrt{\mu_{\text{eff}}} \sin \psi \ln \left(\frac{W+t+2d}{W+t} \right)} \frac{(kR)^2 - 1}{2kR} \quad (5.36)$$

$$Q_L = 0.689 \frac{\mu}{\kappa} \quad (5.37)$$

where t is the thickness of the stripline center conductor. At the circulator center frequency, $B = 0$ because $J_1'(kR) = 0$. B' is the susceptance slope

parameter. Equation (5.37) is the classic approximation for Q_L , which is replaced by (5.29) in Helszajn's paper.

Insofar as this paper is about weakly magnetized ferrites, we again apply the approximation of (5.28). A more accurate expression for B' can be obtained by deriving the product of (5.34) and (5.29).

The paper offers equations for the design of a quarter-wavelength impedance transformer to match the circulator junction impedance to the system characteristic impedance. One of these is

$$Z_t = \frac{1}{\sqrt{rG_rY_0}} \quad (5.38)$$

G_r in this equation is calculated from the specifications for the circulator—(5.30). After G_r , B' , and Q_L are calculated from the circulator specifications using (5.30) to (5.32), the junction parameters are adjusted until the results from (5.29), (5.34), and (5.36) match the previously calculated values.

“Design Data for Radial-Waveguide Circulators Using Partial-Height Ferrite Resonators,” a paper by Helszajn and Tan [6], presents design information for H -plane waveguide junction circulators. The three geometries considered in the paper are shown in Figure 5.7. Figure 5.7(a) depicts a half-wavelength long ferrite cylinder open-circuited at both ends, 5.7(b) shows two quarter-wavelength ferrite disks coupled in the middle of the waveguide junction, and a single quarter-wavelength ferrite disk resonator is shown in Figure 5.7(c). The analysis of all three geometries is very similar. The performance of all three is also similar, but (c) is the simplest and uses the least amount of ferrite. The geometry shown in Figure 5.7(c) also has better parameter flexibility than the other two.

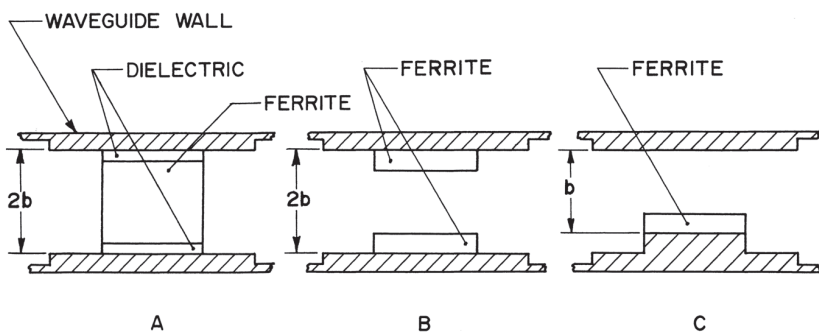


Figure 5.7 Waveguide junction circulator geometries (edge views).

Helszajn and Tan state the circulator boundary conditions in terms of scattering matrix coefficients. They assert that $kR = 1.84$ for the degenerate case of the counter-rotating modes. The configurations described support axially resonating modes associated with the HE_{11} dielectric waveguide mode. The junction resonances can also be quantified using the theory of open dielectric resonators. The solution recommended in the paper is that of the TM_{111} resonator. The equation to be used for selection of resonator R and d dimensions is

$$k_0 R = \frac{1}{\sqrt{\epsilon}} \sqrt{\left(\frac{\pi R}{2d}\right)^2 + (1.84)^2} \quad (5.39)$$

where $k_0 = 2\pi/\lambda_0$. The value of d is the ferrite disk thickness in Figures 5.7(b) and (c), and half the ferrite cylinder length in Figure 5.7(a). There are many possible values of d and R that will satisfy (5.39). For large R/d , the resonance frequency depends mainly on d .

Where an image plane (an imaginary plane between the two coupled ferrite in Figure 5.7(b) or a waveguide wall is in close proximity to a ferrite resonator, the resonant frequency will be perturbed. Helszajn and Tan suggest a correction factor for the resonator length (d):

$$\Delta d = \frac{1}{\beta} \tan^{-1} \left[\frac{\epsilon \sqrt{k^2 - k_0^2}}{\beta} \tanh(s \sqrt{k^2 - k_0^2}) \right] - d \quad (5.40)$$

where β is a wave number that can be approximated by $\pi/2d$. The spacing between resonators or between resonator and image plane is represented by s .

The concept of the characteristic plane is discussed in this paper. The characteristic plane has several useful properties. First, it determines the point in the H plane where the impedance transformer should be connected. The admittances at each port of the circulator junction relative to the characteristic planes are related in a specific manner. Another property of the characteristic plane is that if there is a short circuit placed at this plane of one port, a sympathetic short circuit will also occur at the characteristic planes of the other ports. If a short circuit is placed at the output characteristic plane of a circulator, the input signal will be entirely reflected and the third port theoretically nulled.

The locations of the characteristic planes are specified by R_0 , the radial distance from the center of the circulator junction to the plane. The value of $k_0 R_0$ is approximately 3.45 when $k_0 R = 1$, and $k_0 R_0$ does not vary greatly with $k_0 R$, but climbs slightly when $k_0 R$ goes above or below 1; $k_0 R_0$ does not usually exceed 4.

Helszajn and Tan indicate that a suitable value for the physical dimensional ratio d/b is between 0.7 and 0.85.

In the paper “Planar Triangular Resonators with Magnetic Walls,” Helszajn and James [7] present field patterns for triangular ferrite resonators and magnetic field equations obtained by duality from TE mode equations.

The $TM_{1,0,-1}$ mode is dominant for a triangular resonator, and this is the mode for the counter-rotating circulator modes. The resonance frequency for this mode can be calculated from

$$kA = 3.63 \quad (5.41)$$

where A is the altitude or height of the triangle. The value of A needs to be corrected, say Helszajn and James, to compensate for fringing because the edges of the triangle are not ideal magnetic walls:

$$A_{\text{eff}} = A + \frac{d}{4} \quad (5.42)$$

Again, d is the ferrite thickness. Equation (5.42) applies when $A/d > 4$.

The paper presents some experimental data for two circulators: one built with a disk resonator, and one built with a triangular resonator. The data show that the insertion loss of the triangular junction is about 17% lower than the disk junction loss.

The paper by Davies [8] is a circulator analysis that describes matching cylindrical modes in the ferrite to associated modes in the waveguide junction outside the post, then in turn matching these modes to the rectangular waveguide modes. This results in a large number of equations and unknowns, but because some waveguide modes can be ignored, approximations emerge.

Perfect circulation is predicted for certain values of ferrite radius, κ , and μ . The basic concepts presented in this paper are the same as those already summarized, but the approach of mode matching is a little different.

Auld [9] presents a scattering-matrix method of synthesizing waveguide junction circulators. He asserts that once a particular symmetry for the circulator has been selected, the nature of the adjustments required to obtain the specified performance are suggested by the symmetry, and the range of adjustment must be experimentally determined.

Auld proposes that adjustments to the circulator junction should take the form of bending and denting the waveguide walls and placing any type of material in the junction. He later states that only the ferrite radius and magnetic field need to be adjusted.

According to Auld, the ferrite radius should be determined experimentally. This is done without magnetic bias, adjusting the ferrite radius until the VSWR is 2:1. The radius is then readjusted after magnetic bias is applied to achieve circulation.

He states that the adjustment of the circulator (determination of ferrite radius) is simplified if a metal pin is added axially through the center of the ferrite. Auld suggests that the ferrite should be rotated to cancel asymmetries.

Simon [10] describes the experimental development of a series of octave-bandwidth circulators covering 0.6–8.0 GHz. These are all below-resonance stripline devices.

He writes of the development process as primarily an impedance-matching problem. His first step was to study the impedance characteristic of the basic circulator junction, varying ferrite and structural parameters to arrive at a combination that was easy to match. For a broad bandwidth match, the reactive component of the impedance must be as low as possible.

The striplines, including those between the ferrite disks, were chosen to have a characteristic impedance of 50Ω in air. The ground-plane spacings for the 1–2 GHz and 2–4 GHz circulators were 0.500 and 0.265 inches, respectively. The stripline center conductors had geometries as depicted in Figure 5.8.

The ferrite disk diameters suggested by Simon for the octave-bandwidth circulators are presented in Figure 5.9 in graphical form, as he presents them.

His second step in the development process was to develop matching structures to achieve the desired octave-bandwidth performance. The impedance characteristics from the first step were adjusted to be approximately resistances, lower in value than 50Ω . Simon found that quarter-wavelength transformers (one at each port) were all that was required to achieve 20 dB isolation, 0.5 dB insertion loss, and 1.25:1 VSWR over the octave bandwidth

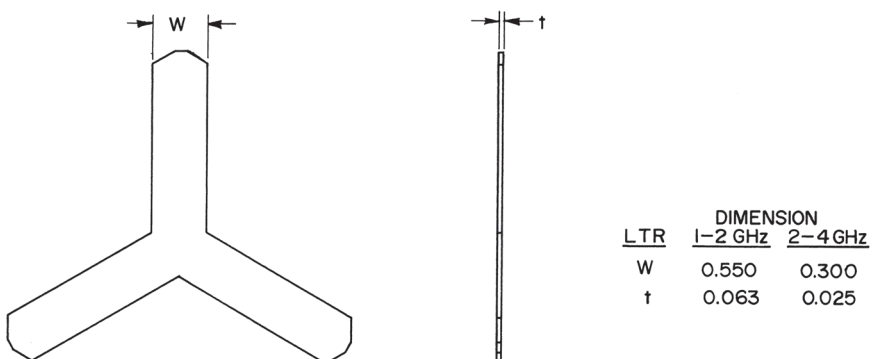


Figure 5.8 Stripline center conductor geometries used by Simon [10].

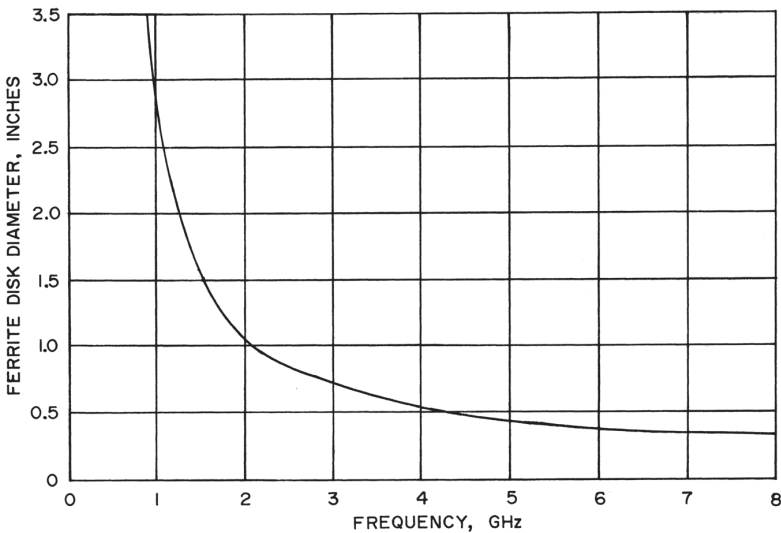


Figure 5.9 Suggested ferrite disk diameters for octave-bandwidth circulators from Simon [10].

for most of the circulator junctions. The lowest frequency circulator also required the use of a quarter-wavelength open-circuited stub, to cancel the reactive component of the junction.

Green and Sandy [11] characterized the microwave permeability of some partially magnetized ferrites and present this data along with empirical equations that closely match the measured data in their paper.

The permeability measurements were made using ferrite rods in cylindrical TM_{110} cavities. Although junction circulators do not normally utilize partially magnetized ferrites, the equations presented are useful for the design of other ferrite devices.

The first equation is from Rado:

$$\kappa' = \frac{\gamma 4\pi M}{\omega} \quad (5.43)$$

where $4\pi M$ is the ferrite magnetization, not to be confused with the saturation magnetization. The permeability for the completely demagnetized state, by Schloemann, is

$$\mu_0' = \frac{2}{3} \sqrt{1 - \left(\frac{\gamma 4\pi M_S}{\omega} \right)^2} + \frac{1}{3} \quad (5.44)$$

Finally, Green and Sandy present two equations for which no physical basis is claimed. Because the ferrite is not saturated, the permeability in the direction the dc magnetic field is applied (z -axis) is not 1:

$$\mu_z' = \mu_0' \left(1 - \frac{4\pi M}{4\pi M_s}\right)^{5/2} \quad (5.45)$$

$$\mu' = \mu_0' + (1 - \mu_0') \left(\frac{4\pi M}{4\pi M_s}\right)^{3/2} \quad (5.46)$$

Some of the variable symbols in the papers summarized here do not match the symbols anywhere in this book; we want to keep variable symbols internally consistent.

Having completed the descriptions of some of the more important papers regarding the synthesis of circulators, we now proceed to develop design procedures for several classes of junction circulators.

5.1.3 Above-Resonance Approximations

First, we will consider the above-resonance stripline junction. Bosma's paper [3] deals with the above-resonance device, so we utilize some of the equations he presented. If the ferrites are magnetically biased far above resonance, it is true that $\omega_0^2 \gg \alpha^2$ because ω_0 is proportional to H by virtue of (1.7). Insofar as α is proportional to the ferrimagnetic resonance losses—(1.9)—we can also write $\omega_0^2 \gg \alpha^2$ due to the fact that we have chosen our magnetic operating point far above resonance. Using the preceding assumptions and (1.30), ignoring the loss component, which should be insignificant (see (1.31)), and substituting, as in (1.7), γH_{dc} for ω_0 , we arrive at (5.10).

Because κ is much smaller than μ for practical above-resonance operating points, we reduce (5.6) (also a factor in (1.37)) to $\mu_{eff} = \mu^2/\mu = \mu$.

We can find the resonator radius if we know the wavelength for which we want it to be resonant, the ferrite permeability (μ_{eff}), and the ferrite dielectric constant. From the circulator specifications we know the wavelength, and from the specifications for the ferrite material chosen we know the dielectric constant. We must calculate the effective permeability from H_{dc} and M_0 .

Insofar as the ferrite material will be saturated by the dc magnetic field, the ferrite magnetization (M_0) will equal the ferrite saturation magnetization

$(4\pi M_S)$. Having already selected ferrite material, we know the saturation magnetization. We now select a value of magnetic field, H_{dc} . Bosma suggests that the field should be at least four times greater than the field required for resonance, so we adopt a rule of thumb with the help of (1.7):

$$H_{dc} = \frac{4\omega}{\gamma} = 1.4f_0 \text{ (MHz), Oe} \quad (5.47)$$

Two other considerations influence the choice of H_{dc} : the desired bandwidth and maximum allowable insertion loss. If H_{dc} is set too low, resonance losses will occur at the upper-band edge of the circulator response. Figure 5.10 shows insertion loss *versus* H_{dc} for several values of resonance line width. A saturation magnetization of 1800G was used to calculate these curves, but this is not a critical parameter. For an above-resonance circulator, the resonance losses are highest at the upper-band edge, so this frequency should be used to evaluate the loss.

We calculate the losses using (1.30) to (1.33), (5.6), and (5.23). The unloaded Q is μ_{eff}'/μ_{eff}'' and Q_L is approximated by (5.27).

The bandwidth without any impedance transformers or matching circuits is related to the amount of splitting between the resonant frequencies of the counter-rotating modes by (5.15).

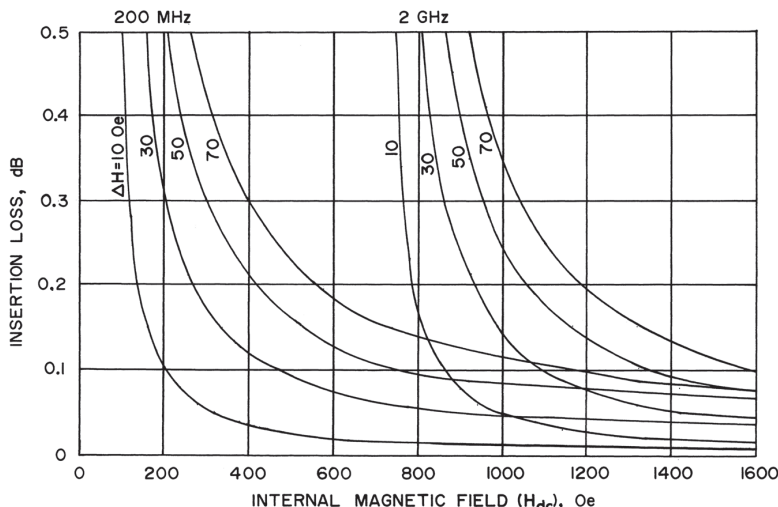


Figure 5.10 Insertion loss versus internal magnetic field. $4\pi M_S = 1800$ G.

From (5.10) and (1.27) we can derive an approximation for κ/μ based on the previously stated assumptions:

$$\frac{\kappa}{\mu} = \frac{M_0 \omega}{\gamma H_{dc} (H_{dc} + M_0)} \quad (5.48)$$

We see from this expression that decreasing H_{dc} will increase bandwidth (but also increase insertion loss), as will increasing M_0 .

Once we have established H_{dc} , we proceed to calculate the resonator disk radius using (5.9) and (5.10). Next, we find the required loaded Q (Q_L) and resonator conductance (G_r) from the specified circulator VSWR and bandwidth with (5.30), (5.32), and (5.33). Fay and Comstock also presented equations to calculate Q_L from bandwidth and VSWR, but the equations due to Helszajn are useful for a broader range. The ferrite disk radius can be read from Figure 5.11, where it is plotted against μ_{eff} for several values of dielectric constant. Curves for Q_L and G_r , versus bandwidth with VSWR as a parameter are shown in Figures 5.12 and 5.13, respectively. The bandwidth in (5.30), (5.32), and (5.33) and in the figures is the bandwidth that can be achieved using one quarter-wavelength impedance-matching transformer at each port.

From Q_L and G_r , we compute the ferrite disk thickness using (5.21). We must avoid two pitfalls here. One is that the ferrite may be so thin that it

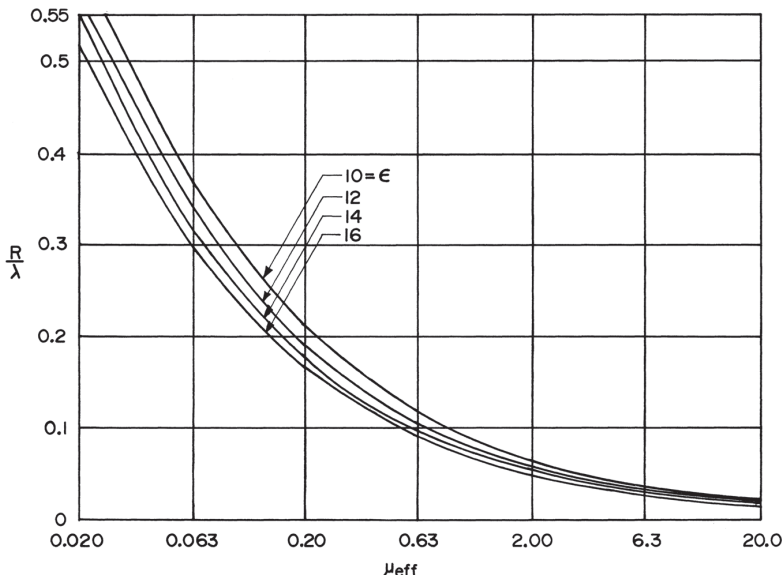


Figure 5.11 Disk radius versus μ_{eff} .

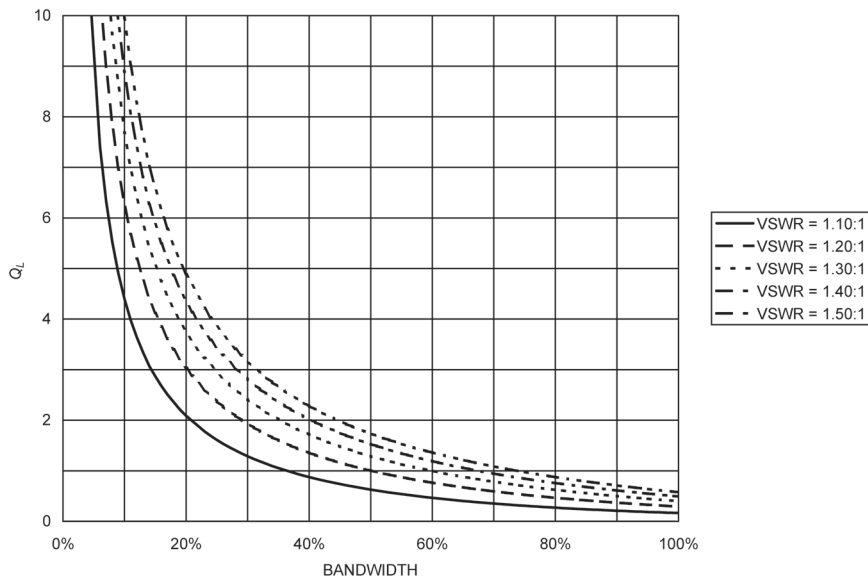


Figure 5.12 Ferrite disk resonator loaded Q versus bandwidth for one quarter-wavelength transformer.

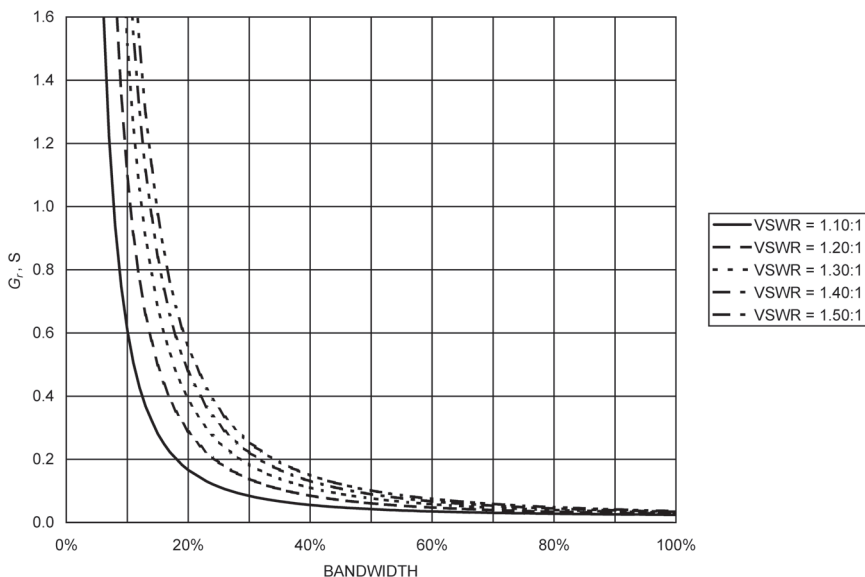


Figure 5.13 Ferrite disk junction conductance versus bandwidth for one quarter-wavelength transformer.

cannot be manufactured. The solution to this problem is to increase the bandwidth, which will result in a thicker ferrite disk. The advantage of a narrow bandwidth is low loss in the ferrite, but this may be negated by high circuit losses because the high junction conductance requires impedance-matching circuitry having inherently higher losses.

The other pitfall is that the disk may be so thick, and hence the ground plane spacing so large, that higher-order modes can propagate. The cut-off wavelength of the first higher-order mode is approximately given [12] by

$$\lambda_C = \sqrt{\epsilon}(2W + 3.172d) \quad (5.49)$$

Another approximation is to see that $d \ll \lambda/4$ at the operating frequency of the circulator.

The stripline width (W) at the circulator junction has an effect on the amount of coupling to the resonator. A wider strip increases the coupling because it couples into the two counter-rotating modes over a wider range of frequencies. The angular position of the nodes and antinodes of the standing-wave pattern in the ferrite disk changes with frequency, so a wider strip accommodates a wider range of frequencies.

If the width is chosen too wide, the RF magnetic field in the ferrite is substantially reduced, which is undesirable. A narrow strip width may result in high circuit losses and large stray fields.

As a starting point, we introduce another rule of thumb: set W equal to the width that gives a stripline characteristic impedance of 50Ω , assuming air dielectric. This rule is presented without proof, as its basis is largely empirical. Equations (5.13) and (5.14) should hold true for the chosen strip width.

The stripline characteristic impedance can be determined [13] using one of two sets of equations:

$$Z_0 = \frac{60}{\sqrt{\epsilon}} \ln \frac{4b}{W} \left[1 + \frac{t}{\pi W} \left(1 + \ln \frac{4\pi W}{t} + 0.51\pi \frac{t^2}{W^2} \right) \right] \pi \quad (5.50)$$

valid for $W/b < 0.35$ and $t/b < 0.25$; t is the stripline thickness and b is the ground plane spacing ($b = 2d$ for small t). For $W/b > 0.35$,

$$Z_0 = \frac{94.15}{\left(\frac{W}{b} + \frac{C_f'}{0.0885\epsilon} \right) \sqrt{\epsilon}} \quad (5.51)$$

where

$$C_f' = \frac{0.0885\epsilon}{\pi} \left[\frac{2}{1 - \frac{t}{b}} \ln \left(\frac{1}{1 - \frac{t}{b}} + 1 \right) - \left(\frac{1}{1 - \frac{t}{b}} - 1 \right) \ln \left(\frac{1}{\left(1 - \frac{t}{b}\right)^2} - 1 \right) \right] \quad (5.52)$$

Many reference books present curves for stripline Z_0 , and microwave circuit design software packages can be used to compute stripline parameters.

An important concept in circulator design is that of frequency scaling. Because the disk radius or triangle altitude is proportional to wavelength, as are magnetic field and saturation magnetization, designs can be scaled. By this, we mean that if we have a working design with center frequency f , we can generate another design with center frequency f' that has very similar (if not identical) electrical performance. If we denote the new design parameters by R' , M'_0 , and H_{dc}' , and the old design parameters by R , M_0 , and H_{dc} , we can write

$$R' = \frac{f'}{f} R \quad (5.53)$$

$$M'_0 = \frac{f'}{f} M_0 \quad (5.54)$$

$$H_{dc}' = \frac{f'}{f} H_{dc} \quad (5.55)$$

M_0 need not be changed for an above-resonance design, and H_{dc} for a below-resonance device need only be changed to just saturate the ferrite. This scaling technique is valid only for small changes in frequency (less than 1.5:1), and we do need to change other parameters along with the ones in (5.53) to (5.55).

5.1.4 Below-Resonance Approximations

For the below-resonance operating region, we use magnetic fields lower than the fields for above-resonance circulators. We make the simplifying assumption that the internal magnetic field in the ferrite is 0. This is the case when the ferrite is just magnetized. Dropping the loss terms, we derive (5.28) from (5.6), (1.30), and (1.32). Note that $\mu = 1$ in (5.28).

We find the ferrite disk radius in the same manner as we do for above-resonance circulators, using (5.9) or Figure 5.11 and (5.28). The effective permeability, hence the disk radius, is only a function of the ferrite material selected and the operating frequency of the circulator. The magnetic field does not have a strong influence on the loss and bandwidth as it does with the above-resonance junction, but the ferrite saturation magnetization is more critical.

We can compare the calculated disk radius with the disk radii that Simon empirically found to be optimum. These radii are presented in Figure 5.9. The disk radii found by either method should be similar, but the radii due to Simon will, without a doubt, lead to working octave-bandwidth designs.

Next, we compute Q_L and G , the same way we do for the above-resonance circulator, using (5.30), (5.32), and (5.33) or Figures 5.12 and 5.13. We approximate the required κ/μ using (5.27).

If $\kappa/\mu < 0.3$, we can use Helszajn's design expressions. We find a more exact value of κ/μ from (5.29). If $\kappa/\mu > 0.3$, or we do not wish to calculate a more accurate κ/μ , we simply use the previously approximated value from (5.27).

We present two equations that relate Q_L and κ/μ because each has advantages. Clearly, both are approximations, as are most circulator design expressions. Equation (5.27) is the simpler of the two, hence easier to use. It also provides reasonably accurate results over a fairly wide range of values. Helszajn's expression, (5.29), includes a second-order polynomial correction factor that presumably improves accuracy, but only for $\kappa/\mu < 0.3$. It is more difficult to use because of the polynomial factor, particularly if we are solving for κ/μ .

The ferrite thickness should be arbitrarily set to about $\lambda/16$ (wavelength in air), which is the approximate dimension that Simon used. The ferrite thickness is not critical as other adjustments later on such as stripline width and center conductor geometry will compensate for inaccuracies in disk thickness.

For the case of $\kappa/\mu < 0.3$, we calculate the stripline width from (5.34). Otherwise, we again set W equal to the width that gives a stripline characteristic impedance, with air dielectric, of 50Ω .

There are several other design considerations that apply to both above-resonance and below-resonance circulators. One of these is the impedance transformer. If the specified circulator bandwidth dictates that one or more quarter-wavelength impedance transformers are needed, we must design these transformers. The circulator bandwidth without any transformers or matching circuits is given by (5.15). Most octave-bandwidth below-resonance circulators contain at least one quarter-wavelength transformer at each port, and often two are used.

We compute the characteristic impedance of a single transformer using (5.38). If two transformers are used, the impedances are given by

$$Z_{t1} = G_r^{-3/4} Y_0^{-1/4} \quad (5.56)$$

$$Z_{t2} = G_r^{-1/4} Y_0^{-3/4} \quad (5.57)$$

where Z_{t1} is the characteristic impedance of the transformer nearest the junction.

To minimize discontinuities and transformer size, it is a good idea to set the dielectric constant of the dielectric surrounding the transformer center conductor equal to or close to the ferrite dielectric constant. Transformers may be folded to minimize the amount of space they occupy.

Lumped-element impedance-matching techniques can be used in low-frequency circulators. The important thing to remember is that the equivalent circuit of the circulator junction is typically a parallel-resonant circuit.

The ferrite disk junctions can easily be converted to their equilateral triangle equivalents by using the following conversion, derived from (5.41) and (5.42):

$$A = 1.97R - \frac{d}{4} \quad (5.58)$$

valid for $A/d > 4$. The thickness of the triangle is the same as the disk thickness.

An important approximate circulator design concept is that of frequency scaling, which is described in Section 5.1.3.

5.1.5 Network Synthesis

After circulator specifications have been established, one design option [14] is to proceed to synthesize an appropriate network that will enable the circulator to meet its electrical requirements. The exact synthesis processes for networks having one or two quarter-wavelength impedance transformers are described in this section. After a network has been synthesized, the next step is to determine the values of the circulator resonator parameters so that the network can be realized. This network synthesis scheme is independent of the circulator topology; it applies to stripline, waveguide, and microstrip junction circulators.

As presented in Section 5.1.2, the equivalent circuit of circulator junction, over a narrow bandwidth, as seen from one port, is a parallel-resonant

RLC circuit or “tank.” To obtain optimum circulator performance, we need to closely match the impedance of the parallel-resonant circuit to the system characteristic impedance. There are many ways this can be accomplished, by using various configurations of lumped-element (discrete capacitors and inductors), distributed (transmission lines), or a mixed approach, often called a semi-distributed or semi-lumped circuit. If the circulator bandwidth or electrical performance is not critical, then the circulator junction impedance is unimportant, and design of the impedance matching structure can be simple and straightforward, as described in Sections 5.1.3 and 5.1.4.

The most common impedance-matching structures in junction circulators consist of one quarter-wavelength transmission line at each port or two cascaded quarter-wavelength transmission lines at each port, which serve as impedance transformers. From circulator specifications of center frequency, bandwidth, and maximum VSWR, we can readily synthesize the matching network parameters: the transformer characteristic impedance(s) and the resonator R , L , and C values. The resonator can also be described in terms of admittance: G_r and B' (susceptance slope) or G_r and Q_L .

Figures 5.12 and 5.14 show loaded Q as functions of bandwidth with maximum VSWR as a parameter, for networks having one and two quarter-wavelength transformers, respectively. Similarly, plots of G_r appear in Figures 5.13 and 5.15. Figures 5.12–5.15 can be used to estimate the required Q_L and G_r from VSWR and bandwidth; VSWR can be estimated from bandwidth and Q_L , or bandwidth can be estimated from the other parameters.

An alternative to the use of the lumped *RLC* circuit to represent the circulator resonator is to use a short-circuited quarter-wavelength transmission line section in parallel with a resistor. This is sometimes referred to as a “stub-r” or “stub-resistor” load.

We can use one of several ways to synthesize the matching network:

1. Determine the values of the network parameters empirically, using a “cut and try” method. This is very slow and can require modification of hardware to optimize electrical performance.
2. Look up the network parameters in tables, such as those in [15]. This may require some interpolation, and the results may not be very precise if the desired parameters cannot be read directly from a table.
3. Using circuit simulation software, such as Ansys® Designer, optimize the network parameters to meet the specified VSWR over the required bandwidth. This method can provide accurate results, but the time required to perform multiple optimization iterations may be long.

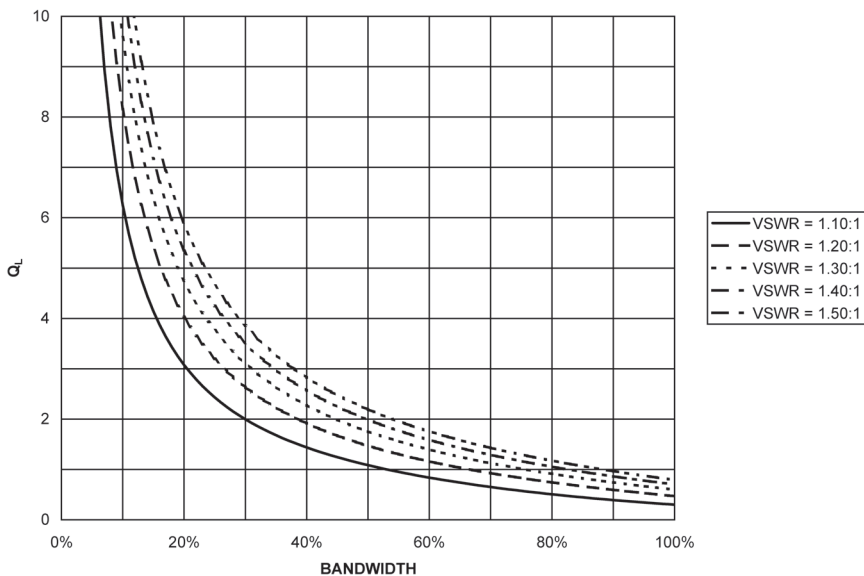


Figure 5.14 Ferrite disk resonator loaded Q versus bandwidth for two quarter-wavelength transformers.

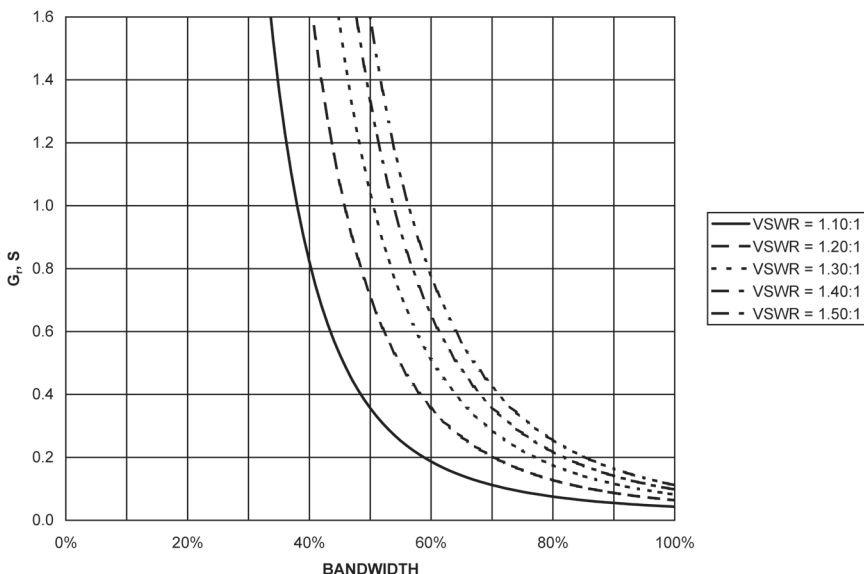


Figure 5.15 Ferrite disk junction conductance versus bandwidth for two quarter-wavelength transformers.

4. Use the equations presented in this section to compute the values of the network parameters. This method is accurate, and very fast if the equations are solved using a computer program or spreadsheet.

Two sets of network synthesis equations [15] follow, one set for the single-transformer case and another set for the two-transformer case. The solution of the two-transformer case requires much more computation than the solution of the single-transformer case. Two transformers have higher insertion loss than one, so only one transformer should be used unless the bandwidth requires the use of two transformers.

In the following equations, f_1 , f_2 , and f_0 are the lower frequency band edge, upper band edge, and center frequency, respectively, and S_{\min} and S_{\max} are the minimum and maximum VSWR in the frequency band. The transformer characteristic impedances are Z_t for the single-transformer case, and Z_{t1} and Z_{t2} for the two-transformer case. Y_s is the characteristic admittance of the short-circuited stub of the resonator equivalent circuit.

For the case of a single quarter-wavelength transformer ($n = 2$), we have

$$w = \frac{f_2 - f_1}{f_0} \quad (5.59)$$

$$K^2 = \left(\frac{S_{\min} - 1}{2\sqrt{S_{\min}}} \right)^2 \quad (5.60)$$

$$\varepsilon^2 = \left(\frac{S_{\max} - 1}{2\sqrt{S_{\max}}} \right)^2 - K^2 \quad (5.61)$$

$$\theta_0 = \frac{(2 - w)\pi}{4} \quad (5.62)$$

$$\beta = \tan^2 \theta_0 + \frac{\tan \theta_0}{\cos \theta_0} \quad (5.63)$$

$$a = K^2 + \varepsilon^2 \quad (5.64)$$

$$b = 2\beta\varepsilon^2 - K^2 \quad (5.65)$$

$$c = \beta^2 \varepsilon^2 \quad (5.66)$$

$$n_1 = \sqrt{2\sqrt{(a+1)c} - b + 1} - \sqrt{2\sqrt{ac} - b} \quad (5.67)$$

$$n_2 = \sqrt{a+1} - \sqrt{a} = \frac{1}{\sqrt{S_{\max}}} \quad (5.68)$$

$$d_0 = 2\sqrt{c} \quad (5.69)$$

$$Z_t = \frac{n_2}{Y_0 n_1} = \frac{1}{\sqrt{S_{\max} G_r Y_0}} \quad (5.70)$$

$$G_r = Y_0 n_1^2 \quad (5.71)$$

$$B' = \frac{Y_0 n_1 d_0 \pi}{4} \quad (5.72)$$

$$Q_L = \frac{B'}{G_r} = \frac{d_0 \pi}{4 n_1} \quad (5.73)$$

$$Y_s = Y_0 n_1 d_0 = \frac{4 B'}{\pi} \quad (5.74)$$

And for the case of a two quarter-wavelength transformers ($n = 3$), using (5.59–5.62) to find K^2 , ε^2 , and θ_0 , we have

$$p = - \left[2 + \frac{\varepsilon^2}{1 + K^2} \left(\frac{2 + \sin \theta_0}{\cos \theta_0} \right)^2 \right] \quad (5.75)$$

$$q = 1 - \frac{2\varepsilon^2}{1 + K^2} \frac{\sin \theta_0 (2 + \sin \theta_0)(1 + \sin \theta_0)}{\cos^2 \theta_0 (1 - \sin \theta_0)} \quad (5.76)$$

$$r = - \frac{\varepsilon^2}{1 + K^2} \left(\tan \theta_0 \frac{1 + \sin \theta_0}{1 - \sin \theta_0} \right)^2 \quad (5.77)$$

$$\alpha = q - \frac{p^2}{3} \quad (5.78)$$

$$b = 2\left(\frac{p}{3}\right)^3 - \frac{pq}{3} + r \quad (5.79)$$

$$n_{32} = \sqrt{1 + K^2} \quad (5.80)$$

If $(b/2)^2 + (a/3)^3 \geq 0$, then we use (5.81–5.90):

$$A = \sqrt[3]{-\frac{b}{2} + \sqrt{\left(\frac{b}{2}\right)^2 + \left(\frac{a}{3}\right)^3}} \quad (5.81)$$

$$B = \sqrt[3]{-\frac{b}{2} - \sqrt{\left(\frac{b}{2}\right)^2 + \left(\frac{a}{3}\right)^3}} \quad (5.82)$$

$$X_1 = -\left(\frac{A+B}{2} + \frac{p}{3}\right) \quad (5.83)$$

$$X_2 = \frac{\sqrt{3}}{2}(A - B) \quad (5.84)$$

$$t_1 = \sqrt{A + B - \frac{p}{3}} \quad (5.85)$$

$$|t_2|^2 = \sqrt{X_1^2 + X_2^2} \quad (5.86)$$

$$t_2 + t_2^* = \sqrt{2(X_1 + \sqrt{X_1^2 + X_2^2})} \quad (5.87)$$

$$n_{22} = \Sigma_1 \sqrt{1 + K^2} = (t_1 + t_2 + t_2^*) \sqrt{1 + K^2} \quad (5.88)$$

$$n_{12} = \Sigma_2 \sqrt{1 + K^2} = \left[|t_2|^2 + t_1(t_2 + t_2^*) \right] \sqrt{1 + K^2} \quad (5.89)$$

$$n_{02} = \Sigma_3 \sqrt{1 + K^2} = t_1 |t_2|^2 \sqrt{1 + K^2} \quad (5.90)$$

Or, if $(b/2)^2 + (a/3)^3 < 0$, then we use (5.91–5.97):

$$\phi = \tan^{-1} \left[\frac{-2\sqrt{-\left(\frac{b}{2}\right)^2 - \left(\frac{a}{3}\right)^3}}{b} \right] \quad (5.91)$$

$$X_1 = \sqrt{2\sqrt{-\frac{a}{3}} \cos \frac{\phi}{3} - \frac{p}{3}} \quad (5.92)$$

$$X_2 = \sqrt{-\frac{p}{3} - \sqrt{-\frac{a}{3}} \cos \frac{\phi}{3} + \sqrt{-a} \sin \frac{\phi}{3}} \quad (5.93)$$

$$X_3 = \sqrt{-\frac{p}{3} - \sqrt{-\frac{a}{3}} \cos \frac{\phi}{3} - \sqrt{-a} \sin \frac{\phi}{3}} \quad (5.94)$$

$$n_{22} = \Sigma_1 \sqrt{1 + K^2} = (X_1 + X_2 + X_3) \sqrt{1 + K^2} \quad (5.95)$$

$$n_{12} = \Sigma_2 \sqrt{1 + K^2} = (X_1 X_2 + X_2 X_3 + X_1 X_3) \sqrt{1 + K^2} \quad (5.96)$$

$$n_{02} = \Sigma_3 \sqrt{1 + K^2} = X_1 X_2 X_3 \sqrt{1 + K^2} \quad (5.97)$$

After the calculations of (5.75–5.80) and either (5.81–5.90) or (5.91–5.97) have been performed, if $K > 0$, we replace $1 + K^2$ with K^2 and repeat the calculations. For good housekeeping, when the calculations for K^2 are performed, we replace variable names n_{22} , n_{12} , and n_{02} with n_{21} , n_{11} , and n_{01} , respectively. If $K = 0$, then we use

$$n_{21} = \varepsilon \frac{2 + \sin \theta_0}{\cos \theta_0} \quad (5.98)$$

$$n_{11} = 0 \quad (5.99)$$

$$n_{01} = \varepsilon \tan \theta_0 \frac{1 + \sin \theta_0}{1 - \sin \theta_0} \quad (5.100)$$

Continuing with the computations,

$$n_{31} = K \quad (5.101)$$

$$n_3 = n_{32} - n_{31} \quad (5.102)$$

$$n_2 = n_{22} - n_{21} \quad (5.103)$$

$$n_1 = n_{12} - n_{11} \quad (5.104)$$

$$d_0 = n_{02} + n_{01} \quad (5.105)$$

$$Z_{t1} = \frac{n_2}{Y_0(n_1 + n_3)} \quad (5.106)$$

$$Z_{t2} = \frac{n_3}{n_1} Z_{t1} \quad (5.107)$$

G_r , B' , Q_L , and Y_S can then be computed using (5.71–5.74), as for the single-transformer ($n = 2$) case.

If desired, the lumped parallel RLC circuit parameters can be computed using

$$R = \frac{1}{G_r} \quad (5.108)$$

$$L = \frac{1}{2\pi f_0 Q_L G_r} \quad (5.109)$$

$$C = \frac{Q_L G_r}{2\pi f_0} \quad (5.110)$$

Figure 5.16 shows a VSWR response for a single-transformer ($n = 2$) network that was generated using Ansys Designer circuit simulation software, with $G_r = 0.1409 \text{ S}$, $B' = 0.2818$, and $Z_t = 16.85 \Omega$. We generated these network parameters from $S_{\min} = 1.00$, $S_{\max} = 1.25$, and $w = 32.3\%$. The general schematic for the network is shown in Figure 5.17. Figure 5.18 shows a Smith-chart plot of the complex impedance of the resonator of the same circuit, with the transformer removed. The parallel-resonant nature of the resonator is obvious. When the transformer is in the circuit, the response is folded over on itself as shown in Figure 5.19, creating the characteristic double-tuned response of the $n = 2$ network.

When it is desirable to change the network parameters, or to obtain less VSWR ripple, and still maintain the same maximum VSWR, S_{\min} can be changed. For example, if we set $S_{\min} = 1.15$ and keep the same S_{\max} and

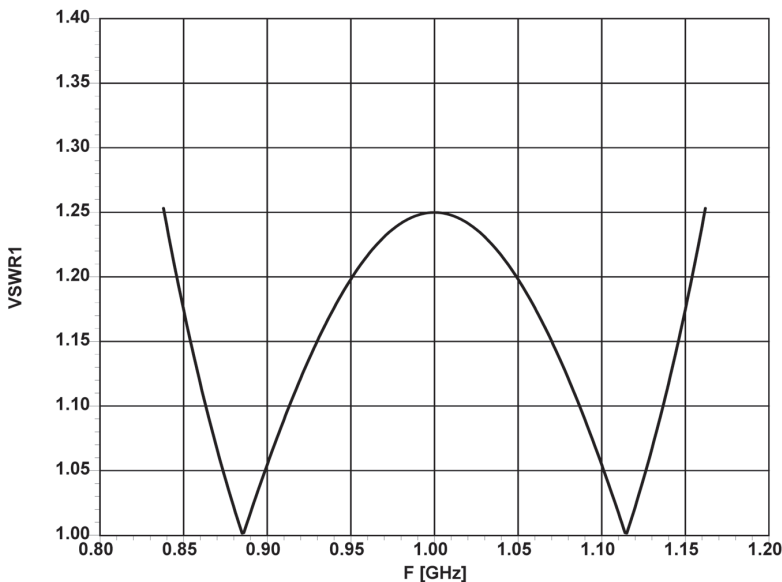


Figure 5.16 Simulated VSWR response of single-transformer network. $G_r = 0.1409 \text{ S}$, $B' = 0.2818$, and $Z_t = 16.85\Omega$.

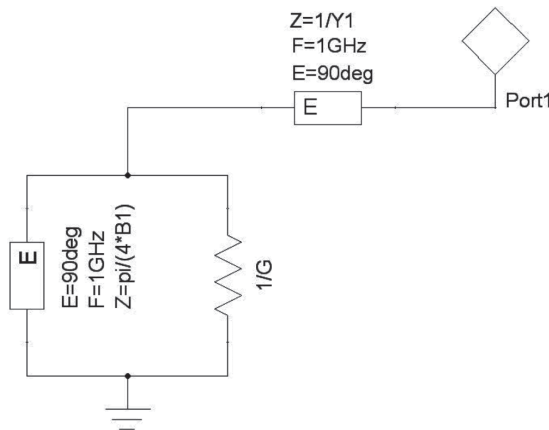


Figure 5.17 Schematic of single-transformer network.

ω values as in the previous example, we find that G_r and B' are decreased to 0.08423S and 0.1700 , respectively, and Z_t is increased to 21.79Ω . The simulated VSWR response of this new network is shown in Figure 5.20, and its corresponding Smith-chart plot appears in Figure 5.21.

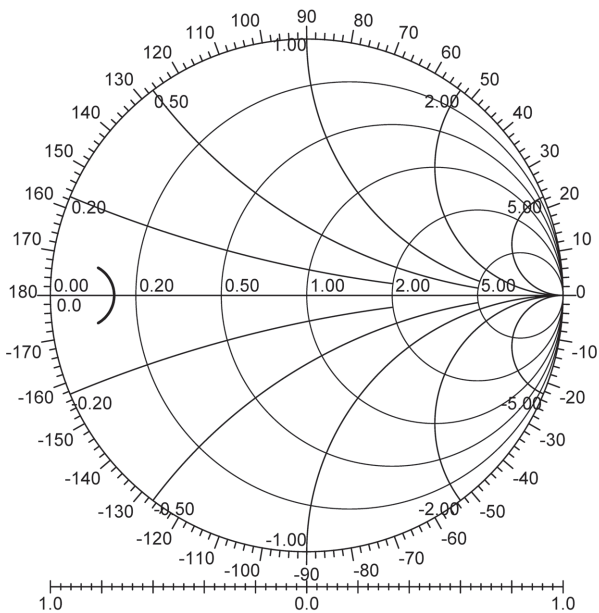


Figure 5.18 Simulated reflection response of resonator with transformer removed.

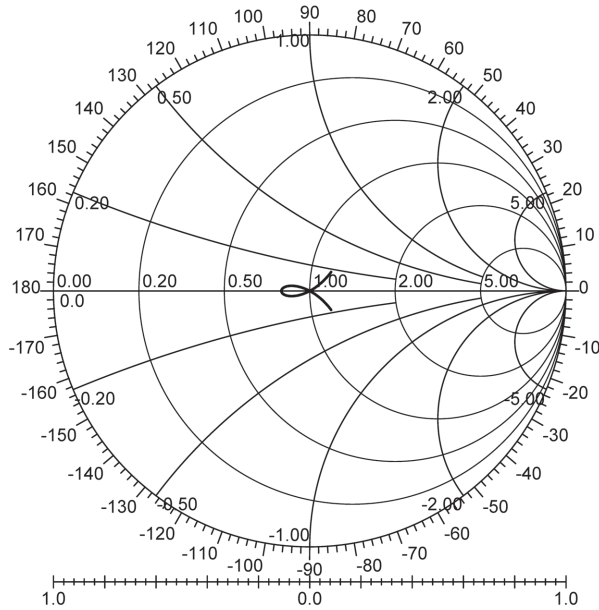


Figure 5.19 Simulated reflection response of single-transformer network.

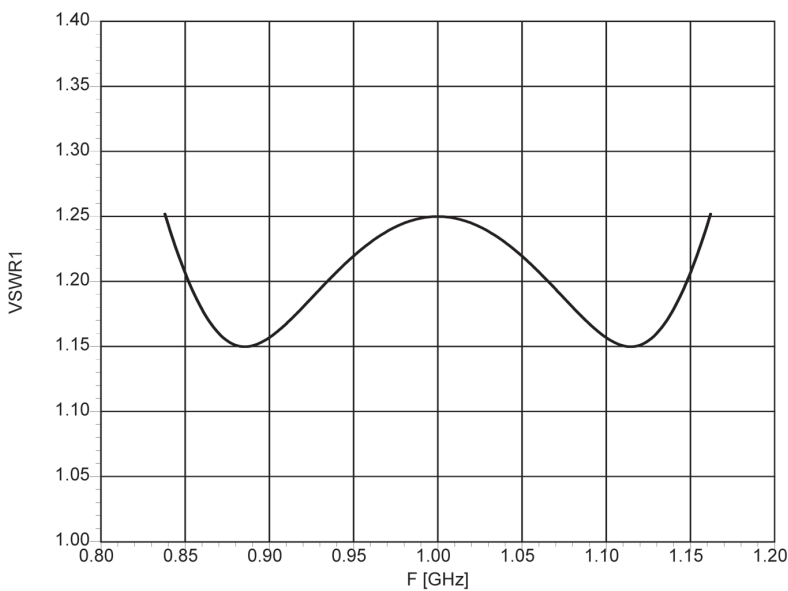


Figure 5.20 Simulated VSWR response of single-transformer network with $S_{\min} = 1.15$.

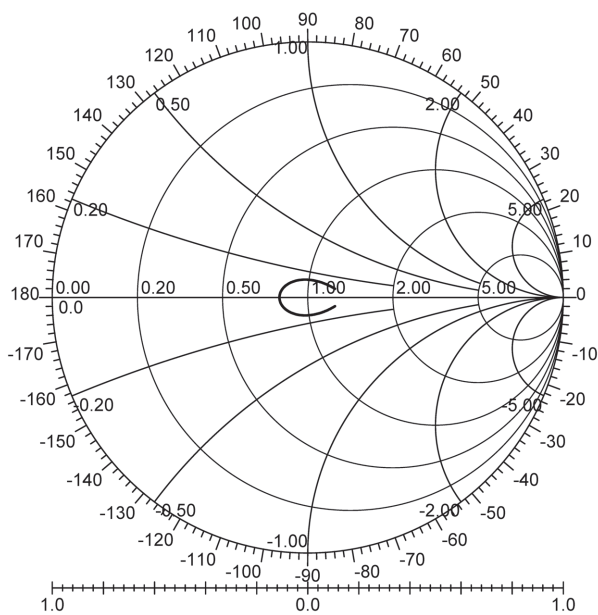


Figure 5.21 Simulated reflection response of single-transformer network with $S_{\min} = 1.15$.

The triple-tuned VSWR response of a network having two transformers ($n = 3$) is shown in Figure 5.22, and Figure 5.23 shows its Smith-chart plot. The variable values corresponding to these simulated responses are $S_{\min} = 1$, $S_{\max} = 1.06$, $w = 69.1\%$, $G_r = 0.07696$, $B' = 0.03852$, $Z_{t1} = 38.46 \Omega$, and $Z_{t2} = 19.60 \Omega$. Figure 5.24 is a general schematic for a two-transformer ($n = 3$) network with a lumped parallel RLC resonator.

5.1.6 Center Conductor Geometries

A wide variety of center conductor geometries are utilized in commercial circulators, some of which are depicted in Figure 5.25. For the novice circulator designer, a simple disk between $3R/2$ and $2R$ diameter will work well with a ferrite disk, and for the ferrite triangle, a hexagon that just fits inside the triangle is a good starting point.

It is helpful to characterize the geometries shown in Figure 5.25 in terms of resonant frequency or kR (for disks) or kA (for hexagons and triangles), and their susceptance slope (B') and conductance (G_r). Generally, changes in the geometry have only a weak effect on Q_L [16, 17], but have substantial effects on B' and G_r . There is interaction of the coupling angle (ψ) and the gyromagnetic splitting factor (κ/μ) with the geometry, so changes in geometry will not have exactly the same effects in every instance.

Disk resonators, as shown in Figure 5.25(a), have similar B' and G_r to hexagonal resonators, as in Figure 5.25(b). The apex-coupled triangular

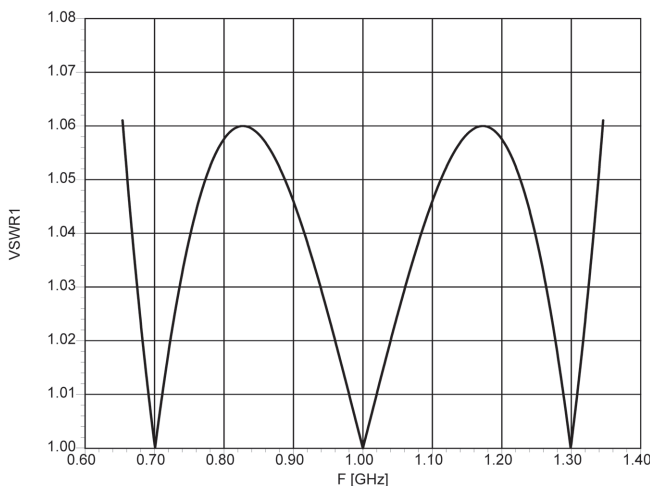


Figure 5.22 Simulated VSWR response of two-transformer network. $G_r = 0.07696$, $B' = 0.03852$, $Z_{t1} = 38.46 \Omega$, and $Z_{t2} = 19.60 \Omega$.

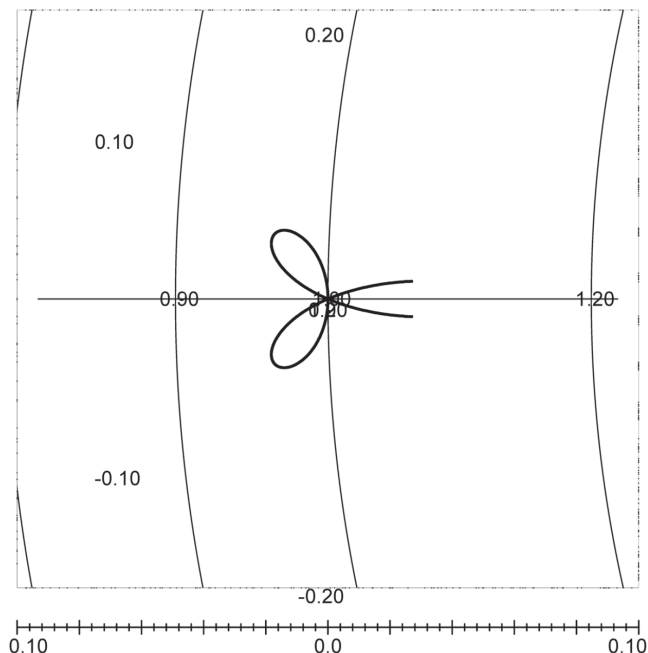


Figure 5.23 Simulated reflection response of two-transformer network.

resonator shown in Figure 5.25(c) can produce B' and G_r values of roughly one-third those of the hexagonal resonator. The side-coupled resonator of Figure 5.25(e) may provide B' and G_r values three times those of the hexagonal resonator. Thus, simply by changing the geometry of the center conductor,

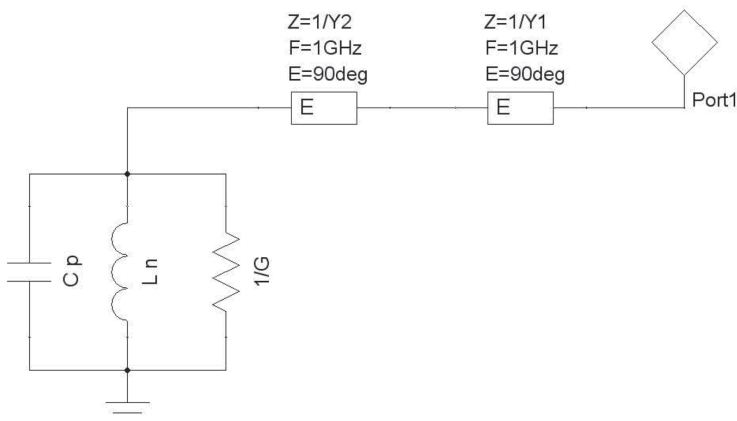


Figure 5.24 Schematic of two-transformer network.

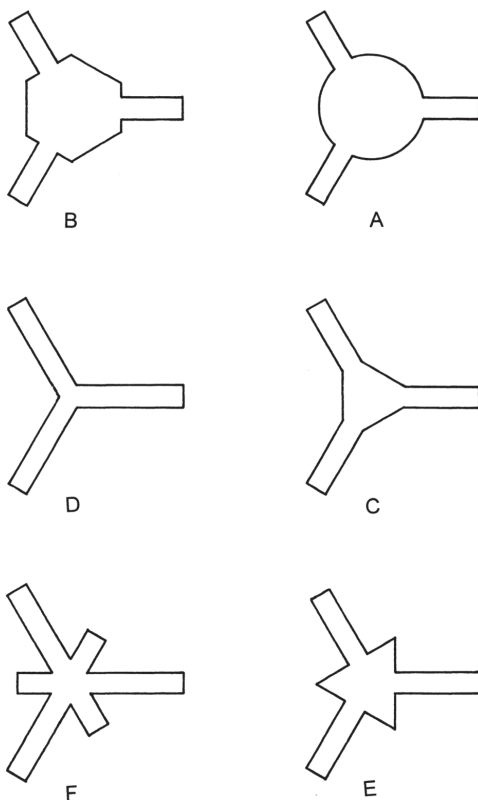


Figure 5.25 Center conductor geometries.

B' and G_r can be varied over a 9:1 range. The wye geometry of Figure 5.25(d) can have low values of B' and G_r , and the wye with stubs of Figure 5.25(f) can have very high values of B' and G_r , depending on the stub dimensions.

Many other center conductor geometries have been used. A circulator design engineer once told me that I should use heart-shaped resonators because I “would love them.” Cloverleaf-shaped resonators, the four-leaf variety luckier than the three-leaf ones, have been widely studied [18], as have resonators having magnetic walls/slots.

Because both B' and G_r are (approximately) inversely proportional to the ferrite thickness (d), if it is desirable to use a thinner or thicker ferrite, this can be accomplished by modifying the center conductor geometry. For example, if the initial design is based on disk center conductor geometry, and we desire to use a thinner ferrite, we can switch to an apex-coupled triangular resonator and make the ferrite roughly one-third of the original thickness.

Similarly, if we desire to make the ferrite thicker, then we could switch to a side-coupled triangular resonator and make the ferrite three times the original thickness. There are many options for center conductor geometry to adjust ferrite thickness or susceptance slope and resonator conductance as needed.

As κ/μ approaches zero (i.e., a very weakly magnetized condition), kR for the disk resonator approaches 1.84 as stated in Section 5.1.2. For the hexagonal resonator, with dimensions as defined in Figure 5.26, we have $kR = 2.00$ [16], or with a little trigonometric manipulation, $kA = 3.46$. For the triangular resonator, $kR = 2.45$ [16], or $kA = 3.68$. Figure 5.27 shows superimposed disk, hexagonal, and triangular resonators having the same resonant frequency.

Some resonators, such as the wye ones in Figure 5.25(d) and (f), are not as readily analyzed as are some others. There is no clearly defined boundary between the wye and the striplines, and in the case of the stubbed wye, there can be considerable variation in the width and length of the stubs. We can readily evaluate these resonators or others either experimentally or by using electromagnetic simulation software, such as Ansys® HFSS™. All that is required is to measure the reflection magnitude and phase (S_{11}) of one port,

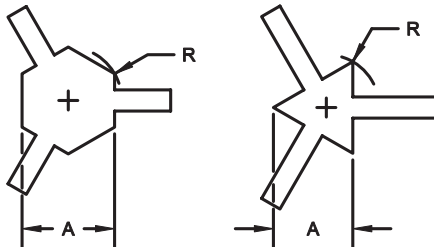


Figure 5.26 Dimensions A and R of hexagonal and triangular resonators.

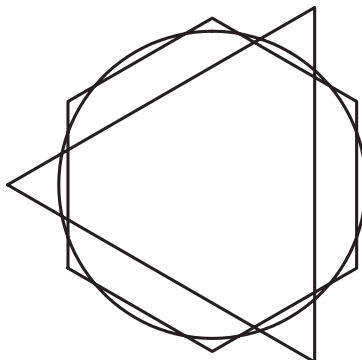


Figure 5.27 Superimposed disk, hexagonal, and triangular resonators having the same resonant frequency.

with the other two ports terminated in reflectionless terminations to prevent unwanted reflections. It must be possible to de-embed the measured data to the edge of the resonator, or the point to which a transformer will ultimately be connected. Experimentally, we can use stub tuners or automatic tuning devices to match two of the three ports. In HFSS, we simply renormalize the ports to an appropriate impedance to provide for minimal reflections.

Figure 5.28 shows an example Ansys HFSS model of a circulator resonator, which contains a hexagonal stripline resonator between hexagonal-shaped ferrites, surrounded by dielectric material having the same dielectric constant as the ferrite. Also shown in the figure is the de-embedding dimension for a port. The results of the electromagnetic simulation are shown in Figure 5.29. In this example, it was necessary normalize two of the ports to 13 ohms, providing a good impedance match, as shown by the two superimposed traces passing near the center of the Smith chart. The third trace, at the left of the Smith chart, shows the measured impedance of the loaded resonator, normalized to 50Ω . We convert the measured data to admittance values, then locate the resonant frequency, where B crosses zero. At this frequency, we note the G_r value and compute B' using (5.124).

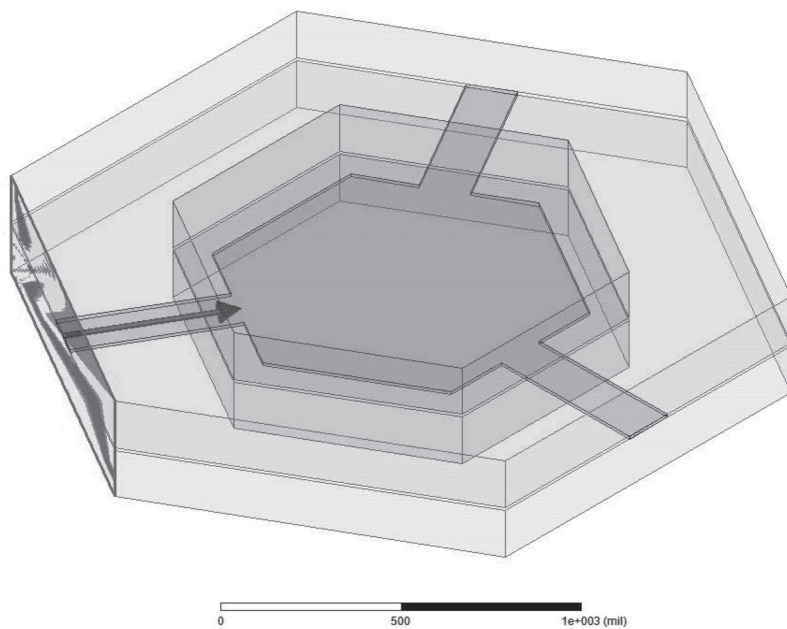


Figure 5.28 Ansys® HFSS™ model for a circulator resonator evaluation.

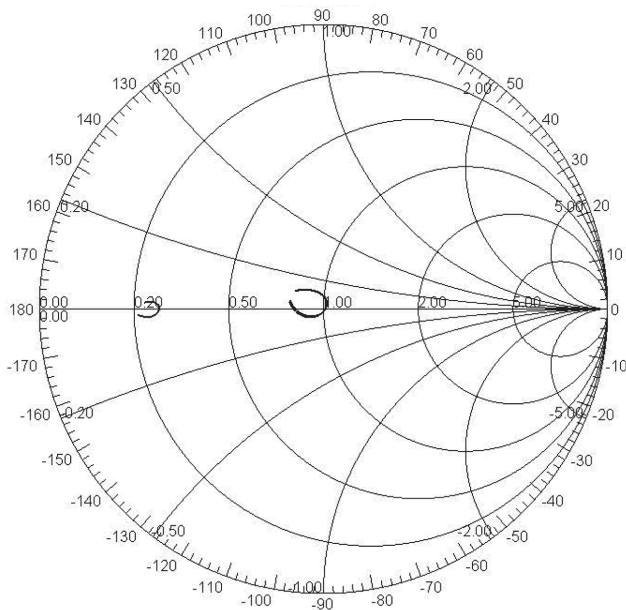


Figure 5.29 Simulated reflection from the circulator resonator of Figure 5.28.

The transitions from coaxial line to stripline need attention. Figure 5.30 shows the details of a typical transition. Both coax and stripline operate in the *TEM* mode, so what is required of the transition is to make a smooth change from the symmetrical coax mode to the distorted stripline mode. Ideally, we would like the stripline ground-plane spacing to be equal to the outer diameter of the coaxial dielectric. When the stripline spacing is larger than this diameter, the transition is fairly good without extensive compensations.

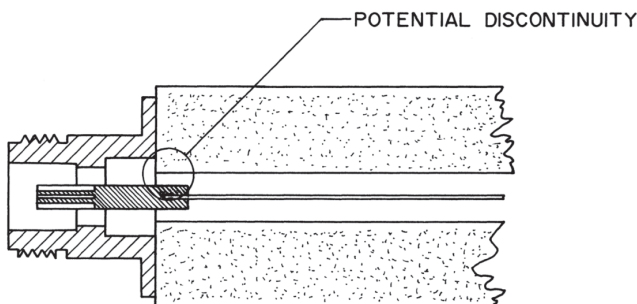


Figure 5.30 Coaxial-stripline transition.

When the ground-plane spacing is smaller, we need to add an intermediate section to step down the size of the center conductor. This section can take the form of a round hole bored into the side of the circulator where the connector attaches. The center conductor inside this bore can be either round or flat, like the stripline. Transition design for the circulator can be borrowed from other types of stripline devices. We can analyze and optimize transitions using electromagnetic simulation software, such as Ansys HFSS, or the design can be accomplished by cut-and-try methods.

5.1.7 Waveguide Junction Geometries

Most of the variation in center conductor geometries is typically in one plane, with ground plane spacing the only variation in the third dimension. Compared to center conductor geometries, waveguide junction geometries typically are uniform in the plane of the junction, but have greater diversity along the junction axis. There are different waveguide heights, different filling factors (the ratio of ferrite thickness, d , to dimension b in Figure 5.7), and different numbers of ferrites. Most junctions have only one or two ferrites, but Okada designs, discussed in Section 5.1.11, may have many more.

Because of the wide variation in waveguide junction geometries, any practical equations that could be used for design are either applicable to only one topology or are approximations. Fortunately, there is a wealth of literature [6, 19–23] available regarding waveguide junctions. To illustrate the effects of some of the variables, we have run electromagnetic simulations of a number of waveguide junctions using Ansys® HFSS™, and plotted derived values of Q_L and normalized G_r against filling factor (d/b). The results of these simulations are shown in Figures 5.31 and 5.32 for the one-cylinder topology (Figure 5.7(a)), Figures 5.33 and 5.34 for the two-disk topology (Figure 5.7(b)), and Figures 5.35 and 5.36 for the single-disk topology (Figure 5.7(c)). Some of the data in the figures are for half-height waveguide.

The waveguide used for the simulations was WR-975, and the frequencies were about 1 GHz. The results readily scale to other waveguide sizes and frequencies. In the simulations, depending on the geometry and κ/μ , the resonant frequency changed. No attempt was made to maintain the same frequency for all combinations of variables, so the values of Q_L and normalized G_r are all at slightly different frequencies. The height of the pedestal in the single-disk (Figure 5.7(c)) simulations was 25% of the waveguide height.

It is clear from the figures that we can adjust both the Q_L and G_r by changing the filling factor or the topology. As expected, Q_L increases for lower values of κ/μ . G_r increases for higher values of κ/μ .

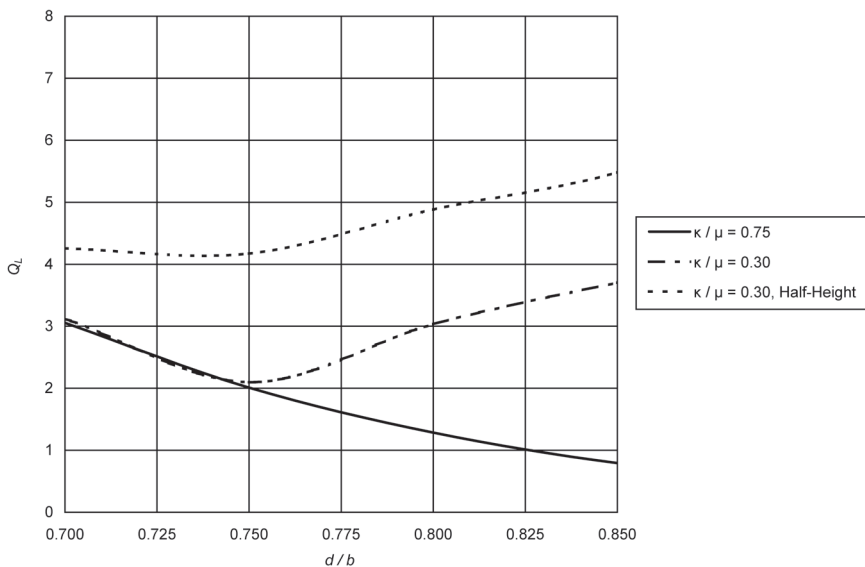


Figure 5.31 Simulated loaded Q of waveguide junction cylinder topology of Figure 5.7(a).

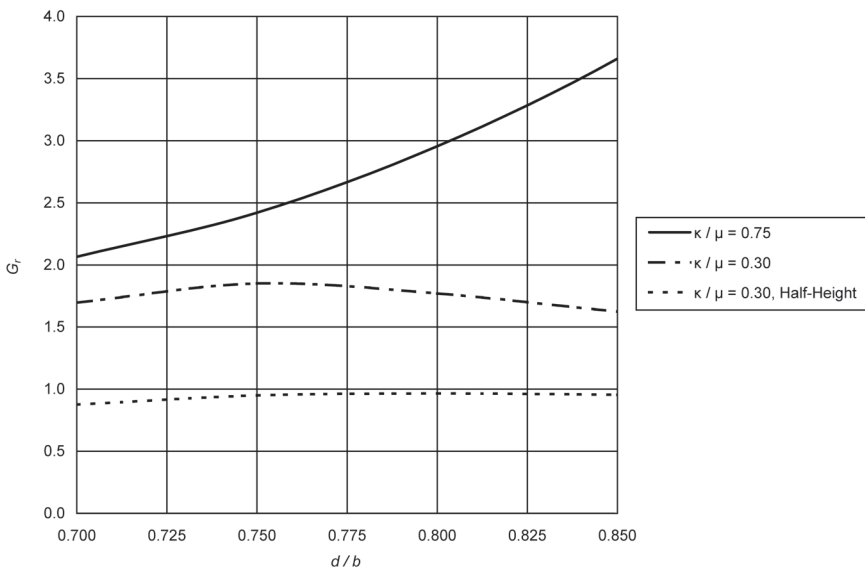


Figure 5.32 Simulated normalized conductance of waveguide junction cylinder topology of Figure 5.7(a).

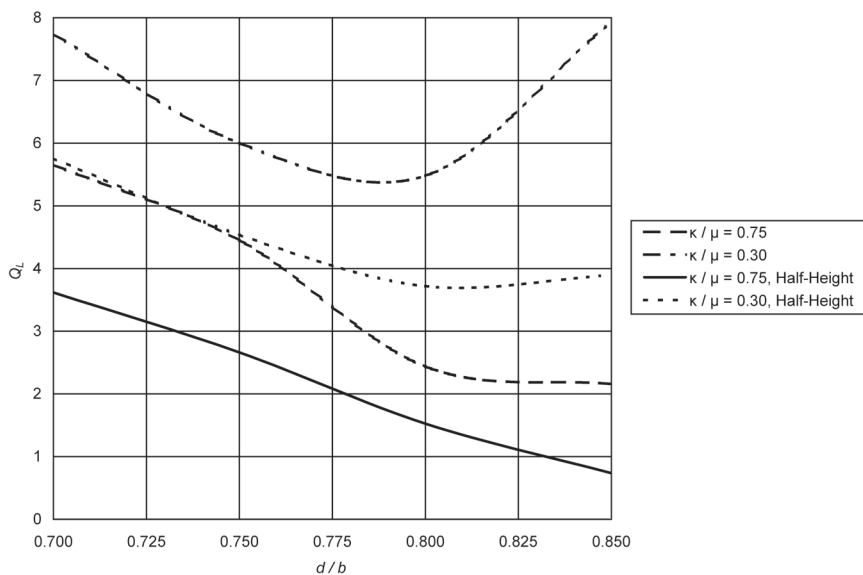


Figure 5.33 Simulated loaded Q of waveguide junction two-disk topology of Figure 5.7(b).

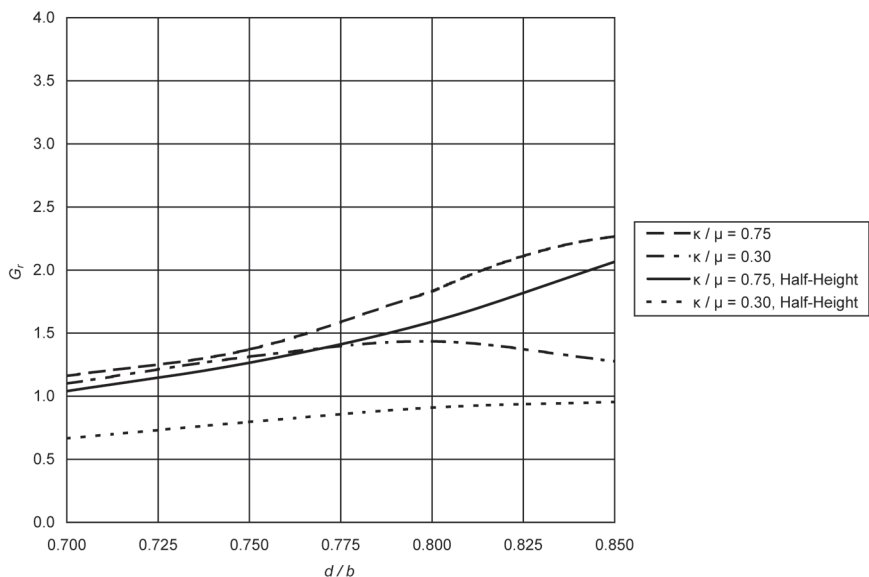


Figure 5.34 Simulated normalized conductance of waveguide junction two-disk topology of Figure 5.7(b).

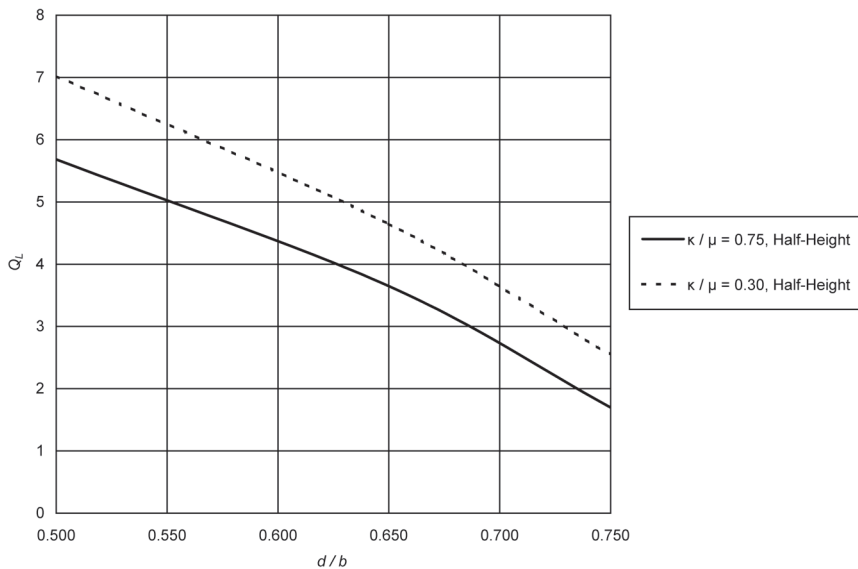


Figure 5.35 Simulated loaded Q of waveguide junction one-disk topology of Figure 5.7(c).

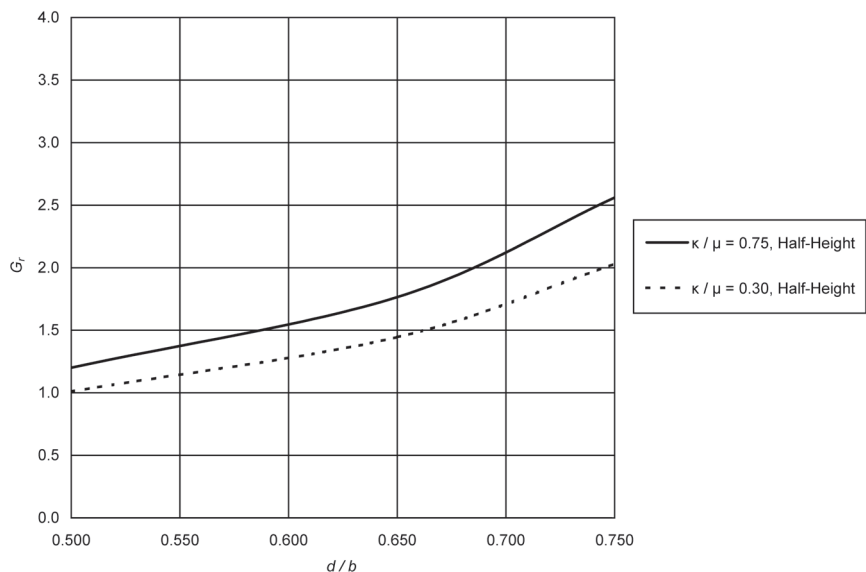


Figure 5.36 Simulated normalized conductance of waveguide junction one-disk topology of Figure 5.7(c).

Ferrites that are triangular or hexagonal in shape produce similar electrical results to ferrite disks, although it is possible to slightly adjust the susceptibility slope of the junction by rotating the ferrite if it is not a disk.

5.1.8 Stripline Circulator Synthesis Algorithm

Circulator synthesis and analysis algorithms are not new; many procedures have been proposed over the past few decades. In addition to the information presented in Section 5.1.2, various algorithms are contained in [14, 24–29]. One thing that all of the algorithms have in common is that they are iterative in nature. Typically, we have to make some initial choices for the values of design variables and then perform some calculations or run an electromagnetic simulation using software such as Ansys® HFSS™. The results of the calculations or simulation often suggest that there are more optimum values for the variables, so we change the values and do more mathematical work. Later in the design process, after hardware is assembled and tested, it may become apparent that more design optimization is necessary.

There is no universal or exact circulator synthesis algorithm. Because some designers have their own personal repertoires of designs or vast corporate-owned design databases available to them, much of their design work already has a firm basis in reality. Other designers may have limited computer resources available to them, or do not need extensive design documentation. In still other cases, time or economic constraints may dictate that design variables be quickly approximated and electrical performance be traded for lowest cost.

Sections 5.1.3 and 5.1.4 present some design approximations, which can be used in many instances. These can be used in combination with experimental results to develop a design or in combination with electromagnetic simulations as well.

Another possibility is to use the network synthesis algorithm of Section 5.1.5; then choose values for the other design variables that will allow the circulator to provide the required complex resonator impedance (and overall electrical performance) over the frequency band of interest. Initial estimates for the values of the design variables can be obtained using the information in Sections 5.1.3 and 5.1.4. Next, we build the circulator and test it, or we analyze the circulator using electromagnetic simulation software, such as Ansys HFSS. Before we perform the electromagnetic simulation, or if simulation software is not available, we have the option of using the following analysis procedure and equations.

This series of equations applies to disk center conductor geometry. Adjustments for other center conductor geometries may be made, as described

in Section 5.1.6. First, we compute the values of κ and μ using (1.30–1.33), the effective permeability of the ferrite using (5.6), and the unloaded Q using

$$Q_u = \frac{1}{\left| \frac{\mu_{eff}''}{\mu_{eff}'} \right| + \tan \delta} \quad (5.111)$$

Then, we calculate kR using

$$kR = \frac{R2\pi\sqrt{\mu_{eff}\epsilon}}{\lambda} \quad (5.112)$$

and the stripline characteristic impedance using (5.50) or (5.51) and (5.52), and ψ using (5.5). If we assume that the stripline has no loss, then $\alpha = 0$ and we have for the propagation constant

$$\Gamma = j\beta$$

where

$$\beta = \frac{2\pi}{\lambda} \sqrt{\epsilon\mu_{eff}}$$

Next, using the equations in [30], we compute

$$Z^0 = Z_0 + Z_{-3} + Z_3 \quad (5.113)$$

$$Z^+ = Z_1 + Z_{-2} \quad (5.114)$$

$$Z^- = Z_{-1} + Z_2 \quad (5.115)$$

where

$$Z_n = \frac{j\beta\sqrt{\mu_{eff}}Z_\psi \sin^2 n\psi}{n^2\pi\psi} \left[\frac{1}{\frac{J_{n-1}(kR)}{J_n(kR)} - n \left(\frac{1 + |\kappa/\mu|}{kR} \right)} \right] \quad (5.116)$$

Z_ψ in this equation is the stripline characteristic impedance. Note that for $n = 0$,

$$\frac{\sin^2 n\psi}{n^2 \psi} = \psi$$

and the negative-order Bessel functions can be replaced with positive-order ones:

$$J_{-n}(x) = (-1)^n J_n(x)$$

Continuing, we next compute

$$A = -\frac{1}{2}(Z^+ + Z^-) + Z^0 \quad (5.117)$$

$$B = \frac{\sqrt{3}}{2}(Z^+ - Z^-) \quad (5.118)$$

$$R_{in} = \frac{-B(B^2 - 3A^2)}{3(A^2 + B^2)} \quad (5.119)$$

$$X_{in} = Z^0 - \frac{AR_{in}}{B} \quad (5.120)$$

The input impedance of the circulator is

$$Z_{in} = R_{in} + jX_{in} \quad (5.121)$$

and we calculate the conductance and susceptance of the parallel-resonant equivalent circuit using

$$G = \frac{R_{in}}{R_{in}^2 + X_{in}^2} \quad (5.122)$$

$$B = \frac{-X_{in}}{R_{in}^2 + X_{in}^2} \quad (5.123)$$

The preceding computations must be repeated for each frequency point. Using the susceptance values, B , of frequency points spaced closely ($\Delta\omega$), we compute the susceptance slope using

$$B' = \frac{\omega\Delta B}{2\Delta\omega} \quad (5.124)$$

from which we calculate the loaded Q

$$Q_L = \frac{B'}{G} \quad (5.125)$$

To analyze circulator performance with stripline impedance transformers, we use [31]

$$Z = Z_0 \frac{Z_{in}\cosh\Gamma L + Z_0\sinh\Gamma L}{Z_0\cosh\Gamma L + Z_{in}\sinh\Gamma L} \quad (5.126)$$

where Z_0 , Γ , and L are the characteristic impedance, propagation constant, and length of the transformer, respectively. If the line is lossless, we can use

$$Z = Z_0 \frac{(Z_{in}/Z_0) + j\tan\beta L}{1 + j(Z_{in}/Z_0)\tan\beta L} \quad (5.127)$$

If there is more than one transformer, (5.126) or (5.127) can be applied iteratively to effectively cascade the transformers. In the usual manner, we compute the circulator performance metrics as follows.

$$\rho = \frac{Z - Z_0}{Z + Z_0} \quad (5.128)$$

where Z_0 is the system characteristic impedance.

$$VSWR = \frac{1 + |\rho|}{1 - |\rho|} \quad (5.129)$$

$$ReturnLoss = -20\log_{10}|\rho| \quad (5.130)$$

$$MismatchLoss = -20\log_{10}\left(1 - |\rho|^2\right) \quad (5.131)$$

$$Loss = -10\log_{10}\left(1 - \frac{Q_L}{Q_u}\right) + MismatchLoss \quad (5.132)$$

In (5.112), an assumption is made that there are no fringing fields at the disk perimeter. These fringing fields make the effective disk radius larger, so it is necessary to make the disk slightly undersize, or the center frequency of the circulator would be too low. Wheeler [32] published formulas for the capacitance of a disk between ground planes, which are applicable to the stripline topology. The computations proceed as follows:

$$C_r = \epsilon_0 \frac{1+\epsilon}{2} 8R \quad (5.133)$$

$$C_a = \frac{\epsilon_0 \epsilon \pi R^2}{d} \quad (5.134)$$

$$C_{2s} = C_r + 2C_a \quad (5.135)$$

$$C_2 = C_{2s} \left(1 - \frac{1}{4 + 2.6 \frac{R}{d} + 2.9 \frac{d}{R}} \right) \quad (5.136)$$

$$R_{\text{eff}} = \frac{C_2}{2C_a} R \quad (5.137)$$

We adjust the disk radius (R) such that the effective radius (R_{eff}) is equal to the value of R used in (5.112). This will result in a smaller radius.

5.1.9 Microstrip Circulator Synthesis Algorithm

Some microstrip circulators exhibit no clear differentiation between the junction portion and the impedance-matching structure. The radius of the junction is sometimes interpreted [33] as the magnet radius. The magnet may be in contact with one face of the ferrite substrate, opposite the microstrip circuitry, or the magnet may be on the circuit face, sometimes with a spacer between the magnet and ferrite substrate. The radius of the junction area (and of the magnet) can be approximated in the usual manner using (5.9), except that the constant 1.84 is reduced to 1.65 because there is no clearly defined edge of the junction.

The thickness of the substrate may be chosen to match the substrate thickness of the circuit with which the circulator is intended to be used. A center conductor geometry utilizing a disk with radius about $0.8R$ will generally work for circulators that do not have demanding specifications,

and microstrip line impedances should be kept as low as possible to achieve reasonable line widths.

Nearly all microstrip circulators operate below resonance. This allows the use of low magnetic fields and avoids regions of ferrite that, in the case of an above-resonance circulator, may inadvertently be biased at resonance, resulting in high insertion loss.

The microstrip circuitry is normally deposited on the ferrite substrate using thin-film techniques. Sometimes, a dielectric ring is placed around a ferrite disk to form the microstrip circulator. This construction is more complicated and has no particular advantage.

Design algorithms for stripline junction circulators, such as those in Section 5.1.8, may be applied to microstrip circulators as well. An important exception is that transmission line impedances must be computed using equations for microstrip rather than equations for stripline. Resonator fringing effects are also computed differently.

Computation of the characteristic impedance of microstrip transmission lines is more complicated than the computations for stripline transmission lines because the dielectrics of a microstrip structure have at least two different relative permittivities. Typically the upper dielectric is air or vacuum, and the substrate to which the microstrip line is attached has a higher permittivity. In most cases, microstrip lines are very thin, so the equations presented here do not include the effects of finite strip thickness.

At microwave frequencies, microstrip transmission lines exhibit frequency dispersion. That is, the characteristic impedance and propagation constant vary with frequency. In addition, the effective permeability of a microstrip structure differs from that of bulk ferrite, although in some cases where the effective permeability is near unity, this is unimportant.

At low frequencies (below about 1 GHz), we compute the *static* characteristic impedance using the following equations [34]. For $w/d < 3.3$,

$$Z_{0S} = \frac{119.9}{\sqrt{2(\epsilon + 1)}} \left[\ln \left(\frac{4d}{w} + \sqrt{16 \frac{d^2}{w^2} + 2} \right) - \frac{1}{2} \left(\frac{\epsilon - 1}{\epsilon + 1} \right) \left(\ln \frac{\pi}{2} + \frac{1}{\epsilon} \ln \frac{4}{\pi} \right) \right] \quad (5.138)$$

and for $w/d \geq 3.3$,

$$Z_{0S} = \frac{119.9\pi}{2\sqrt{\epsilon}} \left\{ \frac{w}{2d} + \frac{\ln 4}{\pi} + \frac{\ln(\epsilon\pi^2/16)}{2\pi} \left(\frac{\epsilon - 1}{\epsilon^2} \right) \right. \\ \left. + \frac{\epsilon + 1}{2\pi\epsilon} \left[\ln \frac{\pi\epsilon}{2} + \ln \left(\frac{w}{2d} + 0.94 \right) \right] \right\}^{-1} \quad (5.139)$$

where w and d are the microstrip line width and substrate thickness, respectively. The effective permittivity is given by [34]

$$\epsilon_{\text{eff}} = \frac{\epsilon + 1}{2} + \frac{\epsilon - 1}{2} \left(1 + 10 \frac{d}{w}\right)^{-0.555} \quad (5.140)$$

which is similar to (5.152) and (5.153). The effective permittivity is useful for computing the electrical length of microstrip line using

$$\beta = \frac{2\pi}{\lambda} \sqrt{\epsilon_{\text{eff}} \mu_{\text{eff}}}$$

and impedance transformation using (5.126) or (5.127).

To adjust for the effects of frequency dispersion above about 1 GHz, we use [34]

$$\epsilon_{\text{eff}}(f) = \epsilon - \frac{\epsilon - \epsilon_{\text{eff}}}{1 + (25.4d/Z_{0S})^{1.33}(0.43f^2 - 0.009f^3)} \quad (5.141)$$

where d is the substrate thickness in inches and f is the frequency in GHz. The effective permeability of the microstrip structure, for $w/d < 2$, is [35]

$$\mu_e = \frac{2\mu_{\text{eff}}}{1 + \mu_{\text{eff}}} \left(\frac{A - B'}{A} \right)^2 \quad (5.142)$$

and for $w/d \geq 2$,

$$\mu_e = \mu_{\text{eff}} \left(\frac{C}{C - D'} \right)^2 \quad (5.143)$$

where μ_{eff} is given by (5.6) and

$$A = \ln \frac{8d}{w} + \frac{1}{32} \left(\frac{w}{d} \right)^2 \quad (5.144)$$

$$B' = \frac{1}{2} \left(\frac{1 - \mu_{\text{eff}}}{1 + \mu_{\text{eff}}} \right) \left(\ln \frac{\pi}{2} + \mu_{\text{eff}} \ln \frac{4}{\pi} \right) \quad (5.145)$$

$$C = \frac{w}{2d} + \frac{1}{\pi} \ln \left[(2\pi e) \left(\frac{w}{2d} + 0.94 \right) \right] \quad (5.146)$$

$$D' = \frac{1 - \mu_{\text{eff}}}{2} \left\{ \ln \left[\frac{\pi e}{2} \left(\frac{w}{2d} + 0.94 \right) \right] - \mu_{\text{eff}} \ln \left(\frac{e\pi^2}{16} \right) \right\} \quad (5.147)$$

The characteristic impedance can then be adjusted for frequency dispersion and effective microstrip permeability (μ_e) using

$$Z_0 = Z_{0S} \sqrt{\frac{\epsilon_{\text{eff}} \mu_e}{\epsilon_{\text{eff}}(f)}} \quad (5.148)$$

and the imaginary component of the propagation constant becomes

$$\beta = \frac{2\pi}{\lambda} \sqrt{\epsilon_{\text{eff}}(f) \mu_e} \quad (5.149)$$

In the same manner that the disk radius (R) for the stripline topology was adjusted in Section 5.1.8 to allow for fringing fields at the disk perimeter, the microstrip disk radius must also be adjusted. Helszajn and Lyon [36] published formulas for the effective radius of a microstrip disk resonator. The computations proceed as follows:

$$\frac{R_{\text{eff}}(0)}{R} = \frac{\pi \frac{d}{R}}{\ln \left(4 \frac{d}{R} - 0.358 + \frac{1}{0.4605 \frac{d}{R} + 0.736} \right)} \quad (5.150)$$

$$R_{\text{eff}}(0) = \frac{R_{\text{eff}}(0)}{R} R \quad (5.151)$$

$$q = 0.5 \left(1 + 5 \frac{d}{R} \right)^{-0.555} \quad (5.152)$$

$$\epsilon_{\text{eff}}(0) = \frac{\epsilon + 1}{2} + (\epsilon - 1) q \quad (5.153)$$

$$Z_0(0) = \frac{120\pi d}{2R_{\text{eff}}(0)} \sqrt{\frac{1}{\epsilon_{\text{eff}}(0)}} \quad (5.154)$$

$$P(f) = \left(\frac{d}{0.03937 Z_0(0)} \right)^{1.33} (0.43f^2 - 0.009f^3) \quad (5.155)$$

where d is in inches and f is the resonant frequency of the disk in GHz.

$$R_{\text{eff}}(f) = R - \frac{R - R_{\text{eff}}(0)}{1 + P(f)} \quad (5.156)$$

$$\epsilon_{\text{eff}}(f) = \epsilon - \frac{\epsilon - \epsilon_{\text{eff}}(0)}{1 + P(f)} \quad (5.157)$$

$$R_{\text{eff}} = R_{\text{eff}}(f) \frac{\sqrt{\epsilon_{\text{eff}}(f)}}{\sqrt{\epsilon}} \quad (5.158)$$

We adjust the disk radius (R) such that the effective radius (R_{eff}) is equal to the value of R used in (5.112). This will result in a smaller radius.

5.1.10 Waveguide Junction Circulator Synthesis Algorithm

Waveguide junction circulators appear to be simple devices, but their design synthesis is not straightforward. As is the synthesis of stripline junction circulators, the design of waveguide junction circulators is iterative in nature. After we make initial choices for design variables, we perform an electromagnetic simulation of the circulator or build a prototype circulator and measure its electrical performance. Then, if necessary, design optimization changes the values of design variables.

Waveguide junction circulators have already been developed for many common waveguide frequency bands. Circulator designers who work frequently with waveguide devices, which are less common than stripline circulators, often have repertoires of designs. Still, in some instances, it may be necessary to develop a new circulator design to optimize certain design aspects for the intended application.

The network synthesis algorithm in Section 5.1.5 may be helpful in determining the electrical requirements (Q_L, B', G_r) for the ferrite resonator. It is possible to design and optimize the ferrite resonator independently of the transformers, initially.

The approximate waveguide junction circulator design procedure we will present applies to the geometries shown in Figure 5.7. The first step is to calculate k_0 , the wave number for the center frequency of the circulator. This parameter is calculated using

$$k_0 = \frac{2\pi}{\lambda_0} \quad (5.159)$$

Next, we select a ferrite thickness (d) between $0.7b$ and $0.85b$ [6]. The dimension b in Figure 5.7(c) and $2b$ in Figures 5.7(b) and 5.7(a) can be taken as the waveguide height, or the junction may be constructed in a reduced-height center section.

Reducing the waveguide height increases the junction conductance. The susceptance slope (B') of the junction is higher for the single-disk geometry of Figure 5.7(c) than it is for the cylinder and two-disk geometries of Figures 5.7(a) and 5.7(b) [20]. Also, B' generally increases with increasing d/b . In Figure 5.7(c), there is the additional variable of the height of the metal pedestal beneath the ferrite. We can adjust Q_L by changing κ/μ , which we compute using (1.30–1.33).

We compute the ferrite disk radius with the aid of (5.39). Another estimate for R can be computed using (5.9). To use a triangular resonator instead of a disk or cylindrical resonator, we substitute $kA = 3.68$ for $kR = 1.84$ in (5.9), or make an appropriate adjustment after the radius is found using (5.39).

Smaller values of d can be selected at the expense of electrical performance. The bandwidth of the waveguide junction circulator is more narrow than that of the stripline circulator because of the inherently narrow bandwidth of waveguide.

Several techniques have been used to improve the performance of waveguide junction circulators, including the addition of dielectric sleeves around the ferrite disks and metal pins through the center of the ferrite.

The preceding information pertains to H-plane waveguide junction circulators, but E-plane circulators have also been produced. E-plane circulators are far less common than H-plane circulators, so we have not given them coverage in this book.

The design of waveguide transformers differs from the design of stripline transformers in important ways. First, the guide wavelength is given by [37]

$$\lambda_g = \frac{1}{\sqrt{\frac{1}{\lambda_0^2} - \frac{1}{\lambda_c^2}}} \quad (5.160)$$

where λ_0 is the free space wavelength and λ_c is the waveguide cutoff wavelength, $\lambda_c = 2a$, for a rectangular waveguide operating in the dominant mode (TE_{10}), where a is the waveguide width.

Because waveguides are not TEM transmission lines, waveguide characteristic impedance is an ambiguous quantity. There are several ways to define the characteristic impedance of a waveguide, but because other quantities can be normalized to the waveguide impedance or admittance, knowing the characteristic impedance is not terribly important. Waveguide impedance varies with frequency, so it is wrong to normalize waveguide characteristic impedance to a constant impedance (like we normalize most coaxial transmission lines to 50Ω or 75Ω) over a wide frequency range. Although it will not be used in further calculations, we can assume a waveguide characteristic impedance of [37]

$$Z_0 = 377 \frac{\lambda_g}{\lambda_0} \quad (5.161)$$

To design a waveguide transformer, we need to know the required transformer characteristic impedance normalized to the system waveguide characteristic impedance. Then, we simply set the height of the waveguide in the transformer section (b_t) so that the ratio of its height to the full waveguide height (b) is equal to the ratio of the impedances (Z_t/Z_0):

$$b_t = b \frac{Z_t}{Z_0} \quad (5.162)$$

It is best to make the steps in waveguide height symmetrical to minimize the electrical discontinuity at the step. Compensation for the steps is discussed in Chapter 7.

5.1.11 Okada Circulators

One of the applications for which Okada [38, 39] developed high-power waveguide junction circulators in the 1970s was breaking concrete and rock with microwave energy. The type of circulator that now bears Okada's name has multiple cells or *unit junctions*, as shown in Figures 5.37 and 5.38, which serve to distribute the dissipated power, thus increasing the power handling capacity of the circulator. The unit junctions are effectively in parallel, so that the incident RF power is distributed between them.

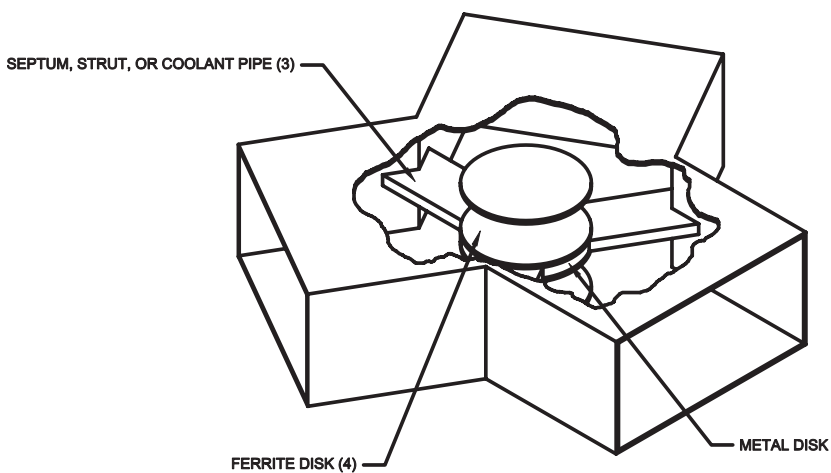


Figure 5.37 Two-cell Okada circulator.

The power level that an Okada circulator can handle depends primarily on the number of unit junctions, the method of cooling, the dimensions of the ferrites, and the microwave losses. Figure 5.37 shows an Okada circulator having two unit junctions, and the circulator in Figure 5.38 has three unit junctions. Theoretically, these circulators should be able to handle at least two and three times, respectively, the average power that a conventional waveguide junction circulator could handle.

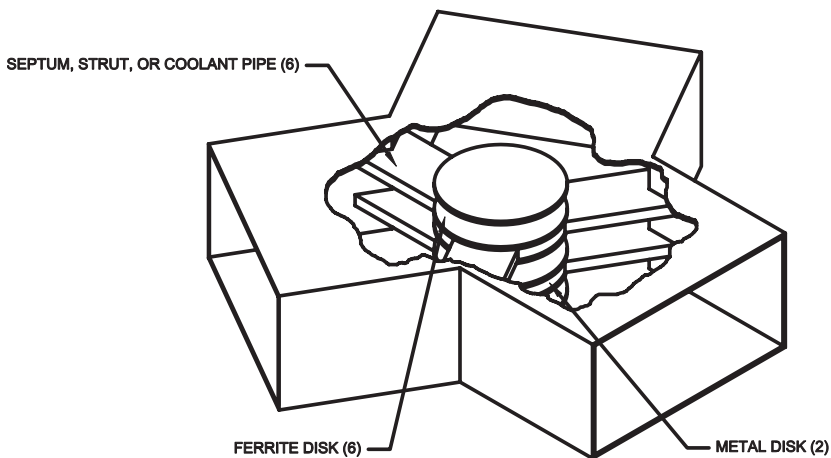


Figure 5.38 Three-cell Okada circulator.

The cooling of the interior ferrites can be accomplished by conduction of heat energy through the metal disk(s) and struts to the waveguide walls. Circulation of liquid coolant inside the struts and disk(s) may provide superior cooling.

The design of a unit junction proceeds initially in the same manner as described in Section 5.1.10 for the design of a conventional waveguide junction circulator. Analysis of a complete Okada circulator is complicated by the presence of multiple unit junctions, the metal disks, and the struts or coolant pipes. Therefore, we rely on measurements of the Okada junction or electromagnetic simulations performed using software such as Ansys® HFSS™. Once the collective junction Q_L and G_r are known, then if necessary, these parameters can be adjusted by varying the waveguide height and the ferrite saturation magnetization or magnetic bias field. If the geometry can be adjusted within the bounds of the thermal design, then the ferrite filling factor (ratio of ferrite thickness to unit junction height) or strut thickness could be adjusted as well.

After acceptable values of Q_L and G_r are established, then our remaining task is to integrate transformers or other impedance-matching structures, as required, with the Okada junction. We do this in the same way as we design the impedance-matching structures for a conventional waveguide junction circulator. Details regarding waveguide impedance transformer design are presented in Section 5.1.10.

5.1.12 Circulators Having Composite Ferrites

In the quest to increase the bandwidth of circulators, one of the outstanding innovations has been the use of composite ferrites. To avoid the frequency limitations of using just one ferrite material in a circulator, this topology uses multiple ferrite materials. US Patent 4,496,915 [40], which has expired, describes this technology. A similar topology, described in US Patent 4,390,853 [41], which has also expired, is to use a special ferrite material having a smoothly varying saturation magnetization or many ferrite materials to produce a saturation magnetization that varies in relatively small steps.

Figure 5.39 shows a circulator layout having two different ferrite materials, one in the form of a ferrite disk and the other material in the form of a ring around the disk. This is a layout for a stripline junction circulator with the top ferrite/dielectric assembly removed so that the center conductor is visible. The design of the circulator in Figure 5.39 is similar to an example detailed in US Patent 4,496,915. A procedure for designing a circulator like this one, suitable for operation over a 100% (3:1) bandwidth follows.

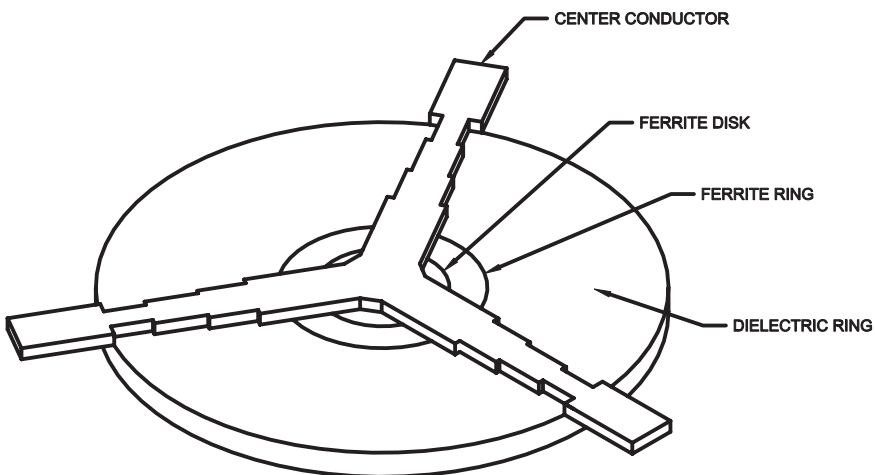


Figure 5.39 Composite ferrite circulator.

First, we choose a relative permittivity (ϵ_D) and diameter (D_D) for the dielectric ring. If the permittivity is too low, the circulator would be large, and if the permittivity is too high, then the circulator would be very sensitive to dimensional variations. The patent suggests a value of $\epsilon_D = 6$. The wavelength in the dielectric ring is given by

$$\lambda_D = \frac{c}{f_0 \sqrt{\epsilon_D}} \quad (5.163)$$

We set the dielectric ring diameter to $1.5 \lambda_D$ to allow sufficient radius for two or three impedance transformers.

We compute the two ferrite saturation magnetization values using

$$4\pi M_{S_{ring}} = \frac{0.817 f_1}{\gamma} \quad (5.164)$$

and

$$4\pi M_{S_{disk}} = \frac{2 \cdot 0.817 \cdot 0.86 f_1}{\gamma} \quad (5.165)$$

where f_1 is the lower frequency band edge in MHz. The diameters of the ferrites are

$$D_{ring} = \frac{c}{2f_1\sqrt{\epsilon_{ring}}} \quad (5.166)$$

and

$$D_{disk} = \frac{c}{2 \cdot 2 \cdot 0.86 f_1 \sqrt{\epsilon_{disk}}} \quad (5.167)$$

Next, we determine the maximum ground-plane spacing using (5.49) or

$$b = \frac{c}{3 \cdot f_2 \sqrt{\epsilon_D}} \quad (5.168)$$

where f_2 is the upper frequency band edge. This ground-plane spacing is approximately equal to that which would support higher-order modes, so a somewhat smaller value of b is desirable to prevent higher-order modes in the frequency band of interest.

Design of the stripline transformers for impedance matching is complicated by the presence of two different ferrite materials. Because of the mathematical complexity, there are two methods available to us for design of the transformers. The first option is to use empirical methods involving arbitrary initial center conductor geometry, measured data, and multiple design iterations. The other option is to simulate the circulator using electromagnetic simulation software such as Ansys® HFSS™ and design an appropriate impedance matching structure based on simulation results.

5.2 Lumped-Constant Circulators

We learned in Section 5.1 that the size of the ferrite resonator disk in a junction circulator is proportional to wavelength. This means that the size of the ferrites becomes prohibitively large at low frequencies. The ferrite size in a lumped-element circulator does not necessarily increase with wavelength.

The lumped-element circulator consists [42] of a ferrite disk with three coils wound on it so that the RF magnetic fields are oriented at 120° with respect to each other. Figure 2.9 shows a ferrite disk with the center conductor (coil) wrapped around it. Other usable geometries are illustrated in Figure 5.40.

The length of the coils is much less than a wavelength at the circulator operating frequency, so they are essentially inductances. The junction

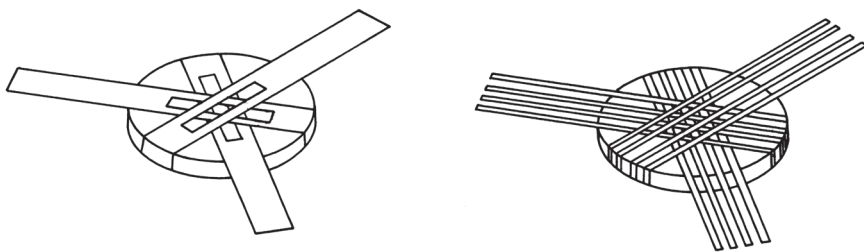


Figure 5.40 Lumped-element circulator geometries.

resonances are formed by connecting capacitances at the three ports. The capacitances can be connected either in the shunt or series configuration, as illustrated in Figure 5.41. The center node of the three nonreciprocally mutual coupled inductances can be either connected directly to ground or grounded through a series-resonant circuit. The series-resonant circuit, suggested by Konishi and Hoshino [43], improves the bandwidth of the circulator by canceling reactive components of the junction impedance at frequencies removed from the center frequency.

In the following discussion, we will consider the directly grounded junction, resonated with series capacitors [44]. The analysis of the shunt-capacitor case would be very similar.

The RF magnetic field in the ferrite disks is shown in Figure 5.42. We let the inductance of each coil, assuming no ferrite is present (inductance in air), equal L_0 . If we think of the propagation in the ferrite as being parallel

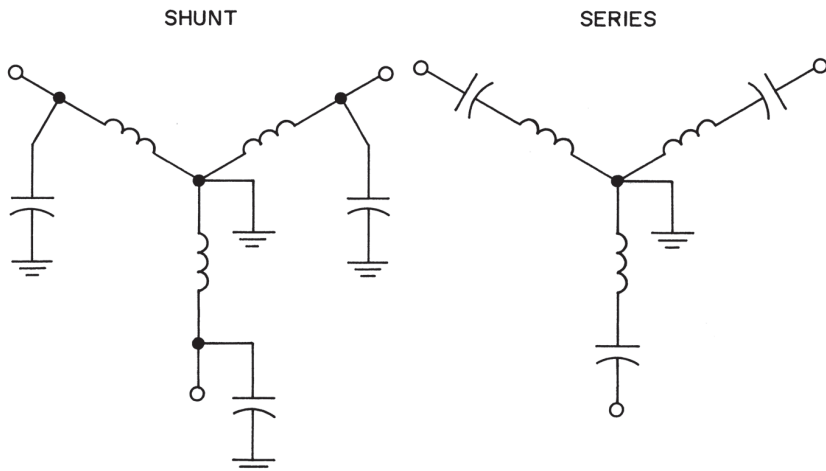


Figure 5.41 Lumped-element circulator capacitor connections.

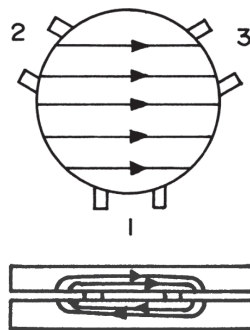


Figure 5.42 RF magnetic field in lumped-element circulator ferrites. Port 1 is excited.

to the applied dc magnetic field, knowing that $L = \mu L_0$, we derive from the factor μ in (1.40):

$$L_+ = L_0(\mu + \kappa) \quad (5.169)$$

$$L_- = L_0(\mu - \kappa) \quad (5.170)$$

where plus and minus signs denote the two counter-rotating modes. The mutual inductance of any pair of coils depends on the direction of signal propagation. We could also analyze the circulator junction using the transverse propagation case and suitable changes in the equations presented here, with little difference in the end result.

For ideal circulation, Dunn and Roberts [44] derive

$$\frac{\omega}{2}(L_+ - L_-) = \frac{Z_0}{1.73} \quad (5.171)$$

$$\frac{\omega}{2}(L_+ + L_-) = \frac{1}{\omega C} \quad (5.172)$$

where C is the capacitance of the series capacitors. We see from these equations that the inductance is an important parameter. The inductance can be achieved with a many-turn coil wrapped around a small ferrite disk or a one-turn coil wrapped around a large ferrite disk.

Neglecting losses, we derive expressions for μ' and κ' from (1.30) and (1.32):

$$\mu' = 1 + \frac{\gamma M_0 \omega_0}{\omega_0^2 - \omega^2} \quad (5.173)$$

$$\kappa' = \frac{\gamma M_0 \omega}{\omega_0^2 - \omega^2} \quad (5.174)$$

By substituting (5.169) and (5.170) into (5.171) and (5.172), we derive

$$1.73\omega L_0 \kappa = Z_0 \quad (5.175)$$

$$\omega^2 L_0 \mu = \frac{1}{C} \quad (5.176)$$

The ferrite disks in a lumped-element circulator are biased above resonance. The techniques described in Section 5.1 for determining the magnetic operating point and bandwidth apply for the lumped-element circulator as well.

To design a lumped-element circulator, we first select an appropriate ferrite material based on the criteria presented in Chapter 4. Next, we choose a value of internal magnetic field, H_{dc} , referring to (5.47), Figure 5.10, and (5.15). κ/μ can be approximated using (5.48) or (5.173) and (5.174).

After we have fixed H_{dc} we can find L_0 from (5.175) and (5.174). We also compute the series capacitor value (C) from (5.176) and (5.173).

The ferrite disk dimensions are somewhat arbitrary. The disk diameter must be much less than a wavelength, or the center conductor coils will not appear as pure inductances. A good rule of thumb is to set the disk diameter equal to $\lambda/16$ or smaller. A larger disk has two advantages: higher average power-handling capacity due to reduced power density in the ferrite and a center conductor with a larger cross section for a given inductance. The disk thickness is even less important. A thin disk is advantageous from both a cost point of view and a thermal consideration. If the disk chosen is too thin, however, the center conductor cross section becomes vanishingly small, negating any power-handling advantages of the thin disk. A good starting point for disk thickness is one-tenth the disk diameter.

The width of the strips wrapped around the ferrite are selected to provide the previously calculated inductance in air (L_0). One strip could be used for each port, but usually two or more strips are connected in parallel. This is done to distribute more evenly the RF magnetic field in the ferrite. Parallelizing also reduces the total inductance at each port.

The inductance of a strip in air can be calculated from the stripline impedance formulas (5.50) to (5.52) if we know that [31]

$$L = 0.08467 Z_0, \text{ nH/in} \quad (5.177)$$

If we opt to use two strips at each port, the inductance of each strip must be twice L_0 . We use $2L_0$ to find the required Z_0 in (5.177), then adjust the strip width to achieve this Z_0 .

The strips from adjacent ports are insulated from each other where they cross with an insulating tape such as Teflon (PTFE) tape. The insulation thickness should be kept to a minimum so that all the strips are close to the ferrites. The crossover points should also have low capacitance. The simultaneous requirements of thin spacing and low capacitance may seem to be conflicting, but they are not. There are two dimensional variables that apply to a parallel-plate capacitor model. One is the spacing between the capacitor plates, and the other is the area of the plates. We can change the amount of capacitance even if we choose to fix one of the dimensional variables—the spacing. To reduce the capacitance at the crossover points, we can make the strips narrower in the vicinity of the cross. This may be necessary if wide strips are to be used. An analysis of the effects of this interstrip capacitance on circulator performance would be quite involved and, in nearly all cases, not justified.

The peak power-handling capacity of lumped-element circulators is limited because of the necessarily thin insulation on the strips.

In practice, lumped-element circulators are not perfectly symmetrical because the strips from one port are not against the ferrites but between the strips from the other two ports. This problem can be eliminated by weaving the center conductor so that all the strips have an equal amount of contact with both ferrites.

If sufficient bandwidth cannot be obtained with just the circulator junction, we add impedance matching (compensation) sections. Because of the low frequencies involved, these networks would be too large if they were constructed with sections of transmission line. Therefore, they are constructed from discrete capacitors and inductors. The circuits usually take the form of bandpass structures, having parallel- and series-resonant sections. It is usually best to evaluate the junction alone before adding the compensation networks.

5.3 Differential Phase Shift Circulators

The operation of the waveguide differential phase shift circulator is described in Section 2.5. There are several methods of implementing the required differential phase shifts. The first method, shown in Figure 5.43, uses identical magic tees or quadrature couplers at each end of the two waveguide sections. One waveguide section has a 180° nonreciprocal (differential) phase shifter, and the other section is dielectrically loaded to produce a reciprocal (not

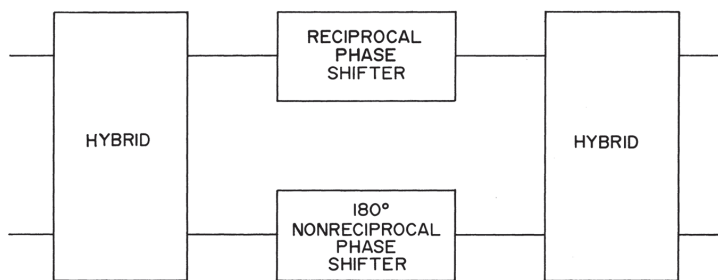


Figure 5.43 Differential phase shift circulator implementation.

differential) phase shift equal to the phase shift, in one direction, of the 180° section.

The second method employs 90° nonreciprocal phasers in both waveguide sections, between identical tees or couplers. One of the waveguide sections also contains a 90° reciprocal phase shifter. This reciprocal phaser could simply be a dielectric slab placed inside the guide. This method of implementation is illustrated in Figure 5.44.

Figure 5.45 shows that the third implementation method is to use 90° nonreciprocal phasers in both waveguide sections, but use different types of couplers at the ends. If a magic tee is used at one end of the waveguides, a quadrature coupler is used at the other end.

Design data for couplers and tees are readily available, and an entire book could be written just about these components, so we will not discuss their design here.

The basic geometry of the differential phase shifter is shown in Figure 5.46. From perturbation theory, Clarricoats [45] derives expressions for propagation constants of ferrite-loaded waveguides. These expressions contain nonreciprocal terms (i.e., the wave traveling through the waveguide suffers

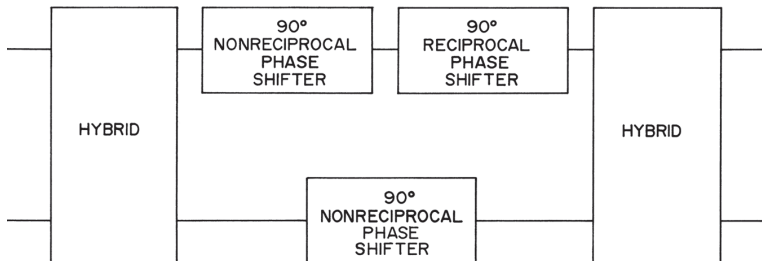


Figure 5.44 Differential phase shift circulator implementation.

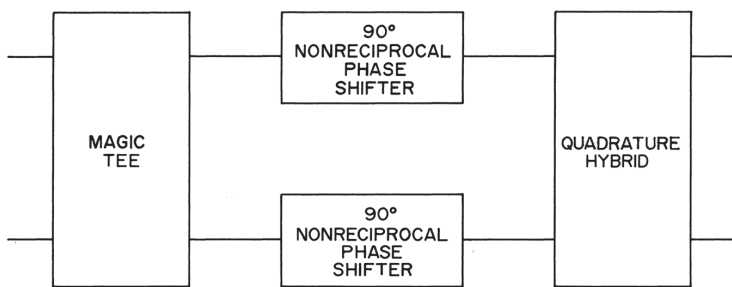


Figure 5.45 Differential phase shift circulator implementation.

different phase shifts depending on the direction of propagation). We have already discussed the reasons for this nonreciprocal behavior in Chapter 1. The only additional information needed is that the ferrite material is located in the waveguide such that the fields in the ferrite are circularly polarized.

There are natural regions of circular polarization in rectangular waveguides that operate in the TE_{10} mode. When ferrite slabs are placed in these

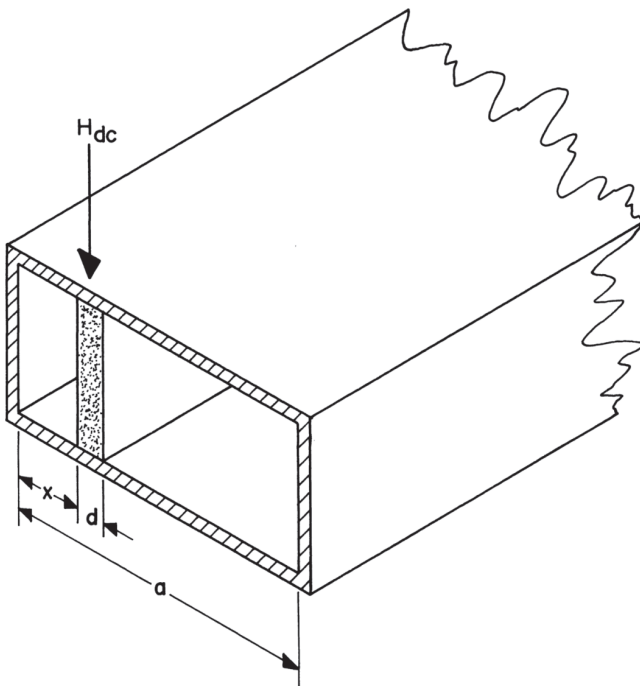


Figure 5.46 Nonreciprocal waveguide phase shifter.

regions, waves with circular polarization are excited in the ferrite. The sense of polarization (left or right hand) depends on the direction of wave propagation in the waveguide. Waves traveling in the forward direction in the waveguide excite circularly polarized waves in the ferrite with one sense of polarization, and waves traveling in the reverse direction excite waves in the ferrite with the opposite sense of polarization.

Because the propagation constants for the two different senses of circular polarization are different as described in Section 1.4, there are different phase shifts associated with the transmission of the two types of waves in the ferrite-loaded waveguide.

The natural regions of circular polarization in rectangular waveguide occur as illustrated in Figure 5.47. As a wave travels down the guide, the loops formed by the magnetic field lines also travel. If we consider the direction and magnitude of the magnetic field at a particular position and instant of time, we have the field vector shown in Figure 5.47. As time progresses, the field vector rotates due to the change in the magnetic field. At a certain position in the waveguide, the magnitude of the magnetic field vector does not change; only

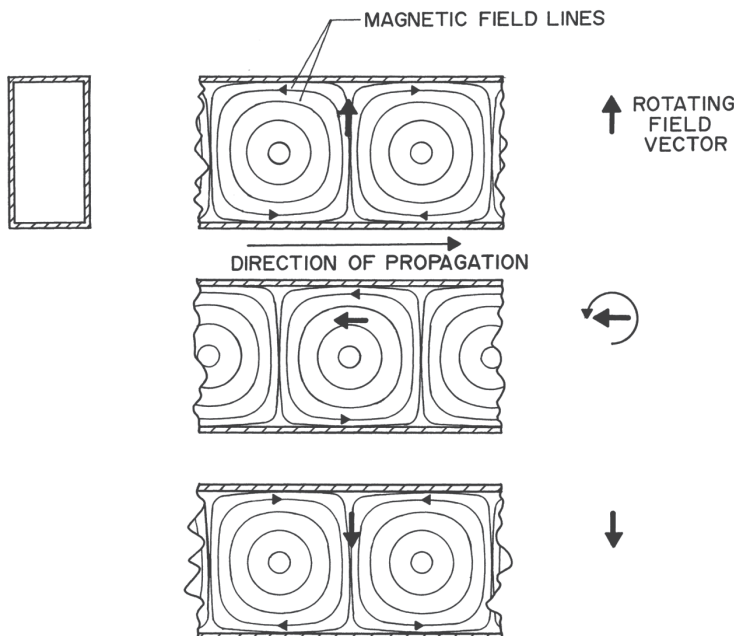


Figure 5.47 Circular polarization in a rectangular waveguide.

the direction changes, and we have circular polarization. Circular polarization occurs at a point in the guide about one quarter of the way across. The sense of polarization (direction of magnetic field vector rotation) is opposite for waves traveling in opposite directions in the waveguide.

The differential phase shift per unit length is given by

$$\beta_+ - \beta_- = \frac{2\pi d}{a^2} \frac{\kappa}{\mu} \sin \frac{2N\pi x}{a} \quad (5.178)$$

where d is the ferrite slab thickness, a is the waveguide width, and N is an integer (we let $N = 1$ for our purposes). The maximum differential phase shift is obtained when $x = a/4$:

$$\beta_+ - \beta_- = \frac{2\pi d}{a^2} \frac{\kappa}{\mu} \quad (5.179)$$

The ferrite slab in a differential phase shifter is biased below resonance, typically in the region where $\mu = \kappa$. When $\mu = \kappa$, we find from (1.30) and (1.32), assuming the ferrite is lossless, that

$$H_{dc} = \frac{\omega}{\gamma} - M_0 \quad (5.180)$$

We see from (5.179) that to achieve a high value of differential phase shift, we need $\mu < \kappa$. The factor κ/μ increases with magnetic field, but the insertion loss climbs as we approach ferrimagnetic resonance.

After selecting an appropriate ferrite material, we establish the dimensions of the slab. The thickness of the slab (d) should be greater than $a/10$ to maximize the differential phase shift, but less than $\lambda/10$ to avoid multimode propagation. The length of the slab is calculated using (5.179), where the desired differential phase shift depends on the particular design but will usually be 90 degrees. The value of κ/μ can be determined by numerical analysis of the insertion loss as a function of H_{dc} as described in Section 5.1. The highest value of κ/μ is obtained with the highest tolerable magnetic field from an insertion-loss point of view. As an alternative to the computations, we can assume $\kappa/\mu = 1$, remembering that the differential phase shift will be higher than the value we calculate using this assumption.

The position x of the ferrite slab is somewhat critical, but should be near $a/4$. There is no nonreciprocal phase shift when the ferrite slab is placed against the waveguide wall or in the center of the guide. The position should be adjusted experimentally to obtain good differential phase shift and, more importantly, minimum variation in phase shift over the frequency band of interest.

The isolation the finished circulator will have as a function of variation in differential phase shift is approximated by

$$\text{Isolation} = -10 \log_{10} \left\{ \sin \left[\frac{\Delta(\beta_+ - \beta_-)}{2} \right] \right\} \quad (5.181)$$

To reduce reflections (VSWR) from the ferrite slab, the ends can be tapered. The length of the taper should be determined experimentally. The bandwidth of the phaser can be increased by dielectric loading techniques, which are also largely empirical in nature.

Improved thermal performance and, consequently, improved power handling can be achieved by using thin ferrite slabs mounted against the guide's broad walls instead of the slab oriented in the E plane, shown in Figure 5.46. This scheme is illustrated in Figure 5.48.

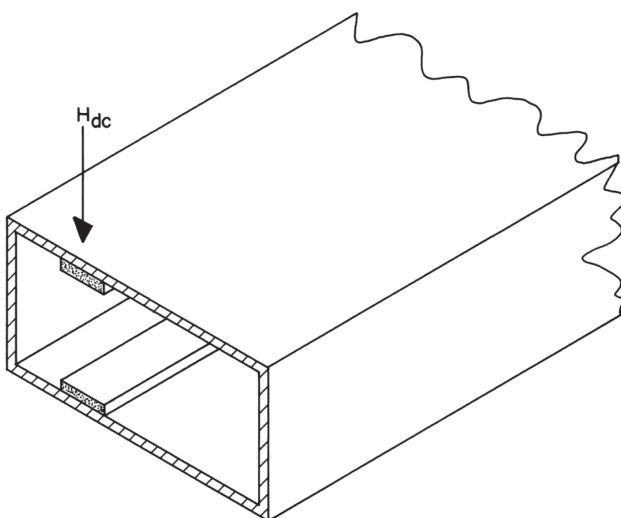


Figure 5.48 Alternative ferrite slab location.

5.4 Resonance Isolators

The resonance isolator is a two-port nonreciprocal attenuator that relies on the absorption of energy at ferrimagnetic resonance. The basic configuration of the resonance isolator is very similar to the differential phase shifter geometry shown in Figure 5.46.

The position of the ferrite slab in the waveguide is such that resonance absorption occurs for only one direction of propagation, as described in Section 2.8. Forward and reverse waves traveling through the waveguide excite circularly polarized waves in the ferrite slab with opposite senses of polarization. The rotation of the reverse circularly polarized mode coincides with the direction of electron precession, so the energy in the reverse wave is coupled into the precession system, and we say it undergoes resonance absorption. Because the electrons can only precess in one direction for a given polarity of applied dc magnetic field, and the direction of rotation of the forward circularly polarized mode does not coincide with the direction of electron precession, the forward wave does not exhibit resonance absorption.

The mechanism of circular polarization in a rectangular waveguide is explained in Section 5.3. The ferrite slab in a resonance isolator is located in a region of circular polarization in the waveguide, so elliptically polarized waves can propagate in the ferrite.

An improvement in the front-to-back ratio of the isolator can be obtained by placing one to four ferrite slabs with their faces against the broad walls of the waveguide, as shown in Figure 5.48. This configuration also increases the average power-handling capacity because the slabs are in good thermal contact with the walls. A disadvantage of not filling the entire height of the guide with ferrite is that a much higher magnetic field is necessary to bias the ferrite slabs. This problem can be minimized, however, by using reduced-height waveguide.

Various methods have been suggested [45] to increase the bandwidth of resonance isolators. One is to use several ferrite slabs with different saturation magnetizations, one for each band of frequencies. Another method is to use nonuniform applied magnetic fields or different ferrite shapes.

Isolation and front-to-back ratio can be improved by employing dielectric loading techniques. In a waveguide isolator, the best location for the dielectric is against the ferrite face nearest the center of the guide, as shown in Figure 5.49.

The magnetic operating point of the resonance isolator is, of course, at resonance. Equation (1.7) describes the relation between resonance frequency and internal magnetic field.

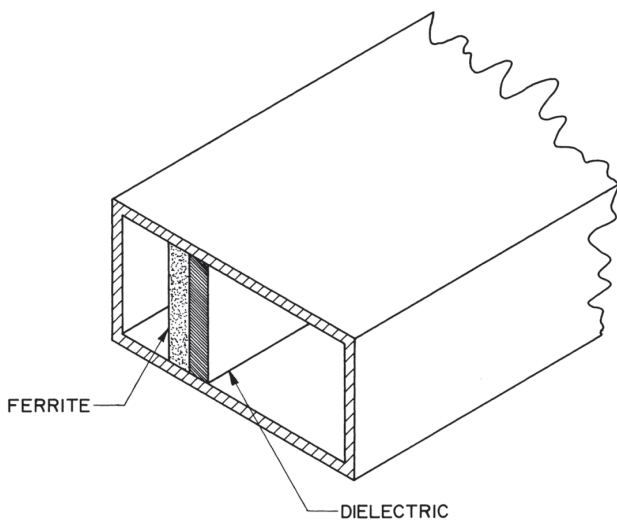


Figure 5.49 Dielectric loading.

The guidelines presented in Section 5.3 for ferrite thickness and positioning also apply to the resonance isolator, but the exact geometry must be determined experimentally.

We must use dielectric material in the construction of coaxial resonance isolators. The dielectric helps create a circularly polarized field at the dielectric-air interface, which would not be present without the dielectric. A cross-sectional view of a coaxial resonance isolator is shown in Figure 5.50.

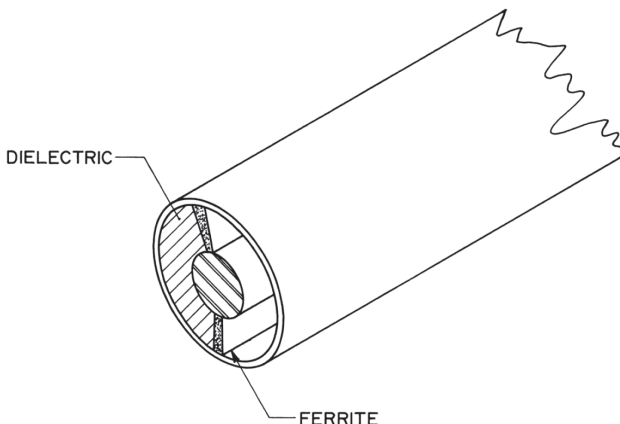


Figure 5.50 Coaxial resonance isolator.

The stripline junction isolator offers better electrical performance, smaller size, and lower cost (in many cases) than the coaxial resonance isolator. For these reasons, the junction isolator is much more popular. We will not present detailed design information for the coaxial resonance isolator because it is unlikely that anyone designing modern equipment will need to design one of these devices. Several other types of circulators have been omitted because they are no longer produced in quantity; one example is the Faraday rotation circulator.

5.5 Dummy Loads for Isolators

Dummy loads, also called terminations and RF loads, are often integrated with circulators to form isolators. Therefore, we will discuss some basic design concepts for these components.

Loads are made for both coaxial and waveguide transmission media. Some typical coaxial loads are shown in Figure 5.51 and waveguide terminations in Figure 5.52. Chip terminations are also widely used.

The absorptive element in a coaxial load could be either a thin-film resistor or bulk absorbing material such as polyiron. Thin-film resistors are often made with beryllium oxide substrates, which have very good thermal conductivity. As an example of the average power-handling capacity of these resistors, a rod 3/8-in diameter by 3/4-in long can dissipate up to 60W continuously if properly cooled. Rod resistors are sold in a wide variety of sizes.

Polyiron, as we call it, is an iron-loaded epoxy-based material that absorbs RF energy. The material is available in different attenuation values; the attenuation is measured using a fully filled length of coaxial line. The

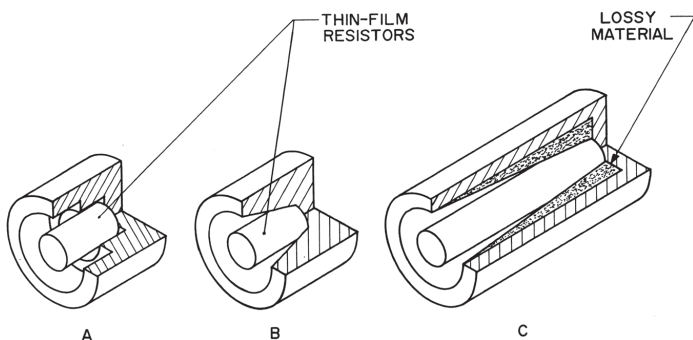


Figure 5.51 Typical coaxial terminations.

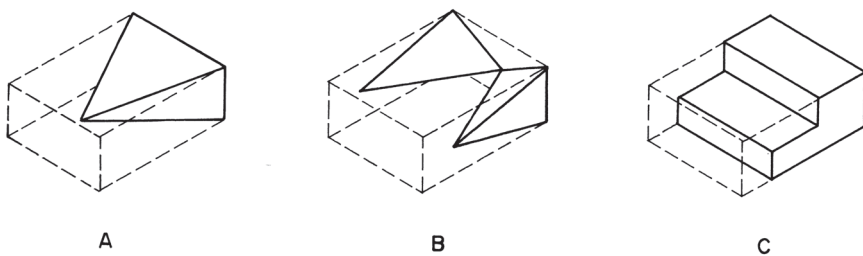


Figure 5.52 Typical waveguide terminations.

attenuation is specified in decibels per unit length at a specific frequency, usually 10 GHz. The attenuation is approximately proportional to frequency. The power-handling capacity of this material is typically about 40 W/in at room temperature.

The key parameters of an RF load are the VSWR, frequency range, and power-handling capacity. To achieve high average power handling, it is important to keep the absorptive element as cool as possible, because the RF energy is converted to heat. The rod resistors have a quite broad frequency range, extending from dc to the frequency where the skin depth is much less than the thickness of the resistive film. As we know, most of the current in the inner conductor of a coaxial line flows at its surface. The skin depth is the depth from the surface where the current decreases to $1/e$ of the current at the surface.

For low VSWR, the outer conductor around the rod resistor must be tapered. This tapering is done to maintain characteristic impedance (between the rod and outer conductor) equal to the resistance of the rod resistor to ground at any point along its length. When the wavelength is much larger than the length of the resistor, a simple step taper like the one shown in Figure 5.51(a) will suffice. The small diameter forms a $25 \Omega Z_0$, and the larger diameter is 50Ω . The best taper is logarithmic, as shown in Figure 5.51(b).

The coaxial loads built with absorptive material (polyiron) have more narrow bandwidths because of the frequency sensitivity of the material. For low VSWR (<1.10:1), the taper illustrated in Figure 5.51(c) should be at least one wavelength long, and the fully filled portion of the line should be at least one outer-conductor diameter long. The taper serves not only to provide a good impedance match, but also to distribute the power more evenly in the absorber. This type of load is usually limited in bandwidth to about one octave. We choose the material so that it has sufficient loss at the lowest frequency in the operating band to achieve the required return loss. The upper frequency limit is then set by the nonuniform thermal distribution in the absorber.

The waveguide absorptive elements can be made from either polyiron or a high-temperature ceramic material. The ceramic (refractory) material has greater power-handling capacity than the epoxy material. Of the three tapers shown in Figure 5.52, the one shown at 5.52(b) has the highest power capacity because it has the greatest contact with the metallic waveguide walls, which can conduct away the heat. The step taper shown in Figure 5.52(c) has the advantage of being small in size and easy to manufacture, but does not offer good bandwidth because the transition to the material is not smooth. The shape in 5.52(a) is easy to remove and install in the guide because it touches only one wall.

Again, a taper length of one wavelength will provide a good match over the full waveguide bandwidth.

A wide variety of commercial RF loads are on the market, many of which are easily integrated with a circulator and are cost effective.

5.6 Temperature Effects

The magnetic properties of ferrites, particularly the saturation magnetization ($4\pi M_S$) and the resonance linewidth (ΔH), vary with temperature. This causes variation in the electrical performance of circulators. Variation in magnet characteristics can also contribute to variation in circulator performance with temperature.

Figures 5.53 and 5.54 show the variations in insertion loss and isolation, respectively, with temperature, for an above-resonance stripline-junction circulator, simulated using Ansys® HFSS™. For generation of these figures, H_{dc} was held constant, which would be the case if the magnetic circuit were capable of producing perfectly constant internal magnetic field in the ferrite. The $4\pi M_S$ values used in the simulations were chosen in accordance with published temperature curves. The design of the circulator is as described in Section 10.2.

We can see in Figures 5.53 and 5.54 that the circulator response moved down in frequency at the cold temperature, and up in frequency at the hot temperature. This behavior is explained by variation in the ferrite effective permeability (μ_{eff}) with temperature. For the above-resonance region, we approximate μ_{eff} using (5.10).

If H_{dc} is constant, then the variation in μ_{eff} with temperature is proportional to the variation in $4\pi M_S$, and it follows that the variation in the circulator center frequency is inversely proportional to the square root of the variation in $4\pi M_S$:

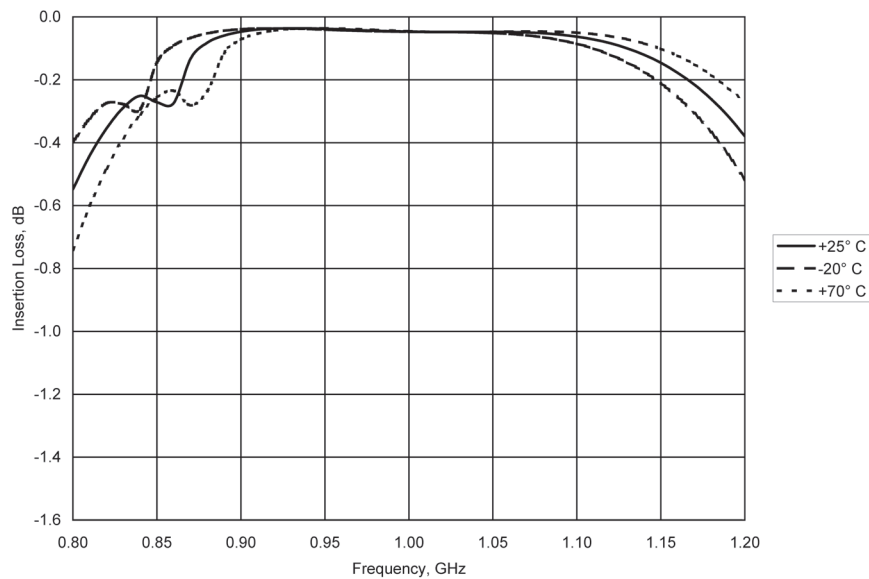


Figure 5.53 Simulated insertion loss of an above-resonance circulator with temperature as a parameter. H_{dc} is constant.

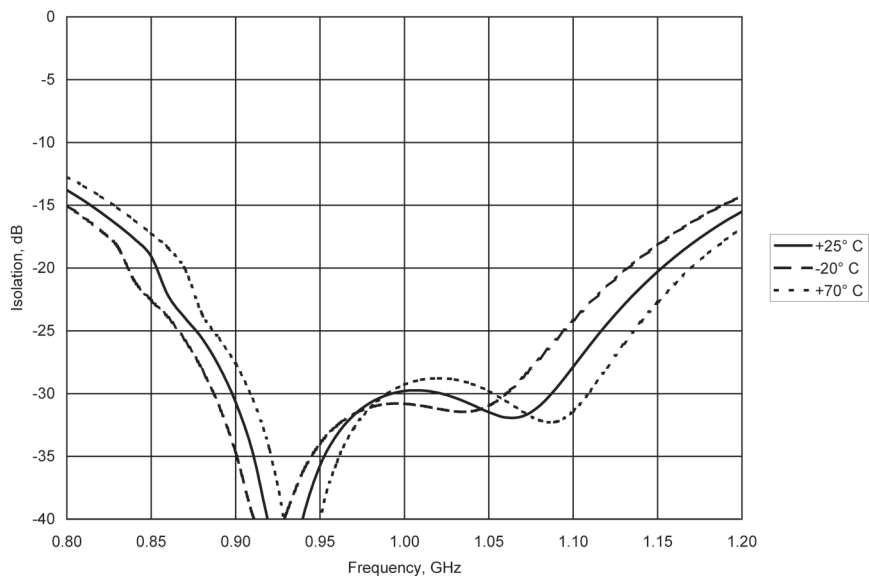


Figure 5.54 Simulated isolation of an above-resonance circulator with temperature as a parameter. H_{dc} is constant.

$$f_0 \propto \frac{1}{\sqrt{\mu_{\text{eff}}}} = \frac{1}{\sqrt{\frac{H_{\text{dc}} + M_0}{H_{\text{dc}}}}} \quad (5.182)$$

If the magnetic circuit is uncompensated, and the external magnetic bias field (H_{ext}) is constant with temperature, then H_{dc} will vary with variation in $4\pi M_S$, as detailed in Section 6.1.1. In this case, the electrical performance of the same stripline-junction above-resonance circulator, having thin ferrite disks, is shown in Figures 5.55 and 5.56. We can see in these figures that the variation in electrical performance is substantial due to the variation in both H_{dc} and $4\pi M_S$.

In the below-resonance region, we approximate μ_{eff} using (5.28).

Below resonance, H_{dc} has a weak effect on μ_{eff} , but $4\pi M_S$ has a relatively strong effect, and the sign is opposite from that in the above-resonance case. Therefore, as shown in Figures 5.57 and 5.58, the circulator frequency response rolls off at the lower frequency band edge at the cold temperature, and it rolls off at the upper frequency band edge at the hot temperature. The design of

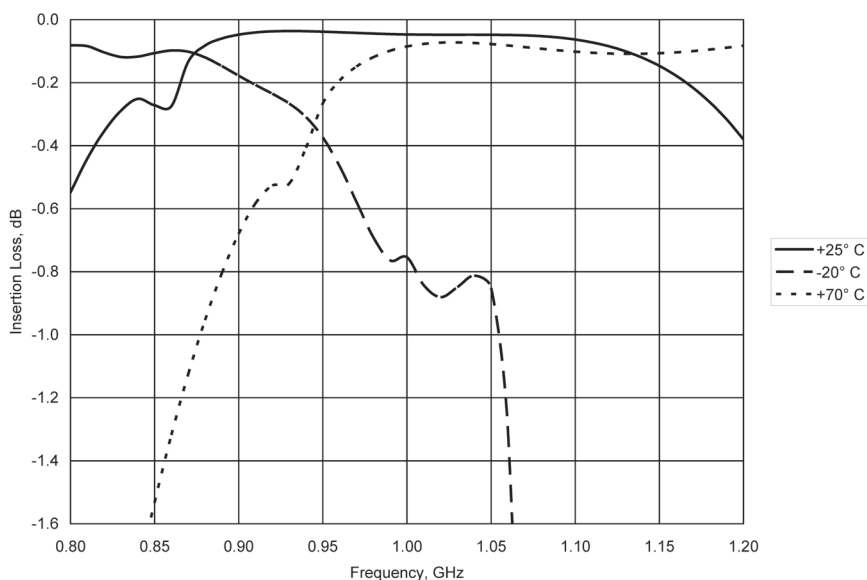


Figure 5.55 Simulated insertion loss of an above-resonance circulator with temperature as a parameter. H_{ext} is constant.

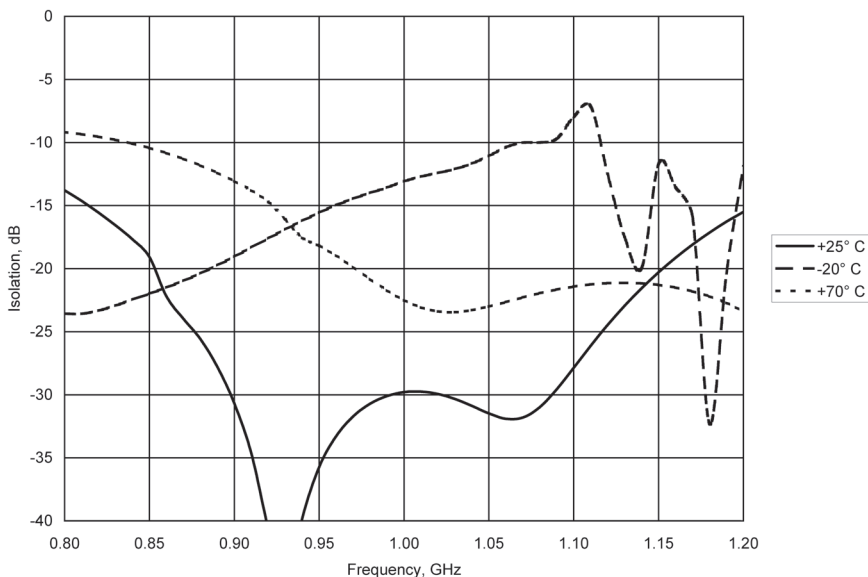


Figure 5.56 Simulated isolation of an above-resonance circulator with temperature as a parameter. H_{ext} is constant.

this below-resonance stripline-junction circulator is as described in Section 10.3, and we simulated its performance using Ansys® HFSS™.

This book is supposed to be about circulator design, so it seems reasonable that after presenting some information about how temperature typically affects circulators, we should next provide some useful design information. Selection of temperature stable ferrite material, as described in Chapter 4, can help with circulator temperature stability. Chapter 6 describes temperature compensation of the magnetic circuit, which also serves to improve circulator temperature stability.

In addition to material selection and magnetic-circuit temperature compensation considerations, another possibility is to choose the magnetic bias field such that the circulator temperature stability is optimum [46]. This technique varies somewhat depending on the particular circulator design and materials used, so some empirical design work or electromagnetic simulation is called for. Yet another design option is to set the circulator reflection phases such that variation in reflection magnitude with temperature is minimized. This is also a stabilization technique that is unique to each particular circulator design.

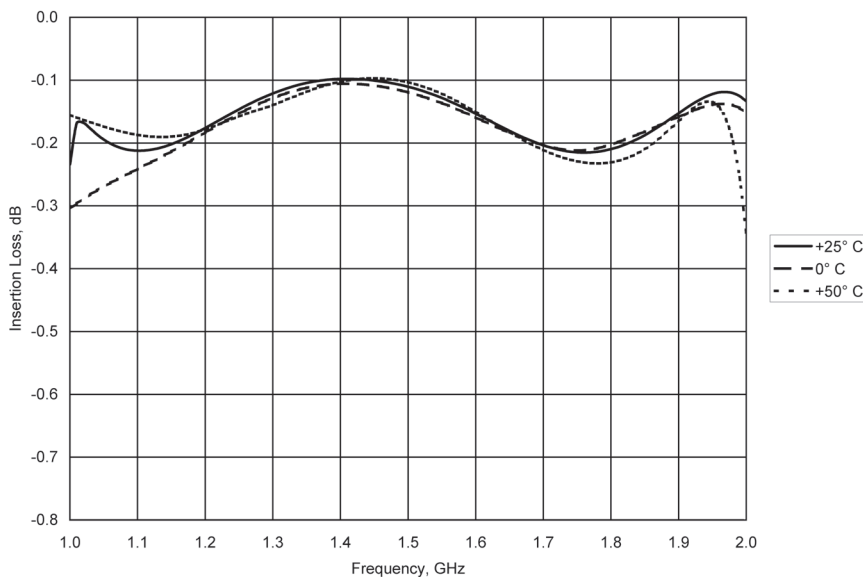


Figure 5.57 Simulated insertion loss of a below-resonance circulator with temperature as a parameter.

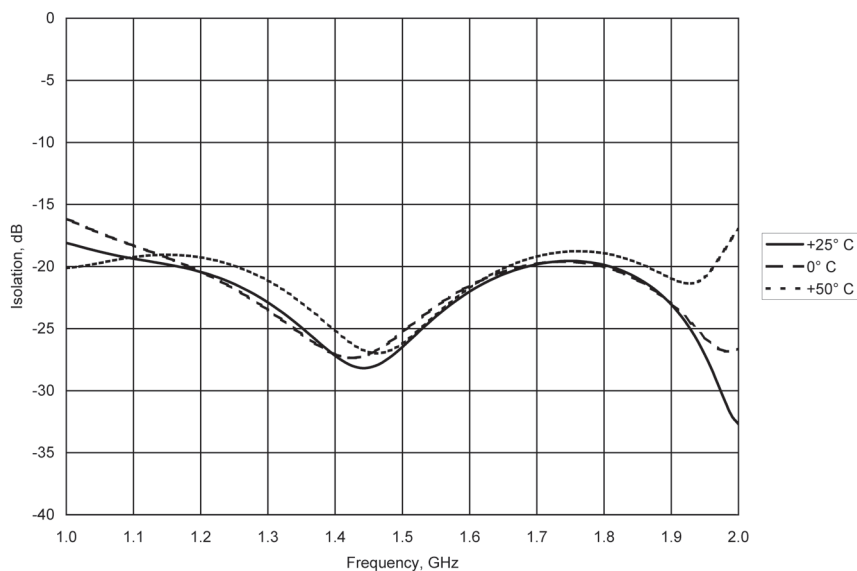


Figure 5.58 Simulated isolation of a below-resonance circulator with temperature as a parameter.

5.7 Intermodulation Distortion

Intermodulation distortion has long been an important consideration in microwave communication systems. With the advent of cellular telephones, and the accompanying numerous co-located transmitters and multiple-carrier transmitters, intermodulation distortion has received more attention. As discussed in Chapter 2, microwave circulators typically introduce more intermodulation distortion than other passive components because of nonlinearity in the ferrite.

Many of the following considerations [47] for minimizing intermodulation distortion in cables and connectors also apply to circulators, but are not as critical as considerations related to the ferrite:

1. Connectors should have large contact surface areas and high contact pressure to maintain low contact resistance.
2. The number of internal connections should be minimized, as should the number of joints in a housing.
3. Soldered joints are preferred over other joint types. Threaded and press-fit joints should be avoided due to the potential for higher contact resistance.
4. Avoid nickel and ferrous metals, as they exhibit nonlinear characteristics. Copper alloys are preferred.
5. Plating on metals should be of silver or a suitable low-intermodulation-distortion alloy. Gold is usually undesirable from an intermodulation distortion perspective unless it can be of sufficient thickness, which makes gold plating expensive.
6. Maintain cleanliness. Loose metal particles or other contaminants can cause intermodulation distortion.

At high RF power levels, steps must be taken to prevent voltage breakdown, covered in Section 5.8.3. Voltage breakdown is a nonlinear effect that can generate intermodulation distortion.

As discussed in Section 5.8.4, spin waves can cause nonlinearity in ferrites, particularly in below-resonance circulators. Spin-wave nonlinearity is a cause of intermodulation distortion in below-resonance circulators, so the factors affecting spin-wave instability should be considered when designing a low-intermodulation-distortion circulator.

A rigorous mathematical analysis of intermodulation distortion in circulators would be quite cumbersome, and is not necessary for the design of circulators. A study of intermodulation distortion in circulators [48] revealed

that κ' , of (1.32), is an important factor, as is the circulator impedance. For lowest intermodulation distortion, minimize κ' and maximize the impedance. Using equations derived from (1.32), we approximate κ' using

$$\kappa' = \frac{\gamma M_0}{\omega} \quad (5.183)$$

for below-resonance circulators and

$$\kappa' = \frac{\gamma M_0 \omega}{\omega_0^2 - \omega^2} \quad (5.184)$$

for above-resonance circulators.

To minimize κ' , avoid magnetic operating points near ferrimagnetic resonance. Below resonance, this means to use a low value of $4\pi M_S$, and above resonance, use a low value of $4\pi M_S$ or increase H_{dc} , which has a stronger effect on κ' . Note that increasing H_{dc} also decreases μ_{eff} , and hence reduces the electrical size of the circulator resonator. To maintain the same electrical size of the resonator, a higher value of $4\pi M_S$ could be used without negating the increase in H_{dc} because H_{dc} has a stronger effect.

To increase the circulator resonator impedance, we generally have to increase the ferrite thickness (d) or modify the structure coupling to the resonator. In the case of a stripline junction circulator, this means to narrow the striplines.

Changes to the magnetic operating point and resonator impedance affect other electrical parameters. There is a tradeoff between circulator bandwidth and performance in terms of intermodulation distortion. Typical levels of circulator intermodulation distortion are presented in Chapter 2.

5.8 RF Power Effects

5.8.1 Steady-State Thermal Effects

The concern when high average powers are present is that the ferrite, dielectric material, center conductor, or solder joints will overheat. We analyze the strip-lines between the circulator junction and the connectors by first determining the insertion loss of these lines, the amount of power dissipated by the line per unit length, and finally the temperature rise of the center conductor and dielectric near it, considering that the heat is conducted through the dielectric

to the ground plane. A complete analysis is beyond the scope of this book, but some of the thermal considerations are discussed further in Chapter 7.

The critical component of the circulator to be designed for high average power is the ferrite junction. The amount of power dissipated in the ferrites must be minimized. This means we want low insertion loss. To keep the surface of the ferrite nearest the center conductor cool, we need to use thin ferrites. This leads to smaller ground-plane spacing and higher losses in the striplines. Also, an extremely thin ferrite disk (or triangle) may produce higher loss in the ferrite, and hence more power dissipated in the ferrite. In addition, other parameters, such as bandwidth and VSWR, may degrade if the ferrite is made too thin. Thus, we have a tradeoff between electrical performance and thermal performance.

The focus of this chapter is on electrical design, so we will describe the electrical effect of overheating ferrite and how to quantify the heat load, which results from the incident RF power and the electrical characteristics of the circulator. The removal of heat from the ferrite and other circulator parts is discussed in Chapter 7, which covers mechanical design.

Typically most of the power dissipated in a circulator is dissipated in the ferrites because magnetic losses dominate dielectric and ohmic losses. The magnitude of the dissipated power can readily be calculated from the incident power and insertion loss, but the distribution of the power is important. Using electromagnetic simulation software, such as Ansys® HFSS™, including output based on Poynting vector theory, we can readily determine the power distribution. Figures 5.59 and 5.60 show the simulated *volume loss density*, or dissipated power distribution, in the ferrite of a stripline junction circulator, similar to the one described in Section 10.2. Figure 5.59 is a top view of the circulator, and Figure 5.60 is an edge view of the same circulator. The scale of the loss density plots is W/m^3 with 1W incident on one port (the right-hand port in Figure 5.59). We see in the figures that the power is dissipated near the edges of the center conductor and mostly along the transmission path (from right to left in Figure 5.59). In this simulation, the circulator output port is terminated in a matched load, so very little power is delivered to the isolated port (the lower left port in Figure 5.59). In Figure 5.60, we can see that the power is dissipated mostly near the surfaces of the ferrites that are in contact with the center conductor.

If it is not possible or practical to accurately compute the distribution of the heat load, we use an empirical estimate of the distribution of the heat load. This approximation is that the heat is dissipated *at the surfaces* of the ferrites nearest the center conductor and is distributed over one half the ferrite surface area.

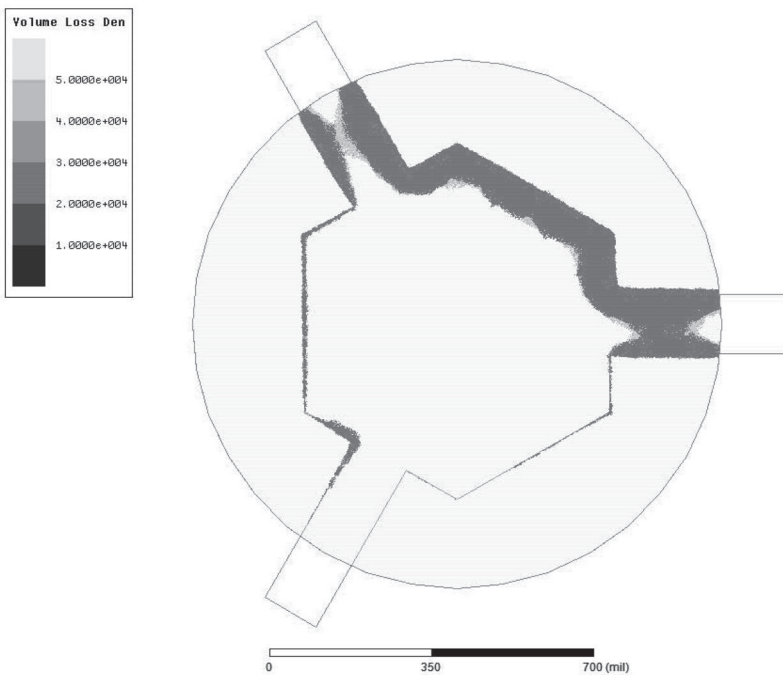


Figure 5.59 Dissipated power distribution in the ferrite of a stripline junction circulator, top view.

Heating of the ferrite raises its temperature and affects circulator electrical performance as described in Section 5.6. The heating effect of RF power is not quite the same as exposure of a circulator to an elevated temperature, however. Ferrite heating from RF power dissipation is nonuniform, so there are temperature gradients in the ferrite. To assume that the temperature of the ferrite is uniform is a reasonable first-order approximation. To accurately predict the electrical performance of a circulator with incident RF power, it would be necessary to analyze the circulator with different ferrite material properties in different regions, depending on temperature. An alternative is to perform RF power testing of a prototype circulator, but this may not be possible if appropriate test equipment is not available. Fortunately, it is rarely necessary to perform this level of analysis or testing.

One method of reducing ferrite temperature is to reduce the power density in the ferrite by increasing the disk diameter or triangle altitude, while not increasing the insertion loss proportionally. The only way we can increase the surface area of the ferrite without changing the operating frequency of the circulator is to decouple the center conductor from the disk.

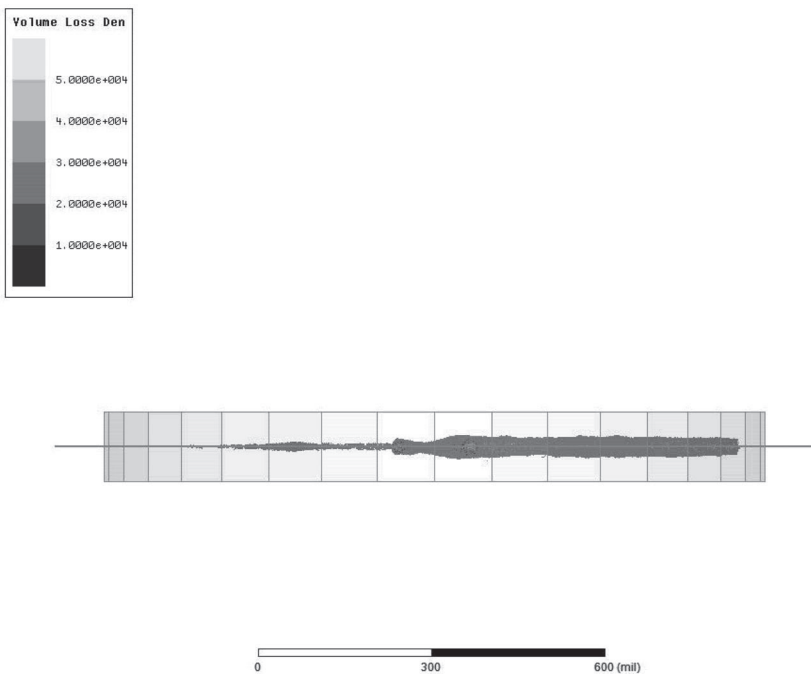


Figure 5.60 Dissipated power distribution in the ferrite of a stripline junction circulator, edge view.

We explain the concept of decoupling by thinking of the ferrite disks (or triangles) and the immediately surrounding volume as a cavity resonator. If this abstract cavity contains no ferrite (only air) it will have a particular resonant frequency for a given mode. If ferrite is added to the cavity, the resonant frequency will generally decrease due to the permittivity and permeability of the ferrite, which are greater than the values for air. The ratio of ferrite volume to air volume in the cavity is described by a quantity called the filling factor. The more ferrite we have in a cavity of given size, the higher the filling factor. A higher filling factor implies a lower resonant frequency.

A larger cavity will also have a lower resonant frequency than a smaller cavity. Our goal is to increase the ferrite volume without changing the operating frequency of the circulator. To do this, we must necessarily increase the cavity volume because the “cavity” of a typical stripline junction circulator is fully filled with ferrite. If we increase the cavity volume without changing the filling factor, the circulator frequency will decrease. We therefore reduce the filling factor to maintain the same circulator operating frequency.

We implement the reduction in filling factor by substituting dielectric material having a lower dielectric constant than ferrite for some of the ferrite. It is desirable to have the ferrites in contact with the ground planes for good thermal conduction (to keep them cool), so we place the dielectric between the ferrite and the center conductor.

The disadvantage of decoupling the center conductor from the disks is that the loaded Q of the junction will increase, which implies a decrease in bandwidth. In general, decoupling a resonant circuit from source and load will increase circuit Q .

Decoupling is accomplished by placing dielectric material between the ferrite and the center conductor. A flexible material such as Teflon works well; at lower microwave frequencies where average or CW power levels are more likely to be high, a good starting thickness is about 0.05 in. The decoupling scheme is illustrated in Figure 5.61.

5.8.2 Transient Thermal Effects

Even if the average power level is insufficient to cause significant thermal drift in electrical performance, a high ratio of peak power to average power (low duty cycle) can cause intrapulse thermal effects, particularly with wide pulses. To determine whether these thermal effects are problematic, we perform a thermal transient analysis. If the heat load magnitude and distribution on and in the ferrite is known (e.g., from an electromagnetic simulation using software such as Ansys® HFSS™), then these data could be used as input to the thermal analysis. Alternatively, the magnitude and distribution of the heat load could be estimated using the same technique described in Section 5.8.1.

Once the heat load is known, commercial thermal transient analysis software is available to perform the thermal portion of the analysis. If thermal

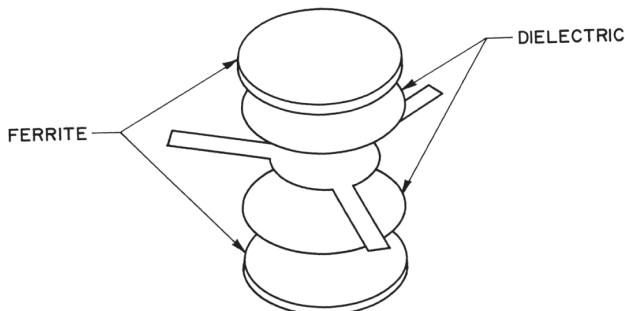


Figure 5.61 Ferrite decoupling scheme.

transient analysis software is not available, then we could use the following numerical technique [49] for estimation of the temperature rise due to the high peak power thermal transient. Figure 5.62 shows a cross section of ferrite mounted on a heat sink, as might be the case in a high-power circulator. The ferrite thickness (d) is divided into a number ($n - 1$) of abstract layers of thickness Δd . The heat load in the figure is applied to the top layer, but could be distributed among several layers. The first subscript of the layer surface temperature T in Figure 5.62 corresponds to the position, and the other subscript corresponds to the elapsed time since application of the transient heat load. In this one-dimensional analysis, we assume that each layer surface temperature is uniform across the layer. Any layer area may be used, but for better resolution, area should be small, and the analysis repeated for each discrete combination of ferrite and heat load. We can achieve increased accuracy by using smaller time steps in this analysis.

In this numerical technique, we calculate the temperature of a layer from the energy entering the layer, the energy leaving the layer, and its previous temperature:

$$T_{(i=1..n),0} = T_{HS} \quad (5.185)$$

$$T_{1,t} = T_{1,(t-\Delta t)} + \frac{Q\Delta t}{0.001CM} - (T_{1,(t-\Delta t)} - T_{2,(t-\Delta t)})F \quad (5.186)$$

$$T_{(i=2..n-1),t} = T_{i,(t-\Delta t)} + (T_{(i-1),(t-\Delta t)} - T_{i,(t-\Delta t)})F - (T_{i,(t-\Delta t)} - T_{(i+1),(t-\Delta t)})F \quad (5.187)$$

$$T_{n,t} = T_{HS} \quad (5.188)$$

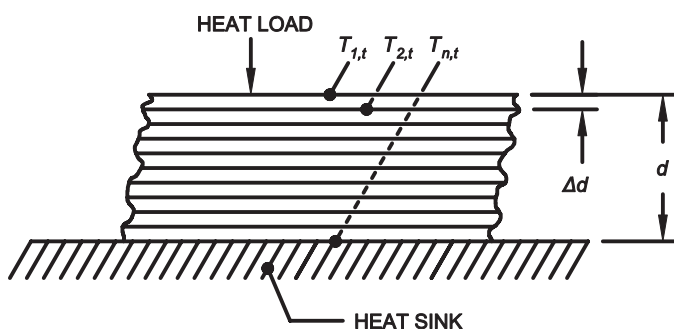


Figure 5.62 Thermal transient analysis.

where T_{HS} is the heat sink temperature, Q is the heat load applied to the top layer in W, t is the elapsed time since the heat load was applied in seconds, Δt is the time step for the analysis, C is the specific heat capacity of the ferrite in J/kg·K, M is the mass of ferrite in each layer in g, and F is the Fourier number,

$$F = \frac{\alpha \Delta t}{0.0006452 \Delta d^2} \quad (5.189)$$

in which Δd is the layer thickness in inches and α is the thermal diffusivity,

$$\alpha = \frac{k}{1000 \rho C} \quad (5.190)$$

where k is the thermal conductivity of the ferrite in W/m·K, and ρ is the ferrite density in g/cm³.

Initially (at $t = 0$), we set the temperatures of all of the ferrite layers to the heat sink temperature. The heat sink temperature serves as a boundary condition, so that the temperature of the surface of ferrite in contact with the heat sink ($T_{n,t}$) is always the same as the heat sink temperature.

For the numerical routine to converge, the time step (Δt) must be small enough so that $F < 0.5$. We repeat the computations of (5.186) and (5.187) for each time (t), incrementing the time by Δt between successive computations. The computations proceed until time has progressed to the end of the RF pulse. Then, we can determine from the ferrite temperature how the electrical performance would be affected using the same analysis technique as for steady-state thermal effects (Section 5.8.1). Intrapulse thermal effects typically manifest themselves as pulse droop (increase in circulator insertion loss during the pulse), as well as degradation in VSWR and isolation.

5.8.3 Voltage Breakdown

Power-handling capacity specifications will affect not only the choice of ferrite material for below-resonance circulators but also ground-plane spacing for both above- and below-resonance devices. At high peak powers, we are concerned with voltage breakdown if the center conductor is too close to the ground plane. The theoretical breakdown power [12] of a stripline in air at sea level with rounded edges and $t/b > 0.05$ is at least $600 \text{ kW/inch}^2 \cdot b^2$, where b is the ground-plane spacing in inches and $Z_0 = 50\Omega$. Generally, the highest characteristic impedance present in a stripline circulator is 50Ω , because

the junction impedance is usually lower. The RF voltage is higher for higher characteristic impedances, so the worst case from a voltage-breakdown point of view is where $Z_0 = 50\Omega$.

Another method of calculating the stripline breakdown power for air at sea level is to use (2.9), substituting $70 \text{ kV} \cdot d$ for V_{dw} , where d is the ferrite or dielectric thickness in inches.

If the ground-plane spacing cannot be increased, two alternatives are to completely fill the space between the center conductor and ground planes with a dielectric material that has a high dielectric strength (such as silicone) or to pressurize the circulator.

Ionization and resulting voltage breakdown of air (and other gasses) can take the form of corona or arcing. For small conductor spacings, as voltage is increased, arcing may occur before inception of corona. For larger spacings, corona will start first, possibly leading to arcing if the voltage increases sufficiently. Paschen's law tells us that the minimum breakdown voltage is a function of the air pressure and the length of the gap between the conductors. Mathematically, the relationship is [50]

$$V = \frac{927pd}{\ln(pd) + 2.132} \quad (5.191)$$

where V is the peak voltage in volts, p is the air pressure in torr, and d is the gap length in inches. Figure 5.63 shows Paschen's curve, which is a graph of (5.191). Different gasses and different conductor materials correspond to different breakdown voltages. Temperature and humidity also play roles, but temperature has a weak effect, so in most practical applications, temperature is relatively unimportant.

To determine the air pressure (p) as a function of altitude, we use the NASA Earth Atmosphere Model [51]. For altitudes (A) up to 36,152 feet above mean sea level (MSL), we use

$$T = 15.04 - 0.001978A \quad (5.192)$$

$$p = 759.8 \left(\frac{T + 273.1}{288.08} \right)^{5.256} \quad (5.193)$$

For altitudes between 36,152 and 82,345 feet,

$$T = -56.46 \quad (5.194)$$

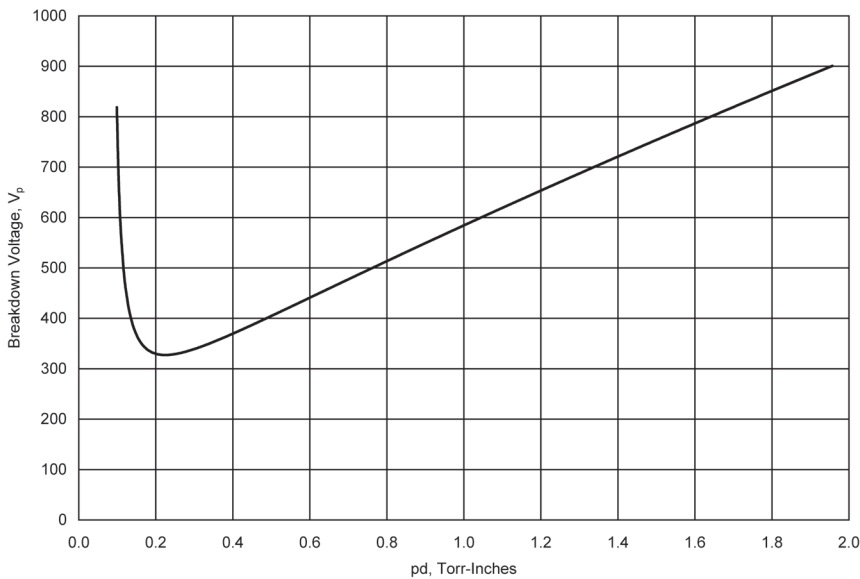


Figure 5.63 Paschen's curve.

$$p = 169.9e^{(1.73 - 0.00004785A)} \quad (5.195)$$

and for altitudes above 82,345 feet,

$$T = -131.21 + 0.0009113A \quad (5.196)$$

$$p = 18.66 \left(\frac{T + 273.1}{216.6} \right)^{-11.388} \quad (5.197)$$

In (5.192–5.197), A is the altitude above MSL in feet, T is the temperature in °C, and p is the pressure in torr.

For low frequencies, the minimum corona inception voltage [52] or minimum arcing voltage is about 327 V_p (about 230 V_{RMS}), corresponding to $pd = 0.22$ torr-inches. For low pd products, breakdown voltages are reduced at higher frequencies [53], but for higher pd products, there is little change in breakdown voltage with frequency. It is interesting to note that for $pd < 0.22$ torr-inches, it is possible for a gap larger than the smallest gap in the device to arc, so counter-intuitively, breakdown could be prevented by making a gap smaller.

A method we can use to prevent arcing is to introduce a long path between conductors by adding dielectric. It is not always possible to have continuous dielectric material between conductors, so there could be a “creep” path on the surface(s) of the dielectric(s) that an arc could follow. Such a creep path is sensitive to humidity and contamination of the surface. A safety factor of three [50], relative to the minimum gap in air, or a maximum voltage gradient of 20 kV_{RMS}/inch [54] at sea level is prudent.

While arc breakdown voltage is sensitive to path length between conductors, corona breakdown voltage is sensitive to conductor radius. For corona on a wire or other rounded surface near a ground plane, the corona inception voltage is given by [55]

$$V = 76200\delta \left(1 + \frac{0.189}{\sqrt{\delta r}}\right) r \ln\left(\frac{2d}{r}\right) \quad (5.198)$$

where r is the radius in inches of the wire or rounded surface, d is the conductor spacing in inches, and δ is the relative air density:

$$\delta = \frac{0.392 p}{273 + T} \quad (5.199)$$

Circulators and other microwave devices that operate in a vacuum, such as those used in spacecraft or (rarely) particle accelerators, may be susceptible to *multipaction*. Multipaction is a secondary electron resonance phenomenon that can occur when the mean free paths of electrons are much longer than the dimensions of gaps between conductors. The mean free path (the average distance a particle travels before it impacts another particle) of an air molecule is [56, 57]

$$\lambda = \frac{0.00197}{p} \quad (5.200)$$

where λ is the mean free path in inches and p is the pressure in torr. The mean free path of electrons in the presence of air molecules is somewhat (5–6 times) longer because electrons are much smaller than air molecules, so (5.200) provides only a rough, order-of-magnitude estimate of the electron mean free path. Also, residual gasses present in the vacuum may not include air, and the specific gasses present would affect the mean free path. Typically multipaction

occurs at pressures below about 10^{-2} torr [58], where the electron mean free path is greater than one inch.

For multipaction to occur, in addition to a pressure below 10^{-2} torr, there must be a gap between conductors of an appropriate length, and an RF electric field. Another requirement is that the surfaces must have secondary electron emission coefficients greater than unity [59]. That is, the number of secondary electrons produced when primary electrons strike the surface must exceed the number of primary electrons. The secondary emission coefficient is a material property, so different materials have different multipaction susceptibility.

In some circulators, electrons may strike the surface of ferrite. It has been shown that ferrite particles can have secondary emission coefficients less than unity [60]. A smooth ferrite surface would likely have a higher secondary emission coefficient, indicating that a rough ferrite surface finish is desirable from a multipaction perspective. The magnetization of the ferrite should be considered, as the secondary electron trajectories may be modified by the magnetic field.

When free electrons having suitable energy levels collide with a conductor surface, secondary electrons are emitted from the surface at a low angle. If the RF electric field oscillation happens to be synchronized with the electron emissions [61], then electrons will be accelerated toward the opposite conductor, where they could impact and release more secondary electrons. Thus, an oscillating electron cloud forms, and ultimately leads to a multipaction avalanche or breakdown.

Multipaction breakdown can be destructive, eroding surfaces, which would cause eventual failure [62]. It can generate electrical noise and cause distortion, as it is a nonlinear effect. Multipaction can also cause outgassing of dielectric materials, which could lead to more-destructive corona or arc discharges.

Fortunately for design engineers, prediction of multipaction is straightforward. NASA Technical Report 32-1500 [63] contains experimental multipaction data, as well as data related to ionization (higher-pressure) breakdown. Graphs showing multipaction regions, with frequency-gap product (fd) as the X-axis and voltage as the Y-axis, are often referred to as *Woo curves*. Figure 5.64 shows multipaction susceptibility regions. We derived the curves in this figure from data presented in ECSS-E-20-01A [64], which contains other valuable information regarding multipaction engineering. A free multipaction calculator [65], which is useful for design work, is available on the Internet.

We prevent multipaction using various techniques [59]: adjustment of the geometry to move the gap dimension into a safe region, use of surface coatings to reduce secondary electron emission, or introduction of a dielectric

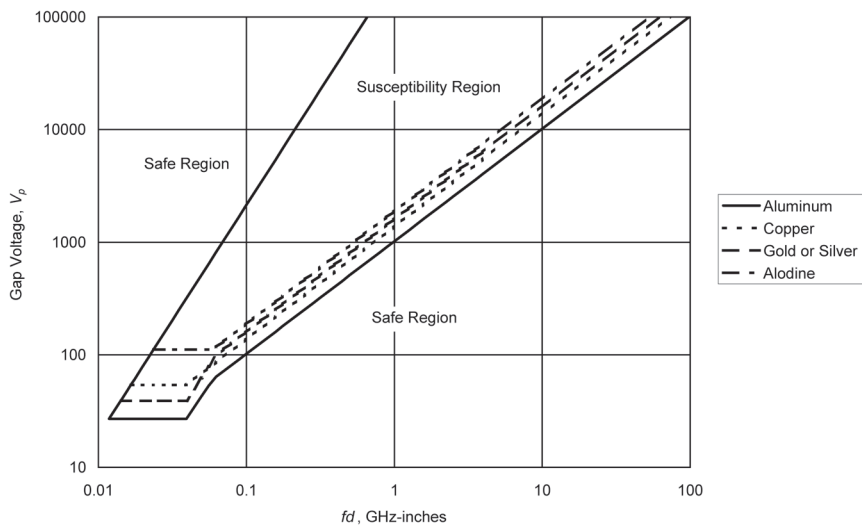


Figure 5.64 Multipaction susceptibility regions.

material to remove the vacuum from the gap. To avoid higher-pressure ionization discharges, vacuum gaps must be properly vented. Pressure in a vacuum gap should be low ($< 10^{-2}$ torr) before RF power is applied, and venting also allows gas generated by an unexpected multipaction event to escape. Design information for vent holes is presented in Chapter 7.

5.8.4 Spin-Wave Instability

As stated in Section 1.4, spin waves are most troublesome in the design of high-power, below-resonance circulators. Under undesirable conditions, as the RF power level increases, the subsidiary resonance grows at the expense of the main ferrimagnetic resonance [66], absorbing energy and causing an increase in insertion loss. If the RF power is pulse modulated, a circulator that is exhibiting nonlinearity due to spin wave effects will typically have low insertion loss for at least the first 100 ns of the pulse. Then, the power transmitted through the circulator will decrease to a limiting value that is substantially independent of the input power.

It is not straightforward to analytically determine the threshold power level for circulator spin-wave instability. This is because of material imperfections and because the exact relationship between the microwave magnetic

field (H_{RF}) and the RF power level is usually unknown. Experienced circulator engineers can rely on past experience, perhaps with circulator failures, to determine power thresholds for similar circulator designs.

Fortunately we can iteratively converge on a circulator design that will have sufficient power threshold to provide linear operation. First, we measure the power threshold of a prototype circulator. We do this by gradually increasing the power level until the circulator insertion loss begins to increase, or in a pulse-modulated system, until the pulse starts to droop. This is the power threshold. Then, by rearranging (4.3), we can determine which design variables could be changed, and how much change is required, to achieve a particular power threshold. The critical microwave magnetic field is

$$H_{RF} = \frac{\omega \Delta H_k}{\gamma_{\text{eff}}^2 4\pi M_S} \quad (5.201)$$

Because H_{RF} is proportional to the RF current, and power is proportional to the square of the current, for the power threshold we have

$$P \propto \frac{\omega^2 \Delta H_k^2}{\gamma_{\text{eff}}^2 4\pi M_S^2} \quad (5.202)$$

To increase the power threshold, we could increase ΔH_k or decrease $4\pi M_S$. We could also reduce H_{RF} corresponding to a given power level by increasing the circulator junction impedance. This is generally accomplished by increasing the ferrite thickness (d). It is noteworthy that the power threshold decreases with decreasing frequency. The power threshold will be lowest at the lowest frequency in the circulator operating frequency range, which for a below-resonance circulator, is closest to the ferrimagnetic resonance. If the magnitude of the required change in the power threshold is known from measurement, then from knowledge of the design variables and the use of (5.202), we can compute the required changes to the design variable(s).

An obvious question is, “why not just design the circulator for maximum power instead of testing a prototype first, and then adjusting the design?” The answer is that designing the circulator for maximum power threshold and ignoring other requirements could result in unnecessarily high insertion loss and narrow bandwidth. High values of ΔH_k correspond to higher ΔH , which results in higher loss, and lower values of $4\pi M_S$ limit the bandwidth. The use of an iterative approach provides the best design compromise.

References

- [1] Soohoo, R. F., *Microwave Magnetics*, New York: Harper and Row, 1985.
- [2] *Tech-Briefs*, Adamstown, MD: Trans-Tech, 1973, p. 16.
- [3] Bosma, H., "On stripline Y-Circulators at UHF," *IEEE Transactions on Microwave Theory and Techniques*, January 1964, pp. 61–73.
- [4] Fay, C. E., and R. L. Comstock, "Operation of the Ferrite Junction Circulator," *IEEE Transactions on Microwave Theory and Techniques*, January 1965, pp. 1–13.
- [5] Helszajn, J., "Quarter-Wave Coupled Junction Circulators Using Weakly Magnetized Disk Resonators," *IEEE Transactions on Microwave Theory and Techniques*, May 1982, pp. 800–806.
- [6] Helszajn, J., and F. C. Tan, "Design Data for Radial-Waveguide Circulators Using Partial-Height Ferrite Resonators," *IEEE Transactions on Microwave Theory and Techniques*, March 1975, pp. 288–298.
- [7] Helszajn, J., and D. S. James, "Planar Triangular Resonators with Magnetic Walls," *IEEE Transactions on Microwave Theory and Techniques*, February 1978, pp. 95–100.
- [8] Davies, J. B., "An Analysis of the M-Port Symmetrical H-Plane Waveguide Junction with Central Ferrite Post," *IRE Transactions on Microwave Theory and Techniques*, 1962, p. 596.
- [9] Auld, B. A., "The Synthesis of Symmetrical Waveguide Circulators," *IRE Transactions on Microwave Theory and Techniques*, April 1959, pp. 238–246.
- [10] Simon, J. W., "Broadband Strip-Transmission Line Y-Junction Circulators," *IEEE Transactions on Microwave Theory and Techniques*, May 1965, pp. 335–345.
- [11] Green, J. J., and F. Sandy, "Microwave Characterization of Partially Magnetized Ferrites," *IEEE Transactions on Microwave Theory and Techniques*, June 1974, pp. 641–645.
- [12] Matthaei, G. L., L. Young, and E. M. T. Jones, *Microwave Filters, Impedance-Matching Networks, and Coupling Structures*, Dedham, MA: Artech House, 1980.
- [13] Howe, H., *Stripline Circuit Design*, Dedham, MA: Artech House, 1974.
- [14] Helszajn, J., "The Synthesis of Quarter-Wave Coupled Circulators with Chebyshev Characteristics," *IEEE Transactions on Microwave Theory and Techniques*, November 1972, pp. 764–769.
- [15] Levy, R. and J. Helszajn, "Specific Equations for One and Two Section Quarter-Wave Matching Networks for Stub-Resistor Loads," *IEEE Transactions on Microwave Theory and Techniques*, January 1982, pp. 55–63.
- [16] Helszajn, J., *The Stripline Circulator: Theory and Practice*, Hoboken, NJ: John Wiley and Sons, 2008.

- [17] Helszajn, J., M. McKay, and D. J. Lynch, "Complex Gyrator Circuit of a Junction Circulator Using Weakly Magnetised Planar Irregular Hexagonal Resonator," *IEE Proceedings on Microwaves, Antennas, and Propagation*, December 1996.
- [18] Helszajn, J., and D. J. Lynch, "Cut-Off Space of Cloverleaf Resonators with Electric and Magnetic Walls," *IEEE Transactions on Microwave Theory and Techniques*, August 1992, pp. 1620–1629.
- [19] Helszajn, J., *Waveguide Junction Circulators: Theory and Practice*, New York: John Wiley and Sons, 1998.
- [20] Helszajn, J., and F. C. F. Tan, "Susceptance-Slope Parameter of Waveguide Partial-Height Ferrite Circulators," *Proceedings of the Institution of Electrical Engineers*, December 1975, pp. 1329–1332.
- [21] Helszajn, J., and F. C. F. Tan, "Mode Charts for Partial-Height Ferrite Waveguide Circulators," *Proceedings of the Institution of Electrical Engineers*, January 1975, pp. 34–36.
- [22] Castillo, J. B., and L. E. Davis, "Computer-Aided Design of Three-Port Waveguide Junction Circulators," *IEEE Transactions on Microwave Theory and Techniques*, January 1970, pp. 25–34.
- [23] Helszajn, J., "Design of Waveguide Circulators with Chebyshev Characteristics Using Partial-Height Ferrite Resonators," *IEEE Transactions on Microwave Theory and Techniques*, August 1984, pp. 908–917.
- [24] Davies, J. B., and P. Cohen, "Theoretical Design of Symmetrical Junction Stripline Circulators," *IEEE Transactions on Microwave Theory and Techniques*, November 1963, pp. 506–512.
- [25] Castillo, J. B., and L. E. Davis, "Computer-Aided Design of Three-Port Waveguide Junction Circulators," *IEEE Transactions on Microwave Theory and Techniques*, January 1970, pp. 25–34.
- [26] Salay, S. J., and H. J. Peppiatt, "An Accurate Junction Circulator Design Procedure," *IEEE Transactions on Microwave Theory and Techniques*, February 1972, pp. 192–193.
- [27] Uzdy, Z., "Computer-Aided Design of Stripline Ferrite Junction Circulators," *IEEE Transactions on Microwave Theory and Techniques*, October 1980, pp. 1134–1136.
- [28] Helszajn, J., "Design of Waveguide Circulators with Chebyshev Characteristics Using Partial-Height Ferrite Resonators," *IEEE Transactions on Microwave Theory and Techniques*, August 1984, pp. 908–917.
- [29] Neidert, R. E., "Computer Aided Approach to the Design of Y-Junction Stripline and Microstrip Ferrite Circulators," *Naval Research Laboratory Final Report ADA251337*, May 5, 1992.
- [30] Helszajn, J., "Operation of Tracking Circulators," *IEEE Transactions on Microwave Theory and Techniques*, July 1981, pp. 700–707.
- [31] *Reference Data for Radio Engineers*, Indianapolis, IN: Howard W. Sams, 1977.

- [32] Wheeler, H. A., "A Simple Formula for the Capacitance of a Disc on Dielectric on a Plane," *IEEE Transactions on Microwave Theory and Techniques*, November 1982, pp. 2050–2054.
- [33] Harrison, G. R., G. H. Robinson, B. Savage, D. R. Taft, "Ferrimagnetic Parts for Microwave Integrated Circuits," *IEEE Transactions on Microwave Theory and Techniques*, July 1971, pp. 577–588.
- [34] Edwards, T. C., *Foundations for Microstrip Circuit Design*, New York: John Wiley and Sons, 1981.
- [35] Pucel, R. A., and D. J. Massé, "Microstrip Propagation on Magnetic Substrates, Part I: Design Theory," *IEEE Transactions on Microwave Theory and Techniques*, May 1972, pp. 304–308.
- [36] Helszajn, J., and R. W. Lyon, "Approximate Determination of Effective Radius and Effective Dielectric Constant of Microstrip Disc Resonators," *Electronics Letters*, January 8, 1981, pp. 46–48.
- [37] Moreno, T., *Microwave Transmission Design Data*, Norwood, MA: Artech House, 1989.
- [38] Okada, F., K. Ohwi, and M. Mori, "The Development of a High-Power Microwave Circulator for Use in Breaking of Concrete and Rock," *Journal of Microwave Power and Electromagnetic Energy*, Vol. 10, No. 2, 1975, pp. 171–180.
- [39] Okada, F., K. Ohwi, M. Mori, M. Yasuda, "A 100 kW Waveguide Y-Junction Circulator for Microwave Power Systems at 915 MHz," *Journal of Microwave Power and Electromagnetic Energy*, Vol. 12, No. 3, 1977, pp. 201–208.
- [40] United States Patent 4,496,915, "Microwave Transmission Device having Gyromagnetic Materials Having Different Saturation Magnetizations," Inventors: Mathew, M. and T. J. Weisz, Assignee: TRW, Inc., January 29, 1985.
- [41] United States Patent 4,390,853, "Microwave Transmission Devices Comprising Gyromagnetic Material Having Smoothly Varying Saturation Magnetization," Inventors: Mathew, M. and T. J. Weisz, Assignee: TRW, Inc., June 28, 1983.
- [42] Helszajn, J., *Passive and Active Microwave Circuits*, New York: John Wiley and Sons, 1978.
- [43] Konishi, Y., and N. Hoshino, "Design of a New Broad-Band Isolator," *IEEE Transactions on Microwave Theory and Techniques*, March 1971, pp. 260–269.
- [44] Dunn, V. E., and R. W. Roberts, "New Design Techniques for Miniature VHF Circulators," *International Microwave Symposium Digest*, 1965, pp. 147–151.
- [45] Clarricoats, P. J. B., *Microwave Ferrites*, New York: John Wiley and Sons, 1961.
- [46] Helszajn, J., and B. Tsounis, "Temperature Stability of Quality Factor of Junction Circulators," *IEE Proceedings on Microwaves, Antennas, and Propagation*, February 1995, pp. 67–70.

- [47] Weinstein, D., "Passive Intermodulation Distortion in Connectors, Cable, and Cable Assemblies," Danbury, CT: Amphenol Corporation.
- [48] Wu, Y., W. H. Ku, and J. E. Erickson, "A Study of Nonlinearities and Intermodulation Characteristics of 3-Port Distributed Circulators," *IEEE Transactions on Microwave Theory and Techniques*, February 1976, pp. 69–77.
- [49] Simonson, J. R., *Engineering Heat Transfer, Second Edition*, New York: Hemisphere Publishing, 1989.
- [50] Cobine, J. D., *Gaseous Conductors: Theory and Engineering Applications*, New York: McGraw-Hill, 1941.
- [51] NASA Earth Atmosphere Model, Internet <http://www.grc.nasa.gov/WWW/k-12/airplane/atmosmet.html>. Last accessed Nov. 14, 2013.
- [52] Karady, G. G., M. D. Sirkis, and L. Liu, "Investigation of Corona Initiation Voltage at Reduced Pressures," *IEEE Transactions on Aerospace and Electronic Systems*, January 1994, pp. 144–150.
- [53] Woo, R., "RF Voltage Breakdown and the Paschen Curve," *Proceedings of the IEEE*, April 1974, p. 521.
- [54] Gartzke, D. G., *Determination of RF Peak and Average Power for Coaxial Connectors*, Port Salerno, FL: Solitron/Microwave, 1982.
- [55] Coppens, M. T., "Effects of AC Corona on EHV Transmission Lines," *The Rose Technic*, April/May 1986, pp. 13–17.
- [56] "Kinetic Theory of Gasses," University of Colorado, Colorado Springs, <http://www.uccs.edu/~tchriste/courses/PHYS549/549lectures/gasses.html>. Last accessed Nov. 14, 2013.
- [57] "1.25. Mean Free Path," Pfeiffer Vacuum, <http://www.pfeiffer-vacuum.com/know-how/introduction-to-vacuum-technology/fundamentals/mean-free-path/technology.action?chapter=tec1.2.5>. Last accessed Nov. 14, 2013.
- [58] Salvesen, H., "Performing Accurate Multi-Paction Measurements," *NASA Tech Briefs*, August 2010, pp. 12–17.
- [59] Woode, A. D., and J. Petit, "Design Data for the Control of Multipactor Discharge in Spacecraft Microwave and RF Systems," *Microwave Journal*, January 1992, pp. 142–155.
- [60] Montero, I., F. Caspers, L. Aguilera, L. Galàn, D. Raboso, "Low-Secondary Electron Yield of Ferromagnetic Materials and Magnetized Surfaces," *Proceedings of the First International Particle Accelerator Conference*, May 2010.
- [61] Fuks, R., "Multipaction Discharge in Coaxial Components," *Microwave Journal*, May 2011, pp. 206–220.
- [62] Clancy, P. F., "Multipactor Control in Microwave Space Systems," *Microwave Journal*, March 1978, pp. 77–83.
- [63] Woo, R., "Final Report on RF Voltage Breakdown in Coaxial Transmission Lines," *NASA Jet Propulsion Laboratory Technical Report 32-1500*, October 1, 1970.

- [64] “Space Engineering: Multipactor Design and Test,” *European Cooperation for Space Standardization ECSS-E-20-01A revision 1*, March 1, 2013.
- [65] Strijk, S. J. G., “Multipactor Calculator Version 1.62,” *ESA/ESTEC*, September 2007, <http://multipactor.esa.int/downloads.html>. Last accessed Nov. 14, 2013.
- [66] Lax, B., and K. J. Button, *Microwave Ferrites and Ferrimagnetics*, New York: McGraw-Hill, 1962.

6

Magnetic Design

6.1 Magnet Sizing

All the circulators described in this book require dc magnetic fields. This magnetic bias causes the electrons in the ferrite material to precess as described in Section 1.3. This precession is essential to the operation of the circulator.

Except in special cases, which we will cover in Section 6.5, the circulator dc magnetic field is provided by permanent magnets. The choice of magnet material was described in Chapter 4; in this section we will concern ourselves with the sizing of the magnets.

A typical junction circulator magnetic circuit is shown in Figure 6.1. We introduce several components here that we have not previously described: shields, pole pieces, shunts, and returns. The purpose of the pole pieces is to make the magnetic flux density in the ferrites more uniform. Without pole pieces, the lines of flux are concentrated near the edges of the magnets, as shown in Figure 6.2. It is very important for the magnetic field applied to the ferrites to be uniform, or homogeneous. If the field is not homogeneous, portions of the ferrites may be only partly magnetized or, worse yet, not magnetized. This situation leads to high insertion loss and generally poor circulator performance. Pole pieces homogenize the magnetic field by conducting magnetic flux from strongly magnetic areas of the magnet to areas that would otherwise be weakly magnetized. The pole pieces are sometimes used to shape the magnetic field applied to the ferrites; this is done when we want to use magnets that are smaller or larger than the ferrites or have a different shape. For example, we may want to magnetize triangular ferrites having 3-in altitudes

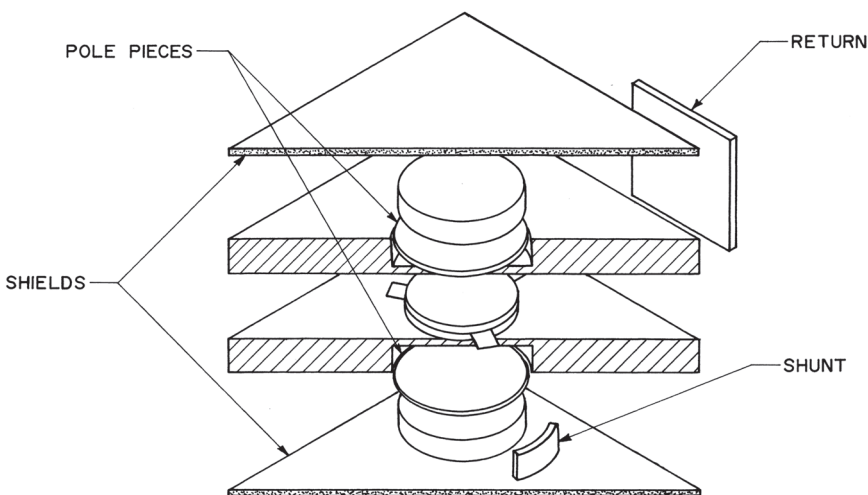


Figure 6.1 Typical junction circulator magnetic circuit.

using 1½-in diameter magnets, which could be accomplished with properly designed pole pieces. We will discuss the design of pole pieces in Section 6.4.

Shunts are used to reduce the magnetic field supplied by the magnet to the ferrites. A shunt effectively short-circuits part of the magnetic flux from the magnet. Where it is undesirable or impossible to demagnetize a magnet, shunts are used. In some instances, we may need to skew the magnetic field to one side or another to compensate for magnetic anomalies; this can be done with shunts.

Returns serve the purpose of making the magnetic circuit more efficient and improving shielding. The return completes the magnetic circuit by returning the magnetic flux to its source, the magnet. Without returns, the outer faces of the magnets would be magnetically linked only by long flux paths through the air. These long paths are not efficient, and the magnets would have to be much larger to supply the needed field.



Figure 6.2 Effect of pole pieces on magnetic field.

Shields not only provide magnetic shielding to prevent interaction between the circulator magnetic circuit and external magnetic fields or ferrous materials, but also improve the circuit efficiency by helping to return magnetic flux in much the same manner as returns. Section 6.2 is devoted to magnetic shielding.

It is important to understand the difference between a shunt and a shield or return. A shunt reduces the magnetic field intensity supplied to the ferrites. Shields and returns usually increase the field by providing a return path for the magnetic flux. These concepts are illustrated in Figure 6.3. The shunt effectively links the two poles of a magnet so that some fraction of the total magnetic flux provided by the magnet is short-circuited and therefore not supplied to the ferrites. The shields and returns link the outer poles of magnets on either side of the ferrites, thus providing a path of low resistance to magnetic flux. This path strengthens the magnetic field applied to the ferrites.

In this book we describe the design of junction circulator magnetic circuits; the magnetic design of other classes of circulators is substantially the same.

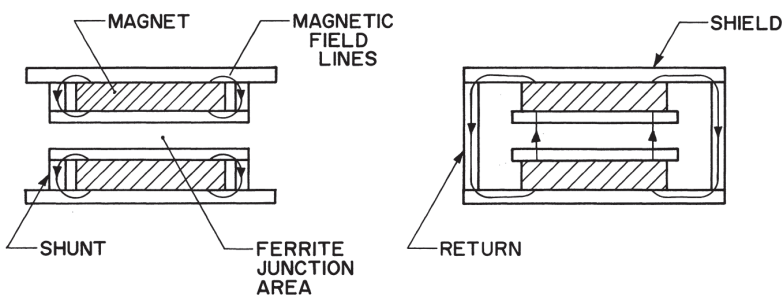


Figure 6.3 Magnetic circuit components. Shunts short-circuit magnetic flux (left); returns and shields strengthen field in ferrite junction area (right).

6.1.1 Ferrite Demagnetization Factors

Before we can size magnets, we must know how much magnetic field is required by the ferrites. After we complete a preliminary electrical design of the circulator as described in Chapter 5, we know the approximate internal magnetic field strength (H_{dc}) needed to bias the ferrites. Until now, we have only worked with the magnetic field inside the ferrite. The external magnetic field, H_{ext} , is different. It is the external magnetic field we use for the magnetic circuit calculations.

The external magnetic field differs from the internal field because of the creation of free magnetic poles [1] at the boundaries of the ferrites. We represent the effect of the free poles by demagnetizing fields that modify the internal magnetic fields. These modified internal fields are

$$h_x = h_{x \text{ ext}} - N_x m_x \quad (6.1)$$

$$h_y = h_{y \text{ ext}} - N_y m_y \quad (6.2)$$

$$H_{\text{dc}} = H_{\text{ext}} - N_z M_0 \quad (6.3)$$

where N_x , N_y , and N_z are demagnetizing factors. We substitute (6.1) and (6.2) into (1.20) and (1.21), and derive

$$m_x = \chi(h_{x \text{ ext}} - N_x m_x) - j\kappa(h_{y \text{ ext}} - N_y m_y) \quad (6.4)$$

$$m_y = j\kappa(h_{x \text{ ext}} - N_x m_x) + \chi(h_{y \text{ ext}} - N_y m_y) \quad (6.5)$$

Solving (6.4) and (6.5) simultaneously for m_x and m_y using determinants, we have for the system determinant:

$$D = \begin{vmatrix} 1 + \chi N_x & -j\kappa N_y \\ j\kappa N_x & 1 + \chi N_y \end{vmatrix} \quad (6.6)$$

Evaluating the determinant, we have

$$D = (1 + \chi N_x)(1 + \chi N_y) - \kappa^2 N_x N_y \quad (6.7)$$

Because the system determinant is the denominator in the expressions for m_x and m_y , and at resonance $m_x = m_y = \infty$ if we ignore losses, D must equal zero at resonance. We substitute (1.25) and (1.27) into (6.7), setting $\alpha = 0$, and derive

$$D = (\omega_0 + N_x \gamma M_0)(\omega_0 + N_y \gamma M_0) - \omega^2 \quad (6.8)$$

Setting $D = 0$, we have

$$\omega = \sqrt{(\omega_0 + N_x \gamma M_0)(\omega_0 + N_y \gamma M_0)} \quad (6.9)$$

Substituting (1.7) into (6.9), we write

$$\omega = \gamma \sqrt{(H_{dc} + N_x M_0)(H_{dc} + N_y M_0)} \quad (6.10)$$

We bring back z -axis magnetic field by substitution of (6.3) into (6.10):

$$\frac{\omega}{\gamma} = \sqrt{[H_{ext} + (N_x - N_z)M_0][H_{ext} + (N_y - N_z)M_0]} \quad (6.11)$$

Insofar as we are writing equations for the resonance frequency, $\omega = \omega_0$ and we can again apply (1.7):

$$H_{dc} = \sqrt{[H_{ext} + (N_x - N_z)M_0][H_{ext} + (N_y - N_z)M_0]} \quad (6.12)$$

This is Kittel's equation [2] relating the internal magnetic field strength to the external field.

An ellipsoid, depicted in Figure 6.4, has the property that when an external magnetic field is applied to it, the demagnetizing field is uniform

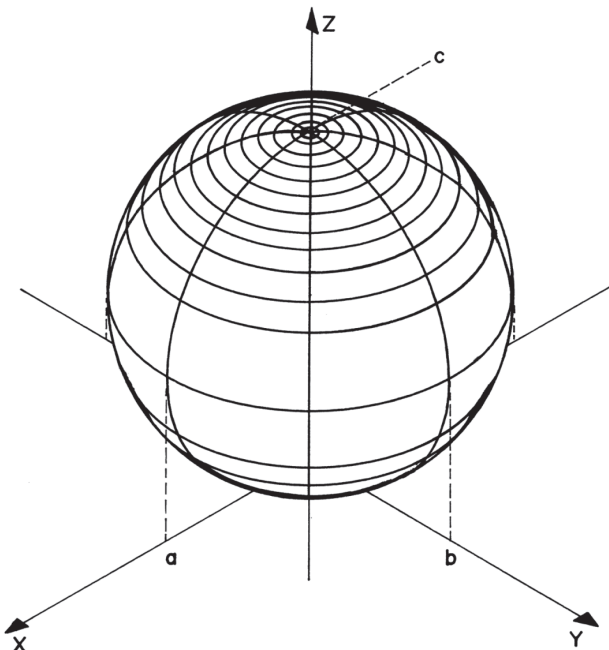


Figure 6.4 The ellipsoid model for demagnetization factors.

throughout the solid. Because of this property, the ellipsoid is used as the model for determining the demagnetization factors. The demagnetizing factors N_x , N_y , and N_z are dependent on the ratios of the axes of the ellipsoid [3]. Let the axes of the ellipsoid be designated by a , b , and c . The demagnetizing factors are inversely proportional to the axes—when a dimension of the ellipsoid is small, the corresponding demagnetizing factor is large. The sum $N_x + N_y + N_z = 1$.

For a ferrite disk, we can approximate the demagnetization factors by letting the disk be an ellipsoid with axes $a = b = 1$ (because the disk is round, its x and y dimensions are equal and arbitrarily 1) and $c = 10^{-10}$ (an arbitrarily small thickness). We find the axis ratios $b/a = 1$ and $c/a = 10^{-10}$. We set the demagnetization factors proportional to the reciprocals of the axis ratios:

$$N_x = \frac{N_x}{a} = N_x \quad (6.13)$$

$$N_y = \frac{a}{b} N_x = N_x \quad (6.14)$$

$$N_z = \frac{a}{c} N_x = 10^{10} N_x \quad (6.15)$$

We then equate the sum of the demagnetizing factors to 1:

$$N_x + N_x + 10^{10} N_x = 1$$

Solving for N_x , N_y , and N_z , we have

$$\begin{aligned} N_x &= 10^{-10} \\ N_y &= 10^{-10} \\ N_z &= 1 \end{aligned}$$

Because N_x and N_y are so much smaller than N_z , we set them equal to zero. For the disk shape, we find that $N_x = N_y = 0$ and $N_z = 1$.

The demagnetizing factors for other shapes can be calculated in the same manner. Table 6.1 summarizes the factors for the more important shapes.

For the thin disk, used in junction circulators, the relationship between H_{dc} and H_{ext} becomes, by substitution of the demagnetizing factors into (6.12):

$$H_{dc} = H_{ext} - M_0 \quad (6.16)$$

Table 6.1
Demagnetizing Factors for Important Shapes

Shape	N_x	N_y	N_z	a	b	c
Thin disk	0	0	1	1	1	0
Slender rod	$\frac{1}{2}$	$\frac{1}{2}$	0	1	1	∞
Sphere	$\frac{1}{3}$	$\frac{1}{3}$	$\frac{1}{3}$	1	1	1
Thin slab	1	0	0	1	∞	∞

For the slender rod, used in Faraday rotators, we have

$$H_{dc} = H_{ext} + \frac{M_0}{2} \quad (6.17)$$

The sphere is used for testing ferrite materials because the internal field is very uniform. The expression for the sphere is

$$H_{dc} = H_{ext} \quad (6.18)$$

For differential phase shift circulators, field-displacement isolators, and resonance isolators utilizing rectangular ferrite slabs, the relationship between internal and external fields is

$$H_{dc} = \sqrt{H_{ext}(H_{ext} + M_0)} \quad (6.19)$$

Equations (6.16–6.19) offer rough order of magnitude relationships between the internal and external magnetic fields. To take a step up in accuracy, we start with (6.15), set $N_x = N_y$ for a ferrite with identical a and b dimensions, and knowing that $N_x + N_y + N_z = 1$, derive

$$N_x = N_y = \frac{1}{\frac{a}{c} + 2} \quad (6.20)$$

$$N_z = \frac{a}{a + 2c} \quad (6.21)$$

$$N_x - N_z = N_y - N_z = \frac{c - a}{a + 2c} \quad (6.22)$$

Equations (6.20–6.22) provide exact results in idealized cases: an infinitely thin disk, a sphere, or an infinitely long rod. In other (practical) cases, these equations provide approximate results. For a disk, results are within < 10% of the correct values based on the ellipsoidal model.

Computation of accurate demagnetization factors can be very involved. Most practical ferrite shapes are not perfectly ellipsoidal, so any computations based on the ellipsoidal model will be approximations. In nonellipsoidal ferrites, the magnetic field is not uniform, which adds more complication to the design of magnetic circuits.

Osborn [4] presented equations for ellipsoidal demagnetization factors. When two dimensions are the same (e.g., if $a = b$ in the case of a disk), an ellipsoid becomes an *ellipsoid of rotation*, or a *spheroid*. For an oblate spheroid (a shape approximating the shape of a disk),

$$N_z = \frac{m^2}{m^2 - 1} \left(1 - \frac{1}{\sqrt{m^2 - 1}} \sin^{-1} \frac{\sqrt{m^2 - 1}}{m} \right) \quad (6.23)$$

where $m = a/c$. When $m \gg 1$ (when the disk is thin), with $\leq 2\%$ error for $m \geq 5$,

$$N_z = 1 - \frac{\pi}{2m} + \frac{2}{m^2} \quad (6.24)$$

Once we know N_z , we calculate

$$N_x = N_y = \frac{1 - N_z}{2} \quad (6.25)$$

and

$$N_x - N_z = N_y - N_z = \frac{1 - 3N_z}{2} \quad (6.26)$$

For a prolate spheroid (a shape approximating the shape of a rod) [4],

$$N_z = \frac{1}{m^2 - 1} \left(\frac{m}{2\sqrt{m^2 - 1}} \ln \frac{m + \sqrt{m^2 - 1}}{m - \sqrt{m^2 - 1}} - 1 \right) \quad (6.27)$$

where in this case, $m = c / a$. When $m \gg 1$ (when the rod is slender),

$$N_z = \frac{1}{m^2} (\ln 2m - 1) \quad (6.28)$$

Another approximation for long cylindrical rods having high permeability is [5]

$$N_z = \frac{4.02 \cdot \log_{10} m - 0.92}{2m^2} \quad (6.29)$$

It is interesting to note that there are nonlinear effects related to the demagnetization factors. In the case of a long rod magnetized along its length, as the magnetic field intensity increases, the permeability at the ends of the rod drop below the permeability at the center of the rod. This effectively moves the poles inward, shortening the magnetic length of the rod.

To find the demagnetization factors for the other axes, we apply (6.25) and (6.26), as for the disk case.

For devices that utilize rectangular ferrite slabs, we have recourse to a lengthy equation [6]:

$$\begin{aligned} N_z = & \frac{b^2 - c^2}{2\pi bc} \ln \left(\frac{\sqrt{a^2 + b^2 + c^2} - a}{\sqrt{a^2 + b^2 + c^2} + a} \right) + \frac{a^2 - c^2}{2\pi ac} \ln \left(\frac{\sqrt{a^2 + b^2 + c^2} - b}{\sqrt{a^2 + b^2 + c^2} + b} \right) \\ & + \frac{b}{2\pi c} \ln \left(\frac{\sqrt{a^2 + b^2} + a}{\sqrt{a^2 + b^2} - a} \right) + \frac{a}{2\pi c} \ln \left(\frac{\sqrt{a^2 + b^2} + b}{\sqrt{a^2 + b^2} - b} \right) + \frac{c}{2\pi a} \ln \left(\frac{\sqrt{b^2 + c^2} - b}{\sqrt{b^2 + c^2} + b} \right) \\ & + \frac{c}{2\pi b} \ln \left(\frac{\sqrt{a^2 + c^2} - a}{\sqrt{a^2 + c^2} + a} \right) + \frac{2}{\pi} \tan^{-1} \left(\frac{ab}{c\sqrt{a^2 + b^2 + c^2}} \right) + \frac{a^3 + b^3 - 2c^3}{3\pi abc} \\ & + \frac{a^2 + b^2 - 2c^2}{3\pi abc} \sqrt{a^2 + b^2 + c^2} + \frac{c}{\pi ab} \left(\sqrt{a^2 + c^2} + \sqrt{b^2 + c^2} \right) \\ & - \frac{(a^2 + b^2)^{3/2} + (b^2 + c^2)^{3/2} + (c^2 + a^2)^{3/2}}{3\pi abc} \end{aligned} \quad (6.30)$$

6.1.2 Leakage Flux Approximation

Due to leakage flux and magnetic circuit reluctance, the lengths of the magnets may have to be increased by as much as 50% for large air gaps. Likewise, the magnet area may need to be increased by a factor of up to 20 to compensate for leakage flux [7]. Most practical circuits do not require *leakage factors* quite this large.

We can determine exact magnet dimensions empirically, but there are leakage factor approximation equations that were developed decades ago [8, 9]. To obtain good results, the equations were optimized for particular geometries. Equations are not available for every conceivable magnetic circuit geometry, although most circulator magnetic circuits seem to fall into the same general categories. For the magnetic circuit shown in Figure 6.1 or the one at the right of Figure 6.3, the leakage factor is given by [8]

$$F = 1 + \frac{1.7 \cdot U \cdot L_g}{A_g} \left[\frac{L_p}{L_p + L_g} + 0.67 \frac{0.67 L_m}{0.67 L_m + L_g + 2L_p} \right] \quad (6.31)$$

L_g and A_g are the length (or height) and area of the working air/ferrite gap, L_m is the length (or thickness) of each magnet, L_p is the thickness of the pole pieces, and U is the perimeter (or circumference) of the pole piece in inches.

For similar magnetic circuits without pole pieces, we have

$$F = 1 + \frac{1.7 \cdot U \cdot L_g}{A_g} 0.67 \frac{0.67 L_m}{0.67 L_m + L_g} \quad (6.32)$$

The leakage factor (F) is the ratio of total magnetic flux required, including leakage flux, to the useful working gap flux [10]. It can also be expressed in terms of permeance:

$$F = \frac{P_g + P_{leakage}}{P_g} = 1 + \frac{P_{leakage}}{P_g} = \frac{P_t}{P_g} \quad (6.33)$$

where P_g is the permeance of the working gap, $P_{leakage}$ is the permeance due to leakage flux, and P_t is the total permeance. Sections 6.1.3 and 6.1.4 describe how we apply the leakage factor approximation equations in practice.

6.1.3 Approximate Design of Magnetic Circuits

Fortunately for circulator designers, magnetic circuit design need not be exact. Magnetic circuits can be over designed at little additional cost; we can use magnets that are larger than the minimum necessary size and simply demagnetize them until we achieve the desired level of magnetic intensity in the ferrite.

We now have equations we can use to compute the amount of external magnetic field required, assuming we know the desired internal field. The

ferrite material should always be saturated to avoid low-field losses and, as a result, we can replace the magnetization, M_0 , with the ferrite material saturation magnetization. For a junction circulator with the ferrites just saturated ($H_{dc} = 0$), $H_{ext} \approx 4\pi M_S$.

The size of the magnets will depend not only on the field required by the ferrites but also on the reluctance of the entire magnetic circuit. We break the reluctance down into two components: the reluctance of the air gap (R_g) and the reluctance of the steel or iron path (R_i).

Reluctance is the magnetic equivalent of electrical resistance. It is also the reciprocal of permeance, which is analogous to electrical conductance.

The saturated ferrite material, aluminum, brass, copper, and other non-ferrous metals all have permeabilities of essentially 1 (relative to air). The permeability of the iron or steel used in the magnetic circuit depends on the material and on the flux density in it. Figure 6.5 shows some B/H characteristics for ferrous metals used in circulators. If the magnetic intensity or flux density in the metal is known, the permeability can be read from these curves ($\mu = B/H$).

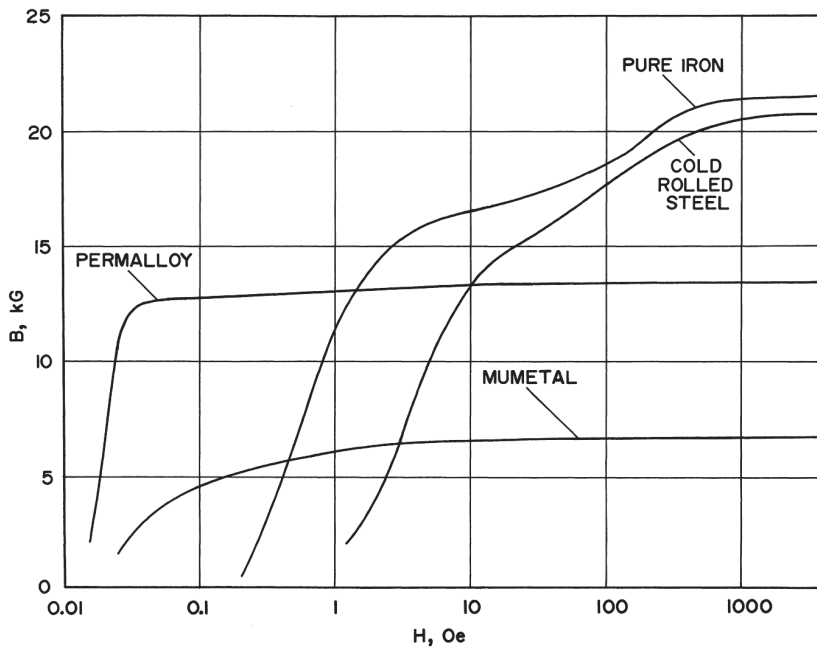


Figure 6.5 Magnetization characteristics of ferrous metals used in circulator design.

For the air gap, including ferrite and nonferrous metals,

$$R_g = \frac{L}{A} \quad (6.34)$$

and for the materials with $\mu > 1$,

$$R_i = \frac{L}{\mu A} \quad (6.35)$$

In both equations, L is the magnetic path length and A is the cross-sectional area of the path. Parallel paths can be combined in the same manner as parallel resistances, and series paths are simply added together [11].

The magnet length and area are calculated using [7]

$$L_m = \frac{B_g L_g}{H_d} \quad (6.36)$$

$$A_m = \frac{B_g A_g}{B_d} \quad (6.37)$$

B_g , the flux density in the air gap (also the flux density in the ferrite), is equal to H_{ext} because $\mu = 1$. A_g is the area of the air gap, or the area of the ferrite face. L_g , the effective gap length, can be calculated from

$$L_g = (R_g + R_i)A_g \quad (6.38)$$

B_d and H_d are the flux density and magnetic field strength of the magnet at the chosen operating point, which can be read from the magnet material demagnetization curve. Rearranging (6.36) and (6.37), and incorporating the leakage factor (F), we derive

$$L_m = \frac{H_{ext} A_g (R_g + R_i)}{H_d} \quad (6.39)$$

$$A_m = \frac{F H_{ext} A_g}{B_d} \quad (6.40)$$

These expressions can be used to size the magnets. The resulting length from (6.39) and (6.40) should be divided in half and one magnet placed on each side of the junction.

If it is necessary to recalculate the flux density in the ferrous portions of the magnetic circuit to iteratively determine permeability or to determine whether the steel is saturated, we can use

$$B_i = \frac{H_{\text{ext}} A_g}{A_i} \quad (6.41)$$

where A_i is the cross sectional area of the iron or steel.

To obtain maximum energy from the magnets, the operating point should be selected so that the product $B_d H_d$ is maximized. This point is found using the demagnetization curve for the chosen material.

6.1.4 Simulation of Magnetic Circuits

The availability of software for magnetostatic simulation of magnetic circuits enables quick, accurate design of magnetic circuits. There are many magnetostatic simulation software packages on the market. We chose to use Ansys® Maxwell® for the magnetostatic simulations that we performed during the preparation of this book.

The equations in this chapter provide a means to jump start iterative simulations to rapidly converge on a solution or to provide an approximate solution that can be empirically optimized without the use of simulations.

To illustrate the use of magnetostatic simulations, we will design a simple magnetic circuit for a junction circulator. Once we know the magnitude of the required H_{ext} , which we compute from H_{int} using the equations in Section 6.1.1, we proceed to select a magnet material and size the magnets. For this example, we will design for $H_{\text{ext}} = 2$ kOe in a working (air) gap that is one inch in diameter and 0.1 inches thick. To keep this example simple, we will omit ferrite from the air gap and use a very-low-reluctance return path. The return path has a large cross section (3.927 in^2), and the iron has high permeability ($\mu = 4,000$) and unlimited saturation magnetization. The magnet material for this circuit will be Ceramic 8.

Initially, we choose an operating point for the magnet near its maximum energy product, at $H_d = 1930 \text{ Oe}$, $B_d = 2,000 \text{ G}$. First applying (6.36) to determine a preliminary magnet thickness, we have

$$L_m = \frac{B_g L_g}{H_d} = \frac{2\text{kG} \cdot 0.1 \text{ inches}}{1930 \text{ Oe}} = 0.104 \text{ inches}$$

We divide this magnet thickness in half to use two 0.052-in-thick magnets. Using (6.31) with 0.050-in-thick pole pieces to find the leakage factor,

$$\begin{aligned} F &= 1 + \frac{1.7 \cdot U \cdot L_g}{A_g} \left[\frac{L_p}{L_p + L_g} + 0.67 \frac{0.67 L_m}{0.67 L_m + L_g + 2L_p} \right] \\ &= 1 + \frac{1.7 \cdot 1 \text{ inch} \cdot \pi \cdot 0.1 \text{ inch}}{\pi \cdot \left(\frac{1 \text{ inch}}{2} \right)^2} \left[\frac{0.050 \text{ inch}}{0.050 \text{ inch} + 0.1 \text{ inch}} + \frac{0.67 \cdot 0.67 \cdot 0.052 \text{ inch}}{0.67 \cdot 0.052 \text{ inch} + 0.1 \text{ inch} + 2 \cdot 0.050 \text{ inch}} \right] \\ &= 1.29 \end{aligned}$$

This leakage factor tells us that we have to either make A_m larger than A_g by a factor of 1.29, if $B_d = 2 \text{ kG}$, or let $A_m = A_g$ and change the operating point of the magnet so that $B_d = 1.29 \cdot 2 \text{ kG} = 2580 \text{ G}$. We choose to let $A_m = A_g$ and set $B_d = 2580 \text{ G}$. From the demagnetization curve for Ceramic 8 material, $H_d = 1380 \text{ Oe}$. This new magnet operating point requires us to adjust the magnet thickness:

$$L_m = \frac{B_g L_g}{H_d} = \frac{2 \text{kG} \cdot 0.1 \text{ inches}}{1380 \text{ Oe}} = 0.145 \text{ inches}$$

We iteratively solve for L_m and F using the preceding equations until we converge on a magnet thickness as shown in Table 6.2.

Table 6.2
Iterative Computation of Magnet Thickness (L_m)

Iteration	H_d	B_d	L_m	F
1	1930 Oe	2000 G	0.052	(none)
2	1930	2000	0.052	1.29
3	1380	2580	0.072	1.32
4	1320	2640	0.076	1.32

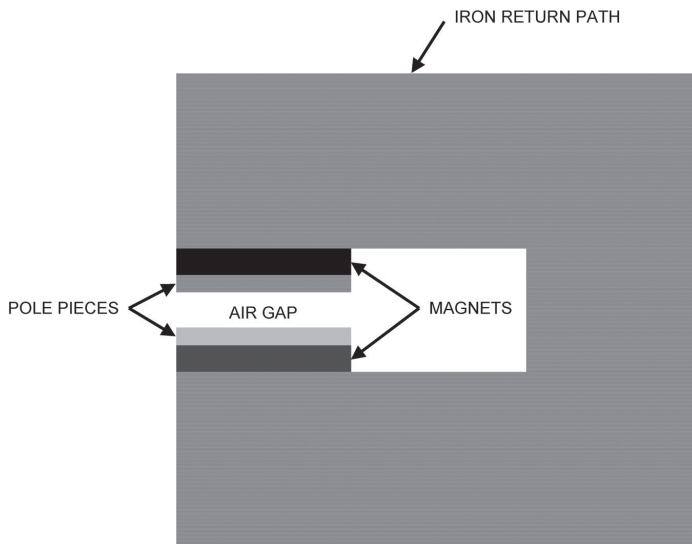


Figure 6.6 Axisymmetric model of magnetic circuit for 2-D magnetostatic simulation.

Using the magnet length that we converged upon, we built a geometric model of the magnetic circuit, shown in Figure 6.6. This is an axisymmetric model of disk magnets, disk pole pieces, and the iron return path. We performed a 2-D magnetostatic simulation of the magnetic circuit using Ansys® Maxwell® 2D. We found that the flux density at the center of the air gap was 1986G, close enough to 2,000G for practical circulator purposes.

Figure 6.7 shows a field plot result from the magnetostatic simulation. The magnetic vectors are vertical in the gap between the pole pieces. To the right of the gap, we see the vectors forming curved leakage paths between the edges of the pole pieces. In this example, we placed the vertical part of the return path far from the edges of the magnets and pole pieces to prevent interaction. If the return iron were close to the magnet and pole piece edges, then we would need to consider these additional leakage paths.

6.2 Shielding

Magnetic shielding of a circulator serves three purposes. First, it helps prevent magnetic fields external to the circulator from degrading its performance. Second, it reduces magnetic flux leakage, protecting other magnetically

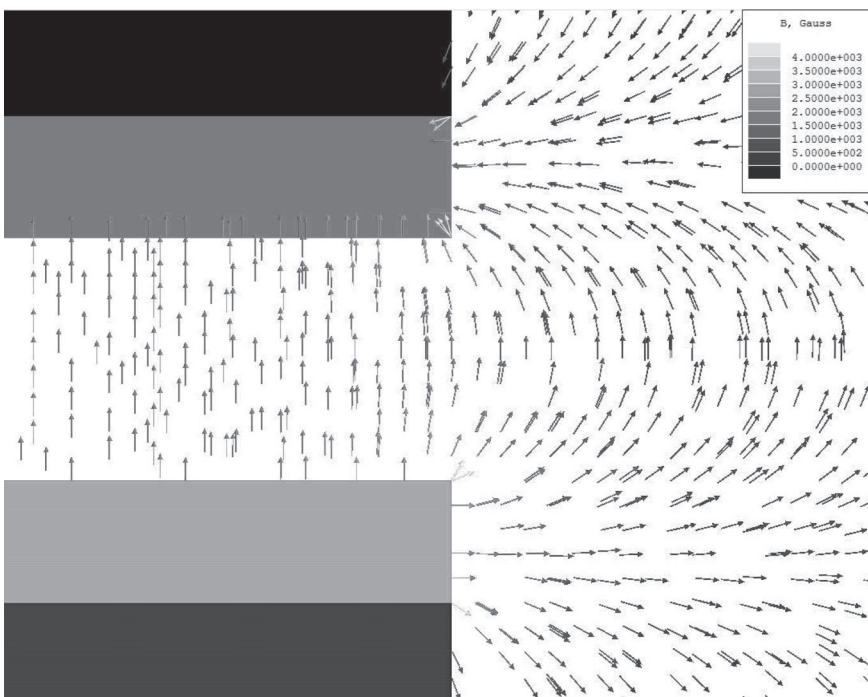


Figure 6.7 Results of 2-D magnetostatic simulation showing leakage flux.

sensitive components in close proximity to the circulator from the circulator's field. In spaceflight applications, shielding helps to minimize the net magnetic dipole moment of the circulator. This is important because the magnetic moment of the circulator could react with Earth's magnetic field, exerting a torque on the spacecraft. Third, the shielding improves the circulator magnetic circuit efficiency by providing a low-reluctance path for flux that would otherwise be leakage flux.

The key to good magnetic shielding is to keep the magnetic flux provided by the circulator magnets inside the circulator and external flux outside the circulator. The shielding material should be chosen so that large amounts of magnetic flux can be conducted with very low reluctance. This means high permeability and high maximum flux density for the material. Unfortunately, high-permeability materials typically have lower saturation flux densities.

Low reluctance can be achieved either by high permeability or large cross section. Thus, if size is not important, we can use shields of large cross

section. Where low levels of flux are present, the high-permeability materials provide the best shielding for a given cross section.

It is important to keep the number of mechanical joints in the shielding material to a minimum to avoid magnetic discontinuities, which degrade shield effectiveness. In addition, smooth bends rather than abrupt ones make for better shielding.

When we compute the cross-sectional area of the shield material, we must consider not only the flux from the circulator magnets, but also flux from outside sources that may be present. If the external flux is high, it could easily saturate the shielding, after which the circulator would have no protection. We need to keep in mind that permanent magnets are not perfectly uniform flux sources. There will be regions where the flux density is higher (usually at the magnet edges). The shielding will have to accommodate flux densities in some areas larger than might be expected if the magnets provided a perfectly homogeneous field.

The flux density in the shielding material can be computed using (6.41). The length of the shielding will, of course, be long enough to reach around the circulator. For optimum shielding, the greatest possible surface area of the circulator should be covered. In extreme cases, it may be necessary to use two layers of shielding, one inside the other.

The procedure for shield design is to first determine the allowable leakage flux from the circulator, and the amount of flux from any outside sources. Keep in mind that if ferrous materials are to be located near the circulator, these materials will provide a lower-reluctance path for leakage flux from the circulator, thus increasing the field applied to the ferrites. Next, we select a shield material and compute its minimum cross section based on the maximum flux density for the material. Remember to include the flux from the circulator magnets—(6.41)—and external flux ($B_i = \text{flux lines}/A_i$). We then spread out this cross section over as much of the circulator surface as possible. If the shielding is designed after the magnets are sized, it will be necessary to resize them because of the lower-reluctance path.

6.3 Temperature Compensation

To design a circulator with a wide operating temperature range, it is often necessary to apply temperature compensation to the magnetic circuit. Magnet manufacturers strive to produce magnets that provide a nearly constant flux regardless of temperature, but for most circulators we want a decrease in flux

as temperature increases. Some devices may require an increase in flux with temperature.

Most compensating materials decrease in permeability as temperature increases. Thus, their position in the magnetic circuit will determine whether the circulator junction flux will increase or decrease with temperature. If the compensating material is placed in series with the magnetic path, flux decreases. If the material is in parallel, flux increases.

The effects of adding compensation material to the magnetic circuit will not be uniform over wide temperature ranges. Typically compensation material will have a stronger effect at hot temperatures than at cold ones.

Ferrite compensating material in series is usually placed between the magnets and the pole pieces. Metallic compensators in series can be used in the same way, or as returns, and in parallel as magnet shunts. Compensating material should not be used as pole pieces. The material may homogenize the bias field well at cool temperatures, but at higher temperatures, the pole piece would not be functional.

Manufacturer's data for the compensating materials state how the permeability of the material varies with temperature for a specific magnetic field strength, as shown in Figure 6.8.

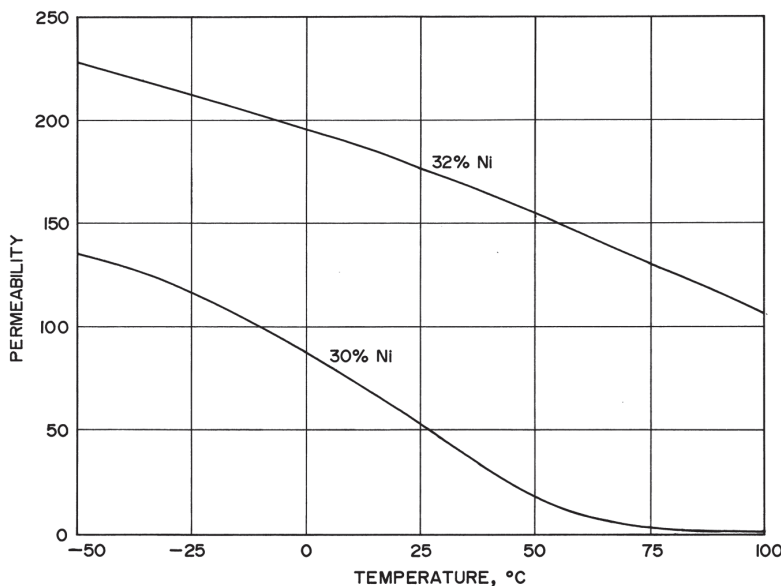


Figure 6.8 Permeability versus temperature for typical iron-nickel alloys. $H = 50$ Oe.

The first step in temperature compensation is to determine the required flux density as a function of temperature, either by calculation or testing. Then an appropriate compensating material can be selected. The magnetic operating point should be set according to the manufacturer's data by adjusting the dimensions of the material to achieve the correct flux density. The flux density can be computed using (6.41).

Circulators that contain discrete capacitors in their impedance-matching circuits, such as lumped-constant devices, can be temperature-compensated by selecting capacitors with different temperature coefficients.

Magnet and ferrite selection play an important part in the temperature stability of circulators, as do proper mechanical design and assembly.

6.4 Completing the Circuit

In this section we will discuss pole pieces, the one remaining component of the magnetic circuit for which we have not presented design information.

The purpose of the pole piece is twofold: to homogenize the magnetic field and to shape the field. For low levels of magnetic field, such as those used for low frequency below-resonance circulators, pole pieces are usually not needed. Where higher magnetic fields are utilized, as in above-resonance devices, pole pieces are a necessity, particularly with triangular magnets.

We cannot present exact designs for pole pieces, because the magnetic homogeneity of magnets varies dramatically for different magnets and shapes. For most triangular magnets used in larger above-resonance circulators, 16-gauge cold-rolled steel pole pieces are adequate. The pole pieces should have altitudes or diameters slightly larger than the magnet altitudes or diameters to be sure the leakage flux at the edge of the magnet is caught by the pole piece. In some cases, it may be necessary to make the pole piece the same size as the magnet, but the pole should never be smaller than the magnet unless the ferrite altitude is much smaller than the pole altitude.

Cold-rolled steel is used for pole pieces for several reasons. First, it has a permeability almost as high as that of pure iron at high flux densities. It is much less expensive than pure iron, which requires special processing to achieve high purity. Cold-rolled steel has a high saturation flux density, higher than the saturation levels of such high-permeability alloys as Mumetal and Permalloy. Finally, cold-rolled steel typically has a smooth finish that does not require further machining, unlike hot-rolled steel, which typically has a scaled surface.

For higher-frequency below-resonance circulators with round magnets, pole pieces about half the thickness of the triangular ones previously discussed will serve. The diameter should be a little larger than the magnet diameter.

To change the shape of the magnetic field supplied by a magnet, we ideally want pole pieces machined to form smooth transitions in shape. It is possible to increase the magnetic field strength in the air gap by using conical pole pieces like the ones in Figure 6.9. The increase in field strength, or gain, is given by [8]

$$g = \frac{H_{\text{ext}}'}{H_{\text{ext}}} = \frac{FA_g B_d'}{F' A_g' B_d} \quad (6.42)$$

H_{ext}' , F' , A_g' , and B_d' are the values with the conical pole pieces, and H_{ext} , F , A_g , and B_d are values with straight pole pieces. We calculate F' using (6.31), substituting A_g' for A_g . When F' is large ($F' \gg 2$), the gain will be low or there will be a loss ($g < 1$).

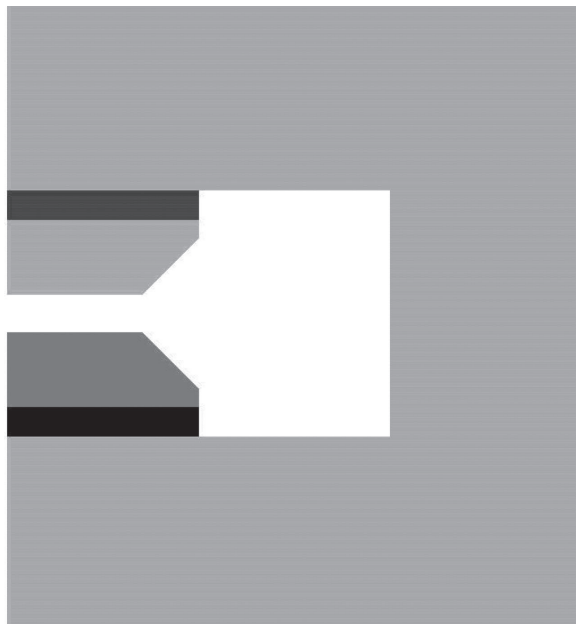


Figure 6.9 Axisymmetric model of magnetic circuit having conical pole pieces to achieve gain.

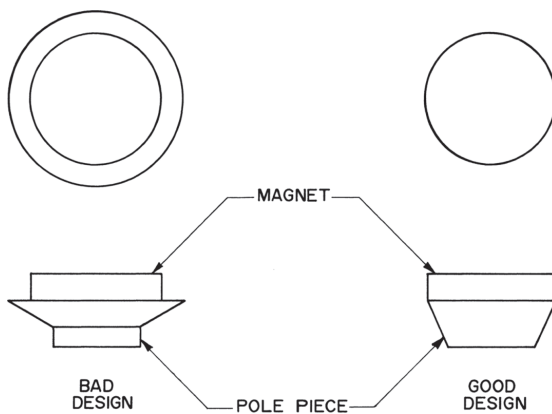


Figure 6.10 Pole piece design: smooth transitions are best.

Figure 6.10 shows two pole-piece designs, one good and one bad. The bad pole-piece design uses a rather abrupt change in cross-sectional area, which leads to a large amount of leakage flux. The good design, on the other hand, accomplishes a lesser change in cross section but the absence of an abrupt dimensional change reduces the amount of leakage flux. Either design could work, but the good design would not require as large a magnet as the bad design.

An optimum pole-piece design will minimize the amount of leakage flux caused by the pole piece. The pole piece should not be any thicker than necessary to homogenize the magnetic field so as not to cause excessive magnetic path reluctance. The thickness required will depend on the particular magnets used and the magnetic field intensity. In addition, the required degree of field homogeneity is a factor. Leakage flux minimization is done mainly by avoiding abrupt dimensional changes.

Pole-piece performance can be analyzed using magnetostatic simulation software to quantify the leakage flux and determine the shape of the magnetic field. Alternatively, pole-piece designs can be derived empirically. We should also stress that pole-piece design is not critical—many topographies are usable.

6.5 Special Cases

6.5.1 Switching Circulators

In some cases the magnetic bias is furnished by an electromagnet or by the retentivity of the ferrite itself. Usually a current pulse through a wire loop supplies the energy to set the amount and polarity of magnetic retention. Various

ferrite geometries are used for switching circulators [12]. These geometries have in common a closed ferrite path around the latching wire to minimize reluctance, in turn maximizing magnetic retention. Figure 6.11 shows one geometry, and Figure 6.12 shows the magnetic induction vectors in the ferrite with current flowing in the wire.

Ferrite retentivity is measured in gauss. The retentivity, or remanence, is the flux density in the ferrite when the external magnetic field is removed. Figure 6.13 is a typical hysteresis loop for a ferrite material. The retentivity is the amount of magnetic induction (flux density) where the loop crosses the B axis.

Switching circulators and phase shifters use retentive ferrites. The amount of energy we need to magnetize the ferrite can be determined from [13]

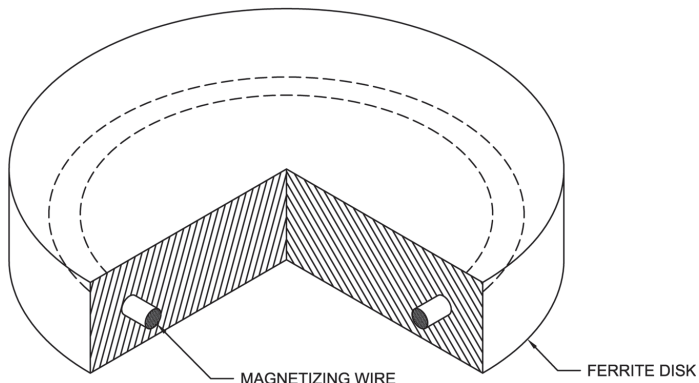


Figure 6.11 A ferrite disk for use in a switching circulator.

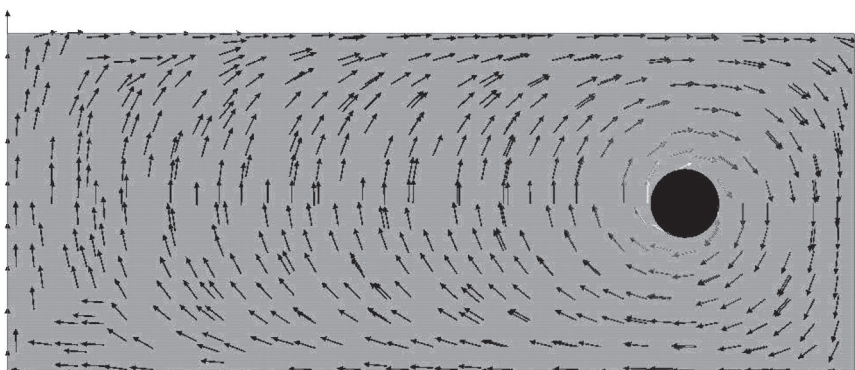


Figure 6.12 Axisymmetric view of magnetic (B) vectors in a ferrite disk of a switching circulator, with current flowing in the wire.

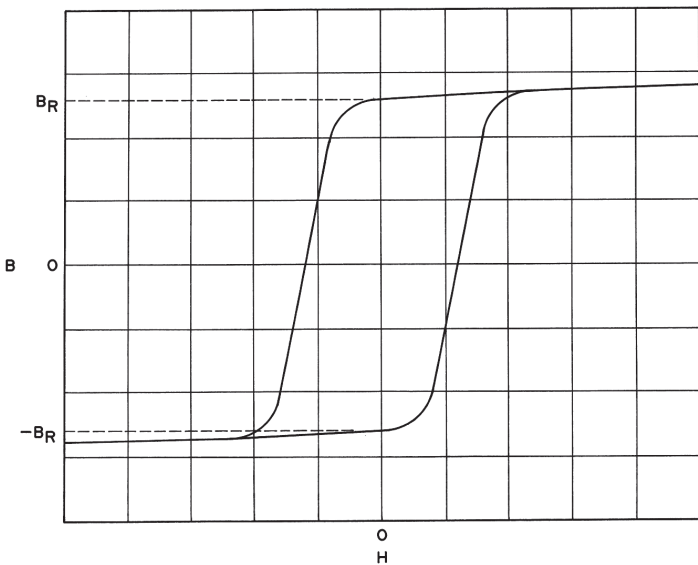


Figure 6.13 Typical ferrite material hysteresis loop (B_R = retentivity).

$$W = \int \left(N \frac{d\phi}{dt} + L \frac{di}{dt} + Ri \right) idt \quad (6.43)$$

where ϕ is the magnetic flux, N is the number of turns of wire around the magnetizing core, i is the current flowing in the wire, L is the leakage inductance of the circuit, and R is the winding resistance. The circuit is shown schematically in Figure 6.14.

If the required magnetic flux is known, we can determine the amount of energy the current pulse must have using (6.43). To change the energy level, we can change the wire loop (or coil) parameters. We calculate the required flux as described in Section 6.1.

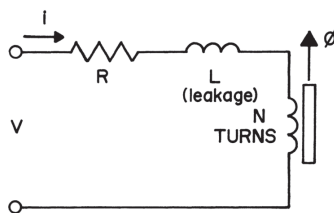


Figure 6.14 Charging circuit for retentive ferrite devices.

Where the dc magnetic field must be varied in an analog fashion, or retentive ferrites are not used, we use an electromagnet. The electromagnet is simply a coil of wire around an iron core. Ideally, the core should have a high permeability and a high saturation flux density. The magnetomotive force delivered by an electromagnet is equal to the product Ni (ampere turns). We discussed earlier in this chapter how to determine the required magnetic field, from which the electromagnet coil can be designed. The procedure for designing the coil is much the same as that for inductor or transformer design. Insofar as this design information is readily available, we will not present it here.

6.5.2 Self-Biased Circulators

To ensure that the ferrite of self-biased circulators is magnetically saturated, the aspect ratio of the ferrite must be such that [14]

$$N_z < \frac{H_C}{4\pi M_S} \quad (6.44)$$

where H_C is the ferrite coercivity. This equation establishes an upper limit for the ratio R/d in terms of ferrite disk dimensions, for a particular ferrite material. Sadly, good circulator design often dictates the use of a large R/d ratio, and not all hexaferrites have high enough H_C to tolerate this.

6.5.3 Considerations for Microstrip Circulators

To minimize cost, size, and weight, microstrip circulators often utilize open, unshielded asymmetrical magnetic circuits. Because the magnet and pole piece, if one is used, usually do not cover the entire surface of the ferrite, the dc magnetic field in the ferrite is nonuniform. Figure 6.15 shows a typical microstrip circulator magnetic circuit. We see in the figure that the magnetic vectors in the ferrite point in different directions depending on position. In some areas, the field is parallel to the direction of microwave propagation, and in other areas, it is transverse, but in the opposite direction from the vectors under the magnet.

Microstrip circulators having nonuniform bias as shown in the figure will require empirical optimization of electrical performance or magnetostatic simulation of the magnetic circuit in combination with microwave electromagnetic simulations. Microwave simulations or calculations based on a uniform field assumption would not produce the most favorable results.

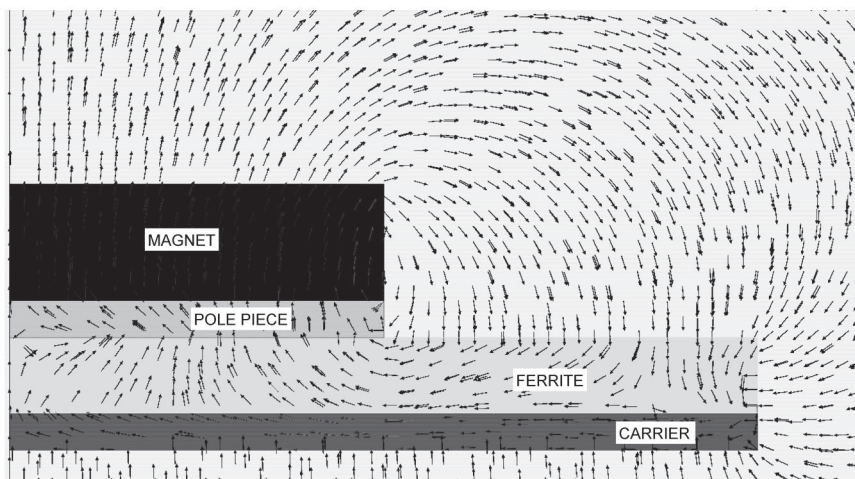


Figure 6.15 Axisymmetric view of microstrip circulator magnetic circuit showing magnetic (B) vectors.

Above-resonance microstrip circulators that have nonuniform magnetic bias are likely to have high insertion loss. This is because some of the weakly magnetized regions of ferrite may be biased at ferrimagnetic resonance, resulting in RF power absorption. To avoid high loss in above-resonance circulators, all of the ferrite in the microwave circuit must be uniformly biased, or part of the ferrite could be replaced with nonmagnetic dielectric material, which would not require magnetic bias.

References

- [1] Clarricoats, P. J. B., *Microwave Ferrites*, New York: John Wiley and Sons, 1961.
- [2] Kittel, C., "On the Theory of Ferromagnetic Resonance Absorption," *Physical Review*, January 15, 1948, pp. 155–161.
- [3] Soohoo, R. F., *Microwave Magnetics*, New York: Harper and Row, 1985.
- [4] Osborn, J. A., "Demagnetizing Factors of the General Ellipsoid," *Physical Review*, June 1945, pp. 351–357.
- [5] Bozorth, R. M., and D. M. Chapin, "Demagnetizing Factors of Rods," *Journal of Applied Physics*, May 1942, pp. 320–326.
- [6] Aharoni, A., "Demagnetizing Factors for Rectangular Ferromagnetic Prisms," *Journal of Applied Physics*, March 1998, pp. 3432–3434.

- [7] Magnet Catalog P5A, Hicksville, NY: Permag Corp., 1986.
- [8] Tenzer, R. K., "Estimating Leakage Factors for Magnetic Circuits by a Simple Method," *Applied Magnetics*, Valparaiso, IN: The Indiana Steel Products Co., April–June, 1957.
- [9] Roters, H. C., *Electromagnetic Devices*, New York: John Wiley and Sons, 1941.
- [10] *Bulletin M303*, Indianapolis, IN: Thomas & Skinner.
- [11] *Advanced Electronics*, AE-4, Los Angeles: National Technical Schools.
- [12] Helszajn, J., *Waveguide Junction Circulators: Theory and Practice*, New York: John Wiley and Sons, 1998.
- [13] Betts F., D. H. Temme, and J. A. Weiss, "A Switching Circulator: S-Band; Stripline; Remanent; 15 Kilowatts; 10 Microseconds; Temperature-Stable," *IEEE Transactions on Microwave Theory and Techniques*, December 1966, pp. 665–669.
- [14] O'Neil, B. K. and J. L. Young, "Experimental Investigation of a Self-Biased Microstrip Circulator," *IEEE Transactions on Microwave Theory and Techniques*, July 2009, pp. 1669–1674.

7

Mechanical Design

7.1 Thermal Considerations

For proper mechanical design of a circulator, we must consider how the ferrites and transmission lines will be cooled. This is particularly important for high-power circulators. To determine the proper type of cooling for an isolator, we need to also consider the power dissipated in the internal termination. This power depends on the VSWR of the load connected to the isolator output.

While it is possible to derive the thermal aspects of a circulator design using thermal simulation software, in most cases the thermal design of a circulator is relatively straightforward. Also, except in extreme cases, it is generally not difficult to provide substantial thermal design margin. For these reasons, the thermal design procedures we present here should suffice in most instances.

7.1.1 stripline Power Handling

We can use the following heat conduction formula [1] to compute the power-handling capacity of a strip transmission line:

$$\Delta T = \frac{Qd}{kA} \quad (7.1)$$

Q is the dissipated power in the strip, calculated from the average input power (P_{in}) and the insertion loss in decibels, using

$$Q = P_{in}(1 - 10^{-loss/10}) \quad (7.2)$$

$d = (b - t) / 2$ is the dielectric or ferrite thickness, k is the dielectric or ferrite thermal conductivity from Table 7.1, A is the cross-sectional area of dielectric or ferrite through which heat is conducted, and ΔT is the temperature drop through the dielectric or ferrite.

First, we find the insertion loss of the line per unit length; then we calculate the power dissipated in the line using (7.2). The spreading of thermal flux between the strip transmission line and the ground planes can be approximated as shown in Figure 7.1 [2]. The trapezoidal areas above and below the strip in Figure 7.1 represent the volume per unit length through which heat is conducted. Thus, the effective thermal conduction area per unit length of the stripline is

$$A = 2 \cdot W + b - t = 2\left(W + \frac{b-t}{2}\right) \quad (7.3)$$

Finally, we can compute the temperature rise of the strip and dielectric above the ground plane temperature and decide whether the maximum temperature is acceptable. Alternatively, knowing the maximum allowable temperature of the center conductor or dielectric, we can plug appropriate values into (7.2, 7.3, and 7.1) and come up with a maximum average power, Q .

A similar algorithm, with the upper dielectric and ground plane removed from the calculations, could be used for microstrip transmission lines.

Table 7.1
Thermal Conductivities of Common Materials

Material	Thermal Conductivity (W/in °C)
Aluminum	5.5
Brass	3.1
Copper	10.0
Steel	1.7
Air	0.0007
Alumina	0.7
Beryllia	5.0
Epoxy (conductive)	0.02
Heat sink compound	0.01
Teflon	0.005
Ferrite	0.16

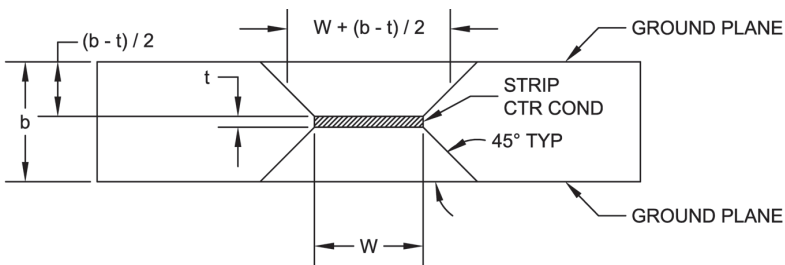


Figure 7.1 Thermal flux spreading in a stripline structure.

7.1.2 Power Dissipation in Ferrites

Thermal considerations also influence the selection of web thickness (the thickness of the metal between the ferrite and the magnet or pole piece). If we know the Curie temperature for the ferrite material to be used and the insertion loss of the ferrite junction, either by calculation or measurement, we can compute the temperature the ground plane must be to avoid severe electrical performance degradation due to RF heating of the ferrites. The thermal conductivities [1] of some materials commonly used in circulators are given in Table 7.1.

Section 5.8 discusses power dissipation in ferrites. If it is not possible to accurately determine the distribution of the heat load, we can make the safe assumption that all RF heating takes place at the surface of the ferrite, and apply (7.1) to compute the temperature drop across the ferrite. In this application of (7.1), Q is the power dissipated in the circulator junction, calculated from the average input power and the insertion loss in decibels using (7.2), d is the ferrite thickness, k is the ferrite thermal conductivity from Table 7.1, and A is the cross-sectional area of the ferrite. Because the power is not evenly distributed on the surface of the ferrite, we need to apply a factor to compensate for this. If we use a factor of 2 (which implies that the power is dissipated in only half of the ferrite), and remember that there are actually two thermal paths, one for each ferrite and ground plane, we find that (7.1) already includes the compensation factor.

Once we know the temperature drop across the ferrite, we subtract this from the ferrite Curie temperature to find the maximum ground-plane temperature. At temperatures below the ferrite Curie temperature, circulator electrical performance may drift significantly. If it is not possible to determine the electrical effects of ferrite heating, either by simulation or by testing, another option is to apply a safety or de-rating margin. For example, we could decide

to keep the ferrite temperature at least 100° C below its Curie temperature. If the maximum ground-plane temperature is significantly below the ambient air temperature, methods of cooling the circulator or decreasing the power density in the ferrite must be investigated.

7.1.3 Cooling of Ferrites

Conduction cooling is the most commonly used cooling method when thermal demands are not too extreme. When conduction cooling is specified, maximum circulator case temperature must also be specified. Without a maximum temperature, the cooling system designer will not be able to do his or her job properly. It is helpful to the user to know the approximate amount of power dissipated in the circulator.

If more power must be removed from the circulator than can readily be removed by conduction cooling, or if there is no controlled-temperature mounting surface for the circulator, we can resort to radiation and natural convection. In a vacuum, such as in space, air convection cooling would not be available, but radiation cooling would be an option.

The approximate amount of power that can be transferred to the ambient air by a natural-convection heat sink is shown in Figure 7.2 as a function of the temperature difference between the heat sink and the ambient air.

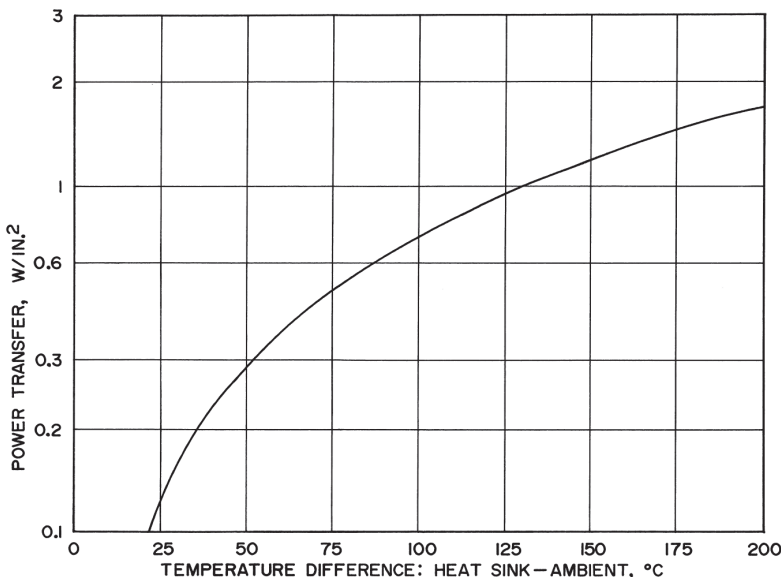


Figure 7.2 Power transferred by a natural-convection heat sink versus temperature rise [1].

A more drastic cooling measure is forced-air cooling. Before we can apply this cooling method, the power dissipated in the ferrite has to be conducted to the surface of the circulator. To calculate how much lower than the ground-plane temperature the circulator surface must be held, we apply (7.1) to all segments of the thermal path from the ground plane to the surface, summing the temperature drops. The length of each segment is d , the cross-sectional area is A , and the appropriate thermal conductivity (k) is used. Other equations can be used for special geometries; they are beyond the scope of this book.

The temperature rise of a forced-air-cooled (fan-cooled) heat sink per watt of power dissipation is approximated by [1]

$$\frac{\Delta T}{Q} = \frac{140w}{n^{0.2}z^{0.2}F^{0.8}L} \quad (7.4)$$

where w is the heat-sink fin spacing, n is the number of fins, z is the fin height, F is the air flow in ft^3/min (CFM), and L is the length of the heat sink. The dimensions of w , n , z , and L are in inches.

If the average power level is very high and the ground-plane temperature must be held very low, water (or other liquid) cooling is indicated. Water cooling is accomplished by placing a water jacket between the ferrite and magnet or pole piece, in place of the web. The temperature rise of the water jacket above the water temperature per watt of power dissipation is given by [1]

$$\frac{\Delta T}{Q} = \frac{0.72A^{0.4}}{F^{0.8}L} \quad (7.5)$$

where A is the cross-sectional area in inches^2 of a cooling duct of circular cross section, F is the water flow in gallons/minute (GPM), and L is the length of the cooling duct in inches. The assumption is made that the flow rate is high enough so that the flow is turbulent; that is,

$$\frac{F}{A^{0.5}} \gg 0.69 \quad (7.6)$$

7.2 Venting

Circulators that are destined to operate in vacuum or in ambient pressures that differ substantially from atmospheric pressure require venting to equalize

pressure between the circulator interior and the circulator's ultimate surroundings. In some applications, such as a rocket launch, a venting rate or maximum pressure differential may be specified. In these cases, the rate of venting must be considered. In a vacuum, it is desirable to vent as much of the residual atmospheric gases as possible to avoid a partial-pressure voltage breakdown.

At pressures above one torr, the gas flow is generally *viscous* in nature, and the flow rate through a vent hole is much higher than it is when the pressure is very low. Other than to ensure that a device does not build up significant pressure relative to its environment, venting rate is not a significant concern at higher pressures. In vacuum, when the mean free path of gas molecules is greater than the vent hole dimensions, flow is *molecular*, and for a tube or hole of circular cross section, the flow rate of air is approximately [3]

$$C = 78.19 \frac{D^3}{L + \frac{4D}{3}} \quad (7.7)$$

where D is the hole diameter in inches, L is the length of the hole in inches, and C is the flow rate, or *pumping conductance* in vacuum technology parlance, in l/s. Vent holes must have sufficient pumping conductance to maintain a low pressure in the vicinity of any gaps that could potentially multipact. The outgassing rates of the materials that are present should be considered. The outgassing rate of the surfaces of metals can be as high as 10^{-5} torr-l/s per square inch [4], so the vent holes should at least be able to maintain high vacuum (10^{-3} torr or lower pressure) with this outgassing rate. The ultimate steady-state internal pressure in torr of the device is given by

$$P = \frac{QA}{C} \quad (7.8)$$

where Q is the outgassing rate of the interior surface (10^{-5} torr-l/s per square inch worst case for metals), A is the interior surface area in inches², and C is the pumping conductance of the vent hole in l/s.

If venting is insufficient, then the vent hole could be made larger, but if the hole is too large, it could allow RF radiation. We can think of the hole as a circular waveguide, for which the cutoff frequency in gigahertz of the lowest-order mode is given by [5]

$$f_c = \frac{1.84c}{10^9 \pi D} \quad (7.9)$$

The microwave attenuation in decibels provided by a circular waveguide opening below cutoff is approximately

$$\text{Attenuation} = 32 \frac{L}{D} \sqrt{1 - \left(\frac{f}{f_c}\right)^2} \quad (7.10)$$

If radiation is problematic, then multiple smaller holes could be used to achieve the same venting.

7.3 Coaxial Junction Circulators

7.3.1 Packaging Techniques

The final stage in the circulator design process is the mechanical design. In this stage, we package the ferrites, magnets, connectors, and other components, forming a microwave device that meets specifications. The specifications for the circulator may include not only electrical parameters and environmental factors but also cost. The type of mechanical design used will be dependent on the available manufacturing facilities as well as specifications.

Most coaxial junction circulators are based on stripline techniques. There are five basic packaging schemes for stripline circuits [6]. The first is flat-plate construction. This is an inexpensive and simple technique where two flat metal plates are placed outside the center conductor and dielectric material (or ferrite), one on each side. The plate thickness is chosen to provide rigidity to the circuit and to allow screw holes for connector mounting at the edges. However, it is not imperative that the connectors be mounted at the edges. Broad-wall launching could be used.

The plates are usually held together with screws; we use metal spacers between the plates if the dielectric is not firm enough to prevent bending the plates when the screws are tightened. A drawback of this construction is that the edges of the device, between the ground plates, must be sealed to prevent RF radiation and to protect the circuitry from the environment and foreign objects. Figure 7.3 illustrates the flat-plate construction.

The second packaging scheme we will discuss is the bonded-substrate construction, shown in Figure 7.4. Dielectric materials are available that have aluminum plates already bonded to them. This scheme reduces the amount of machining required, but the plates are usually too thin to have connectors screwed to them. Consequently, we must use either special connectors or

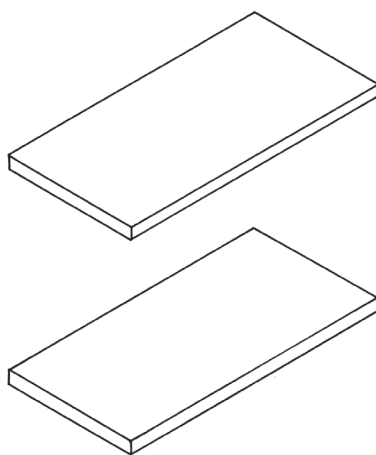


Figure 7.3 Flat-plate construction.

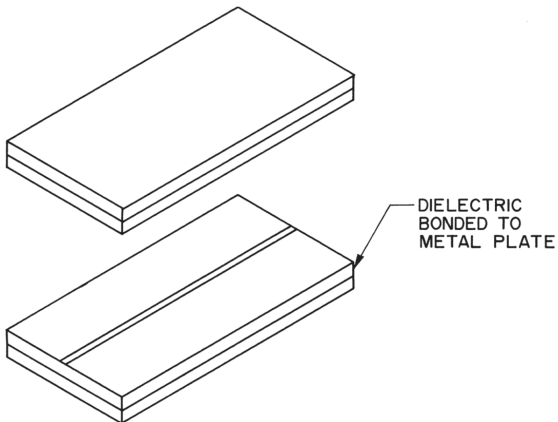


Figure 7.4 Bonded-substrate construction.

manufacture blocks for connector mounting. The bonded-substrate construction also requires that we seal the edges of the device.

Figure 7.5 depicts another stripline technique that utilizes metal plates with channels cut into them. The edges of a device constructed using this technique do not usually require additional sealing. A disadvantage of this scheme is that the dielectric material must be cut to fit into the channels, unless air is the dielectric. In this case, the center conductor must be properly supported. The plates can be channeled by various means, including milling, electrical-discharge machining, drawing, casting, and high-energy-rate forming [7].

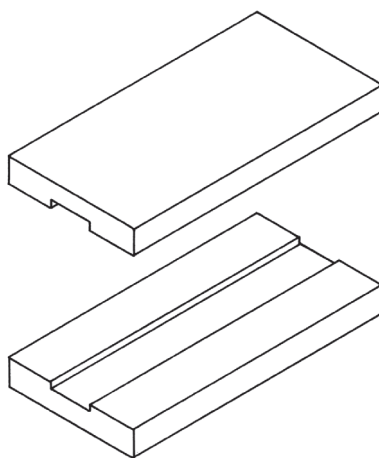


Figure 7.5 Channeled-plate construction.

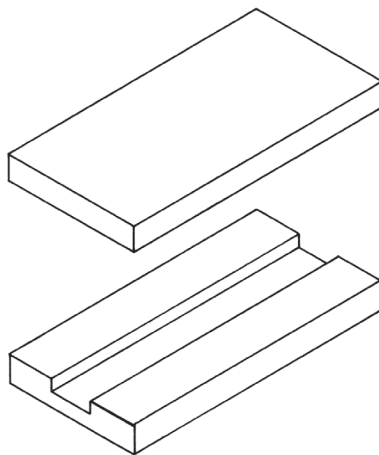


Figure 7.6 Box-and-cover construction.

Box-and-cover construction, shown in Figure 7.6, is very similar to the channeled-plate construction. The box-and-cover technique does not require that both plates be channeled; only the box plate is channeled. This construction reduces the amount of machining to produce a pair of plates, but different machine setups may be needed to produce each plate. In addition, more time is spent generating drawings for a box and cover than would be spent on drawings for two channeled plates, because the two channeled plates could be designed as symmetrical mirror images of one another. Symmetrical mirror-image

parts can be machined using the same setup. The only necessary difference between the parts is related to the screws that hold them together—one will have tapped (threaded) screw holes, and the other will have clearance holes.

The decision between the channeled-plate construction and the box-and-cover construction should be made based on the quantity of parts to be manufactured.

The fifth stripline packaging scheme is the bonded-stripline construction. This technique uses dielectric sheets with copper ground planes on the outside. The circuit is etched on the other side of one or both dielectric sheets. The sheets are held together by a resin bond formed by heat and pressure [8]. The resulting assembly is highly resistant to humidity and salt spray and is very lightweight, but cannot be repaired and does not offer rigid support to components. Bonded stripline techniques are unsuitable for circulators because of the lack of support given to the ferrites.

The metal plates in the first four packaging schemes can be replaced by metalized plastic parts. Such parts are used more frequently where weight is an important parameter.

Of the five stripline packaging techniques, three are most suitable for circulators. As previously mentioned, bonded stripline does not offer support to the ferrites. The bonded-substrate configuration does not lend itself to circulator design because we would need ferrite slabs with the ground planes bonded to them, which would lead to difficulties in machining the combination and to wasted ferrite. We are left with the box-and-cover construction, the channeled-plate technique, and the flat-plate construction.

An important difference between the flat-plate construction and the other two is that the edges of the flat-plate device must be sealed. An advantage of the flat-plate scheme is that intimate contact between the ferrites and the ground plane is achieved by tightening the screws to the correct torque. Good contact between the ground plane and the ferrite can be obtained with the other two constructions only by imposing tight dimensional tolerances.

Two popular packaging variations, one on the box-and-cover scheme and one on the flat-plate scheme, are shown in Figures 7.7 and 7.8, respectively. The circulator in Figure 7.7 uses a steel housing and cover to complete the magnetic circuit, and the threaded cover maintains good contact between internal parts. Ground contact between the ground planes and interior housing walls is typically made by interference fits or by conductive gaskets. The circulator of Figure 7.8 uses three magnets placed alongside the ferrites, with thick pole pieces top and bottom to complete the magnetic circuit. This type of circulator is typically placed inside a nonmagnetic housing to retain all the parts.

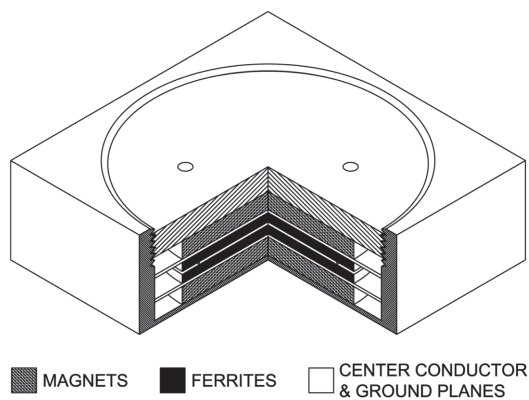


Figure 7.7 Threaded steel housing.

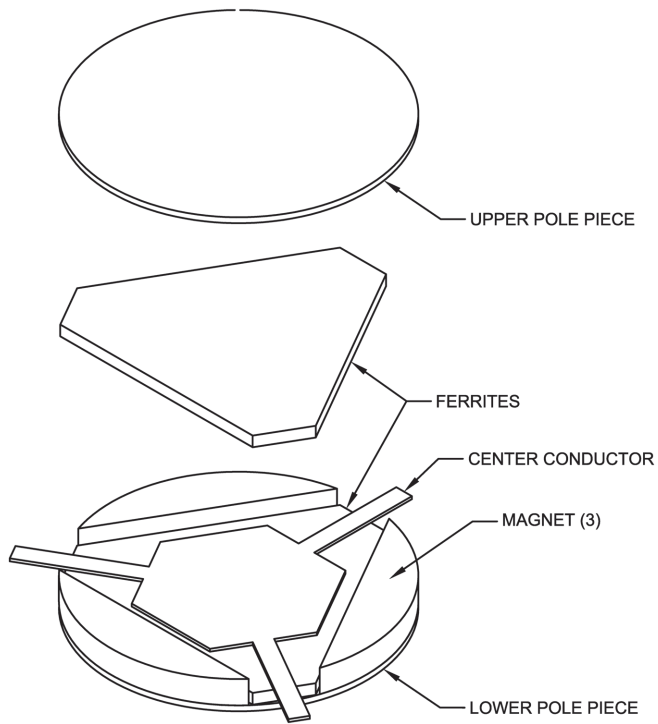


Figure 7.8 Side-magnet construction.

The magnets are typically placed in wells so that the plates can be thicker than the web thickness between the magnet and ferrite. These magnet wells are positioned so that the ferrites are centered beneath the magnet. Some engineers believe that they can achieve better performance from the circulator by deliberately skewing the magnetic field off to one side. This technique may optimize one parameter but will degrade others. At best, it is a compromise of circulator performance.

Where magnet wells are not used, as in the flat-plate construction, the magnets must be held in position by epoxy or mechanical means.

7.3.2 Dimensional Tolerances

Imperfect contact between the ferrites and the ground planes can cause undesired resonances and generally poor electrical performance. It is therefore imperative that the ground planes be very flat and very smooth. Circulator housings (also called bodies) that have channels are usually dimensioned so that there is a slight amount of compression applied to the ferrite junction, ensuring intimate contact between ferrite and ground plane. If the depths of the channels in the housing are relied on to set up the appropriate compression, the tolerance on the ground-plane spacing must be tight: ± 0.001 inch or so. Figure 7.9 illustrates the effect of incorrect ground-plane spacing. When the spacing is too large, the ferrites are not in contact with the ground planes. When the spacing is too small, the ground plane bows up at the center of the ferrite, not making good contact. In extreme cases, the ferrites may be broken when the circulator is assembled. The ground plane may be permanently bent up in the center so that it will never make good contact with the ferrite. A good amount of interference (compression) with which to design is about 0.001 in, although this depends on the web thickness, ferrite diameter or altitude, and the size of the cavity. We should remember that ferrites are hard and are not compressible as are many dielectric materials.

Compression can be achieved with channeled circulator housings using two methods that do not rely on the channel depth to set up the ground-plane

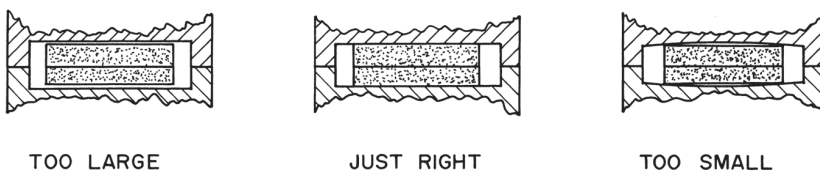


Figure 7.9 Effects of incorrect ground-plane spacing.

spacing. One method is to set the channel depth slightly less (0.010 to 0.020 in) than the depth required for ferrite contact. Then, the screws that hold the housing halves together can be tightened to a torque that provides for good ferrite contact. This technique defeats the purpose of the channels and the circulator must be sealed.

The second method is to place a compressible, elastic material between the ferrites and the ground planes. Ground continuity must be maintained by laying thin metallic foil between the ferrites and the compressible material. When the housing halves are assembled, the compressible material provides a force, pushing the ground foil against the ferrite. This method is shown in Figure 7.10. The elastic material also may serve as shock mounts for the ferrites. The disadvantage of this technique is that the ground will not be perfectly flat and smooth because the thickness of the compressible material may vary. The compressible material may degrade with age, depending on the chosen material.

The thickness of the metal between the ferrite and the magnet or pole piece (web thickness) should be thick enough so that it will not flex much when the circulator is assembled. There are practical limits to how thin the web can be made from a machining point of view as well. Circulator housings are often machined from solid blocks of aluminum. If a very thin (flexible) web is specified, chances are good that the milling cutter will accidentally punch right through the web, destroying the part; it could happen if the cutter is pulling up on the web and the web is flexing so that it is cut when it should not be.

It is desirable to have a thin web from a magnetic point of view because this will reduce the air gap in the magnetic circuit, thus reducing the magnet size. Typically, webs can easily be made as thin as 0.030 in. However, webs on the order of 0.100 in thick are desirable electrically because they usually provide flatter ground planes.

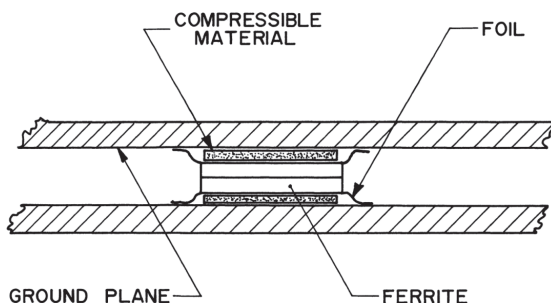


Figure 7.10 Ferrite junction compression achieved using compressible material.

The magnet wells should be sized so that the pole piece and magnet will easily fit inside, but not so large that the performance of the circulator changes because the magnet moves around. The bottom of the magnet well must be parallel to the ground plane, or field asymmetry will result.

7.3.3 Controlling Cavity Resonances

In stripline circulators, we often place the ferrites and center conductor inside a cavity, as shown in Figures 7.11 and 8.2 in Chapter 8. For ferrite disks, the cavity is cylindrical. If the ferrites are triangular, then the cavity may also be triangular, with similar margins.

If the cavity is not properly sized, its resonant frequency may fall within the operating frequency band of the circulator, wreaking havoc with circulator performance. Even very small gaps between the ferrites and ground planes or between the ferrites and center conductor can excite cavity modes and impact circulator electrical performance [9].

There are several ways to minimize or eliminate the effects of cavity resonances:

1. Reduce excitation of spurious modes by eliminating gaps between ferrites and the center conductor and between ferrites and ground planes.
2. Size the cavity so that its resonant frequency is outside the circulator frequency band.
3. Use conductive features, such as a metal pin through the center of the ferrites and center conductor, to prevent excitation of spurious modes.

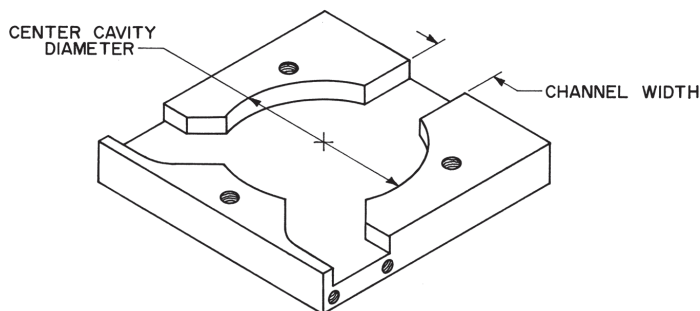


Figure 7.11 Dimensions of box-and-cover or channeled-plate housing half.

4. Strategically place microwave absorptive material (*mode suppressors*) to reduce the cavity Q, effectively reducing the impact of the cavity resonance on circulator performance.

Despite best efforts, it is not always practical to eliminate all gaps between ferrites and conductive surfaces. Metal pins cause other problems, such as bandwidth limitation and increased manufacturing cost. Cavities are not always properly sized due to physical size limitations, so the use of mode suppressors has long been the most popular option.

Early in my career, an eccentric, experienced engineer gave me a rule of thumb. He said, “Make the cavity diameter at least 1.3 times the diameter of the ferrite.” I vaguely understood that this had something to do with cavity resonances, but I did not ask for the derivation of this rule. I suspected that this information was passed from one circulator engineer to the next without full explanation. Your author has recently worked tirelessly, having embarked on a mathematical journey of discovery, to find the origin of this rule of thumb, which undoubtedly appears somewhere in the excessive reams of circulator literature.

We know from rearranging (5.9) that the resonant wavelength of a stripline junction circulator is

$$\lambda = \frac{2\pi R \sqrt{\mu_{\text{eff}} \epsilon}}{kR} \quad (7.11)$$

and the resonant wavelength for the TM_{010} mode of a cylindrical cavity is [10]

$$\lambda = 2.61 R_C \sqrt{\mu_{\text{eff}}} \quad (7.12)$$

where R_C is the radius of the cavity. Setting (7.11 and 7.12) equal to each other and solving for the ratio R_C/R , we have

$$\frac{R_C}{R} = \frac{2\pi}{2.61 kR} \quad (7.13)$$

When $kR = 1.84$, which is the case for weakly-magnetized below-resonance circulators or strongly-magnetized above-resonance circulators, $R_C/R = 1.3$, our rule of thumb. The ratio R_C/R varies with kR , but is independent of ferrite material properties, so it is widely applicable.

It might seem that as R_C/R is increased, the resonant frequency of the air cavity would be impacted in a not-so-predictable fashion by the decrease in ferrite filling factor in the cavity. For large filling factors, the cavity resonant frequency is not strongly dependent on filling factor [11]. Figure 7.12 shows cavity resonant frequency versus filling factor of ferrite for $R_C = 0.5$ in, $\epsilon = 15$, and $\mu_{\text{eff}} = 1$. For filling factors ≥ 0.6 , the cavity resonant frequency is within $< 10\%$ of the fully filled value. In Figure 7.13, we see that for $R \leq R_C < 1.3R$, the cavity resonant frequency is above the circulator frequency, and for $R_C > 1.3R$, the cavity frequency is below the circulator frequency.

For most practical circulators ($R/d \geq 2.2$), the next higher-order mode would be the TM_{110} one, which has a resonant frequency about 1.59 times that of the dominant TM_{010} mode. The cavity diameter must be large enough so that it is resonant below the lower circulator frequency band edge:

$$\frac{R_C}{R} > \frac{4\pi}{2.61(2 - w) kR} \quad (7.14)$$

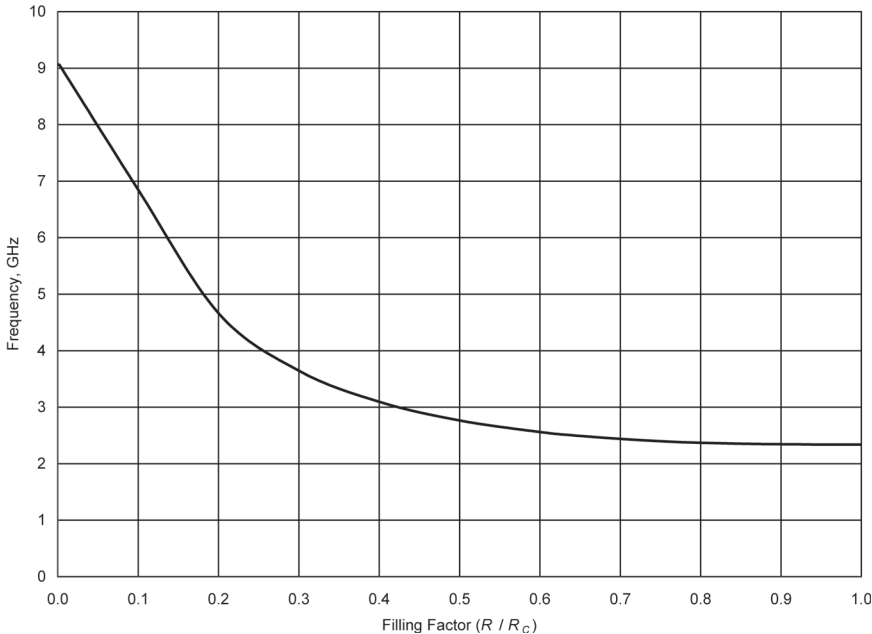


Figure 7.12 Ferrite-filled cavity resonant frequency. $\epsilon = 15$, $\mu_{\text{eff}} = 1$, and $R_C = 0.5$ in.

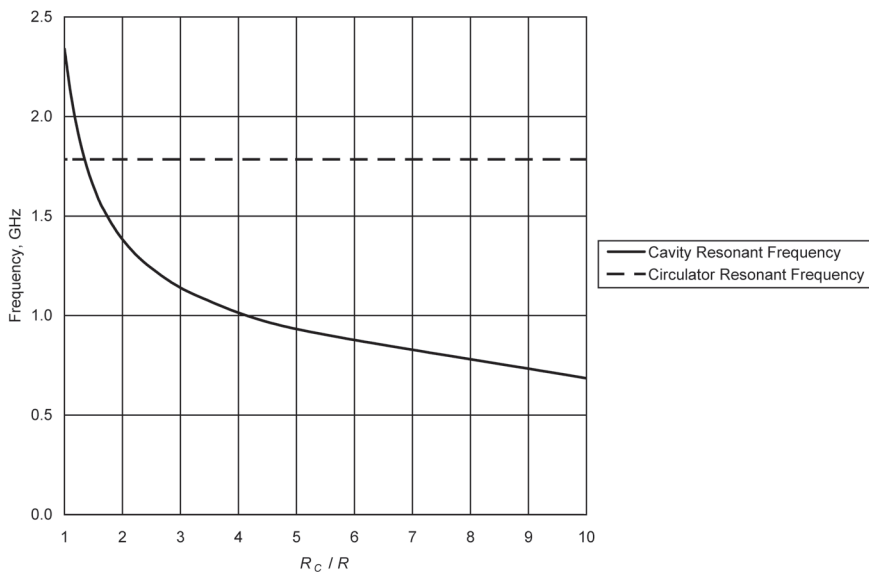


Figure 7.13 Resonant frequency versus normalized cavity radius. $\epsilon = 15$, $\mu_{\text{eff}} = 1$, and $R = 0.5$ in.

yet small enough that the next higher-order mode does not fall below the upper edge of the circulator band:

$$\frac{R_C}{R} < \frac{4\pi}{1.64(2+w)kR} \quad (7.15)$$

Equations (7.14) and (7.15) constrain the maximum mode-free fractional bandwidth (w) to about 45%, which corresponds to $R_C/R = 1.7$. It is not possible to obtain mode-free operation of circulators having $> 45\%$ bandwidth only by adjusting cavity diameter.

Sometimes package size constraints prevent sizing the cavity adequately. In these cases, and others where cavity size alone won't prevent cavity resonances, mode suppressors can be used. Absorber material, such as polyiron, should be strategically placed in the circulator housing, near the ferrites but away from strip lines. The strategy is to reduce the Q of the cavity significantly so that sharp resonances do not appear in the circulator frequency band, but avoid increasing insertion loss by coupling too much energy into the mode suppressors.

For both the box-and-cover construction and channeled-plate construction, we need to determine the widths of the channels and the size of the center cavity. These dimensions are indicated in Figure 7.11. Note that the exterior shape of the circulator housing shown in Figure 7.11 is rectangular. The shape could also be round, triangular, or hexagonal. The rectangular shape is normally used because it is easily integrated into a system. Shapes with three-way symmetry can be difficult to mount without wasting space.

The size of the center cavity, which will be either round or triangular depending on the ferrite shape, is determined from the size of the resonator, ferrite, and any dielectric material that may be attached to the ferrite. Where impedance transformers are used, dielectric material may be either located in the channels connecting the center cavity and the connectors or immediately adjacent to the ferrite in the center cavity. If two quarter-wavelength transformers are used (a typical construction for octave-bandwidth circulators), and these transformers are located adjacent to the ferrite, the center cavity diameter will be increased by approximately a wavelength, as shown in Figure 7.14. A cavity of this size will support circular resonance modes, which may result in high insertion loss at some point in the band. These circular modes can be suppressed by strategic location of absorbing material such as polyiron. The dielectric material can be cut into slabs and placed in the channels. If we use this technique, we do not have the problem of circular modes, but more machining is required on the dielectrics.

If the dielectric ring illustrated in Figure 7.14 is used, the center cavity should be dimensioned so that the dielectric just fits, allowing for dimensional tolerances. When the cavity size is based only on the ferrite diameter or

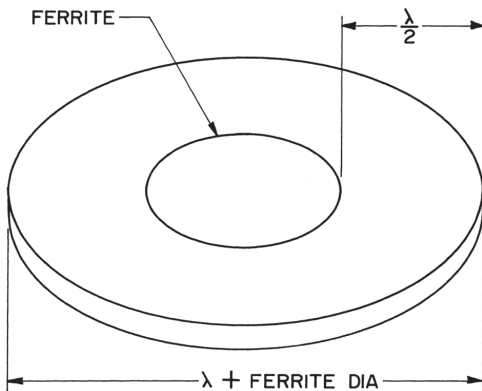


Figure 7.14 Ferrite disk in dielectric ring for dual quarter-wavelength transformers at each port.

altitude, we dimension the cavity so that the walls are far enough away from the ferrite to prevent them from being part of the circuit. Usually the walls have little influence on the ferrites if the space between a wall and the ferrite is approximately equal to the ground plane spacing.

We select the channel widths such that they will not affect the characteristic impedance of the striplines. There is certainly no significant change in Z_0 if the walls are two line widths from the center conductor, and the spacing can be as little as one-half the line width depending on the impedance. Stripline design data are available that include the effect of the walls, if it is necessary to make the channels very narrow.

The channels should be located 120° apart or the circulator will not be symmetrical electrically. It is also desirable to make the channels straight, if possible, to avoid discontinuities.

The flat-plate construction has neither channels nor center cavity. Because the inside of a circulator made using this method of construction is completely open, several different types of resonances can occur. To help eliminate these parasitic resonances and couplings, we can place screws around the ferrites and along the sides of the striplines, spaced an eighth of a wavelength or less apart. Some resonances may not show up until the circulator is sealed. Absorbing material can also be useful in the reduction of resonances. The exact location of this material is best determined empirically.

7.3.4 Transitions

In any type of stripline circulator, it may be necessary to make transitions in stripline characteristic impedance. These transitions could be between transformer sections or between a transformer and a 50Ω section. Step transitions are the simplest, but create the worst discontinuity. We can select one of two other commonly used techniques: the triangular compensation method illustrated in Figure 7.15, or a contour method [12].

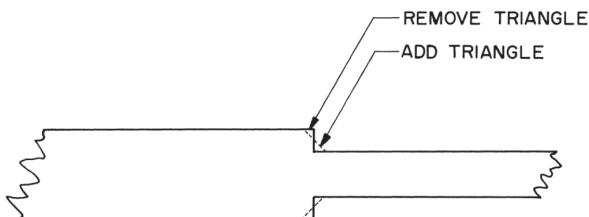


Figure 7.15 Stripline-transition triangular compensation technique.

A stripline step transition discontinuity can be modeled using the equivalent circuit shown in Figure 7.16(a). This is an approximate equivalent circuit, where the inductance is given by [13]

$$L = \frac{60\pi b}{\omega\lambda} \ln \left[\csc \left(\frac{\pi Z_{t2}}{2Z_{t1}} \right) \right] \quad (7.16)$$

where b is the ground-plane spacing and Z_{t1} and Z_{t2} are the low and high characteristic impedances of the two striplines, respectively.

If the inductance added by the step transition is unacceptable, we can use the triangular compensation method. In this method, we attempt to minimize the discontinuity equivalent inductance by removing and adding triangular sections as shown in Figure 7.15. The amount to be removed or added can be determined by breaking up the transition into small steps and computing the discontinuity inductances for each of the steps. If the length of these steps for analysis is much less than a wavelength, the analysis will be fairly accurate. Other ways to determine how large the triangles to be removed and added should be is to use an experimental (cut-and-try) method or use electromagnetic simulations of the transition.

A more accurate stripline-transition discontinuity model is shown in Figure 7.16(b). This model could be applied along with a technique to maintain a constant characteristic impedance up to the actual transition, resulting in a contoured transition. The details of such a compensation technique are beyond the scope of this book, but [12] at the end of this chapter describes a computer program to help reduce discontinuities.

We frequently use waveguide-height transitions in waveguide circulators. These may be symmetrical, as shown in Figure 7.17, or asymmetrical, as shown in Figure 7.18. The equivalent circuit of this step discontinuity is a shunt capacitance at the plane of the waveguide height change. For the symmetrical case, the normalized susceptance is [14]

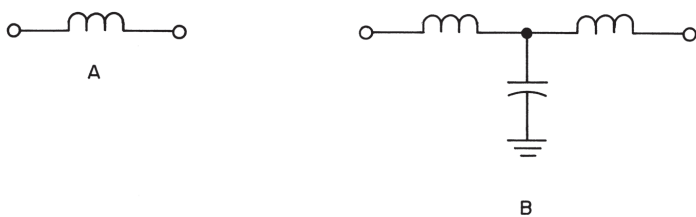


Figure 7.16 Stripline-transition discontinuity equivalent circuits.

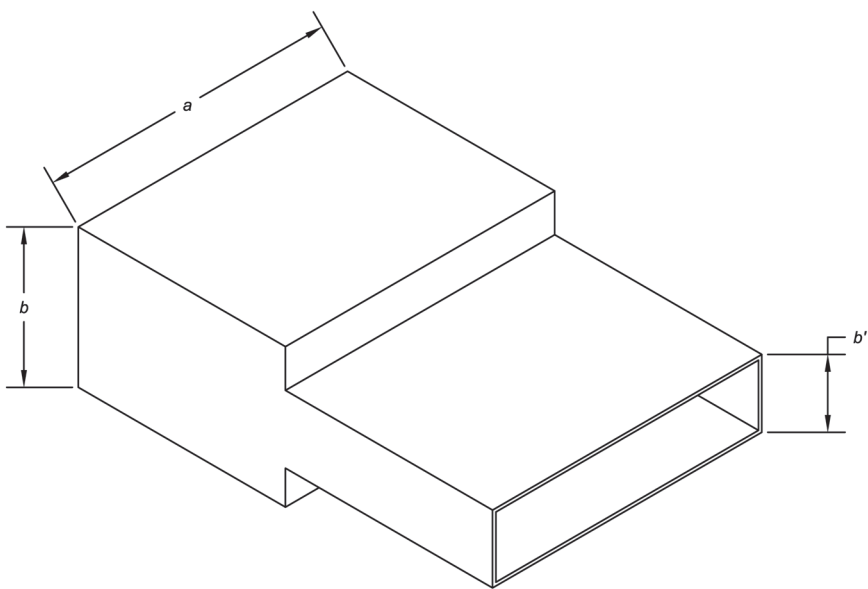


Figure 7.17 Symmetrical waveguide height transition.

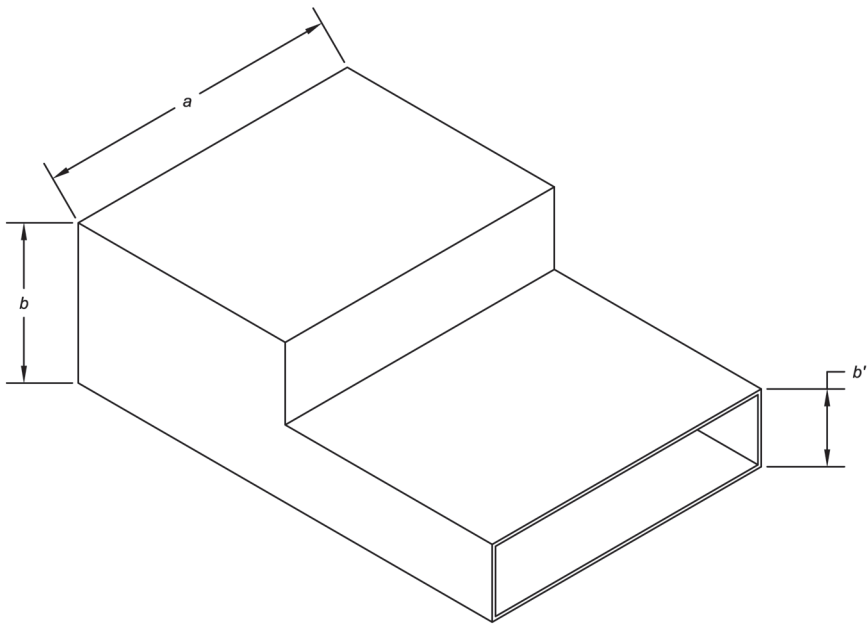


Figure 7.18 Asymmetrical waveguide height transition.

$$\frac{B}{Y_0} = \frac{2b}{\lambda_g} \left\{ \ln \left[\left(\frac{1-\alpha^2}{4\alpha} \right) \left(\frac{1+\alpha}{1-\alpha} \right)^{\left(\frac{\alpha+1}{2-2\alpha} \right)} \right] + 2 \frac{A+A'+2C}{AA'-C^2} \right. \\ \left. + \left(\frac{b}{4\lambda_g} \right)^2 \left(\frac{1-\alpha}{1+\alpha} \right)^{4\alpha} \left(\frac{5\alpha^2-1}{1-\alpha^2} + \frac{4\alpha^2 C}{3A} \right)^2 \right\} \quad (7.17)$$

where λ_g is the guide wavelength, given by (5.160), $\alpha = b'/b = Y_0/Y'_0$, and

$$A = \left(\frac{1+\alpha}{1-\alpha} \right)^{2\alpha} \frac{1 + \sqrt{1 - \left(\frac{b}{\lambda_g} \right)^2}}{1 - \sqrt{1 - \left(\frac{b}{\lambda_g} \right)^2}} - \frac{1+3\alpha^2}{1-\alpha^2} \quad (7.18)$$

$$A' = \left(\frac{1+\alpha}{1-\alpha} \right)^{\frac{2}{\alpha}} \frac{1 + \sqrt{1 - \left(\frac{b'}{\lambda_g} \right)^2}}{1 - \sqrt{1 - \left(\frac{b'}{\lambda_g} \right)^2}} + \frac{3+\alpha^2}{1-\alpha^2} \quad (7.19)$$

$$C = \left(\frac{4\alpha}{1-\alpha^2} \right)^2 \quad (7.20)$$

For the asymmetrical case, use (7.17–7.20), except replace λ_g with $\lambda_g/2$.

After we know the normalized susceptance (B/Y_0), we can compute the required phase adjustment to compensate for the step discontinuity [13]:

$$X = \frac{1}{2} \left[\tan^{-1} \left(\frac{B}{Y_0} \frac{\alpha}{1-\alpha} \right) + \tan^{-1} \left(\frac{B}{Y_0} \frac{\alpha}{1+\alpha} \right) \right] \quad (7.21)$$

We then shorten the length of the reduced-height waveguide section (typically a transformer) by

$$\Delta L = \frac{X\lambda_g}{360^\circ} \quad (7.22)$$

if X is in degrees. If X is in radians, then the denominator of (7.22) would be 2π .

7.3.5 RFI Control

We need to seal the finished circulator, especially if it is of flat-plate construction, to prevent RF radiation and to protect the inside of the circulator from humidity, rain, salt spray, and dust. One of the most frequently used sealing schemes for circulators is to epoxy edge covers (of aluminum or steel) in place. Epoxy is also used to seal joints. The disadvantage of epoxy is that it is difficult to repair the circulator once it is sealed.

We can use gaskets, either ordinary or of the RFI variety, to seal the circulator edges. This is a good method if the circulator is to be pressurized to increase the power-handling capacity and to reduce RF radiation.

Another sealing method is the use of metal tape with adhesive. We use this tape to seal the edges and joints of the circulator.

Where hermetic sealing is required, we use glass-bead connector interfaces and solder or weld the housing together. If the soldering or welding is done properly, the circulator will not be overheated, because only the immediate area of the joint will be heated.

7.3.6 Dissimilar Metals

As presented in Section 4.5, if dissimilar metals are placed in contact with each other, steps must be taken to prevent corrosion. MIL-STD-889B [15] contains a table listing the compatibility of metal combinations in various environments and a list of recommended surface treatments for corrosion protection.

Metals that are far apart in the galvanic series should not be placed in contact with each other without surface protection, as severe corrosion of the more anodic metal will occur. If dissimilar metals must be placed in contact, choose metals that are close together in the galvanic series, and ensure that the surface area of the more anodic metal is much larger than the area of the more cathodic metal.

7.3.7 Finishes

Finishing is an aspect of circulator design we do not want to overlook. Where dissimilar metals such as steel and aluminum are in contact with one another, it is important to plate one or both metals to make them compatible. Failure to do so results in galvanic action and erosion of one of the metals. Steel should not be left bare in any case because it rusts. Either zinc or cadmium plating can be used to protect the steel, although cadmium plating is not as widely used as it once was because of the toxicity of cadmium. Aluminum is frequently finished with a chemical-conversion coating such as iridite.

The outside finish on a circulator will depend on the severity of the environment. Finishes range from attractive plating such as chrome or nickel to epoxy coatings and paint.

7.4 Lumped-Constant Circulators

The mechanical design of lumped-element circulators differs from that of stripline junction circulators. The operating frequency range is usually lower; resonances are not normally a problem. The location of magnets relative to the ferrites is very similar to the junction circulator magnetic circuit, but in the lumped-element circulator there must be space for impedance-matching capacitors and inductors between the ferrites and the connectors. A typical lumped-element circulator housing is shown in Figure 7.19.

The type and size of matching circuit components will determine the amount of space needed in the housing and the method of access to the components for tuning. For low-power circulators, tuning can be accomplished using trimmer capacitors, which can be mounted so that adjustment is possible

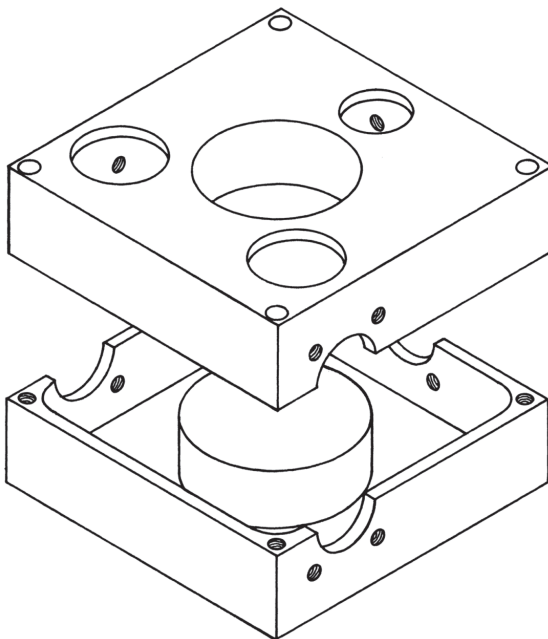


Figure 7.19 A typical lumped-element circulator housing.

without access holes. For higher-power circulators, it may be necessary to design access holes so that the matching circuit components can be adjusted without opening the circulator; this is necessary because the ferrite junction will behave in quite a different manner when the upper ground plane and magnet are removed.

After the component values for the impedance-matching circuits have been determined by evaluation of the ferrite junction itself and application of appropriate network synthesis methods, we proceed with the mechanical design of the inductors and capacitors. At low power levels, we can use off-the-shelf components. High power levels demand that we design our own components to ensure adequate electrical performance.

The first step in the inductor design procedure [16] is to compute the expected RF current. From this, we calculate the necessary wire diameter (in inches) using

$$d = \frac{I_{RF}(f)^{1/4}}{500} \quad (7.23)$$

where f is the frequency in megahertz and I_{RF} is the RF current in amperes. The suggested spacing between turns of the coil [16] is one wire diameter. Next, we compute the coil diameter (in inches) for optimum Q :

$$D = 8.9(Ld^2)^{1/3} \quad (7.24)$$

where L is the required inductance in microhenries. If the diameter is impractically large, we reduce the diameter to a practical value and calculate the number of turns:

$$N = \frac{40Ld}{D^2} + \left[\left(\frac{40Ld}{D^2} \right)^2 + \frac{18L}{D} \right]^{1/2} \quad (7.25)$$

Lead inductance and stray capacitance depend on how the coil and its leads are positioned, so it is best that coil adjustments to compensate for these factors be done experimentally. Large coils need to be supported. Teflon rods serve well as coil supports. If there is a danger that the coil or leads will short to each other or ground, Teflon tubing should be placed over the wire.

To design a capacitor, we first compute the RF voltage across the capacitor and then select a dielectric material and thickness that will safely stand off this voltage. Teflon is a good choice because of its high dielectric strength and

low loss factor. For a parallel-plate (or parallel-disk) capacitor, the capacitance is given by [10]

$$C = \frac{0.225\epsilon A}{t} \quad (\text{pF}) \quad (7.26)$$

where A and t are the plate area and dielectric thickness, in inches, respectively. A cylindrical-coaxial capacitor may have a more convenient shape than the parallel-plate capacitor. Its capacitance is [10]

$$C = \frac{0.614\epsilon}{\log_{10}(b/a)} \quad (\text{pF/inch}) \quad (7.27)$$

where b and a are the outer and inner diameters of the dielectric and ϵ is the relative permittivity of the dielectric.

Some lumped-element circulators use a series-resonant circuit from the common node of the three mutually coupled inductors wrapped around the ferrites to ground. In these circulators, the ferrites cannot be in direct contact with the ground planes and dielectric material must be placed in the gap. In low-power circulators, a soft material such as Teflon may be used, but for higher powers, the dielectric must be a good heat conductor in order to keep the ferrites cool. In this case, alumina and beryllia are good materials to use.

Many of the design concepts presented in Sections 7.1–7.3 for coaxial junction circulators, such as those for cooling, sealing, compression, and finishing, also apply to lumped-element circulator design. As mentioned previously, the primary differences lie in the operating frequency (parasitics are of less concern with regard to lumped circulators), space required for discrete capacitors and inductors in the lumped circulator, and provisions for tuning.

7.5 Waveguide Circulators

Two types of waveguide circulators have been presented in this book: the waveguide junction circulator and the differential phase shift circulator. Many of the concepts we discussed in Sections 7.1 and 7.3 with regard to coaxial junction circulators also apply to waveguide junction circulators. The waveguide versions are constructed using the channeled-plate or box-and-cover methods. For large (low-frequency) circulators, sections of waveguide may be welded or

brazed together to form a Y or star, because machining the circulator housing from solid blocks of metal would not be economical.

The remarks in Section 7.1 about web thickness and cooling are applicable here as well. An important difference in the mechanical design of waveguide junction circulators is in the quality of machining. If the waveguide is machined into a metal plate, as in the channeled-plate and box-and-cover constructions, the dimensions of the guide (depth and width) must be very accurate and meet the specifications for the particular waveguide size. The maximum allowable perpendicularity [17] deviation of the walls is typically 0.5° . Military specification MIL-DTL-85K states that the maximum allowable bow of the narrow wall is 0.00042 in/in and 0.00083 in/in for the broad wall. The waveguide cannot be twisted more than 0.083° per in of length. The inside surface roughness should be 32 microinches or better and any scratches present must not be more than 0.001 in deep. Circulators designed to be pressurized must be tightly sealed to prevent leakage. The mating surfaces of the waveguide flanges must be very smooth and flat, and the bolt holes should be the correct size and in the correct locations. The type of waveguide flange to be used should be included in the circulator specifications.

It is doubtful that the circulator performance would be severely degraded if we did not adhere to the preceding specifications. It is true, however, that the machining of waveguide circulators, especially those for high frequencies, is more critical than coaxial circulator housing machining.

The ferrites in a waveguide junction circulator are typically located as shown earlier in Figure 5.7. For geometries (b) and (c), we mount the ferrites to the waveguide wall using adhesive or solder. The adhesive is an epoxy; conductive epoxy will provide a good ground plane at the ferrite face. The ferrites can be metalized on one face and then soldered inside the waveguide. This provides a good thermal and electrical path if there are no air pockets in the solder. We can also hold the ferrites in place with nonmetallic clamps or screws if the thermal and electrical properties of the interface are not critical.

The mounting of the ferrite post in Figure 5.7(a) is somewhat simpler because the entire space between the waveguide walls is filled. If we apply pressure to the waveguide walls (webs) from the outside, the dielectric spacers and ferrite post are held in place without using solder or adhesive. If the circulator must withstand shock and vibration, some method of captivating the ferrite and dielectric is necessary.

The mechanical design of differential phase shift circulators includes the design of a magic tee and quadrature coupler and the design of differential phase shifters. Design data for couplers and tees are readily available elsewhere,

so we will not discuss their design here. Purchased tees and couplers could be used in the construction of differential phase shift circulators.

Mechanically, a differential phase shifter is little more than a section of waveguide with a ferrite slab or slabs inside and magnet outside. The external magnetic circuit, which may be just the magnet itself, is usually C-shaped, the ends of the C contacting the waveguide walls as shown earlier in Figure 2.16.

When the ferrite slab is positioned as previously shown in Figure 5.46, it can be held in place by filling the guide with a dielectric foam. Foams are available that have dielectric constants near unity, so they will not significantly affect the operation of the phaser. Sometimes dielectric slabs are placed alongside the ferrite slab; they help to hold it in place.

When the ferrite slabs are placed against the broad wall of the waveguide as shown in Figure 2.23, they are usually held in place with adhesive as used for waveguide junction circulators.

A final mechanical consideration of differential phase shift circulators is to make sure we check the dimensions and orientations of the tee, coupler, phasers, and dummy load (in the case of an isolator) to be sure all the components fit together properly.

7.6 Resonance Isolators

The mechanical design of waveguide resonance isolators is very similar to the design of differential phase shifters. Dielectric slabs are normally placed against the ferrite face nearest the center of the guide. The difference between the resonance isolator and the differential phaser is the magnetic operating point, the resonance isolator requiring a stronger magnetic field. In addition, reverse power is absorbed in the ferrite of a resonance isolator, so more consideration needs to be given to the cooling of the ferrite slabs, particularly at high power levels. The thermal analysis methods presented in Section 7.1 can be applied here.

Coaxial resonance isolators are constructed from straight sections of coaxial transmission line, which are not difficult to design. Perhaps the most difficult aspect of resonance isolator manufacture is the machining of the dielectric insert.

We do not present detailed design information for the coaxial resonance isolator here because the coaxial junction isolator is currently more popular and offers better electrical performance for most applications.

References

- [1] Scott, A. W., *Cooling of Electronic Equipment*, New York: John Wiley and Sons, 1974.
- [2] Schiffres, P., "How Much CW Power Can Stripline Handle?" *Microwaves*, June 1966, pp. 25–34.
- [3] Van Atta, C. M., *Vacuum Science and Engineering*, New York: McGraw-Hill, 1965.
- [4] Woode, A. D. and J. Petit, "Design Data for the Control of Multipactor Discharge in Spacecraft Microwave and RF Systems," *Microwave Journal*, January, 1992, pp. 142–155.
- [5] Pozar, D. M., *Microwave Engineering, Second Edition*, New York: John Wiley and Sons, 1998.
- [6] Howe, H., *Stripline Circuit Design*, Dedham, MA: Artech House, 1974.
- [7] Jensen, C., and J. Helsel, *Engineering Drawing and Design*, New York: McGraw-Hill, 1979.
- [8] Laverghetta, T. S., *Modern Microwave Measurements and Techniques*, Norwood, MA: Artech House, 1988.
- [9] Helszajn, J., *The Stripline Circulator: Theory and Practice*, Hoboken, NJ: John Wiley and Sons, 2008.
- [10] *Reference Data for Radio Engineers*, Indianapolis: Howard W. Sams, 1977.
- [11] Hui, H., and E. Yung, "Dyadic Green's Functions for the Inhomogeneous Cylindrical Waveguide and Cavity and their Applications," *Journal of Electromagnetic Waves and Applications*, Vol. 11, 1997, pp. 1121–1138.
- [12] Hutchings, J. L., J. R. Nortier, and D. A. T. Lambert, "Contour Program Smoothes Strip Discontinuities," *Microwaves and RF*, November 1987, pp. 129–138.
- [13] Matthaei, G. L., L. Young, and E. M. T. Jones, *Microwave Filters, Impedance-Matching Networks, and Coupling Structures*, Dedham, MA: Artech House, 1980.
- [14] Marcuvitz, N., *Waveguide Handbook*, New York: McGraw-Hill, 1951.
- [15] Military Standard MIL-STD-889B, July 1976.
- [16] Bostick, G., G. F. Kinnetz, and T. W. Parker, "Designing High-Power Series Inductors and Shunt Capacitors," *Microwaves and RF*, October 1987, pp. 97–107.
- [17] Military Specification MIL-DTL-85K, June 2011.

8

Assembly and Testing

8.1 Assembly Techniques

Before analysis and simulation tools and fast computers on which to run them were widely available, assembly and testing were a necessary part of the design process. Empirical optimization of the circulator design was nearly always required. Today, we still have to verify circulator performance after the circulator design work is finished, even if little or no design optimization is needed.

There are different philosophies regarding the circulator design process and what it should encompass. These depend on the size of the firm, the quantity of circulators to be produced, and to what extent production is to be automated. A very small firm, such as a garage shop or even one person making circulators, is likely to produce only small quantities of circulators and not have sufficient capitalization to handle production of large quantities of circulators. On the other hand, a very large firm, such as a Fortune Global 500 firm, is likely to seek opportunities to produce large quantities of circulators and avoid small orders. A small order could be for just one or two circulators, customized for a particular application. Large orders could be for tens of thousands or more circulators. Most circulator designs are produced only in relatively small quantities (< 1,000 circulators). Obviously, investment in automation for circulator assembly is not always justified, and sometimes the use of human labor is less expensive and more flexible than the use of automation.

A small firm producing small quantities of circulators will typically have just one designer, who uses a *sequential engineering* (SE) approach. Because only one person is involved in the design process, there is no parallel effort, and the designer is forced to perform one step after another. This is not to say

that the designer cannot consider other design aspects when working on one; these are just not parallel considerations by other people/departments. A large firm designing for production of a large quantity of circulators is more likely to use a multidisciplinary team, involving such functions as marketing and manufacturing with design engineering throughout the design process. Such an approach is called *concurrent engineering* (CE). CE is not new, and similar design philosophies have names such as *integrated cross-functional engineering* or *design for manufacturing* (DFM).

This book is about the design of circulators. The design process always includes testing of one or more circulators to verify or optimize the design. The circulator designer needs an understanding of the assembly process, either to do the assembly work or to instruct others how it should be done. We will leave writing a book about high-volume circulator manufacturing for another time, but CE/DFM require that we consider during the design process how the circulator will ultimately be assembled.

The assembly process, more than any other aspect of circulator design, involves hands-on work prior to testing to gather information about circulator performance. We will consider two distinct categories of assembly processes. One is for small quantities, for initial design verification and optimization, and sometimes also for delivery of circulators to a customer. The other category or extreme is for high-volume production of circulators. In this category, assembly work is not done for design purposes, although it could be for a *pilot production* or *low-rate initial production* (LRIP) run. However, this high-volume assembly process should be considered during the design process.

As with most microwave and RF components, circulators do not always perform exactly according to the design specifications. We must test circulator performance, compare test results with desired performance parameters, and in some cases redesign all or parts of the circulator to improve certain aspects.

Circulator assembly differs from general electronic assembly work in several ways. First, circulators are often very precisely machined. To maintain this precision, certain special assembly techniques or fixturing must be used. Sometimes the fixturing can be part of the circulator design itself. For example, features could be added to a housing to center the ferrites. Second, circulators use strong magnets that require care in handling and installation. Circulators, being RF components, differ substantially from dc and 60 Hz ac wiring with which most electronic assemblers are familiar.

Rather than present specific assembly techniques for each class of circulator, we will present general techniques, most of which apply to any given type of circulator. It will be obvious which techniques apply to the particular circulator class being assembled. For example, information on coaxial connector

assembly obviously does not apply to waveguide units, and bonding ferrites to waveguide walls obviously does not apply to coaxial units.

A good rule to follow in circulator assembly is to trust no one. Check individual circulator components carefully before assembly. Dimensions are typically very important. If the ground-plane spacing or ferrite thickness of a coaxial junction circulator are incorrect, the result could be fractured ferrites (ferrites, particularly large ones, are not cheap). If the pin depth of a coaxial connector is incorrect, expensive test equipment could be ruined when the circulator is connected. If the ferrite slabs in a waveguide circulator are not properly secured, they could work loose, degrading electrical performance and possibly causing failure of a very expensive RF power source. Checking individual parts to drawings does not necessarily guarantee that they are correct; the drawings could be wrong. It is best to check parts against each other as well as against drawings.

Anyone involved in circulator assembly or solving problems related to circulator assembly should know how to use precision measuring tools. The most commonly used tools are the caliper and the micrometer. Calipers are usually capable of inside, outside, and depth measurements; micrometers usually measure only one parameter, depth or outside dimension. For most work with circulators, resolution to 0.001 inch is sufficient, but at times we need to resolve to 0.0001 inch. Reading dial calipers and micrometers to one thousandth of an inch is fairly straightforward so long as the operator realizes that calipers are not a monkey wrench and a micrometer is not a C-clamp. With the advent of inexpensive digital measuring devices, dimensional measurements can be easy. However, we cannot overemphasize that skill in precision dimensional measurements is an important attribute of anyone involved in building circulators. Reading calipers or micrometers to high precision and reading vernier scales can be challenging.

We explain how to read a vernier scale with the aid of Figure 8.1. The vernier scale of a micrometer that is shown consists of 11 thin lines [1], scribed parallel to the sleeve long line, marked 0 through 10. When the thimble mark does not line up exactly with the sleeve long line, we examine the vernier scale to read the fraction of the thousandth increment on the thimble. One of the vernier lines will be aligned better with one of the thimble marks than all the others. The number corresponding to this vernier line is the number of ten-thousandths to be added to the thimble reading. The reading shown in Figure 8.1 is 0.1633 inch.

After the individual parts of the circulator are checked, they should be cleaned and dried if necessary. It is particularly important for the ferrites to be free of any coolant residue left over from the grinding operation. The ferrites

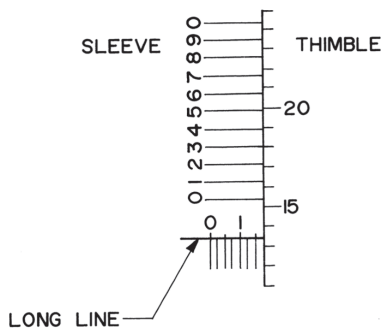


Figure 8.1 Reading a vernier scale.

can be washed in a volatile solvent and then baked to drive this solvent out of the pores and cracks.

Ferrite materials are easily confused with one another. Because the materials in bulk form are so similar in appearance, it is typically impossible to tell them apart by looking at them. Two relatively simple tests help us discriminate between materials if they become mixed up. We test the ferrite density and Curie temperature. Different ferrite materials are likely to have different densities or different Curie temperatures, so we can discriminate between the two if we know which is denser or which has a higher Curie temperature. In some cases, different ferrite materials will have similar or identical densities and Curie temperatures. In these cases, other testing would be required to discriminate between the two materials.

The density is determined by weighing a sample of the material in question and dividing the weight by its volume. The volume can be either calculated from the ferrite dimensions or taken as the volume of water the sample displaces.

We compare Curie temperatures by sticking samples of the two materials under investigation on a magnet and placing the magnet on the ceiling of an oven. We turn on the oven (high temperature) and wait for the oven to warm up. When we hear a ferrite drop from the magnet, we know that the ferrite still on the magnet probably has a higher Curie temperature. Not all ferrites can be compared using this method because most ovens do not reach high enough temperatures to accommodate ferrites having high Curie temperatures. If the ferrite that falls breaks into a hundred pieces and is the only one of its type and the one you needed, you did something wrong.

The next step in the assembly procedure is to mount the ferrites. Particularly for volume production, in some cases, ferrites are metalized using either a thin-film or thick-film process, and soldered in place or bonded with

conductive epoxy. We make an effort to eliminate air pockets between the ferrite and ground plane or waveguide wall. The quantity of solder or epoxy should be sufficient to form a good bond, without oozing onto the ferrite edges.

In coaxial junction circulators being assembled for initial design verification or for a very small quantity production run, the ferrites can be temporarily held in place (until final assembly, when compression will hold the ferrites) using silicone grease or petroleum jelly. A very thin coating is all that is necessary; use only enough grease to maintain ferrite position temporarily. The grease tends to fill any air pockets that may be present on the ferrite surface, improving thermal conductivity and RF ground contact. Because the quantity of grease used is so small, it does not significantly affect electrical performance. When the ferrites are firmly held in place, it is not necessary to use assembly grease. The ferrites must be properly positioned, usually centered over a magnet well. In addition, the ferrites should be in registration with each other. Figure 8.2 illustrates ferrite centering. Ferrites may be automatically centered by mechanical means, such as housing features or, when the circulator will be produced in large quantities, an assembly fixture. Ferrites usually need to be centered within a few thousandths of an inch to ensure good electrical performance in the microwave frequency range. We offer no proof for this figure. When only small quantities of circulators are assembled, ferrites can be centered visually. Most people can see that something is off center a few thousandths on the scale of a typical circulator.

To improve electrical contact between the ferrite faces and ground planes in small quantities of circulators that do not utilize metalized ferrites or ferrites bonded to the ground planes, we can treat the ferrites with aluminum or other conductive metallic foil. A thin coating of adhesive or grease is applied to the ferrite face. Then we spread a piece of foil on the ferrite face nearest the ground plane. The foil must be free of wrinkles and air pockets. The electrical contact is improved in many cases because the ground plane may not be perfectly smooth, but the foil bridges any valleys that exist in the

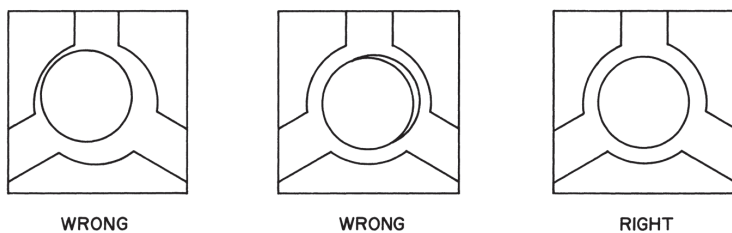


Figure 8.2 Ferrite centering.

ground plane surface. The foil does not significantly affect the ground-plane spacing because most foils are much less than 0.001 inch thick.

After the ferrites are installed, we proceed to install the connectors of a coaxial circulator. There are usually no other internal components of a waveguide circulator, with the possible exception of dielectric slabs. In the case of the lumped-element circulator, the ferrites are not installed until after the web-like center conductor has been wrapped around them. The coaxial connectors should be attached to the bottom half (the half with the threaded holes for holding the housing halves together) so that they will stay with this half when the top half or cover is removed. If the connectors and center conductor (which is usually soldered to the connectors) stay with the top half when the circulator is disassembled, it is more likely that the ferrites will move around if they are not captivated by housing features or fixturing. In addition, we usually want to look at the center conductor when the circulator is disassembled, as the reason for disassembly is for tuning purposes. The top cover or half is defined as the part with the clearance holes for the assembly screws because it makes more sense to work with the circulator when it is positioned with the screw heads on top for easy access. Figure 8.3 illustrates a partially assembled coaxial junction circulator.

Coaxial connectors with uncaptivated center pins are often used for circulators because they save the space normally occupied by the captivation mechanism. When the circulator is assembled, the center conductor is soldered to the connector center pin, providing the means of captivation.

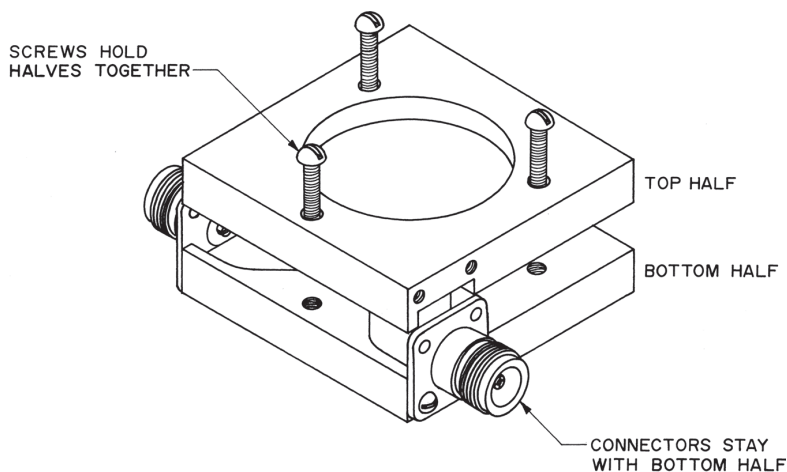


Figure 8.3 Partially assembled coaxial junction circulator.

Where the circulator center conductor provides the means of captivation, a strong mechanical joint must be made between connector pin and center conductor. We make this joint by brazing, silver soldering, or conventional soldering, in order of decreasing strength [2]. Before and after we make the connection, we must be sure the connector pin depth is correct. We can do this most accurately using a connector gauge. We can also measure the pin alignment with conventional measuring tools. A simple method of holding the connector pins at the correct depth during the soldering process is to mate the connector with another connector that will hold the center pin in alignment and at the correct depth. Special connector fixtures could also be used. Dimensions for connector pins are available from connector manufacturers and various reference books [3].

The next step in the circulator assembly process is temporarily closing the housing. We do not permanently close the circulator at this point because we may have to open the unit later to perform mechanical modifications for tuning or perform other tuning operations. At low frequencies, it is not necessary to install all of the screws that secure the coaxial connectors. The circulator can be electrically tested with missing connector screws. At higher frequencies it is necessary to install most or all of the connector screws to avoid degradation of electrical performance due to poor grounding of the connectors.

Unless the magnets will be charged during circulator tuning, we need to start with oriented (magnetized; charged) magnets. The magnets can be either purchased already magnetized or magnetized just before installation. Several types of magnet chargers are available. One of these is the capacitive-discharge magnetizer. This device utilizes capacitors that are charged to a specific voltage depending on the magnetizing force required. To charge the magnet, the capacitors are connected, usually via a silicon-controlled rectifier (SCR), to a low-resistance electromagnet. The magnet is placed in a magnetic circuit with the electromagnet so that the current pulse and resulting magnetic pulse charges the magnet. Another type of charger operates by rectifying the ac line voltage and applying the resulting dc pulses to the charging electromagnet. The amount of magnetizing force depends on which portion of the ac line half cycle is applied to the electromagnet; this is also done with SCRs.

After we charge the magnets, we thermally stabilize them if they are to be used in a circulator with a broad operating temperature range. The stabilization may follow the tuning of the circulator if magnetic field adjustment is used as a tuning adjustment. Magnets experience an irreversible loss of magnetic field when they are exposed to a temperature cycle [4]. We can thermally stabilize the magnets by cycling them several times between temperature extremes equal to or greater than the specified temperature range for the circulator.

Where both operating and storage temperature ranges are specified, the storage range is usually more severe and should be used for cycling the magnets. The magnets should not be recharged after temperature cycling because this would defeat the purpose of thermal stabilization.

The pole pieces and magnets should be temporarily installed in the circulator. The magnets may have to be removed for adjustment by partial demagnetization unless equipment is available that will enable the magnets to be calibrated (adjusted) while they are installed in the magnetic circuit. It is best, especially with regard to circulators that are engineering development models, not to install the magnetic shields until the circulator is nearly completed. If the shields are not present, the magnetic field intensity can be experimentally adjusted by either holding other magnets near the magnets in the circulator or placing pieces of steel against the magnets to increase the magnetic field.

8.2 Testing

8.2.1 Finding the Operating Point

After the preliminary assembly of the circulator is complete, we proceed to find the operating point. By this, we mean we adjust the magnetic field intensity until no further improvement in electrical performance can be obtained. The best electrical performance may not be obtained at the correct operating frequency of the circulator, and it may not meet the specifications. Nevertheless, magnetic adjustment is a good starting point for several reasons.

First, it is difficult for the beginner to design a magnetic circuit accurately so that no adjustments are required because there may be empirical factors due to leakage flux, as we discussed in Section 6.1. Second, magnetic adjustment is easy. To determine in which direction the adjustment must be made, we can simply hold a magnet near the circulator in either a bucking or aiding orientation. Bucking refers to the orientation that reduces the magnetic field supplied by the internal circulator magnetic circuit, and aiding is the orientation that increases the field. Magnetic adjustments made by demagnetizing or magnetizing the circulator magnets are not permanent—we can always recharge the magnet one more time. Electrical adjustments made by mechanical modifications are not so easily undone. Finally, changes in magnetic field typically have a profound effect on circulator performance compared to small changes in impedance-matching circuit component values, which are not so easily changed in many cases.

We start by connecting the circulator to a calibrated circulator test setup. Many different test setups are used in the industry, ranging from antique signal generators and slotted lines (not so common anymore) to automatic vector network analyzers. A typical test installation was previously depicted in Figure 2.3.

Scalar measurement techniques (techniques that do not include phase measurements) can be used to test most circulators; however, phase information can be quite useful for determining how electrical adjustments should be made. For this reason, it is advisable to use test equipment that will provide complex transmission and reflection information, if at all possible. To test differential phase shift sections that will be part of differential phase shift circulators, the transmission phase shift information is a necessity.

The most important electrical parameter to monitor as we adjust the magnetic field is the insertion loss. Insertion loss tells us not only about magnetic losses in the circulator, but also about the VSWR. If the VSWR were high, then the insertion loss would be impacted by the mismatch loss. The phase shift is also important for differential phase shifters. If the magnetic field is not correct, the insertion loss will be high over all or part of the circulator operating frequency range. Below resonance (in the magnetic domain, not the frequency domain), insufficient magnetic field leads to unsaturated ferrite and low-field losses. If the magnetic field intensity is set too high, resonance losses will occur. For resonance isolators, the magnetic field must be set at resonance. At resonance, the insertion loss of the isolator is at a minimum and the isolation (reverse loss) is maximal. Above resonance, insufficient magnetic field intensity leads to resonance losses. Excessive magnetic field reduces κ/μ —see (5.48)—hence the splitting between the two counter-rotating modes, reducing the circulator bandwidth and increasing insertion loss at the band edges. Figure 8.4 shows insertion-loss frequency-response curves for above- and below-resonance circulators with incorrect magnetic field intensities.

Our goal in finding the operating point is to adjust the magnetic field intensity until no further improvement in electrical performance can be obtained. Most circulators require only that we minimize the insertion loss over the operating frequency range. We do not need to make permanent changes to the magnetic circuit yet, because we will very likely have to readjust the magnetic bias later on, after we have performed some electrical adjustments.

Unless reference magnets or some other means of measuring magnetic field polarity are on hand, we will not know in which direction the circulator is circulating. It is important to remember that the magnetic field polarities for above- and below-resonance circulators are opposite for a given circulation direction. We must determine the direction of circulation before we can

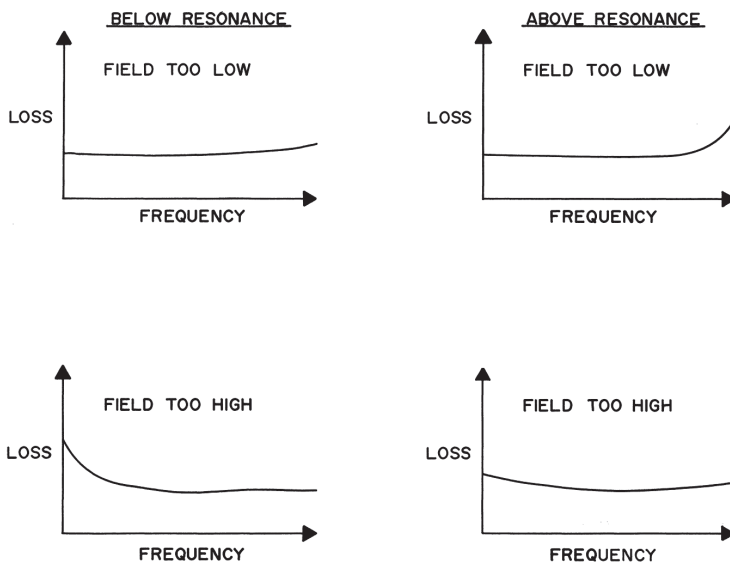


Figure 8.4 Frequency-response curves for circulators with incorrect magnetic field.

monitor the insertion loss. This is easily done by trial and error. We know from our magnetic circuit design computations approximately how much magnetic field will be needed to bias the ferrites. If we start with this level of magnetic field, the circulator will probably have higher insertion loss in one direction than in the other. The direction that has lower loss should be taken as the forward (insertion loss) direction. If we have specified a particular port as the circulator or isolator input, we have a 50-50 chance of installing the magnets correctly the first time. We will surely get it right the second time.

We need not be concerned if the insertion loss does not meet specification after preliminary magnetic adjustments are made. If the insertion loss is high because the VSWR is high (mismatch loss), we may be able to bring the insertion loss within specification by making some electrical adjustments. If the VSWR is within specification but the loss is too high, it may be that our operating point is not exactly right. We may have to change the magnetic field intensity and then electrically tune the circulator. Both of these situations and others will be discussed in more detail in Chapter 9.

We can make the temporary magnetic field adjustments described in this section by stacking up magnets of various sizes and shapes on top of the circulator magnets. Small magnets make small changes in the magnetic field and large magnets make large changes (assuming all the magnets are made of the same material and are charged to the same degree). The magnets can

either aid or buck the circulator magnets. We can reduce the magnetic field by placing more pole pieces or spacers between the circulator magnets and pole pieces. The field can be increased by small amounts using pieces of steel or iron placed in contact with the magnets.

8.2.2 Taking Data

Because circulator design is typically an iterative process involving prediction and experimentation, data collection and manipulation form a very important aspect of any circulator design algorithm. It would be absurd to synthesize a circulator on paper, build it, and install it in a system without ever checking the performance of the unit. We must be able to measure the electrical parameters of the circulator and record them for future use in an intelligent manner.

Several terms describe various qualities of measurement systems [5]. Perhaps the most important is accuracy. Accuracy is the deviation of a reading from a known input. We should know the accuracy of our test equipment, because the accuracy of the data and the quality of the circulator depend on it. Precision is the ability of an instrument to reproduce a certain reading with a given accuracy. Precision does not imply accuracy; an instrument may display five digits but have an accuracy of $\pm 1\%$. In this case, three of the five digits displayed may not be correct. It is of no help to record five digits if we are certain that three of them may be wrong unless we are only comparing measurements made using the same instrument. Engineers often speak of measurement uncertainty. The uncertainty of a measurement is the plus-minus range of the instrument accuracy.

Calibration of test equipment is important to ensure accuracy. Most facilities have calibration procedures that are used to maintain instrument accuracy. Instruments are checked against either a primary or secondary standard on a regular basis. A primary standard might be (in the United States) one at the National Institute of Standards and Technology (NIST) and a secondary standard could be an instrument similar to the one being calibrated but of known accuracy. Most calibrated test equipment has accuracy somehow traceable to NIST.

Circulator isolation and insertion loss are normally measured in decibels. Reflection can be expressed in terms of voltage reflection coefficient, return loss, or VSWR. Equations (2.4) and (2.5) are useful for performing conversions between these units.

Electronic S-parameter files or a bound notebook should be maintained to record circulator performance data. It will be necessary to look at the data when we decide how to make electrical and magnetic adjustments. Test data

are often sent along with circulators if they are shipped. If anything unusual or significant is observed during the circulator development, this information could be used later on for other circulators or could become part of a patent application.

Most modern microwave test equipment is capable of storing test data in electronic format or producing test reports of one kind or another. If such equipment is not available, the test results are recorded by hand. Whether the data are recorded in tabular or graphical format, enough points should be used to describe adequately the shape of the circulator frequency response. It is often helpful to take data over a broader range of frequencies than the circulator's operating frequency range. Broadband data may provide additional clues as to how to tune the circulator.

8.2.3 RF Power Testing

Circulators destined for high-power applications should have their transmission (insertion loss and isolation) and reflection (VSWR or return loss) characteristics measured using a test installation such as the one in Figure 8.5 [3]. Incident and reflected power at one circulator port and transmitted power to another port can be measured with this setup. Depending on the circulator and power level, it may be necessary to provide some form of cooling to the circulator.

Calibration of the test setup includes accurate measurement of the coupling and insertion loss values for the directional couplers and attenuation values of the attenuators. These must be measured at each test frequency. From these measured calibration factors, we can determine offsets for the power meters so that we can accurately measure RF power. In addition, a through connection could be used to calibrate for insertion loss measurement of the circulator under test.

8.2.4 Intermodulation Testing

IEC 62037 [6] describes intermodulation (IM) level testing of passive microwave devices, including circulators. Figure 8.6 shows the block diagram of a typical circulator IM test installation. When the two test frequencies are spaced far apart, the combiner can take the form of a filter diplexer, and the notch filters could be replaced with a filter of lower complexity. More commonly, the frequencies are closely spaced, so a hybrid coupler, such as a quadrature hybrid, is used as the combiner. If the signals at the power amplifier outputs have significant harmonic content, low-pass filters may be needed to reject the

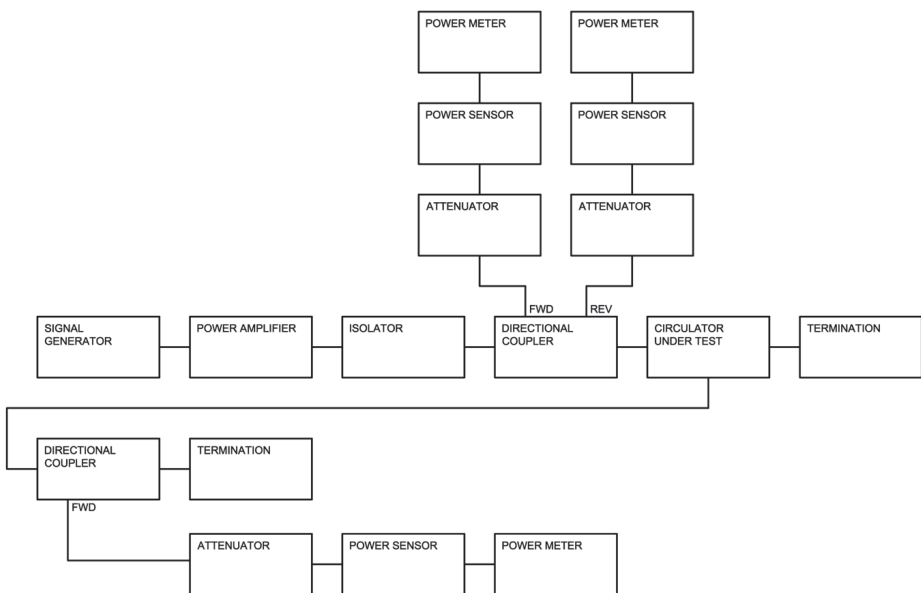


Figure 8.5 Typical circulator power test installation.

harmonic energy. The isolators help prevent IM in the amplifiers and ideally should have better IM performance than the circulator under test. Terminations that are constructed using film resistive elements often have poor IM performance, so linear terminations must be used. These can be implemented as long sections of coaxial cable, terminated at the far ends. To prevent IM in the LNA or receiver, the notch filters are used to reject the two test frequencies. Depending on the expected level of IM products and the noise figure of the receiver, the LNA may not be required.

The test installation in Figure 8.6 is for *forward* IM testing. With some setup configuration changes, the same equipment could be used for reverse testing.

8.2.5 Multipaction Testing

ECSS-E-20-01A [7] provides multipaction test methods, as well as other multipaction engineering information. Figure 8.7 shows a relatively simple test installation for detection of noise that is close in frequency to the carrier. The noise would result from multipaction activity in the circulator under test.

Two other methods of multipaction detection that are applicable to circulators are the return loss and harmonic ones. Very small changes in return

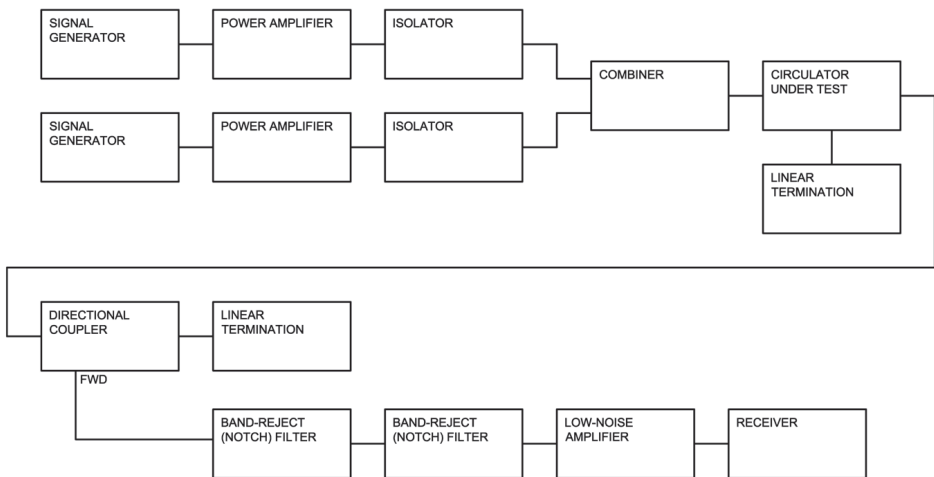


Figure 8.6 Typical circulator intermodulation test installation.

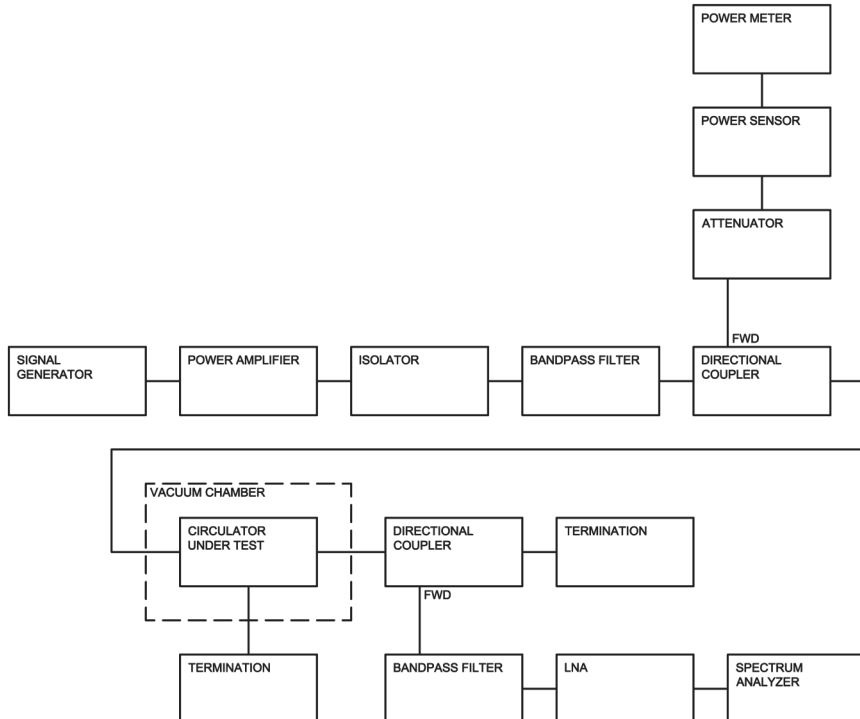


Figure 8.7 Multipaction test installation for detection of close-in noise.

loss may be evidence of multipaction. These changes are detected by nulling a sample of the incident power to the circulator under test with a sample of the reflected power. The null is maintained during testing using a variable attenuator and variable phase shifter, and monitored using a spectrum analyzer. The spectrum analyzer displays any fast changes in return loss.

Multipaction activity generates harmonics, which can be detected and provide evidence of multipaction. Typically the third harmonic of the test signal is monitored, and any fast increases in third-harmonic level may be indicative of multipaction.

Electron seeding should be used during multipaction testing to ensure an adequate supply of free electrons. Radioactive sources (beta emitters), such as Strontium-90 or Cesium-137 are versatile electron sources. The electrons from these sources have sufficient energy to penetrate metal circulator housings, provided that the metal is not too thick.

8.2.6 Magnetic Moment Measurement

There are several ways to measure the magnetic moment of a circulator, depending on the precision required and the availability of equipment. Magnetic moment can be estimated without any special equipment simply by suspending the circulator to be tested with its magnetic poles aligned with Earth's field. The circulator is set into oscillation about Earth's field, and then from the period of oscillation, the circulator's mass moment of inertia, and the magnitude of Earth's field, the magnetic moment of the circulator can be calculated. Imagine what people would think when they would see you watching a suspended circulator twist!

Although some spacecraft use magnetic devices that interact with Earth's field to maintain spacecraft attitude, Earth's field is not constant; it is slowly changing. In 2011, the primary airport runway designation in Tampa, Florida, was changed from 18R/36L to 19R/1L because of movement of the magnetic North pole.

To make a more precise magnetic moment measurement, we measure magnetic flux density at a distance from the circulator, along its magnetic axis, and then calculate [8]

$$M = \frac{4\pi}{\mu_0} \cdot \frac{1}{\frac{R - \frac{1}{2}}{\left(R^2 - RL + \frac{L^2}{4}\right)^{3/2}} - \frac{R + \frac{1}{2}}{\left(R^2 + RL + \frac{L^2}{4}\right)^{3/2}}} \cdot B \quad (8.1)$$

In this equation, $\mu_0 = 4\pi \times 10^{-7}$ H/m is the permeability of free space, R is the distance in m from the center of the circulator magnetic circuit to the point at which the magnetic flux density is measured, L is the length of the circulator magnetic circuit along its magnetic axis in m, and B is the measured flux density in T. M is the magnetic moment in units of A·m².

To obtain an accurate result, R must be large enough, preferably $R \geq 10L$, yet not so large that it is difficult to distinguish the measured flux density from background flux or instrument noise. It is advisable to calculate M from B values measured at increasing distances from the circulator until M does not change significantly from one point to the next. To cancel the effect of Earth's field on measurements, invert the circulator and repeat the measurements. Then average together the measured values of B for the two polarities.

In cases where high accuracy is not needed and $R \gg L$, (8.1) can be approximated by [9]

$$M = 5 \times 10^6 \cdot B \cdot R^3 \quad (8.2)$$

8.2.7 Measurement Uncertainty and Gauge Studies

Modern vector network analyzers have built-in error correction, referred to as 12-term error correction. Network analyzer manufacturers publish information regarding the measurement uncertainty of the instruments. Agilent and Anritsu offer uncertainty calculators [10, 11] that can be downloaded from the Internet and used to determine measurement uncertainty.

For test installations that do not incorporate mathematical error correction, such as the one in Figure 8.5, we estimate the uncertainty in measured voltage reflection coefficient using [12]

$$\Delta\rho = A + B\rho + C\rho^2 \quad (8.3)$$

where A is the directivity of the directional coupler used to make the reflection measurement, expressed in voltage coefficient:

$$A = 10^{(\text{Directivity in dB}/-20)} \quad (8.4)$$

$B = 0$ if an open/short calibration technique is used. If an open/short calibration technique is not used, then $B = A + C$. The measured voltage reflection coefficient is designated by ρ :

$$\rho = \frac{VSWR - 1}{VSWR + 1} = 10^{(\text{Return Loss in dB}/-20)} \quad (8.5)$$

C , a source match term, is given by

$$C = \rho_D - \tau_D A \quad (8.6)$$

where ρ_D is the reflection coefficient of the main line of the directional coupler, which we can compute using (8.5), and τ_D is the transmission coefficient of the main line of the directional coupler:

$$\tau_D = 10^{(\text{Insertion Loss in dB}/-20)} \quad (8.7)$$

The uncertainty in measured voltage *transmission* coefficient due to mismatches is [12]

$$\Delta\tau = \frac{1 \pm \rho_S \rho_L}{(1 \pm \rho_S \rho_C)(1 \pm \rho_C \rho_L) \pm (\rho_S \tau_F \tau_R \rho_L)} \quad (8.8)$$

where ρ_S and ρ_L are the source and load reflection coefficients of the test equipment, and ρ_C is the reflection coefficient of the circulator under test, which is assumed to be the same at all ports. τ_F and τ_R are the voltage transmission coefficients of the circulator under test, in the forward and reverse directions, respectively.

The uncertainty in measured transmission coefficient due to directivity of the directional coupler is [13]

$$\Delta\tau = \rho \cdot A \quad (8.9)$$

The preceding uncertainty equations do not include the effects of drift or harmonic energy in the test signal. Sometimes it is necessary to include a low-pass filter in test installations to remove harmonic signals. The effects of drift should be understood, and can be minimized by allowing equipment to warm up and stabilize before making measurements. It is also important to control the ambient temperature to avoid drift.

We use gauge studies, also known as repeatability and reproducibility (R & R) studies, to evaluate the variability in measurements. Gauge studies typically evaluate the following:

1. Repeatability: variation in measurements made by the same person, using the same equipment, under the same conditions, of the same circulator.

2. Reproducibility: variation in measurements of the same circulator attributable to changes in personnel, equipment, or other conditions.
3. Stability: variation in measurements caused by time.

To determine the repeatability, reproducibility, and stability of measurements, we design an experiment that involves measurements of one or several similar circulators by two or more test technicians, using two or more test installations. This could be a full-factorial experiment or a reduced matrix.

After the trials are performed, we analyze the data using statistical techniques, including *analysis of variance* (ANOVA), to quantify the measurement variations. Then, armed with a better understanding of the source of the variations, we may take action to reduce measurement variation and uncertainty.

References

- [1] Stockel, M. W., *Auto Service and Repair*, South Holland, IL: Goodheart-Willcox, 1969.
- [2] Jensen, C., and J. Helsel, *Engineering Drawing and Design*, New York: McGraw-Hill, 1979.
- [3] Laverghetta, T. S., *Modern Microwave Measurements and Techniques*, Norwood, MA: Artech House, 1988.
- [4] *Factors Affecting Magnet Stability*, Valparaiso, IN: Indiana General, 1978.
- [5] Holman, J. P., *Experimental Methods for Engineers*, New York: McGraw-Hill, 1984.
- [6] IEC 62037, *International Standard for Passive RF and Microwave Devices, Intermodulation Level Measurement*, Edition 1.0, Geneva, Switzerland: International Electrotechnical Commission, May 2012.
- [7] “Space Engineering: Multipaction Design and Test,” *European Cooperation for Space Standardization ECSS-E-20-01A revision 1*, March 1, 2013.
- [8] Lee, J., A. Ng, and R. Jobanputra, “On Determining Dipole Moments of a Magnetic Torquer Rod—Experiments and Discussions,” *Canadian Aeronautics and Space Journal*, March 2002.
- [9] *Magnetic Moment Easy Measurement, Application Note NAS01-i*, Serviciencia, October 2003.
- [10] *Downloadable Vector Network Analyzer Uncertainty Calculator*, Agilent Technologies, <http://www.home.agilent.com/agilent/software.jspx?ckey=1000000418%3Aepsg%3Asud&cc=US&lc=eng>. Last accessed Nov. 14, 2013.
- [11] *VNA Measurement Uncertainty*, Anritsu, <http://www.anritsu.com/en-US/Downloads/Software/Drivers-Software-Downloads/DWL8125.aspx>. Last accessed Nov. 14, 2013.

- [12] *High Frequency Swept Measurements, Application Note 183*, Hewlett Packard, December 1978.
- [13] Norton, J., "Directional Power Measurements and the Effects of Directivity," Bird Electronics, March 2005.

9

Tuning

9.1 Interaction Between Magnetic and Electrical Adjustments

To tune a circulator properly, especially a model that has not been built before, we must alternate between magnetic and electrical adjustments. The process usually begins with preliminary magnetic adjustment as described in Chapter 8. The reason for alternating between magnetic and electrical adjustments is that we want to see the results of each to determine whether an improvement in circulator performance has been made. In addition, it is difficult for one person to make both adjustments at the same time.

The last section of this chapter describes the use of *eigenvalues* to evaluate the electrical performance of circulators. Eigenvalue analysis is another tool in our arsenal that, when used in conjunction with measured S-parameter data, can provide additional circulator tuning insight.

9.2 Magnetic Adjustment

If we assume the dc magnetic field applied to the ferrites is uniform, as it should be if the pole pieces are of sufficient thickness and area, the only magnetic adjustment we need to make is to the magnitude of the field. If the circulator is to operate over a broad temperature range or have special magnetic shielding, there may be more tuning involved, but these cases are special. In this

section we present information about how changes in the magnitude of the dc magnetic field affect circulator performance.

Our goal in tuning a circulator is to obtain the necessary bandwidth and minimize insertion loss. We will now consider what effects changes in magnetic field have on these parameters.

9.2.1 Above-Resonance Magnetic Adjustment

For the above-resonance mode, the splitting factor is approximately given by (5.48).

From (5.15), we know that the circulator bandwidth is proportional to the splitting factor. Hence, the bandwidth (by inspection of (5.48)) is roughly inversely proportional to the square of the internal magnetic field:

$$\%BW \propto \frac{1}{H_{dc}^2} \quad (9.1)$$

The bandwidth increases dramatically with decreases in magnetic field.

The calculation of insertion loss as a function of applied magnetic field is rather involved, but can be carried out as described in Section 5.1 from Chapter 5. We can more easily see the effect of changes in magnetic field by examining Figure 5.10. The insertion loss climbs rapidly as we decrease the magnetic field, approaching resonance.

Generally, the best magnetic adjustment for the above-resonance circulator is found as follows. We set the field low enough so that the insertion loss just meets specification at the highest frequency in the band, considering mismatch loss. This will give us the broadest possible bandwidth without sacrificing insertion loss, simplifying the impedance-matching process. Sometimes, for reasons of temperature stability, we choose to use a higher magnetic field intensity. This increases the degree of impedance-matching difficulty and, perhaps, circuit complexity.

Circulators exhibit mismatch losses due to both the input and output VSWRs. Mismatch loss is given by

$$\text{Mismatch Loss (dB)} = -10 \cdot \log_{10}(1 - \rho^2) \quad (9.2)$$

where ρ can be computed from VSWR using (2.4). The two mismatch losses should be added together, assuming that the circulator has reasonably good isolation. The true circulator insertion loss, in a matched condition, is

approximately equal to the measured loss minus the sum of the input and output mismatch losses.

The reason circulators have mismatch losses at both input and output, rather than one mismatch loss as for most low-loss linear components, is that any power reflected from the output port is absorbed in the termination at the third port. In a reciprocal component, the power reflected from the output mismatch would be transmitted in the reverse direction back to the input (with low loss), where it would combine with the power reflected from the input to form a net reflected power that is probably less than the sum of the two reflected signals. This concept is illustrated in Figure 9.1.

9.2.2 Below-Resonance Magnetic Adjustment

For the below-resonance mode, the magnetic field adjustment is not as critical as that for the above-resonance mode. The splitting factor and bandwidth are much more dependent on the ferrite saturation magnetization, as we discussed in Chapter 5. An increase in magnetic field does, however, increase the bandwidth somewhat [1].

The magnetic field intensity must be sufficient to saturate the ferrite material to avoid low-field losses. It is unlikely that the field will ever be so strong that resonance losses occur at the center frequency, because, given the bandwidth of most below-resonance circulators, this would require a field of large magnitude at the frequencies where below-resonance circulators normally operate.

9.2.3 Magnet Charging, Calibration, and Stabilization

As described in Chapter 8, magnets will generally be charged and installed in the circulator as part of the assembly process. Then, some preliminary magnetic adjustment may be performed during initial electrical testing. Our objective

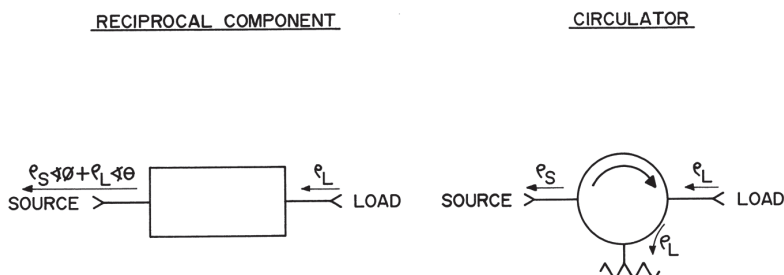


Figure 9.1 Circulator mismatch losses.

in the tuning process, covered in this chapter, is to adjust the magnetic field in conjunction with electrical adjustments to optimize circulator electrical performance.

Magnets can be procured already magnetized, magnetized just before installation, or magnetized after installation in the circulator magnetic circuit. To obtain maximum magnetic field from a magnet, it should be charged in its circuit. This is of particular importance for magnets that have low coercivity, such as Alnico magnets.

As described in Chapter 8, several types of magnet chargers are available. The most common type used for circulator manufacturing is the capacitive-discharge magnetizer. This device utilizes capacitors that are charged to a specific voltage depending on the magnetizing force required. To charge the magnet, the capacitors are connected, usually via a silicon-controlled rectifier (SCR), to a low-resistance electromagnet. The magnet is placed in a magnetic circuit with the electromagnet so that the current pulse and resulting magnetic pulse charges the magnet.

Magnet calibration refers to adjusting the magnetic intensity, or *strength* of the magnet to a specific, lower level than the fully oriented state [2]. This can be accomplished in one or more of several ways:

1. Magnet degaussing (demagnetizing) equipment to calibrate or *treat* the magnets. The equipment may be the same equipment, or equipment of the same type used to charge the magnets initially, or ac demagnetizing equipment may be used. Magnets could be calibrated by removing them from the circulator, demagnetizing them to the desired level, and then re-installing them in the circulator. Alternatively, the entire circulator could be placed in a demagnetizing coil, or an intermediate iron bar (core) can be used to magnetically couple the demagnetizing coil to the circulator.
2. Temperature exposures. The circulator, or the magnets separate from the circulator, can be temperature cycled or exposed to only high temperature to partially demagnetize the magnets. The temperatures used will depend on the expected future circulator environmental exposures and the susceptibility of the particular magnet material to temperatures.
3. Addition of magnetic shunts or removal of magnetic returns. Shunts can be placed on magnet edges to effectively short circuit some magnetic flux, reducing the magnetic field provided to the ferrites. To increase the magnetic intensity in the ferrites, additional magnetic returns can be added to the magnetic circuit.

4. Elapsed time. Depending on the magnet material and the calibration method, elapsed time may have an effect on the ultimate magnetic intensity. This is usually not highly predictable, so other methods of magnet calibration should be used if possible.

Calibration (partial demagnetization) of magnets not only serves to set the magnetic field to the desired level, but also stabilizes the magnets, making them less susceptible to future temperature variations and external magnetic field exposures. If the circulator is destined for use in an application having a broad operating or storage temperature range, additional magnetic stabilization is required. Magnets experience an irreversible loss of magnetic field when they are exposed to a temperature cycle [3]. We can thermally stabilize the magnets by cycling them several times between temperature extremes equal to or greater than the worst-case specified temperature range for the circulator. Where both operating and storage temperature ranges are specified, the storage range is usually more severe and should be used for cycling the magnets.

Because stabilization temperature cycling often reduces the magnetic field, it is necessary to compensate for this effect by leaving the magnetic field a little high during magnet calibration. Several iterations of magnet calibration and stabilization may be required to optimize the process, after which multiple iterations should not be necessary unless design or materials changes are made. A question frequently comes up after the magnet stabilization process: “The magnetic field is a little low. Can I just add a little field and not re-stabilize the magnets?” The answer to this question is “No.” Re-magnetization, whether it is partial or full, affects magnet stability, so the stabilization process must be repeated. Also, if the starting point of the magnet calibration and stabilization processes does not include fully magnetized magnets, then the magnetic intensity level and stability results will be different.

9.3 Electrical Adjustment

The electrical parameters with which we are concerned during tuning are the frequency, bandwidth, insertion loss, isolation, and VSWR. The isolation of a circulator is dependent on the return loss of the isolated port as described in Chapter 2, so we need to look only at the frequency, bandwidth, insertion loss, and VSWR or return loss at all ports.

Tuning a circulator is largely an impedance-matching problem. For a given reactive load, there exists a theoretical limitation on broadband impedance matching. Let us consider Figure 9.2. The lossless impedance-matching

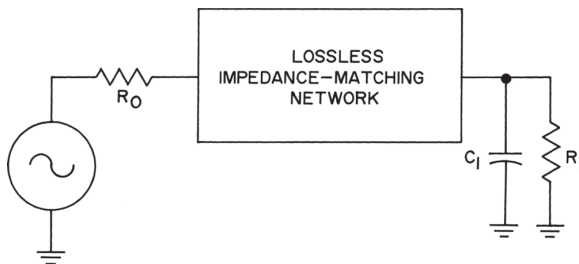


Figure 9.2 Impedance matching of a reactive load.

network is used to match the load, R_1 and C_1 , to the source resistance, R_0 , for maximum power transfer. Bode [4] showed what the impedance-matching limitations were, and Fano [5] later presented more general limitations on the matching of any load.

The equivalent circuit of a circulator junction is typically a parallel-resonant circuit, so the load in Figure 9.2 nicely represents the circulator junction on one side of resonance. The capacitor C_1 could be replaced by an inductance and the same analysis used by duality.

The best possible impedance match is achieved when [6]

$$\int_0^\infty \ln \left| \frac{1}{\rho} \right| d\omega = \frac{\pi}{R_1 C_1} \quad (9.3)$$

where ρ is the voltage reflection coefficient looking into the source side of the impedance-matching network. For the best impedance match in the circulator operating frequency range, we want the reflection coefficient to be equal to unity for all frequencies outside this range. Under this condition, we write

$$\int_{\omega_1}^{\omega_2} \ln \left| \frac{1}{\rho} \right| d\omega = \frac{\pi}{R_1 C_1} \quad (9.4)$$

where ω_1 and ω_2 are the edges of the circulator frequency range. If ρ is constant across the frequency band, we can readily evaluate the integral in (9.4) and write

$$\rho = e^{-\pi/(\omega_2 - \omega_1) R_1 C_1} \quad (9.5)$$

We can see from the preceding equations that we will achieve the best impedance match if the frequency response of the circulator has the shape

of a bandpass filter: high VSWR outside the passband and low VSWR in the passband. We will have a lower passband VSWR if the bandwidth is narrower or if the product R_1C_1 is lower. For a broadband match, we want a low-resistance load with a low reactive component (low Q).

Our goal in tuning a circulator, then, is to make the passband only as broad as necessary, keep the Q as low as possible, and minimize the insertion loss.

We can make changes in the impedance characteristics of stripline junction circulators by modifying the geometry of the portion of the center conductor between the ferrites. If electromagnetic simulation software is available, the effects of these modifications could be analyzed. Otherwise, there is no straightforward method of analyzing the effect of these geometrical modifications.

The first step in an empirical electrical adjustment procedure is to evaluate the impedance of the port or ports to be matched. In order to measure properly the impedance of one port of a three-port circulator, the other two ports should be matched; this can be done with stub tuners or some other temporary means. As a rule of thumb, the two ports should be matched to achieve 10 dB return loss or more. Because a reciprocal three-port junction would ideally exhibit 10 dB return loss at each port with the other two ports terminated in matched loads, and only a nonreciprocal three-port junction can be perfectly matched [7], we know the circulator junction is nonreciprocal (certainly a desired quality) if we have 10 dB or more return loss.

After we have measured the complex impedance of the port to be matched, we need to de-embed the circulator junction or characteristic plane. This process will give us the impedance we wish to transform to the system characteristic impedance (usually 50Ω). The de-embedding process usually stops at the edge of the ferrite material, or at the characteristic plane in the special case of a waveguide junction circulator. Figure 9.3 illustrates the concept of de-embedding.

There are several ways we can perform the de-embedding. One is to use computer analysis (linear circuit simulation) software. This is the fastest and easiest method if the software is available. Another method is to perform the necessary calculations by hand, which is quite tedious. A third method is to use the Smith chart, which is the method we will describe here.

Our impedance calculations fall into two classes: those for transmission lines and those for lumped elements (discrete inductors and capacitors). We will first consider transmission lines.

Having measured the complex impedance, we can proceed to find the impedance at a point inside the circulator, normally at the ferrite edge.

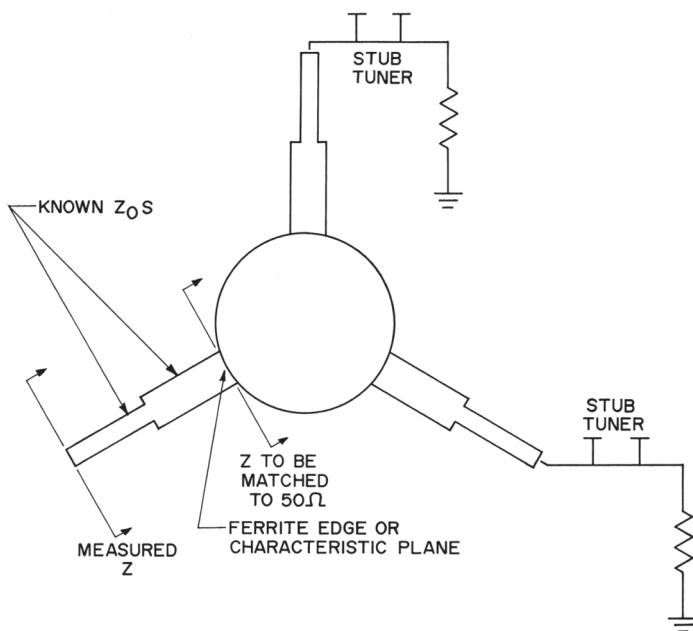


Figure 9.3 Circulator junction de-embedding.

Because we will be moving away from the generator, we need to begin with the conjugate of the measured impedance. This conjugate has the same real component, but the imaginary component has the opposite sign.

For simplicity, we normalize the Smith chart to the characteristic impedance of each transmission line through which we travel. The de-embedding process is best illustrated using an example. Our example is shown in Figure 9.4. The measured impedance is $63 + j10\Omega$. The complex conjugate of this is $63 - j10\Omega$. The first transmission line section in the circulator has a characteristic impedance of 37Ω and an electrical length of 90° . We normalize the Smith chart in Figure 9.5 to 37Ω and plot $63 - j10\Omega$ on the chart; $63 - j10$ is normalized as follows:

$$\frac{63 - j10\Omega}{37\Omega} = 1.70 - j0.27 \quad (9.6)$$

We rotate this point through 180° on the Smith chart (90° transmission length) toward the load, counterclockwise. We arrive at the normalized impedance looking toward the source at point A in Figure 9.4. The impedance at this point is approximately $0.57 + j0.09 = 21.1 + j3.33\Omega$.

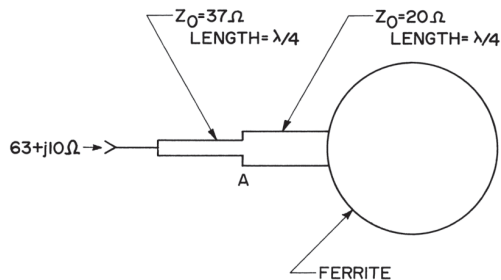


Figure 9.4 Example of de-embedding.

We now renormalize a Smith chart to 20Ω , the characteristic impedance of the transmission line section between point A and the ferrite. We plot $21.1 + j3.33\Omega$ on the chart in Figure 9.6:

$$\frac{21.1 + j3.33\Omega}{20\Omega} = 1.06 + j0.167 \quad (9.7)$$

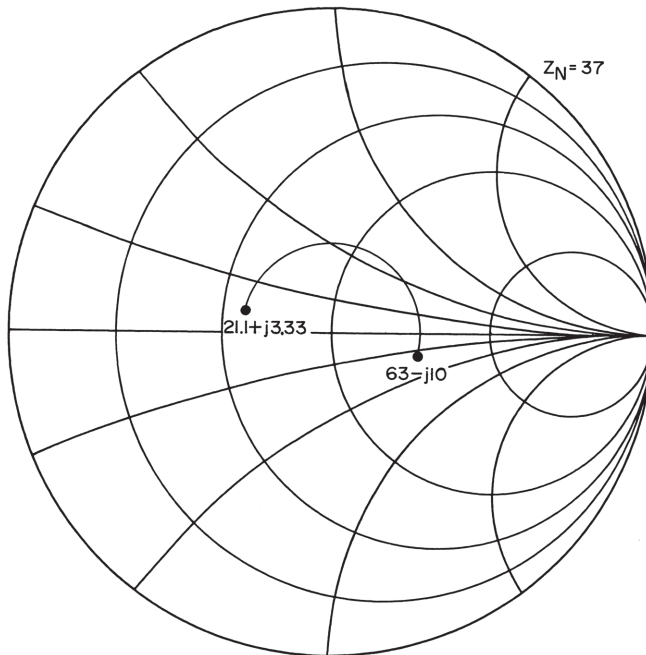


Figure 9.5 First step of de-embedding.

We again rotate the point 90° toward the load and arrive at $0.92 - j0.13 = 18 - j2.6\Omega$, approximately. This is the impedance looking toward the source. The impedance looking into the ferrite is the conjugate of this, $18 + j2.6\Omega$.

From this impedance, we can proceed to design a matching circuit that will match this impedance to 50Ω . In this example we consider only one frequency point. In a real situation, we need to consider a band of frequencies. The general procedure is the same, except for two things. First, the transmission lines have different electrical lengths at different frequencies. Second, we need to consider how various components will affect the circulator frequency response. We do not want to use components that will reduce the bandwidth.

The impedance we want to match, $18 + j2.6\Omega$, has a reactive component that can be handled in one of two ways [8]: by the absorption method or resonance method. In the absorption method we absorb the reactance into the matching network by modifying the original network slightly. The resonance method involves resonating the load reactance with an equal and opposite reactance.

For our example, we choose to use the absorption method because it will actually shorten the length of the transmission lines. This is not always the

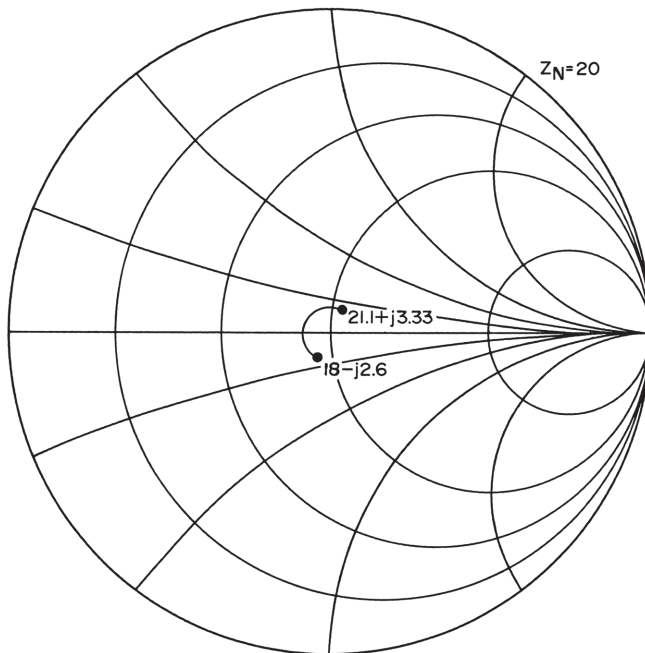


Figure 9.6 Second step of de-embedding.

case, and it is usually undesirable to lengthen the transmission lines because the dielectric for the transmission lines may be ceramic, part of the ferrite assembly, and not easily enlarged. If we use the resonance method, the resonating section can be a shunt element, placed anywhere along the transmission line length without changing the dimensions of the dielectric.

To match $18 + j2.6\Omega$ to 50Ω , we begin with the existing 20Ω transmission line, normalizing the Smith chart in Figure 9.7 to 20Ω . We plot the ferrite impedance ($0.92 + j0.13$). We rotate this point 120° toward the generator to arrive at the real axis of the chart. Thus, we have transformed $18 + j2.6\Omega$ ($0.92 + j0.13$) to $23.6 + j0\Omega$ ($1.18 + j0$) using a 60° length of 20Ω transmission line. We can easily match 23.6Ω (real) to 50Ω using a 90° section of 34.4Ω line. Figure 9.8 illustrates this last transformation.

After designing this new matching circuit, we modify the existing circuit accordingly. Insofar as the circulator is symmetrical, we perform the same modifications at each port.

We describe our de-embedding procedure for lumped-element matching circuits with the aid of Figure 9.9. We plot the complex conjugate of the measured impedance, $40 - j20\Omega$, on a Smith chart with normalized impedance

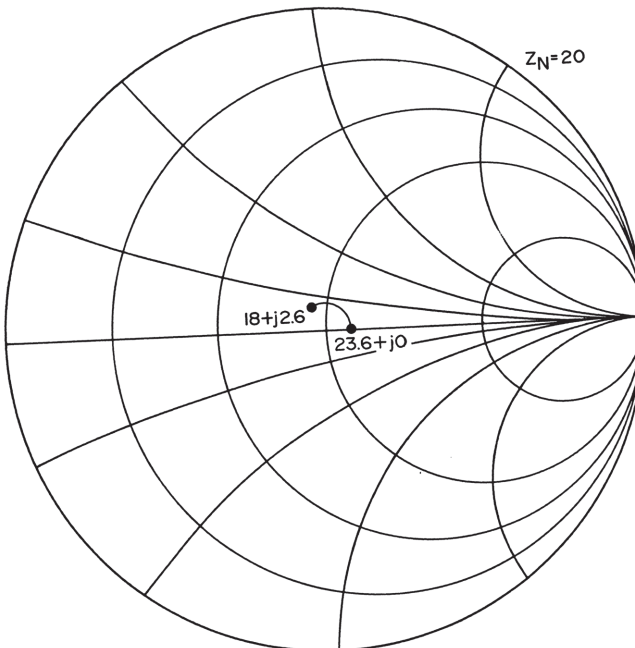


Figure 9.7 First step of matching.

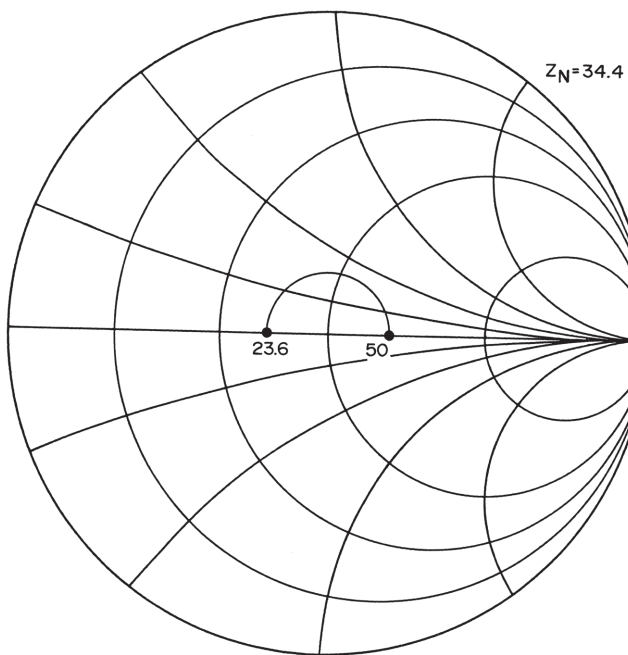


Figure 9.8 Second step of matching.

and admittance coordinates [9] in Figure 9.10. The chart can be normalized to 50Ω ($0.02S$) or any other convenient impedance.

We next calculate the inductive susceptance of the 20 pF shunt capacitor at 200 MHz as 0.0251S . We then normalize this susceptance to the normalization of the chart:

$$\frac{+j0.0251\text{S}}{0.02\text{S}} = 1.26 \quad (9.8)$$

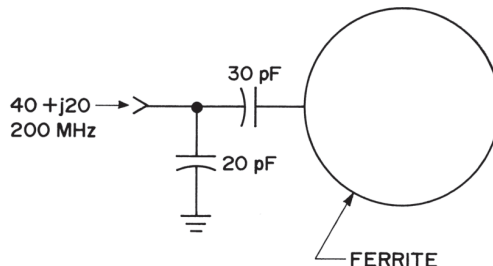


Figure 9.9 Lumped-element de-embedding example.

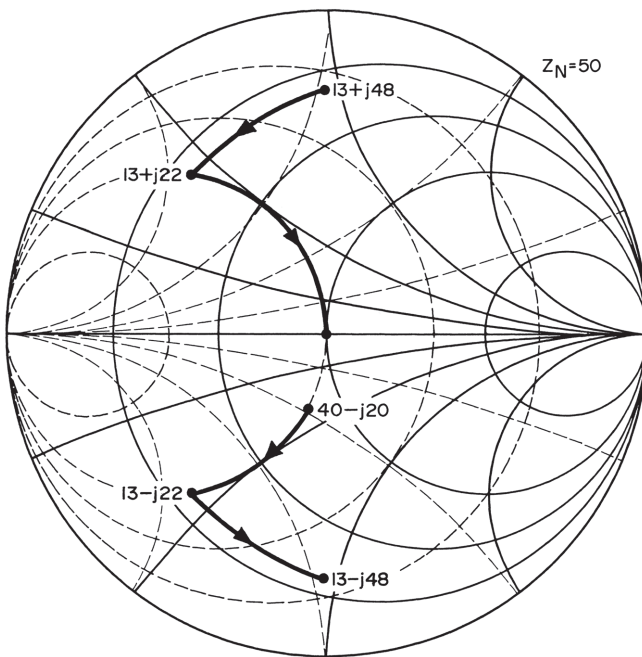


Figure 9.10 Lumped-element de-embedding and matching.

We then increase the inductive susceptance of the source impedance already plotted on the chart by the amount of the inductive susceptance of the shunt capacitor by moving downward along a constant conductance circle 1.26 units. We arrive at an impedance of $0.25 - j0.43$ ($13 - j22\Omega$).

Next, we calculate the reactance of the 30 pF series capacitor at 200 MHz as 26.5Ω . This corresponds to a normalized reactance of

$$\frac{-j26.5\Omega}{50\Omega} = 0.531 \quad (9.9)$$

We increase the capacitive reactance of the last point plotted by moving downward along a constant resistance circle 0.531 units. We arrive at an impedance of $0.25 - j0.96$ ($13 - j48.1\Omega$). The conjugate of this value, $13 + j48.1\Omega$, is the ferrite junction impedance.

By inspection of the Smith chart, we can see that the existing series capacitor brings the ferrite impedance to the $0.02S$ conductance circle. If we simply adjust the value of the shunt capacitor, we will obtain a 50Ω match. Starting with the ferrite impedance and adding the series capacitor in Figure

9.10, we arrive at an admittance of $1.0 - j1.76$. This indicates that if we add an inductive susceptance of 1.76, we will be at the center of the chart. Thus, we calculate the value of shunt capacitance that will give us $(1.76 \times 0.02S =) 0.0352S$. This value is 28 pF. Changing the shunt capacitor value to 28 pF will achieve a 50Ω match as shown in Figure 9.10.

The same circuit modifications should be performed for all ports of a symmetrical circulator.

The effects of adding several different types of lumped components for impedance matching are shown in Figure 9.11. The effects on the circulator bandwidth should also be considered.

The material presented here is by no means complete in terms of impedance-matching techniques, but we have presented some basic concepts. There is often more than one solution to an impedance-matching problem, and it takes experience and knowledge to arrive at the best one.

After an impedance match is achieved at each circulator port, the magnetic field can be adjusted again and the impedance-matching process repeated if there is a possibility of electrical performance improvement.

At microwave frequencies, it is easy to perform impedance matching by empirical means. If the inside of the circulator is accessible while an RF signal

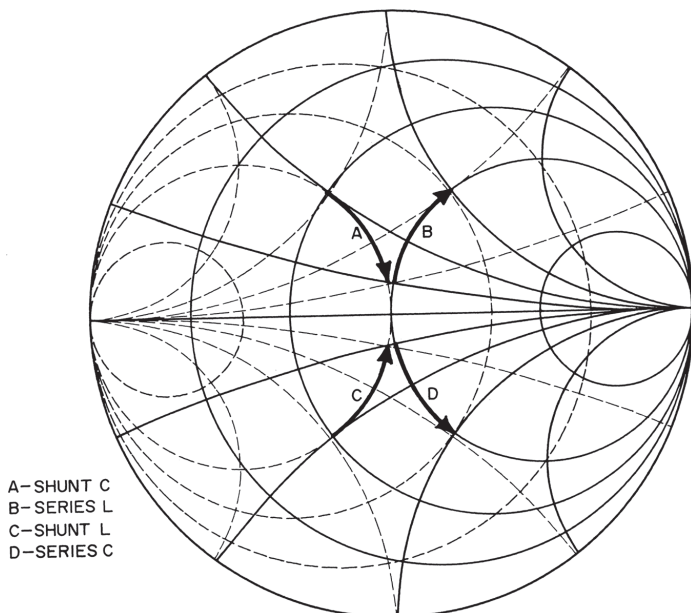


Figure 9.11 Effects of lumped impedance-matching components.

is applied, we can probe inside the circulator with a metallic probe. A probe held in contact with the ground plane and in proximity with the center conductor will simulate shunt capacitance. If this capacitance makes the electrical performance of the circulator better, we can add shunt capacitance at this point. If the response worsens, we know to remove capacitance. Similarly, we can use a magnet and a piece of steel to probe a waveguide unit. The steel is placed inside the waveguide, and the magnet, outside the waveguide, is used to slide the steel around until good electrical performance is obtained. Then we either add a tuning screw at this location or dimple the guide.

9.4 Eigenvalue Evaluation

It is possible to characterize a circulator in terms of its eigenvalues rather than its S-parameters. There are references to eigenvalue test sets in the literature [10, 11], but S-parameter test sets are much more common, and the eigenvalues can be computed from S-parameters. We compute the eigenvalues of the scattering matrix using [10]

$$\mathbf{s}_0 = \mathbf{S}_{11} + \mathbf{S}_{12} + \mathbf{S}_{13} \quad (9.10)$$

$$\mathbf{s}_- = \mathbf{S}_{11} + \mathbf{S}_{12}e^{-j2\pi/3} + \mathbf{S}_{13}e^{j2\pi/3} \quad (9.11)$$

$$\mathbf{s}_+ = \mathbf{S}_{11} + \mathbf{S}_{12}e^{j2\pi/3} + \mathbf{S}_{13}e^{-j2\pi/3} \quad (9.12)$$

For a symmetrical circulator,

$$\mathbf{S}_{11} = \mathbf{S}_{22} = \mathbf{S}_{33}$$

$$\mathbf{S}_{12} = \mathbf{S}_{23} = \mathbf{S}_{31}$$

$$\mathbf{S}_{13} = \mathbf{S}_{21} = \mathbf{S}_{32}$$

so we can rewrite (9.10–9.12) as

$$\mathbf{s}_0 = \mathbf{S}_{11} + \mathbf{S}_{12} + \mathbf{S}_{21} \quad (9.13)$$

$$\mathbf{s}_- = \mathbf{S}_{11} + \mathbf{S}_{12}e^{-j2\pi/3} + \mathbf{S}_{21}e^{j2\pi/3} \quad (9.14)$$

$$\mathbf{s}_+ = \mathbf{S}_{11} + \mathbf{S}_{12}e^{j2\pi/3} + \mathbf{S}_{21}e^{-j2\pi/3} \quad (9.15)$$

These forms of the equations allow us to obtain the eigenvalues more quickly by using only two-port S-parameters. The magnitudes of the eigenvalues are all near unity for low-loss circulators. The phase angles of the eigenvalues are of interest, and it is useful to visualize the eigenvalues using phasor diagrams.

Figures 9.12–9.17 show eigenvalue phasor diagrams superimposed on S-parameter plots for a 2-GHz above-resonance stripline junction circulator. All of the phasor diagrams correspond to the same frequency, 2 GHz. Figure 9.12 represents the electrical performance of a near-ideal circulator. This is a directly coupled circulator with neither transformers nor other impedance-matching circuitry. We see from the S-parameters that the circulator frequency response is centered close to 2 GHz. The s_0 phasor angle of 180° tells us that near-perfect circulation is achieved at 2 GHz; the circulator center frequency is correct. The angle between s_- and s_+ is roughly proportional to the frequency splitting between the counter-rotating modes, which is also proportional to κ/μ . For perfect circulation, the angle between s_- and s_+ is 120° , and they are each 120° from s_0 , indicating symmetrical splitting.

Figure 9.13 shows the performance of the same circulator with a 10%-large resonator diameter. This resonator diameter perturbation shifts the circulator resonant frequency lower. The angle of s_0 , $+169^\circ$, tells us that the center frequency is incorrect and below the frequency corresponding to the

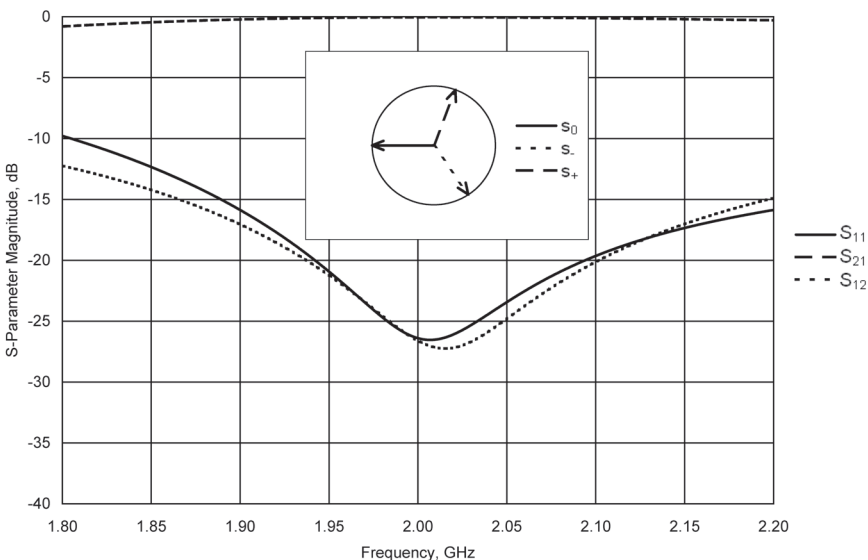


Figure 9.12 S-parameters and eigenvalue phasors for a near-ideal circulator.

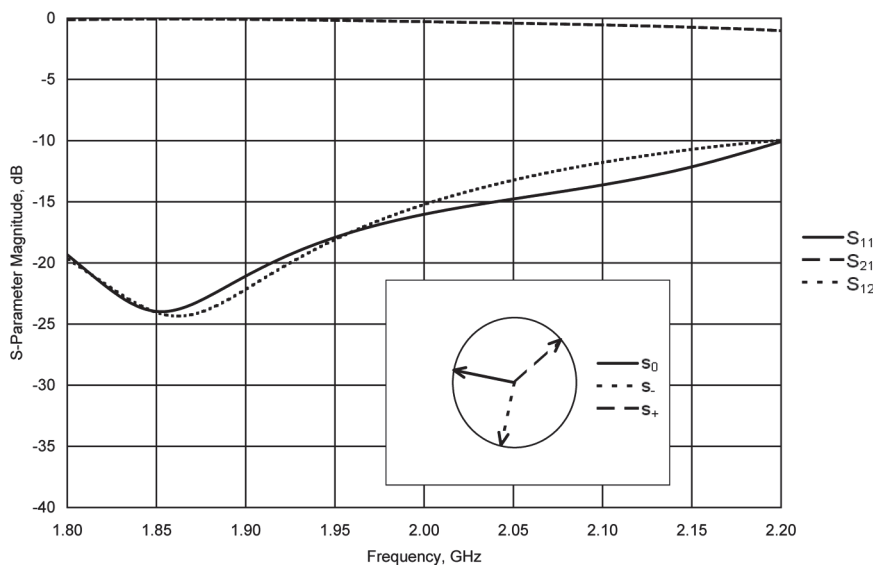


Figure 9.13 S-parameters and eigenvalue phasors for a circulator having 10%-large resonator diameter.

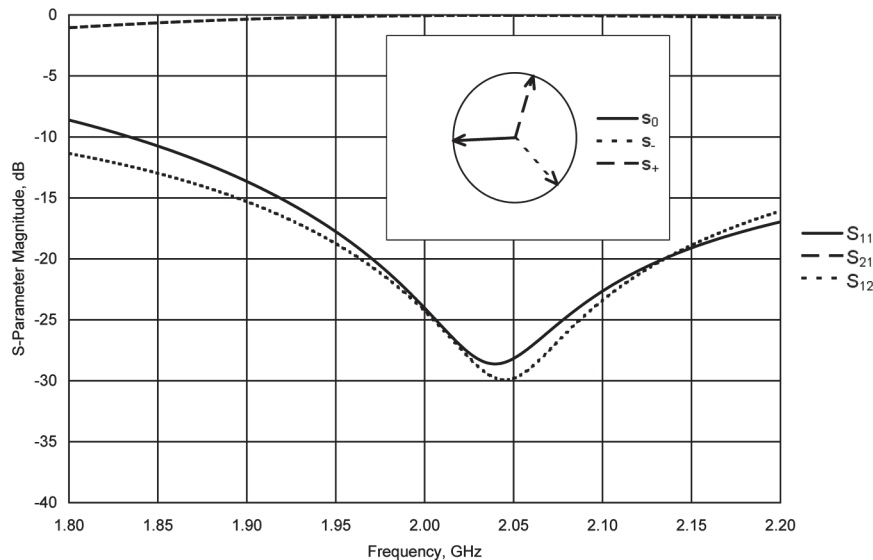


Figure 9.14 S-parameters and eigenvalue phasors for a circulator having 50-Oe high H_{dc} .

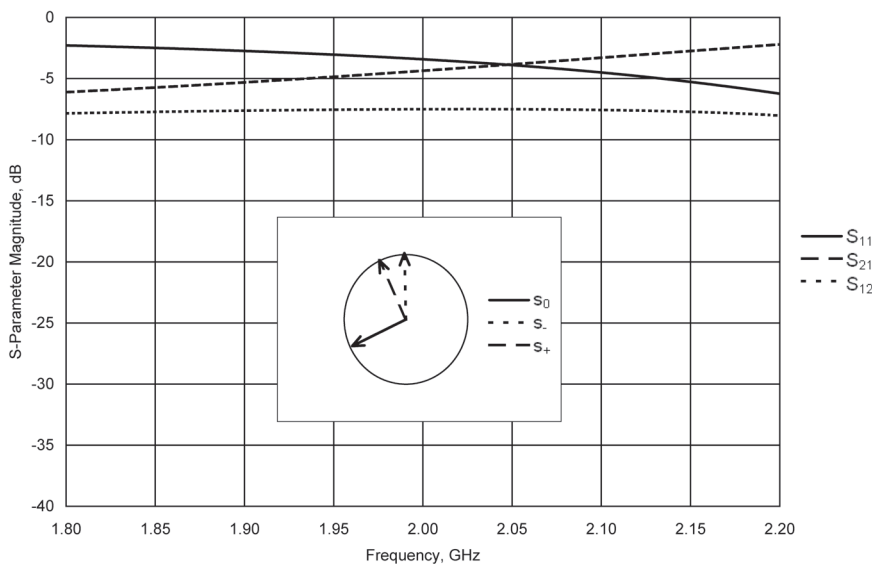


Figure 9.15 S-parameters and eigenvalue phasors for a circulator having very high H_{dc} .

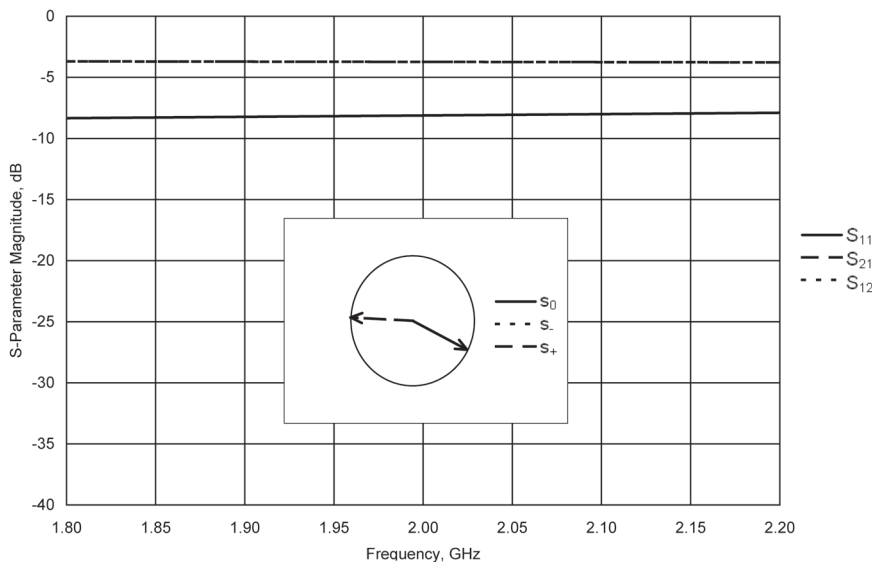


Figure 9.16 S-parameters and eigenvalue phasors for a circulator having no ferrite.

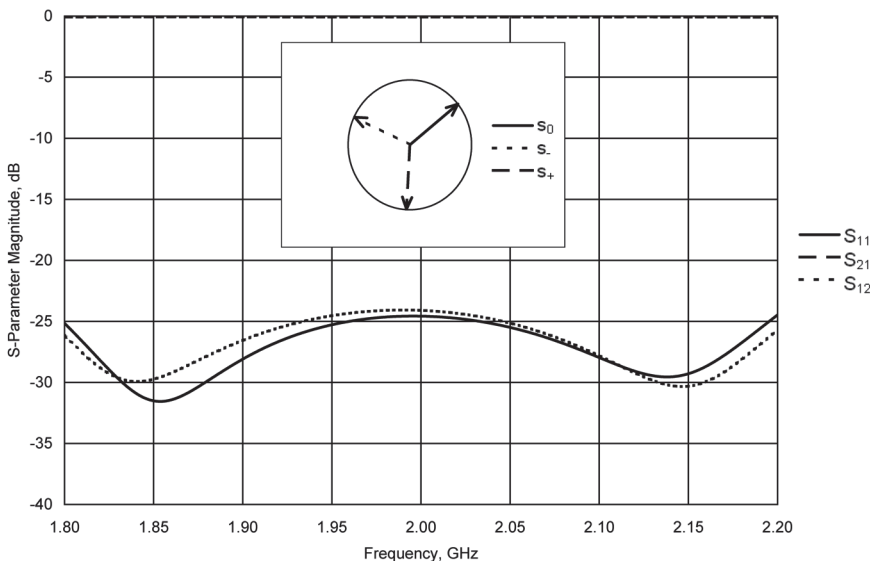


Figure 9.17 S-parameters and eigenvalue phasors for a circulator having quarter-wavelength transformers.

displayed eigenvalue phasors. The splitting angle (angle between \mathbf{s}_- and \mathbf{s}_+) is larger than 120° . For an above-resonance circulator, splitting generally increases with frequency. The phasor diagram also shows that the splitting is slightly asymmetrical. The tuning adjustment indicated by Figure 9.13 to achieve perfect circulation at 2 GHz is a reduction in resonator diameter or an increase in H_{dc} .

In Figure 9.14, we see the effect of a 50-Oe increase (above the value corresponding to Figure 9.12) in H_{dc} . The \mathbf{s}_0 angle is -177° , indicating high center frequency, and splitting is slightly small at 118° . Figure 9.15 shows the effects of a very strong level of H_{dc} . Here, the angle between \mathbf{s}_- and \mathbf{s}_+ is only 24° . This alone, for an above-resonance circulator, indicates that H_{dc} is too high. The \mathbf{s}_0 phasor, at an angle of -155° indicates a circulator center frequency that is too high.

If the ferrites were removed from the circulator, we would see results like those in Figure 9.16. The \mathbf{s}_- and \mathbf{s}_+ phasors are superimposed (no splitting), and are near 180° . The \mathbf{s}_0 phasor is at a small angle near 0° .

When transformers are added to a circulator, the insertion phase of the circulator increases, rotating the \mathbf{s}_0 phasor away from its 180° angle as shown in Figure 9.17. When using the eigenvalue phases to evaluate circulator

performance, it is important to ensure that the S-parameter measurement reference planes are correct. The reference plane positions affect the eigenvalue phases.

In most cases, S-parameter magnitudes, plotted in the frequency domain, provide the same information about a circulator to the experienced eye that an eigenvalue phasor diagram provides. It is interesting to note, though, that eigenvalue evaluation performed at just one frequency may provide enough information for tuning purposes. Eigenvalue phase values can be plotted as functions of frequency to derive more information regarding circulator performance.

References

- [1] Simon, J. W., "Broadband Strip-Transmission Line Y-Junction Circulators," *IEEE Transactions on Microwave Theory and Techniques*, May 1965, p. 339.
- [2] Moskowitz, L. R., *Permanent Magnet Design and Application Handbook, Second Edition*, Malabar, FL: Krieger Publishing, 1995.
- [3] *Factors Affecting Magnet Stability*, Valparaiso, IN: Indiana General, 1978.
- [4] Bode, H. W., *Network Analysis and Feedback Amplifier Design*, New York: D. Van Nostrand, 1945.
- [5] Fano, R. M., "Theoretical Limitations on the Broadband Matching of Arbitrary Impedances," *Journal of the Franklin Institute*, January–February 1950.
- [6] Matthaei, G. L., L. Young, and E. M. T. Jones, *Microwave Filters, Impedance-Matching Networks, and Coupling Structures*, Dedham, MA: Artech House, 1980.
- [7] Simon, J. W., "Broadband Strip-Transmission Line Y-Junction Circulators," *IEEE Transactions on Microwave Theory and Techniques*, May 1965, p. 344.
- [8] Besser, L., *RF Circuit Fundamentals, Part I*, Palo Alto, CA: Besser Associates, 1986.
- [9] Bowick, C., *RF Circuit Design*, Indianapolis, IN: Howard W. Sams, 1982.
- [10] Owen, B., "The Identification of Modal Resonances in Ferrite Loaded Y-Junctions and their Adjustment for Circulation," *The Bell System Technical Journal*, March 1972, pp. 595–627.
- [11] Helszajn, J., *Waveguide Junction Circulators: Theory and Practice*, New York: John Wiley & Sons, 1998.

10

Design Examples

10.1 Introduction to Examples

In this chapter, we present several design examples that serve to illustrate some of the circulator design processes and provide information that is not presented elsewhere in this book. The electrical design processes for these example circulators are more detailed than those typically used in industry. This is because circulator designs are often based on existing designs. When measured data for an existing design are available, it is questionable whether the additional cost of mathematical analysis or electromagnetic simulation is justified. However, sometimes detailed design documentation is required.

In the design examples, we have chosen to focus primarily on electrical design, which is the most challenging and frequently misunderstood aspect of circulator design. To avoid writing another dull book that is only about design examples, we have intentionally omitted mechanical and magnetic design information for the examples. For engineering prototypes, the mechanical structure can often be very simple, such as two sheet-metal plates for stripline circulators. The magnetic bias field can be provided temporarily by stacks of whatever magnets are stuck to the workbench or file cabinet, and scraps of sheet steel. Power handling considerations are mostly ignored in the examples.

The levels of electrical performance of the design examples in this chapter are not intended to impress any reader. These are not examples of fully engineered circulators. An entire book, albeit a sleep-inducing one, could be written about the engineering of just one circulator, so to keep you awake, we spared you the engineering details. To the uninitiated, circulators look simple, but the engineering effort that has been invested in some circulators is staggering.

Circulator engineering is partly about reducing variation: variation in electrical performance from one circulator to the next, and variation with temperature, frequency, RF power, and time. Some types of apparent electrical performance differences cannot readily be reduced. These include the differences we will see in the electrical performance plots later in this chapter (Figures 10.6–10.8, 10.14–10.16, 10.19–10.21, 10.24–10.26, 10.34, and 10.36–10.38).

The design approximations and analysis procedures described in Chapter 5 produce approximate results. These are adequate to produce initial designs that can then be optimized using iterations of electromagnetic simulations or empirical work. We did not expect that the approximate analysis results in the figures would match measured data exactly; these figures represent real-world disagreement. Similarly, the Ansys® HFSS™ simulation results do not agree with measured data. There are several reasons for this: connectors and transitions were not included in the simulations to simplify the geometric models and speed computations, ground planes were perfectly conductive, we used uniform magnetic bias, and the geometries were perfect. Also, because HFSS uses a finite-element solver, results may sometimes approach matching measured data very closely, but because of the mesh discretization, results can never quite be perfect. We made compromises between computation time and the accuracy of results.

Measured results can differ from computed results because dimensions of parts differ from designed nominal dimensions, and material properties also vary. As described in further detail in Section 10.2, Figure 10.9 shows the results of a Monte Carlo analysis of VSWR, performed by randomly perturbing center conductor and ferrite dimensions and ferrite material properties within their typical tolerance ranges. One way to control the effects of variations in dimensions and materials properties is to use tuning adjustments where possible. Steps can be taken to reduce the effects of dimensional and materials properties variations by sorting and matching parts or by allowing less variation in these parameters during manufacturing.

Finally, electrical measurement errors contribute to differences between computed and measured results. Measurement uncertainty is discussed in Section 8.2.7.

10.2 Above-Resonance Stripline Junction Circulator

Above-resonance junction circulators are widely used for low-frequency (typically below 3 GHz) applications and are smaller than their below-resonance counterparts. Above-resonance junction circulators can be made to operate at relatively high power levels because they are not susceptible to spin-wave nonlinearity, but bandwidth is generally limited to 40% or less.

To demonstrate the design process for above-resonance stripline junction circulators, we will design a circulator having a 20% bandwidth centered at 1 GHz. Our electrical specifications for this circulator are as follows:

- Isolation: 26 dB minimum;
- Insertion loss: 0.2 dB maximum;
- VSWR: 1.10:1 maximum;
- Power handling: 1W.

First, we select a ferrite material for the circulator using the criteria presented in Chapter 4. A high value of saturation magnetization ($4\pi M_S$) is desirable to maximize bandwidth, but this is an above-resonance circulator, which requires a strong magnetic bias. We choose to use a moderate $4\pi M_S$ to avoid the use of large or high-energy magnets. The resonance line width (ΔH) of the ferrite material should be as narrow as possible to minimize insertion loss. These requirements of low ΔH and moderate $4\pi M_S$ lead us to select Yttrium Iron Garnet (YIG). Typical properties for YIG are as follows:

- $4\pi M_S$: 1780 G;
- ΔH : 45 Oe;
- ϵ : 15;
- $\tan \delta$: 0.0002.

Next, we select a preliminary value of H_{dc} . H_{dc} must be high enough to maintain low insertion loss, yet low enough to provide for the necessary bandwidth. Because this is to be an above-resonance circulator, we must have H_{dc} greater than the value corresponding to ferrimagnetic resonance at the upper frequency band edge:

$$H_{dc} > \frac{f_2}{\gamma} = \frac{1100\text{MHz}}{2.80\text{MHz/Oe}} = 393 \text{ Oe}$$

Knowing the ferrite material properties, we estimate the insertion loss contribution from magnetic losses as described in Section 5.1.3 using (1.30–1.33), (5.6), and (5.23), with $Q_U = \mu_{eff}' / \mu_{eff}''$ and Q_L approximated by (5.27). The results of this evaluation, performed at the upper frequency band edge (1.1 GHz) where loss is highest, are shown in Figure 10.1. Above 550 Oe, H_{dc} has very little effect on insertion loss. Below 550 Oe, the loss increases significantly as H_{dc} is reduced. To meet our 0.2-dB insertion loss specification, we need to

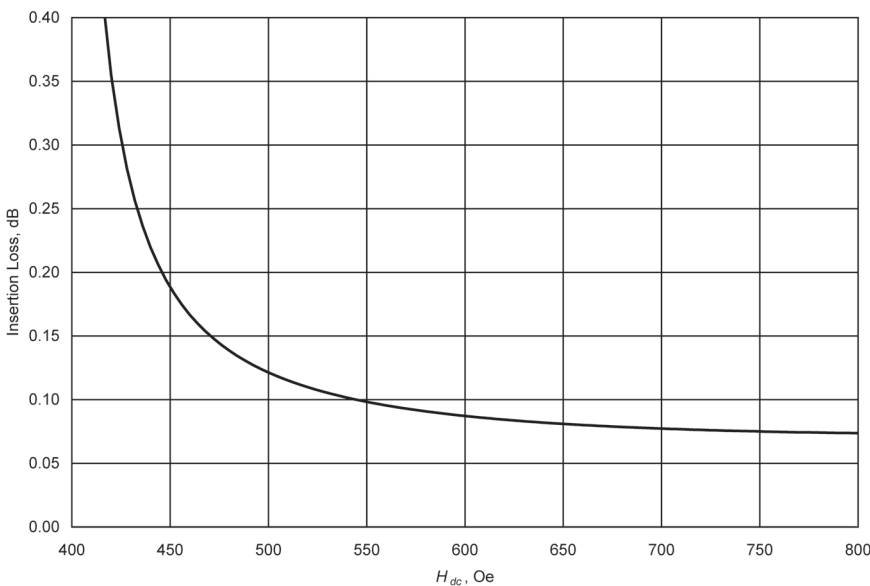


Figure 10.1 Estimated magnetic loss.

allow some loss margin for conductor losses and connector insertion loss, and operation at 550 Oe would leave some margin. To allow for some adjustment later, we tentatively set $H_{dc} = 600$ Oe for this circulator design.

Using (1.30–1.33) again at the center frequency, with find that

$$\frac{\kappa'}{\mu'} = 0.49$$

and applying (5.27),

$$Q_L = \frac{0.71}{\frac{\kappa}{\mu}} = \frac{0.71}{0.49} = 1.4$$

It is possible to vary this Q_L value from 1.3–1.6 by varying H_{dc} from 550–650 Oe. We can see from Figure 5.12 that a single quarter-wavelength transformer at each port will be sufficient, and for a bandwidth = 20% and VSWR = 1.10:1, Q_L should be about 2.1. We could increase H_{dc} to achieve $Q_L = 2.1$, or we could increase bandwidth to about 28% to work with the lower $Q_L = 1.4$ value. However, neither of these solutions provides the best possible performance over the frequency band of interest.

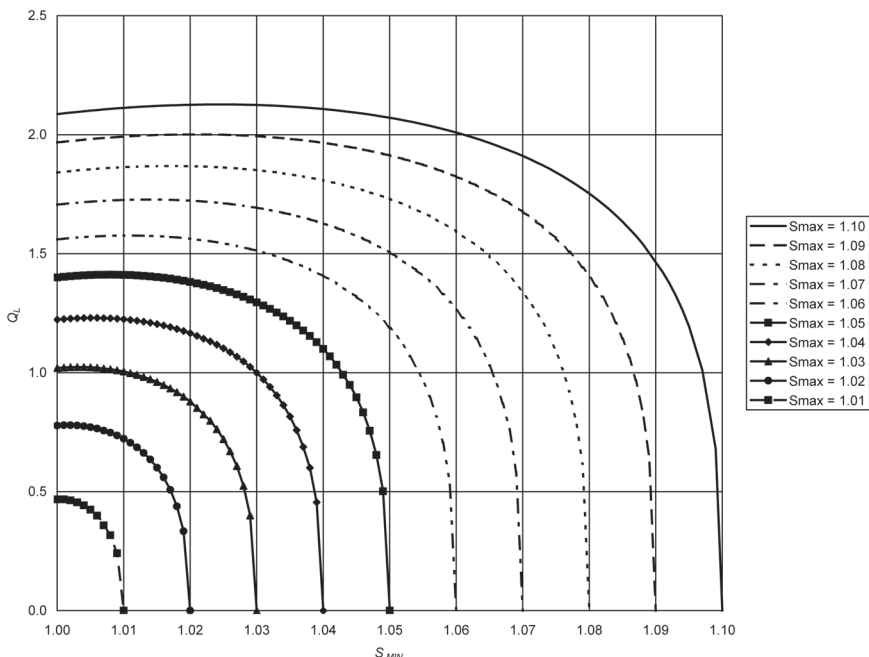


Figure 10.2 Loaded Q versus S_{\min} with S_{\max} as a parameter.

Equations (5.59–5.73) offer a means to explore the values of Q_L corresponding to various combinations of S_{\min} and S_{\max} , with S_{\max} up to 1.10, our specified maximum VSWR. The results of this exploration are shown in Figure 10.2. From this graph, we see that there is a wide range of network solutions corresponding to our $1.3 \leq Q_L \leq 1.6$ range. S_{\max} values from 1.05–1.10 with various values of S_{\min} are possible. Similarly, Figure 10.3 shows G_r versus S_{\min} with S_{\max} as a parameter. For our Q_L range and maximum VSWR specification, we could use a value of G_r in the range of 0.050–0.111S.

Applying (5.9 and 5.10), we estimate

$$\mu_{\text{eff}} = \mu = \frac{H_{\text{dc}} + M_0}{H_{\text{dc}}} = \frac{600 \text{ Oe} + 1780 \text{ G}}{600 \text{ Oe}} = 3.97$$

$$R = \frac{1.84\lambda}{2\pi\sqrt{\mu_{\text{eff}}\epsilon}} = \frac{1.84 \cdot \frac{11.8 \times 10^9 \text{ inch/s}}{1 \text{ GHz}}}{2\pi\sqrt{3.97 \cdot 15}} = 0.448 \text{ inches}$$

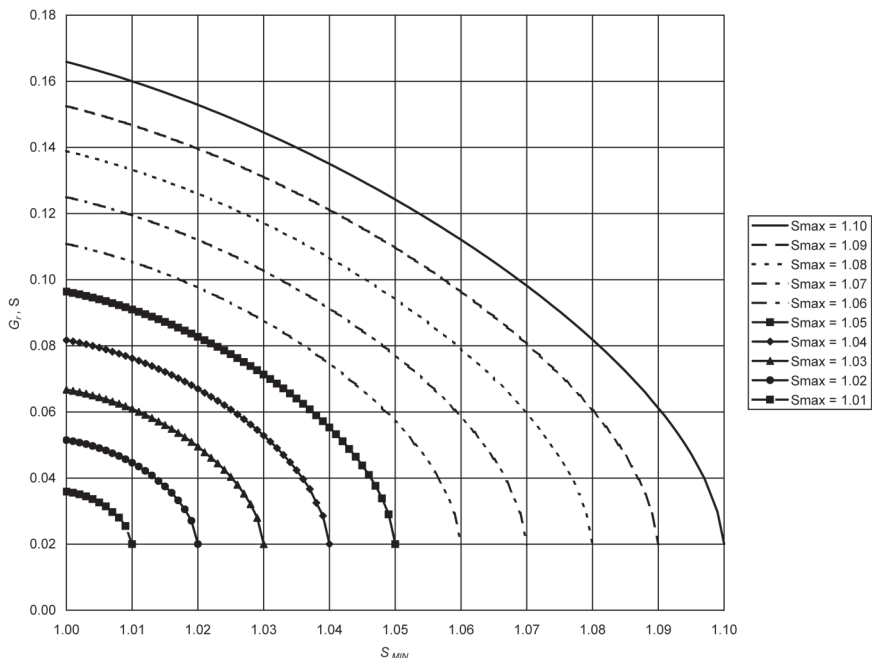


Figure 10.3 Resonator conductance versus S_{\min} with S_{\max} as a parameter.

Then, by re-arranging (5.21), we can find the ferrite thickness (d):

$$d = 1.48 \frac{\omega R^2 \epsilon \epsilon_0}{G_r Q_L}$$

From the previously stated ranges of H_{dc} , Q_L , and G_r , we find that $0.038 \leq d \leq 0.091$ inches. To proceed with the circulator design, we choose $d = 0.060$ inches, near the middle of this range. If $Q_L = 1.4$, this ferrite thickness corresponds to $G_r \approx 0.075S$ and from (5.59–5.73), this network solution corresponds to $S_{\min} = 1.04$ and $S_{\max} = 1.06$. Equation (5.70) gives us the transformer characteristic impedance:

$$Z_t = \frac{1}{\sqrt{S_{\max} G_r Y_0}} = \frac{1}{\sqrt{1.06 \cdot 0.075 S \cdot 0.02 S}} \approx 25 \Omega$$

Now that we have established preliminary values for the circulator design variables, we analyze the electrical performance of the circulator using the analysis procedure outlined in Section 5.1.8 (5.111–5.132). After this analysis and some performance optimization, we arrive at the optimized design values shown in Table 10.1.

Before committing the design to hardware, we will perform an electromagnetic simulation and final optimization of the design using Ansys® HFSS™. Because the previous analysis ignored fringing fields from the resonator edges, we need to first adjust the resonator radius (R) accordingly. Equations (5.133–5.137) tell us that R should be reduced about 5.5% to 0.359 in. The preceding calculations were for a disk resonator, but we will use a hexagonal resonator, so considering the geometric equivalency presented in Section 5.1.6 (i.e., if $kR = 1.84$ for a disk, then $kA = 3.46$ for a regular hexagon), if $R = 0.359$ in for the disk, then $A = 0.675$ in for a hexagon.

Figure 10.4 shows the geometry for the Ansys HFSS electromagnetic simulation. We have chosen ferrite disks having 1.200-in diameter, and the transformers between the ferrite disks were shortened slightly to allow dielectric blocks at the ports for tuning purposes. The lower dielectric blocks are solid dielectric material having $\epsilon_r \approx 10$, and the upper dielectric is silicone, which can easily be added or removed.

Table 10.1
Optimized Design Values for Above-Resonance
Stripline Junction Circulator

Parameter	Preliminary Value	Optimized Value
$4\pi M_s$	1780 G	1780 G
ΔH	45 Oe	45 Oe
ϵ	15	15
H_{dc}	600 Oe	600 Oe
R	0.448 in	0.380 in
kR	1.84	1.62
d	0.060 in	0.060 in
Z_t	25Ω	26.7Ω
t	0.002 in	0.002 in
W_t	0.184 in	0.169 in
L_t	0.369 in	0.275 in

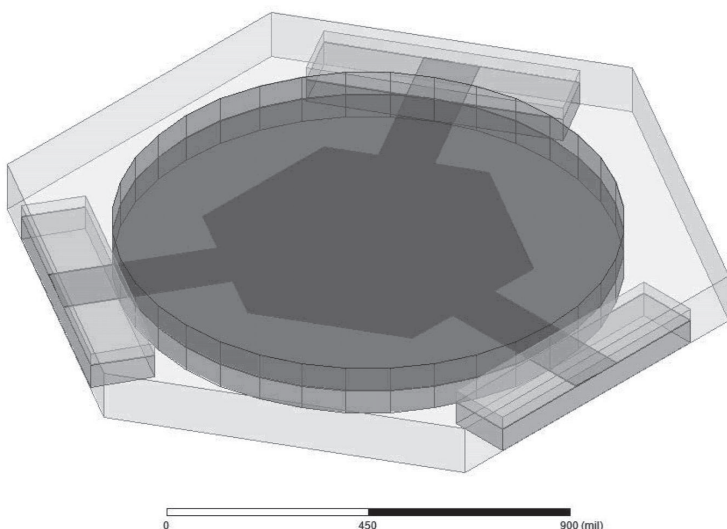


Figure 10.4 Model geometry for electromagnetic simulation.

To further optimize the design of the circulator using Ansys HFSS, we reduced H_{dc} to 550 Oe and narrowed the transformer width slightly to 0.130 in to allow use of the tuning blocks.

Finally, we constructed a circulator, implementing the design described in this section in a package having type N connectors. Figure 10.5 shows the circulator with its upper housing removed. Electrical test results, along with the electromagnetic simulation results and the results of the analysis using the equations in Section 5.1.8, are shown in Figures 10.6–10.8.

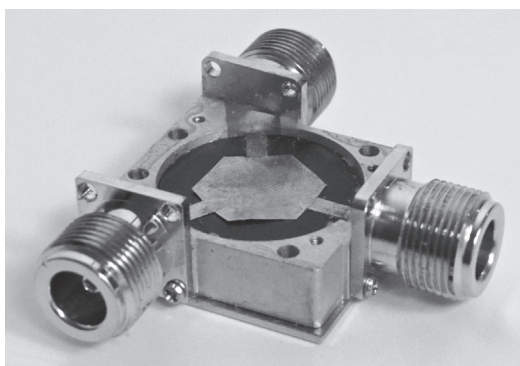


Figure 10.5 Example above-resonance stripline junction circulator.

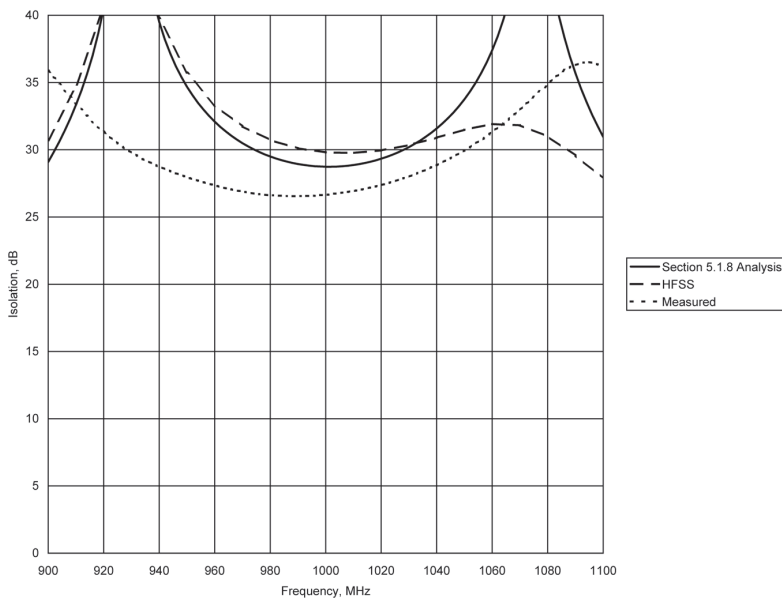


Figure 10.6 Isolation of example above-resonance stripline junction circulator.
(Electrical testing services courtesy of UTE Microwave.)

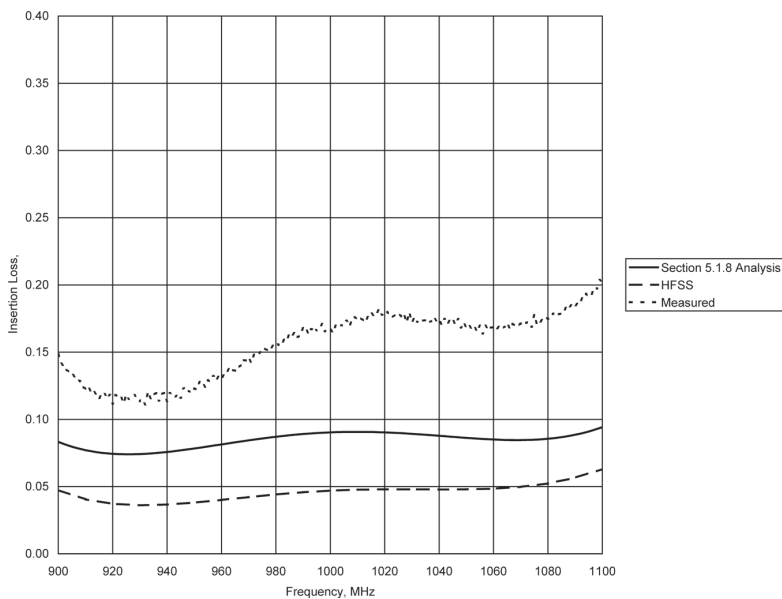


Figure 10.7 Insertion loss of example above-resonance stripline junction circulator.
(Electrical testing services courtesy of UTE Microwave.)

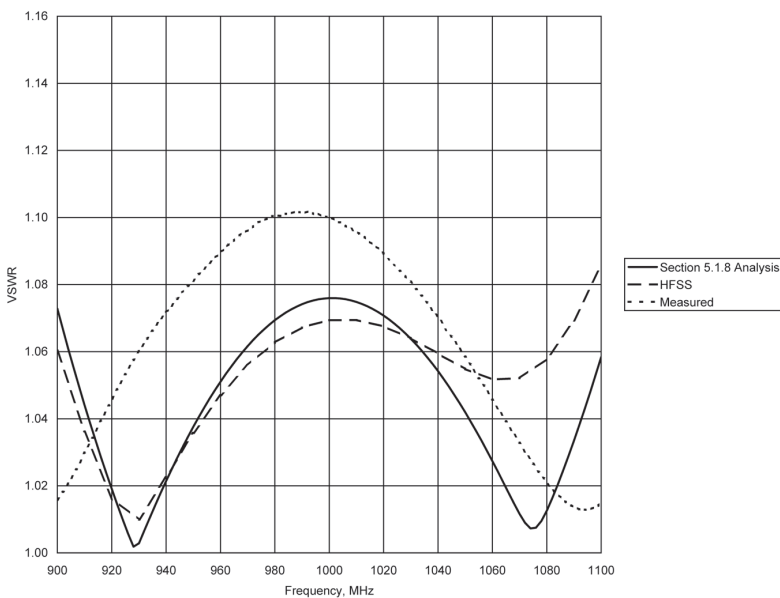


Figure 10.8 VSWR of example above-resonance stripline junction circulator. (Electrical testing services courtesy of UTE Microwave.)

The simulated insertion loss is lower than the measured loss primarily because connector and conductor losses are not included in the simulation or analysis. The analysis and simulation results differ noticeably only when we look at isolation levels of roughly 30 dB and higher, or VSWR levels below 1.08. Insertion loss differs by hundredths of a decibel. In practical cases, these differences are relatively unimportant.

It is important to understand why the real-world measured results differ from the computed not-so-real-world mathematical results. Sometimes despite our best efforts, dimensions of parts differ from the designed nominal dimensions, and material properties also vary about the published nominal values. Figure 10.9 shows the results of a Monte Carlo analysis of VSWR, performed by randomly perturbing center conductor and ferrite dimensions and ferrite material properties within their typical tolerance ranges. The tolerance ranges were ± 89 G for $4\pi M_s$, ± 10 Oe for ΔH , ± 0.75 for ϵ , ± 0.0005 in for center conductor thickness, ± 0.001 in for transformer width and ferrite thickness, and ± 0.005 in for R and transformer length. The band of values in Figure 10.9 suggests that measured VSWR shown in Figure 10.8 is within its normal range of variation, compared to simulation and analysis results. The same is true of the isolation and insertion loss parameters.

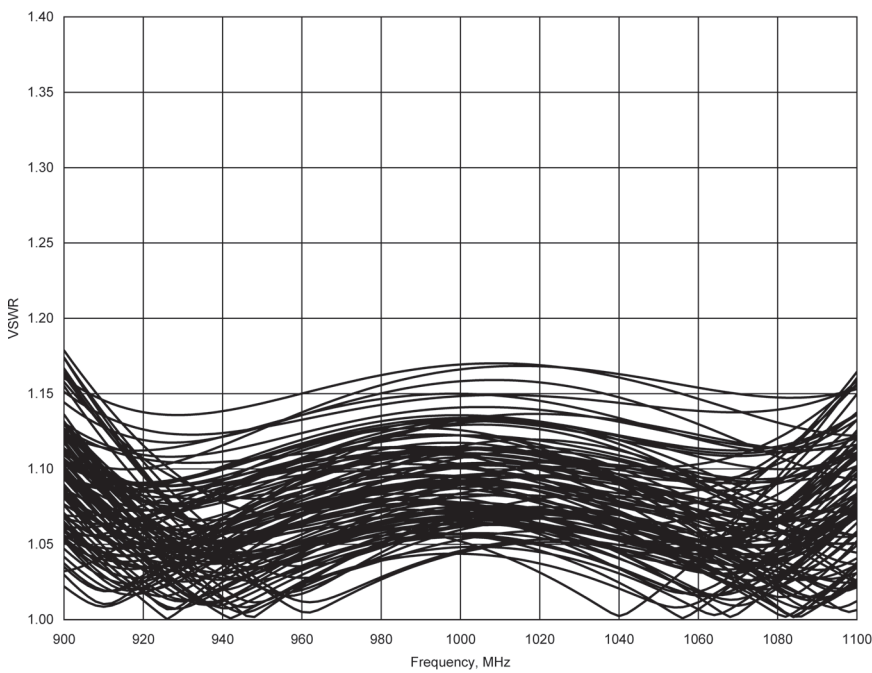


Figure 10.9 Monte Carlo analysis results.

Several general techniques can be used to prevent electrical parameters from straying outside of their specification limits. One is to allow a suitable margin between nominal circulator performance and specification limits. Another is to use tuning adjustments, where possible, to minimize variation. It is not possible to tune every variable, but wisdom should tell us to provide for tuning of the most sensitive variables. Finally, steps can be taken to reduce the effects of dimensional and materials properties variations by sorting and matching parts or taking steps to reduce variation.

10.3 Below-Resonance Stripline Junction Circulator

Below-resonance junction circulators are widely used for frequencies above 500 MHz, but are larger than their above-resonance counterparts. The power handling capability of below-resonance junction circulators can be limited by the onset of spin-wave nonlinearity, but bandwidth can be up to 75%.

The design process for a below-resonance circulator is similar to that of an above-resonance circulator. We will design a circulator having an octave

(67%) bandwidth centered at 1.5 GHz. Our electrical specifications for this circulator are as follows:

- Isolation: 18 dB minimum;
- Insertion loss: 0.8 dB maximum;
- VSWR: 1.35:1 maximum;
- Power handling: 1W.

First, we select a ferrite material for the circulator using the criteria presented in Chapter 4. A high value of saturation magnetization ($4\pi M_S$) is desirable to maximize bandwidth, but the $4\pi M_S$ must not be so high that low field losses are present. Referring to Figure 4.4 and (4.4), we find that a $4\pi M_S$ of 350 G is appropriate. The resonance line width (ΔH) of the ferrite material should be as narrow as possible to minimize insertion loss. These requirements of low ΔH and $4\pi M_S = 350$ G lead us to select a Yttrium Aluminum Iron Garnet. Typical properties for this material are as follows:

- $4\pi M_S$: 350 G;
- ΔH : 45 Oe;
- ϵ : 14;
- $\tan \delta$: 0.0002.

For a below-resonance circulator, the ferrite is just magnetically saturated, so we assume that $H_{dc} = 0$. Using (1.30–1.33) at the center frequency, with find that

$$\frac{\kappa'}{\mu'} = 0.65$$

and applying (5.27),

$$Q_L = \frac{0.71}{\frac{\kappa}{\mu}} = \frac{0.71}{0.65} = 1.09$$

Because of the relatively high value of κ/μ , this equation provides only a rough estimate of Q_L , as the equation is outside of its range of validity. We need a more accurate value of Q_L for network synthesis, which we compute

using (5.112–5.125). Before computing Q_L , we estimate μ_{eff} and R using (5.28) and (5.9):

$$\mu_{\text{eff}} = 1 - \frac{\gamma^2 M_0^2}{\omega^2} = 1 - \frac{(2.80 \text{ MHz/Oe})^2 (350 \text{ G})^2}{(1500 \text{ MHz})^2} = 0.573$$

$$R = \frac{1.84\lambda}{2\pi\sqrt{\mu_{\text{eff}}\epsilon}} = \frac{1.84 \cdot \frac{11.8 \times 10^9 \text{ inch/s}}{1.5 \text{ GHz}}}{2\pi\sqrt{0.573 \cdot 14}} = 0.813 \text{ inches}$$

The stripline characteristic impedance in (5.116) is unimportant for the purpose of computing Q_L , but for a wide-bandwidth design like this one, it is important to converge on a correct value of coupling angle (ψ). This can be done iteratively by computing Q_L , and then synthesizing the network and updating ψ . Ultimately, for a wideband design like this one, the design will converge on a so-called *tracking* solution [1]. In the interest of reducing the quantity of computations, for this design we will start with a value interpolated from values in a table [1]: $\psi = 0.637$.

Applying (5.112–5.125) and adjusting R to achieve the correct resonant frequency, we find that $R = 0.573$ in, $kR = 1.30$, and $Q_L = 0.50$. While we can see from Figure 5.12, based only on Q_L at the center frequency, that a single quarter-wavelength transformer at each port may be sufficient, we can achieve better performance with two transformers. Figure 5.14 shows that we should theoretically be able to achieve a VSWR of less than 1.10:1 with $Q_L = 0.50$.

Using (5.59–5.62) and (5.71–5.107), we find that for $Q_L \approx 0.50$ and 67% bandwidth, various combinations of S_{\min} and S_{\max} , with S_{\max} up to 1.10, correspond to $0.04 \leq G_r \leq 0.08S$. For this design example, we choose $G_r = 0.08S$. This network solution, based on $S_{\min} = 1.000$ and $S_{\max} = 1.056$, yields transformer characteristic impedances (Z_{t1} and Z_{t2}) of $\approx 19\Omega$ and $\approx 38\Omega$.

Again using (5.112–5.125) in an iterative fashion, we find that to obtain $G_r = 0.08S$ with $\psi = 0.637$, based on a disk resonator, we need a ferrite thickness (d) of 0.152 in. To implement the first transformer having $Z_{t1} \approx 19\Omega$, considering the values of the design variables already established, requires a dielectric constant (ϵ_d) of 3.6. Ultimately we will change the resonator shape and increase d so that a higher value of ϵ_d can be used to make the circulator more compact.

Now that we have established preliminary values for the circulator design variables, we analyze the electrical performance of the circulator using the analysis procedure outlined in Section 5.1.8 (5.111–5.132). After this analysis and some performance optimization, we arrive at the optimized design values shown in Table 10.2.

To increase d and still maintain the same value of G_r and Q_L , we can change the shape of the resonator to a side-coupled triangle as described in Section 5.1.6.

Because the previous analyses ignored fringing fields from the resonator edges, we need to adjust the resonator radius (R) accordingly. Equations (5.133–5.137) tell us that R should be reduced about 10.7% to 0.491 in. The preceding calculations were for a disk resonator, but we will use a triangular resonator, so considering the geometric equivalency presented in Section 5.1.6 (i.e., if $kR = 1.84$ for a disk, then $kA = 3.68$ for a triangle), if $R = 0.491$ in for the disk, then $A = 0.982$ in for a triangular resonator.

Before committing the design to hardware, we will perform electromagnetic simulations and final optimization of the design using Ansys® HFSS™. First, we will simulate only the resonator to ensure that its resonant frequency and G_r are correct before attaching transformers. Figure 10.10 shows the geometry for this first Ansys HFSS electromagnetic simulation. In the geometric model, the resonator is sandwiched between two triangular ferrites, which are in turn embedded in hexagonal dielectrics. The ports are de-embedded to the ferrite edges. Figure 10.11 shows the impedance of one port, with the other two ports terminated in essentially reflectionless terminations. The impedance

Table 10.2
Optimized Design Values for Below-Resonance
Stripline Junction Circulator

Parameter	Optimized Value
$4\pi M_S$	350 G
ΔH	45 Oe
ε	14
H_{dc}	0
R	0.550 in
kR	1.33
d	0.152 in
Z_{t1}	18.4Ω
Z_{t2}	35.7Ω
ε_d	3.6
t	0.025 in
W_{f1}	0.655 in
W_{f2}	0.256 in
L_t	1.042 in

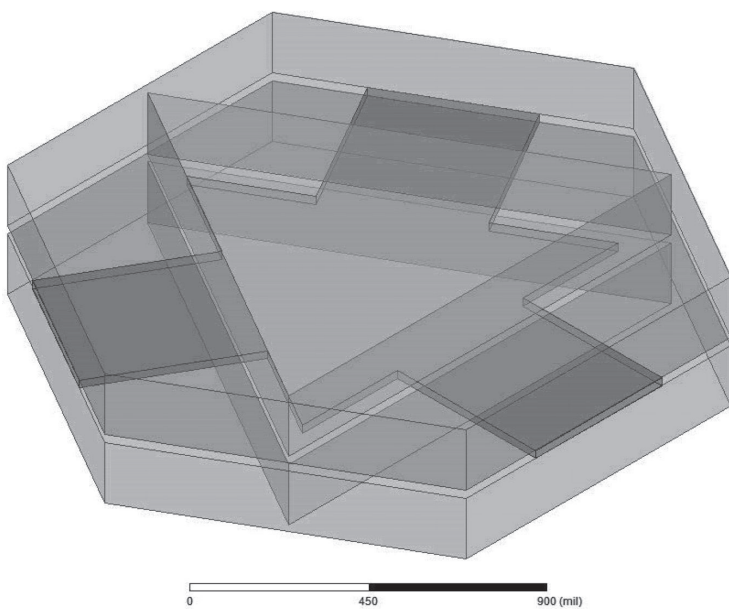


Figure 10.10 Model geometry for electromagnetic simulation of triangular resonator.

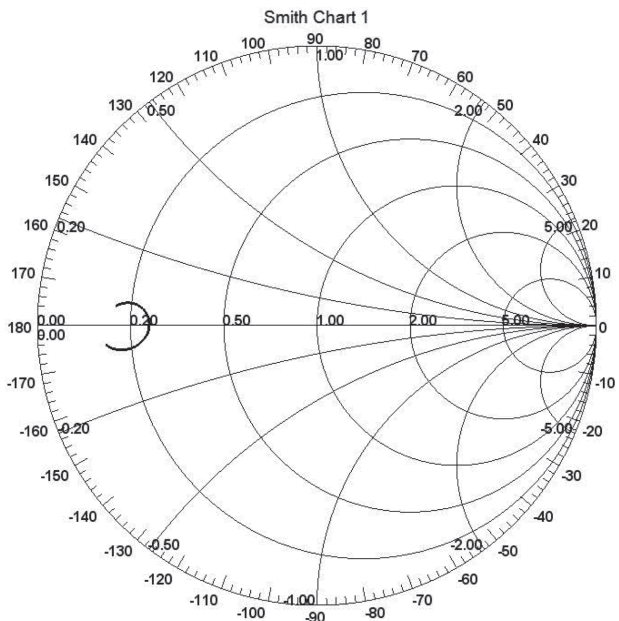


Figure 10.11 Resonator impedance.

at the center frequency is 0.25, normalized to 50Ω , or $0.25 \cdot 50\Omega = 12.5\Omega$. This is equivalent to $G_r = 0.08 \text{ S} = 1 / 12.5\Omega$. The optimized value for d for the triangular resonator is 0.200 in., and the stripline width at the resonator is 0.500 in. The characteristic impedance of this stripline is roughly equal to the resonator impedance, so it provides no impedance transformation. The purpose of this line is to allow connection of the transformers at the periphery of the ferrite disk, as shown in Figure 10.12.

We have chosen ferrite disks having 1.600-in diameter to allow sufficient area for the resonator, and the first transformers are implemented between dielectric rings around the ferrite disks. These dielectric rings have a dielectric constant (ϵ_d) of 9 to shorten the transformers and decrease the size of the circulator. The width of these transformers was adjusted to 0.300 in to optimize electrical performance. The second transformers are implemented as 50Ω air lines with dielectric tuning blocks that can be moved to adjust the impedance match.

We constructed a circulator, implementing the design described in this section in a package having type N connectors. Figure 10.13 shows the circulator with its upper ground plane removed. Electrical test results, along with the electromagnetic simulation results and the results of the analysis using the equations in Section 5.1.8, are shown in Figures 10.14–10.16.

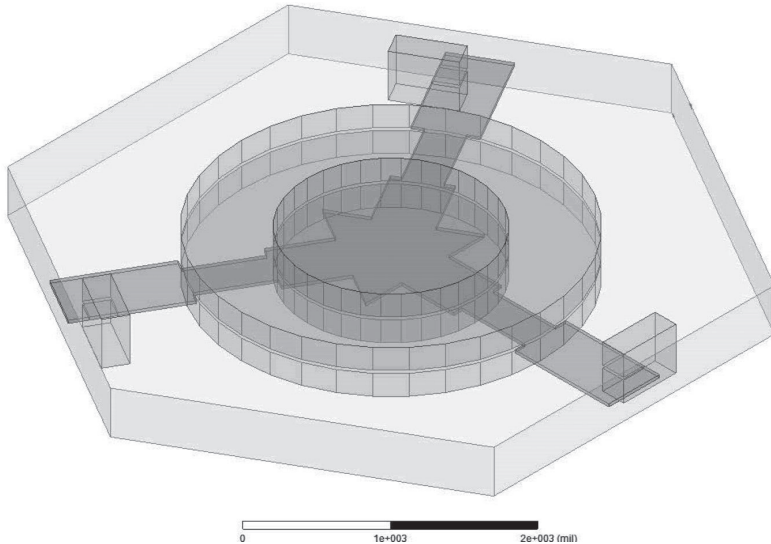


Figure 10.12 Model geometry for electromagnetic simulation.

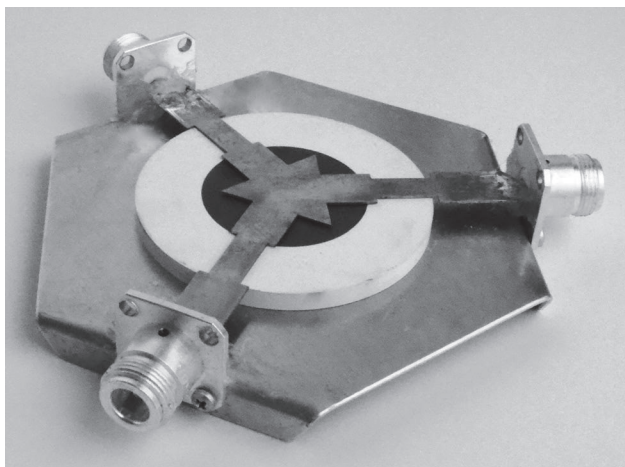


Figure 10.13 Example below-resonance stripline junction circulator.

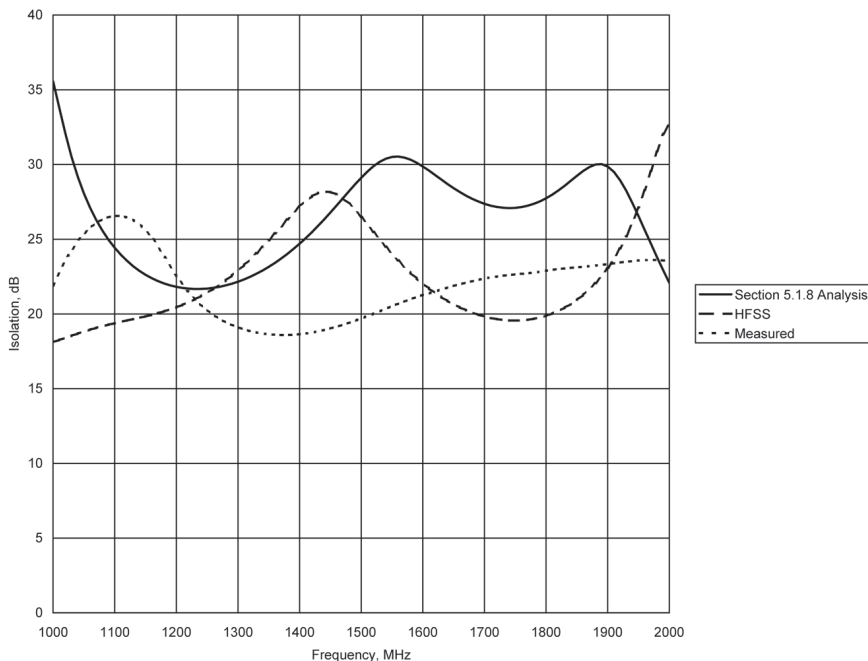


Figure 10.14 Isolation of example below-resonance stripline junction circulator.
(Electrical testing services courtesy of UTE Microwave.)

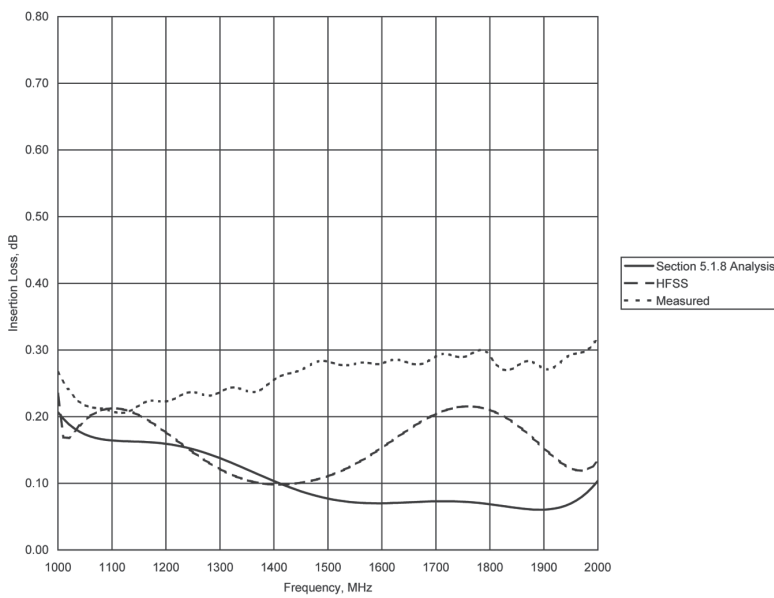


Figure 10.15 Insertion loss of example below-resonance stripline junction circulator. (Electrical testing services courtesy of UTE Microwave.)

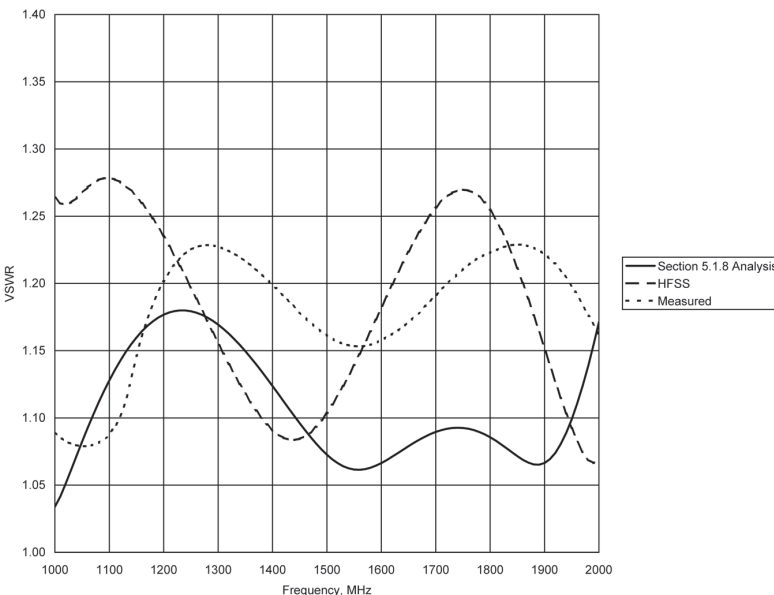


Figure 10.16 VSWR of example below-resonance stripline junction circulator. (Electrical testing services courtesy of UTE Microwave.)

The simulated insertion loss is lower than the measured loss at the higher frequencies primarily because connector and conductor losses are not included in the simulation or analysis. The analysis and simulation results differ because of the added stripline length between the resonator and the first transformer in the simulation. As discussed in Section 10.1, real-world measured results differ from the computed mathematical results because dimensions of parts differ from the designed nominal dimensions, and material properties also vary about the published nominal values.

10.4 Waveguide Junction Circulator

The waveguide junction circulator typically shares the same magnetic operating region as the below-resonance stripline junction circulator, but is designed for use with the waveguide transmission medium.

Most waveguide junction circulators operate below resonance and the design process follows Section 5.1.10. We will design a circulator having a 2-GHz (25%) bandwidth centered at 8 GHz. Our electrical specifications for this circulator are as follows:

- Isolation: 20 dB minimum;
- Insertion loss: 0.2 dB maximum;
- VSWR: 1.25:1 maximum;
- Power handling: 1W;
- Waveguide: WR-112 (inside dimensions: 1.122×0.497 inches).

First, we select a ferrite material for the circulator using the criteria presented in Chapter 4 for a below-resonance circulator. Because the bandwidth of a waveguide junction circulator implemented in rectangular waveguide is limited by the bandwidth of the waveguide itself, we can choose a relatively low value of saturation magnetization ($4\pi M_S$) to reduce magnetic bias field requirements. Referring to Figure 4.4 and (4.4), we find that a $4\pi M_S$ as high as 2750 G could be used at 8 GHz, but we will settle on a value of $4\pi M_S = 1780$ G and use YIG. Typical properties for this material are as follows:

- $4\pi M_S$: 1780 G;
- ΔH : 45 Oe;
- ϵ : 15;
- $\tan \delta$: 0.0002.

For a below-resonance circulator, the ferrite is just magnetically saturated, so we assume that $H_{dc} = 0$. Using (1.30–1.33) at the center frequency, with find that

$$\frac{\kappa'}{\mu'} = 0.62$$

and applying (5.27),

$$Q_L = \frac{0.71}{\frac{\kappa}{\mu}} = \frac{0.71}{0.62} = 1.15$$

Because of the relatively high value of κ/μ , this equation provides only a rough estimate of Q_L , as the equation is outside of its range of validity.

We can see from Figure 5.12 that a single quarter-wavelength transformer at each port will be sufficient, and we should easily be able to meet our electrical specifications, even if there is some error in the Q_L value. Applying (5.59–5.73), we find that the lowest possible VSWR over the 25% bandwidth, with $Q_L = 1.15$, is slightly less than 1.06:1. This network solution yields $G_r = 0.070S$ and a transformer characteristic admittance $Y_t = 0.037S$. These values are valid for a 50Ω system, for which $Y_0 = 0.02S$. Because waveguide characteristic impedance is an ambiguous quantity, we normalize the G_r and Y_t values to the waveguide impedance by dividing them by Y_0 , giving $G_r = 3.5$ and $Y_t = 1.85$. The normalized transformer *impedance* is

$$Z_t = \frac{1}{Y_t} = \frac{1}{1.85} = 0.54$$

Using (5.162), we find that the waveguide height for the transformer is

$$b_t = b \frac{Z_t}{Z_0} = 0.497 \text{ inches} \cdot 0.54 = 0.27 \text{ inches}$$

The transformer length should be one quarter wavelength in the waveguide, or $\lambda_g/4$, where λ_g is given by (5.160):

$$\lambda_g = \frac{1}{\sqrt{\frac{1}{\lambda_0^2} - \frac{1}{\lambda_c^2}}} = \frac{1}{\sqrt{\frac{1}{(11.8 \times 10^9 \text{ inch/s})^2} - \frac{1}{(2 \cdot 1.122 \text{ inch})^2}}} = 1.957 \text{ inches}$$

$$\frac{\lambda_g}{4} = \frac{1.957 \text{ inches}}{4} = 0.489 \text{ inches}$$

Following Section 5.1.10, using the topology shown in Figure 5.7(a), we choose an initial value of $d = 0.775 \cdot b_t = 0.209$ in. We use (5.39) iteratively to estimate that for $d = 0.209$ in, R should be approximately 0.269 in. Note that in Figure 5.7(a), the waveguide height is actually $2b$, and the ferrite thickness would be $2d$, so the value of d used in (5.39) should be half of the 0.209-in dimension. We choose to use a triangular ferrite, and the triangle altitude (A) is approximately equal to $2R = 0.538$ in.

To optimize the circulator design, we will perform electromagnetic simulations using Ansys® HFSS™. Figure 10.17 shows the geometry for the Ansys HFSS electromagnetic simulations. The ferrite is sandwiched between layers of Teflon dielectric.

After the simulations and performance optimization, we arrive at the optimized design values shown in Table 10.3.

The change in the ferrite triangle altitude (A) was probably required because the loading effect of the Teflon dielectric and the proximity of the ferrite to the waveguide walls were not taken into account. The resonant frequency could be adjusted by changing either the A or d dimension. Equation (5.40) could be used to correct the ferrite length for wall proximity. The change in transformer length (L_t) was probably required because of the step discontinuity at the edges of the transformers.

Finally, we constructed a circulator, implementing the design described in this section. Figure 10.18 shows the circulator with its cover removed. Electrical test results, along with the electromagnetic simulation results, are shown in Figures 10.19–10.21.

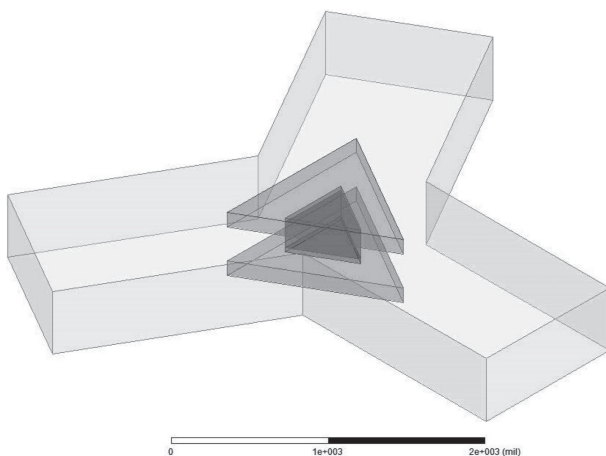


Figure 10.17 Model geometry for electromagnetic simulations.

Table 10.3
Optimized Design Values for Waveguide Junction Circulator

Parameter	Preliminary Value	Optimized Value
$4\pi M_s$	1780 G	1780 G
ΔH	45 Oe	45 Oe
ε	15	15
H_{dc}	0 Oe	0 Oe
A	0.538 in	0.450 in
d	0.209 in	0.200 in
b_t	0.270 in	0.270 in
L_t	0.489 in	0.400 in

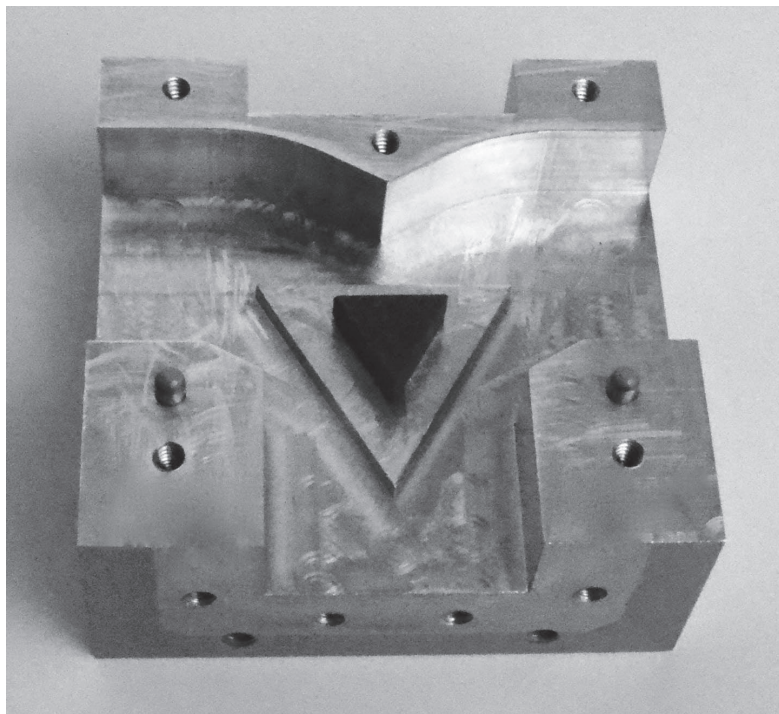


Figure 10.18 Example waveguide junction circulator.

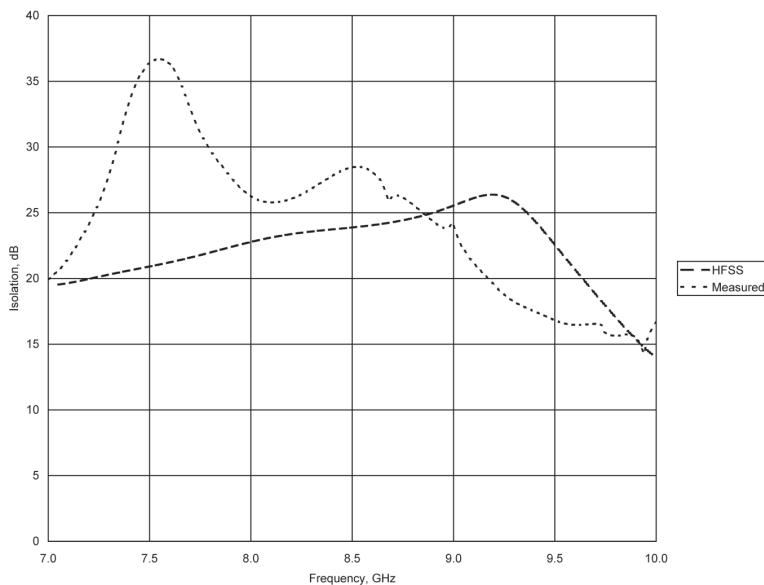


Figure 10.19 Isolation of example waveguide junction circulator. (Electrical testing services courtesy of UTE Microwave.)

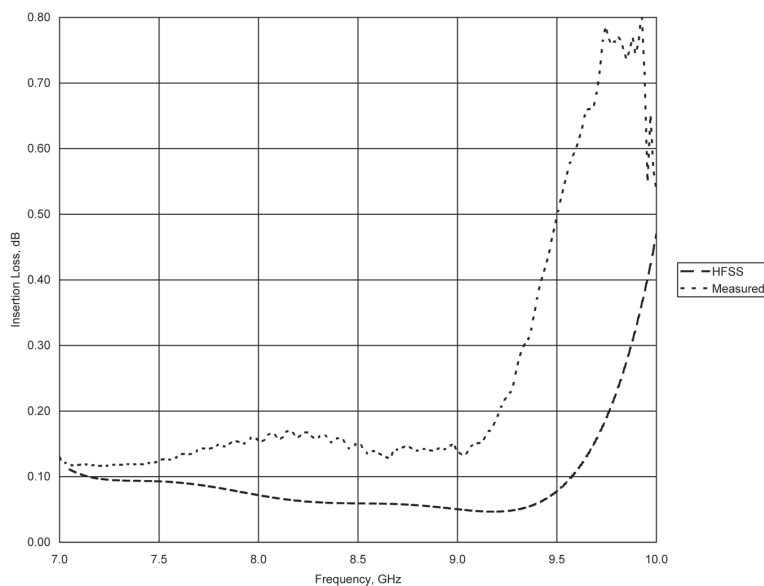


Figure 10.20 Insertion loss of example waveguide junction circulator. (Electrical testing services courtesy of UTE Microwave.)

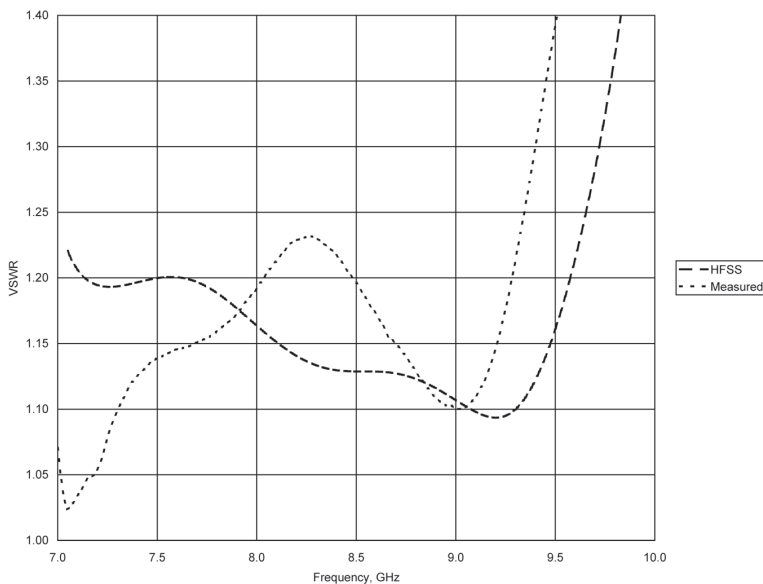


Figure 10.21 VSWR of example waveguide junction circulator. (Electrical testing services courtesy of UTE Microwave.)

10.5 Microstrip Circulator

Microstrip circulators are inexpensive because they lack the housing and connectors of other junction circulators. The lack of these features makes the microstrip circulator more suitable for integration with other circuitry. Bandwidths and power levels for this type of circulator are usually small compared to those of other circulators.

We will use a different design approach for this circulator to help illustrate the differences between microstrip and stripline junction circulators. Initially we will aim for electrical performance similar to that of the circulator we designed in Section 10.2. However, because the design will not be optimum, we expect to meet the following specifications over a narrow (8%) band centered at 1.25 GHz:

- Isolation: 15 dB minimum;
- Insertion loss: 0.5 dB maximum;
- VSWR: 1.30:1 maximum;
- Power handling: 1W.

Above-resonance microstrip circulators are unusual, but for similarity to the circulator of Section 10.2, we will use an above-resonance operating point for this example. We will use the same ferrite material (YIG) and internal magnetic field intensity ($H_{dc} = 600$ Oe) as well.

The stripline circulator of Section 10.2 used a ferrite thickness (d) of 0.060 in and an effective resonator radius (R_{eff}) of 0.380 in for analysis purposes. Knowing that in a microstrip configuration, we will need a thinner ferrite disk to achieve the same resonator impedance, we arbitrarily choose $d = 0.050$ in and a ferrite disk diameter of 1.000 in. Using (5.150–5.158), we determine that $R = 0.343$ in corresponds to $R_{eff} = 0.380$ in. To maintain about the same transformer impedance when transferring the stripline design to microstrip, we need to widen the line considerably. A width of 0.200 in provides us with an acceptable $Z_t = 28.8\Omega$, calculated using (5.138–5.148). We analyze the electrical performance of the circulator using the analysis procedure outlined in Section 5.1.8, (5.111–5.132), substituting microstrip equations (5.138–5.148) for the stripline ones. Table 10.4 summarizes the values determined so far.

The value of the microstrip kR_{eff} is lower than that for the stripline design because ϵ_{eff} for the resonator is less than ϵ for the ferrite. L_t for the microstrip design is the length of microstrip line from the resonator to the ferrite disk edge. It is less than a quarter wavelength because the remaining impedance matching will be implemented with a length of microstrip line in air.

We found during the analysis of this circulator that despite the change to a slightly thinner ferrite and wider transformer strip, the resonator impedance

Table 10.4
Summary of Design Values for Microstrip Circulator

Parameter	Stripline Value	Microstrip Value
$4\pi M_s$	1780 G	1780 G
ΔH	45 Oe	45 Oe
ϵ	15	15
H_{dc}	600 Oe	600 Oe
R	0.359 in	0.343 in
R_{eff}	0.380 in	0.380 in
kR_{eff}	1.62 (at 1 GHz)	1.52 (at 1 GHz)
d	0.060 in	0.050 in
Z_t	26.7Ω	28.8Ω
W_t	0.169 in	0.200 in
L_t	0.275 in	0.157 in

is high and inductive. It is too high to provide for the same level of electrical performance as that of the stripline circulator. To match the microstrip circulator to a 50Ω system impedance, we choose to use a short (0.157-in long) microstrip line on the ferrite disk, followed by a microstrip line in air about 0.470 in long. This matching structure is a semi-lumped one, with the ferrite-loaded line acting as a shunt capacitor, and the air line acting as a series inductance.

To obtain electrical performance like its stripline counterpart, the microstrip circulator would require a much thinner ferrite disk, probably about 0.016 in thick.

Before committing the design to hardware, we will perform an electromagnetic simulation of the design using Ansys® HFSS™. Figure 10.22 shows the geometry for the electromagnetic simulation.

Finally, we constructed a circulator, implementing the design described in this section. Figure 10.23 shows the circulator without its magnets. Electrical test results, along with the electromagnetic simulation results and the results of the analysis using the equations in Section 5.1.8, are shown in Figures 10.24–10.26.

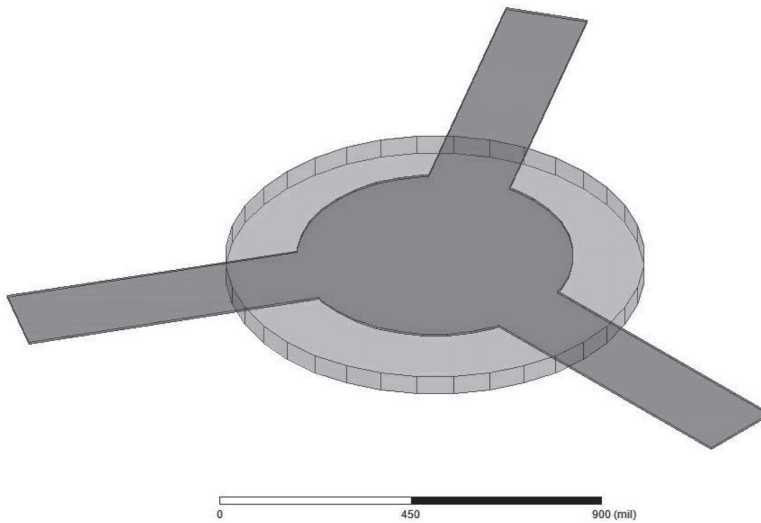


Figure 10.22 Model geometry for electromagnetic simulation.

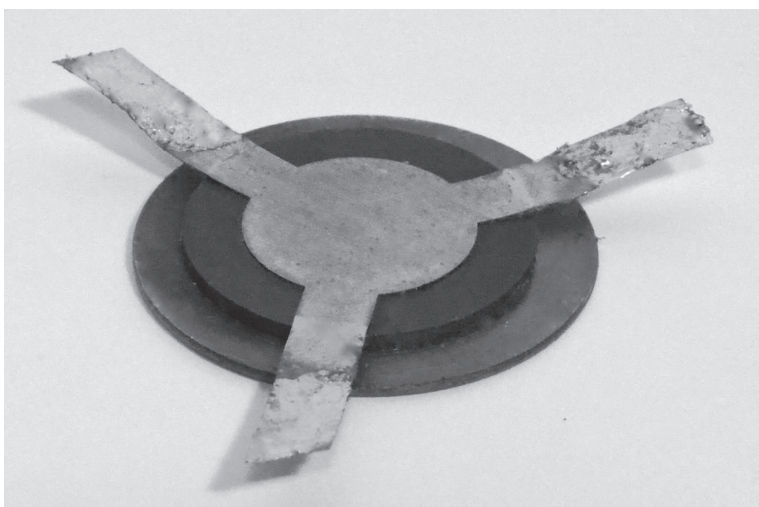


Figure 10.23 Example microstrip circulator.

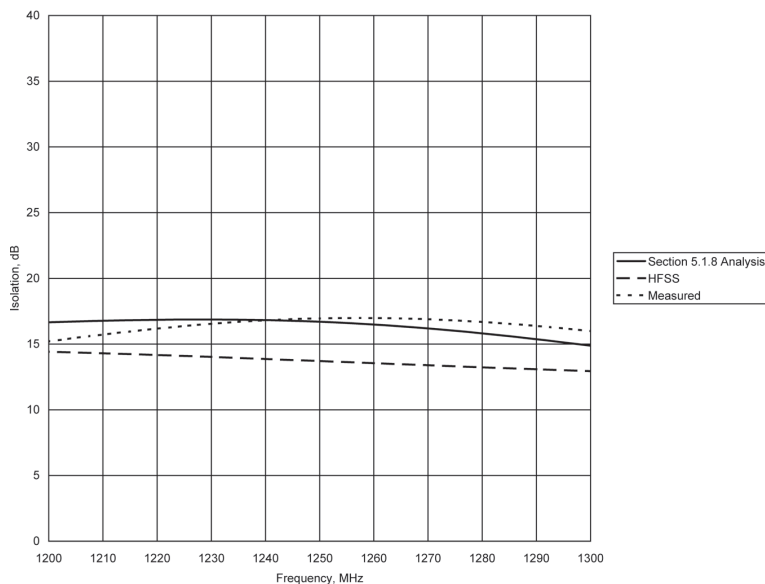


Figure 10.24 Isolation of example microstrip circulator. (Electrical testing services courtesy of UTE Microwave.)

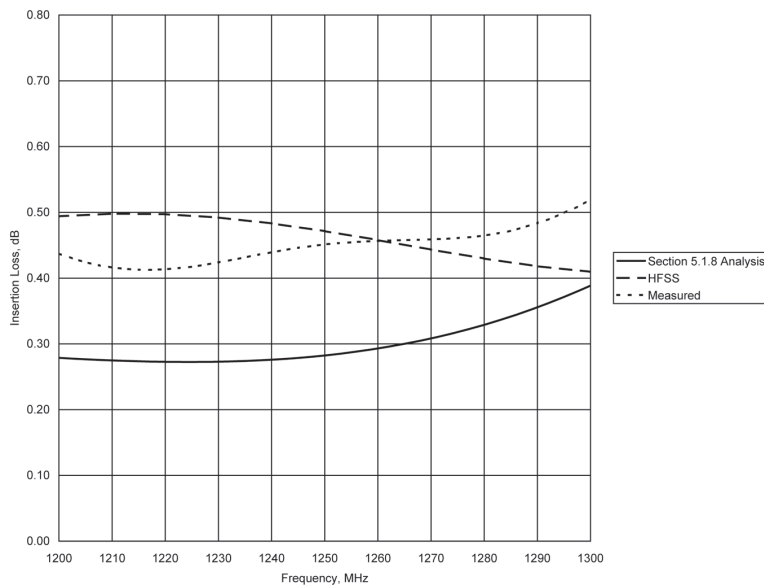


Figure 10.25 Insertion loss of example microstrip circulator. (Electrical testing services courtesy of UTE Microwave.)

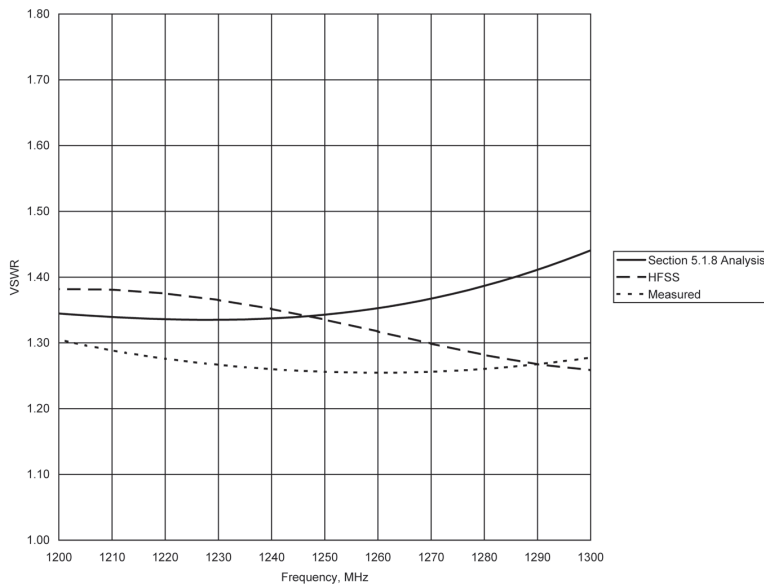


Figure 10.26 VSWR of example microstrip circulator. (Electrical testing services courtesy of UTE Microwave.)

10.6 Differential Phase Shift Circulator

Differential phase shift circulators are waveguide devices, capable of handling very high power levels. They are larger and heavier than lower-power junction circulators. Typically these devices cover narrow bandwidths because the high-power sources they are associated with are often limited in bandwidth. They can be made to cover waveguide bandwidths, though.

In this section, we will design the phase shifters in WR-112 (inside dimensions: 1.122×0.497 in) waveguide for a differential phase shift circulator having the block diagram of Figure 5.43. Although we will not design and fabricate custom hybrids for this example, we will fabricate and test the phase shifters. We will also construct a circulator by connecting the phase shifters between two commercial 180° hybrids (*magic tees*) and test the complete circulator. Our specifications for the differential phase shift circulator, over 7.75–8.00 GHz, are as follows:

- Isolation: 20 dB minimum;
- Insertion loss: 0.4 dB maximum;
- VSWR: 1.25:1 maximum;
- Power handling: 1W.

The nonreciprocal phase shifter topology will be as shown in Figure 5.48, and we will use (5.179) to predict the differential phase shift, with reference to Figure 5.46. If the RF power level were a concern, we could size the ferrite slabs to optimize cooling of the ferrites. Because the power level for this design example is not a concern, we arbitrarily set the length of the ferrite slabs to 5.5 in, so they would conveniently fit inside a 6-in long section of waveguide. The width of the ferrite slabs will be 0.250 in, which is also a somewhat arbitrary choice, and is a little less than one quarter of the waveguide width. We choose 0.093 in as the thickness of the ferrite slabs. None of the ferrite dimensions are particularly critical. Thinner ferrite slabs will generally allow for lower VSWR without any impedance matching structure. A design alternative would be to choose a ferrite material first, then size the ferrite to achieve the desired differential phase shift, but in this example, we chose the ferrite dimensions first.

Next, we need to choose an appropriate ferrite material and internal magnetic field intensity (H_{dc}). Knowing that we need a differential phase shift ($\beta_+ - \beta_-$) of $180^\circ = \pi$ radians over the 5.5-in length, or $\pi/5.5 = 0.571$ radians per in, we rearrange (5.179) to find the desired value of κ/μ :

$$\frac{\kappa}{\mu} = \frac{(\beta_+ - \beta_-) a^2}{2\pi d} = \frac{0.571 \text{ rad/inch} \cdot (1.122 \text{ inches})^2}{2\pi \cdot 0.250 \text{ inches}} = 0.458$$

For a below-resonance operating point, assuming $H_{dc} = 0$, we can approximate $\kappa/\mu \approx \gamma M_0 / \omega$. With a little algebraic manipulation, we find that the saturation magnetization ($4\pi M_S$) of the ferrite material should be

$$4\pi M_S = \frac{\frac{\kappa}{\mu} \cdot \omega}{\gamma} = \frac{0.458 \cdot 7875 \text{ MHz}}{2.80 \text{ MHz/Oe}} = 1290 \text{ G}$$

This value of $4\pi M_S$ is the minimum required to provide the desired 180° differential phase shift, with the ferrite slabs in exactly the right positions in the waveguide. To allow for some inaccuracy in positioning of the ferrites, we choose a somewhat higher value of $4\pi M_S = 1600 \text{ G}$. This could be a nickel spinel material for temperature stability and power handling.

We verified that 180° differential phase shift is attainable by simulating the phase shifter using Ansys® HFSS™. Figure 10.27 shows the geometry used for the simulation. The nonreciprocal phase shifter was fabricated, and we adjusted H_{dc} to achieve 180° differential phase shift at the center frequency, 7.875 GHz.

Next, we need to design a *reciprocal* phase shifter having the same phase shift as the nonreciprocal phase shifter in one direction of propagation. We produced this phase shift by loading another waveguide section with Teflon

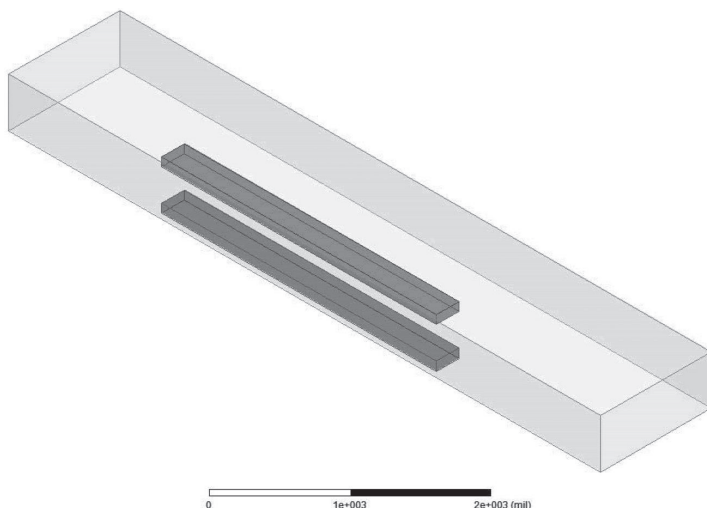


Figure 10.27 Model geometry of nonreciprocal phase shifter for electromagnetic simulation.

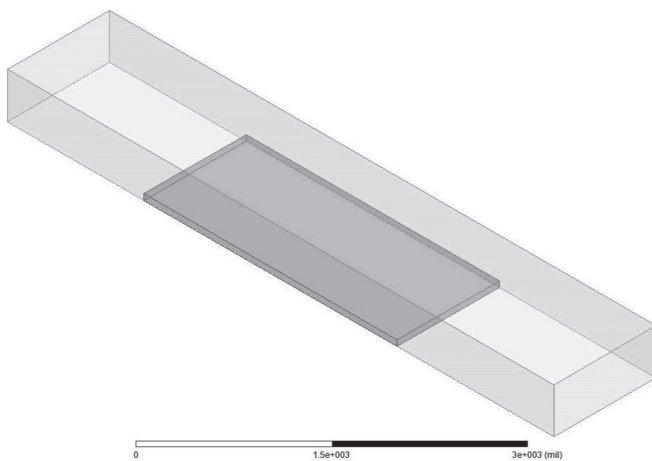


Figure 10.28 Model geometry of reciprocal phase shifter for electromagnetic simulation.

as shown in Figure 10.28. We adjusted the length of the Teflon slab until the phase shift of the nonreciprocal phase shifter in one direction of propagation matched the phase shift of the reciprocal phase shifter.

Finally, we constructed a circulator by connecting the nonreciprocal and reciprocal phase shifters between magic tees using swept H-plane waveguide bends. The assembled example circulator, without its nonreciprocal phase shifter bias magnets, is shown in Figure 10.29. Figures 10.30–10.32 show the electrical test results.



Figure 10.29 Example differential phase shift circulator.

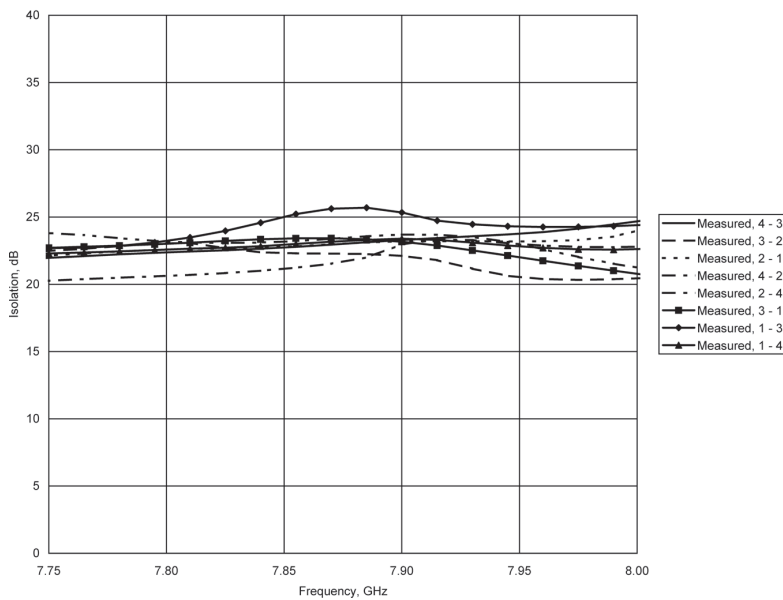


Figure 10.30 Isolation of example differential phase shift circulator. (Electrical testing services courtesy of UTE Microwave.)

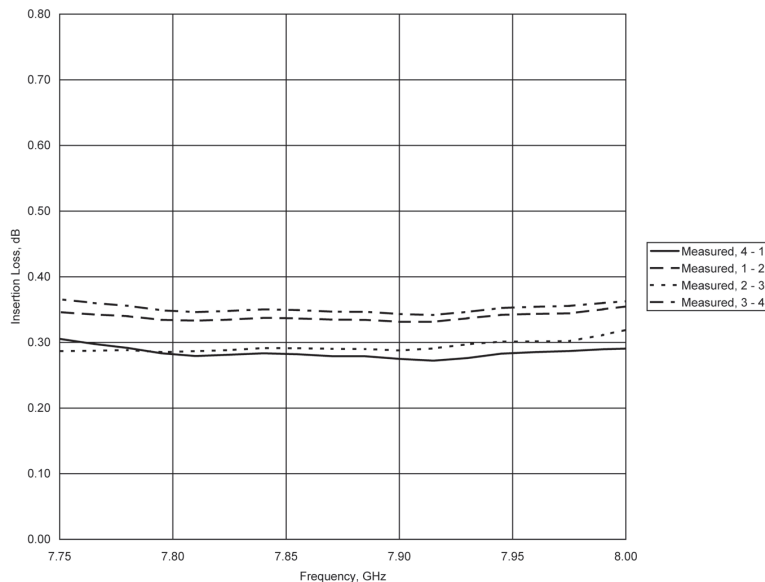


Figure 10.31 Insertion loss of example differential phase shift circulator. (Electrical testing services courtesy of UTE Microwave.)

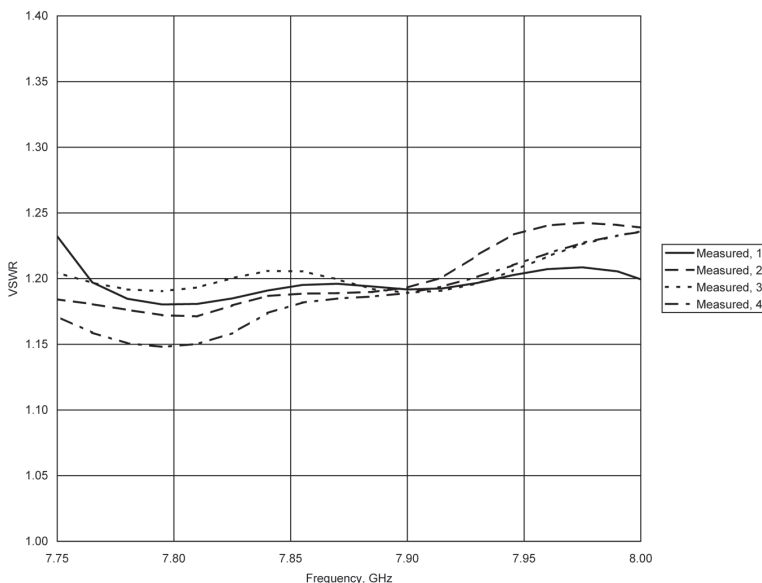


Figure 10.32 VSWR of example differential phase shift circulator. (Electrical testing services courtesy of UTE Microwave.)

10.7 Lumped-Constant Circulator

Lumped-constant circulators fit in small packages, often operating at lower frequencies than their distributed counterparts. The circuit complexity of the circulator is increased, however, and the power handling capability may be reduced below that of junction circulators. Lumped-constant circulators typically cover narrow bandwidths, but can be made to cover bandwidths of 50% or more.

We will design a small (about 1.25 in \times 1.25 in) lumped-constant circulator covering 800–950 MHz. Our electrical specifications for this circulator are as follows:

- Isolation: 17 dB minimum;
- Insertion loss: 0.5 dB maximum;
- VSWR: 1.25:1 maximum;
- Power handling: 1W.

First, we select a ferrite material for the circulator using the criteria presented in Chapter 4. This is an above-resonance circulator, which requires a strong magnetic bias. We choose to use a moderate $4\pi M_S$ to avoid the use of

large or high-energy magnets. The resonance line width (ΔH) of the ferrite material should be as narrow as possible to minimize insertion loss. These requirements of low ΔH and moderate $4\pi M_s$ lead us to select YIG. Typical properties for YIG are as follows:

- $4\pi M_s$: 1780 G;
- ΔH : 45 Oe;
- ϵ : 15;
- $\tan \delta$: 0.0002.

Next, we select a preliminary value of H_{dc} . H_{dc} must be high enough to maintain low insertion loss, yet low enough to provide for the necessary bandwidth. Because this is to be an above-resonance circulator, we must have H_{dc} greater than the value corresponding to ferrimagnetic resonance at the upper frequency band edge:

$$H_{dc} > \frac{f_2}{\gamma} = \frac{950 \text{ MHz}}{2.80 \text{ MHz/Oe}} = 339 \text{ Oe}$$

Knowing the ferrite material properties, we estimate the insertion loss contribution from magnetic losses as described in Section 5.1.3 using (1.30–1.33), (5.6), and (5.23), with $Q_U = \mu_{eff}' / \mu_{eff}''$ and Q_L approximated by (5.27). The insertion loss of this circulator is not critical, and we find from the analysis that the magnetic losses are about 0.25 dB at $H_{dc} = 380$ Oe, so we will use this operating point.

Using (1.30–1.33) again at the center frequency, with find that

$$\frac{\kappa'}{\mu'} = 0.77$$

and applying (5.174 and 5.175),

$$\kappa' = \frac{\gamma M_0 \omega}{\omega_0^2 - \omega^2} = \frac{2.80 \text{ MHz/Oe} \cdot 1780 \text{ G} \cdot 875 \text{ MHz}}{(2.80 \text{ MHz/Oe} \cdot 380 \text{ Oe})^2 - (875 \text{ MHz})^2} = 11.9$$

$$L_0 = \frac{Z_0}{1.73\omega \cdot \kappa} = \frac{50 \Omega}{1.73 \cdot 2\pi \cdot 875 \text{ MHz} \cdot 11.9} = 0.442 \text{ nH}$$

We compute a series capacitor value using (5.173) and (5.176):

$$\mu' = 1 + \frac{\gamma M_0 \omega_0}{\omega_0^2 - \omega^2} = 1 + \frac{2.80 \text{ MHz/Oe} \cdot 1780 \text{ G} \cdot 2.80 \text{ MHz/Oe} \cdot 380 \text{ Oe}}{(2.80 \text{ MHz/Oe} \cdot 380 \text{ Oe})^2 - (875 \text{ MHz})^2} = 15.5$$

$$C = \frac{1}{\omega^2 L_0 \mu} = \frac{1}{(2\pi \cdot 875 \text{ MHz})^2 \cdot 0.442 \text{ nH} \cdot 15.5} = 4.84 \text{ pF}$$

Next, we set the ferrite disk diameter at 0.400 in, or about $\lambda/10$, and the disk thickness at one tenth of this value, 0.040 in. Using two strips, with the strip length equal to the ferrite disk diameter, and with recourse to (5.177), we compute the required strip Z_0 from the previously calculated inductance (L_0):

$$Z_0 = \frac{2L_0}{0.400 \text{ inches} \cdot 0.08467} = \frac{2 \cdot 0.442 \text{ nH}}{0.0339} = 26.1 \Omega$$

Using the stripline characteristic impedance (5.50–5.52), we find that this Z_0 corresponds to a strip width of about 0.035 in.

At this stage, the design of the circulator could be optimized empirically, or using a combination of electromagnetic simulations and circuit simulations. We will perform an electromagnetic simulation using Ansys® HFSS™. Figure 10.33 shows the geometry for the Ansys HFSS electromagnetic simulation. The strip thickness is 0.005 in, and 0.002-in thick Teflon tape will be used between the strips, which will not be interwoven for this design.

Figure 10.34 shows the results of the electromagnetic simulation; a simulated reflection response and measured data for the circulator without its lumped impedance matching components. Both of the traces were generated over the 800–950 MHz frequency range.

We constructed a circulator without its lumped impedance matching components, implementing the design described in this section in a package

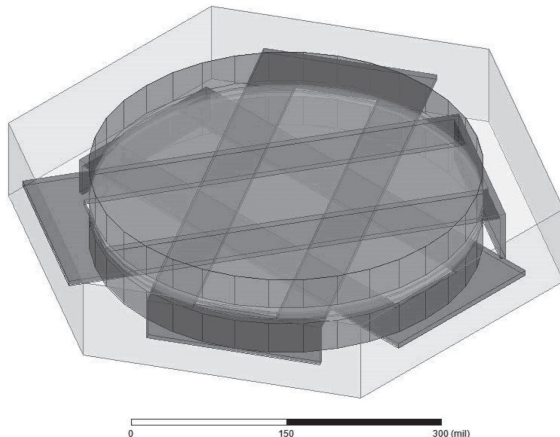


Figure 10.33 Model geometry for electromagnetic simulation of lumped-constant circulator.

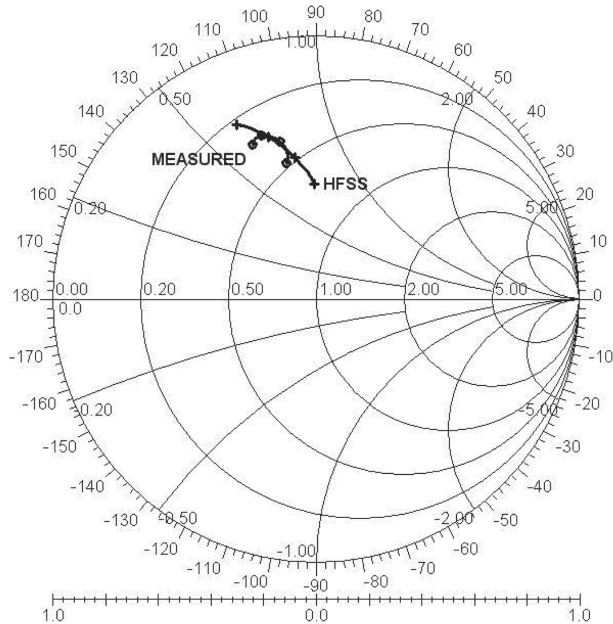


Figure 10.34 Measured and simulated reflection of lumped-constant example circulator over 800–950 MHz.

having SMA connectors. Using measured data and Ansys Designer circuit simulation software, we synthesized and optimized lumped impedance matching networks for the circulator. Figure 10.35 shows the circuits for two of the circulator ports. The circuits (and circulator) are not perfectly symmetrical. One cause of asymmetry is that the strips were not interwoven, so the strips connected to each port have different exposures to the ferrite disks. Electrical test results for the circulator with its impedance matching networks, together with circuit simulation results are shown in Figures 10.36–10.38.

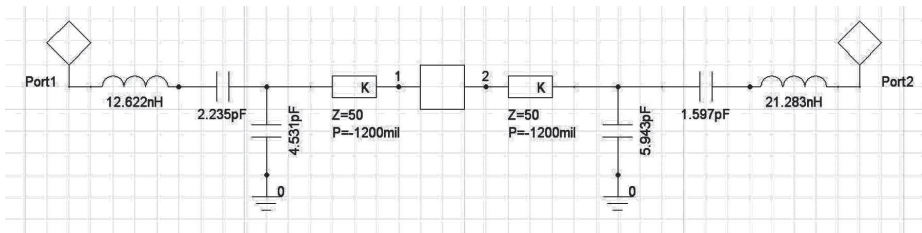


Figure 10.35 Impedance matching circuitry for example lumped-constant circulator.

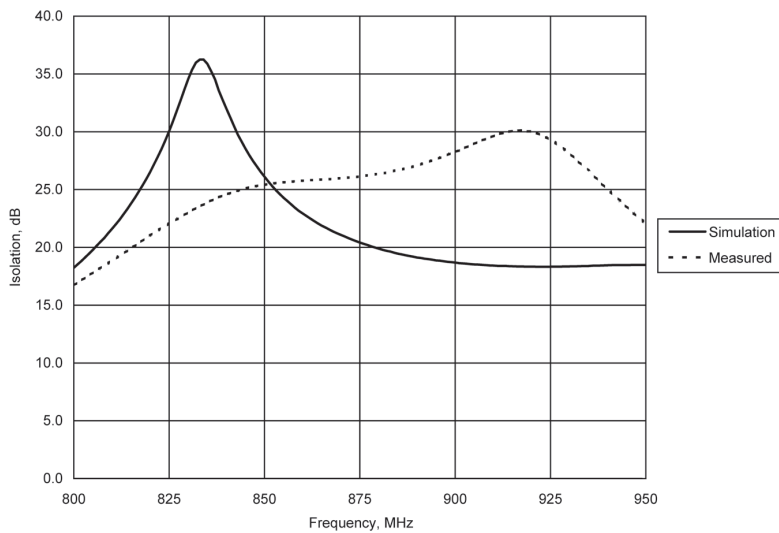


Figure 10.36 Isolation of example lumped-constant circulator. (Electrical testing services courtesy of UTE Microwave.)

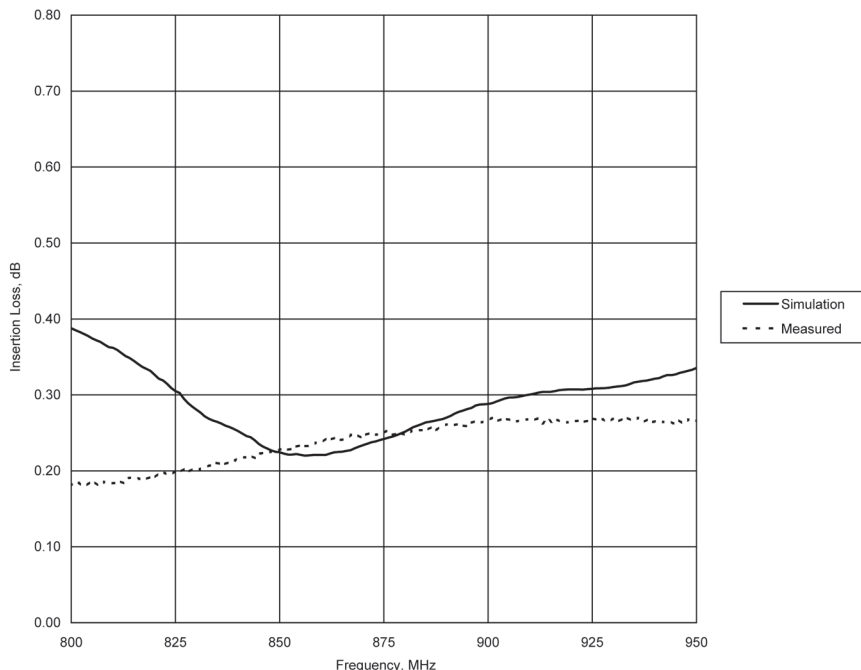


Figure 10.37 Insertion loss of example lumped-constant circulator. (Electrical testing services courtesy of UTE Microwave.)

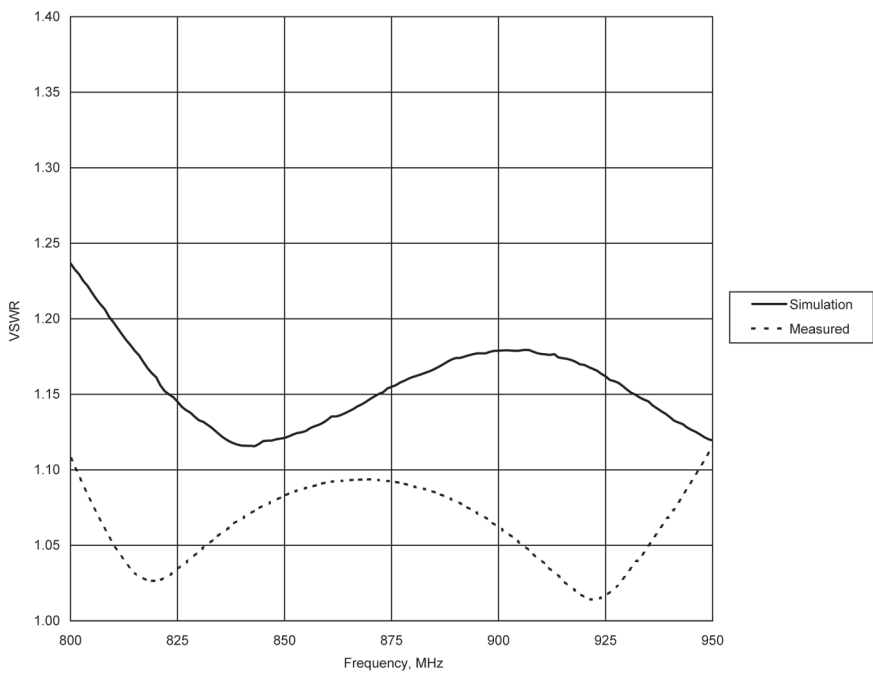


Figure 10.38 VSWR of example lumped-constant circulator. (Electrical testing services courtesy of UTE Microwave.)

Reference

- [1] Helszajn, J., *The Stripline Circulator: Theory and Practice*, Hoboken, NJ: John Wiley and Sons, 2008.

List of Symbols

a = Waveguide width, Coaxial dielectric inner diameter, Intermediate variable in network synthesis, Ferrite dimension along x -axis

b = Magnetic induction, Ground-plane spacing, Waveguide height, Coaxial dielectric outer diameter, Intermediate variable in network synthesis, Ferrite dimension along y -axis

c = Velocity of light = 2.998×10^8 m/s, Intermediate variable in network synthesis, Ferrite dimension along z -axis

d = Ferrite thickness, Wire diameter, Gap length

d_0 = Intermediate variable in network synthesis

e = Unit electron charge = 1.602×10^{-19} coulomb

f = Frequency

f_C = Cutoff frequency

f_0 = Center frequency

f_1 = Lower frequency limit

f_2 = Upper frequency limit

f' = Scaled frequency

g = Landé splitting factor (g factor), Pole piece gain

g_{eff} = Effective g factor

h = Magnetic field intensity, Planck's constant = 6.625×10^{-34} J/s

i = Current in electromagnet

k = Wave number, Thermal conductivity

k_0 = Wave number at λ_0

m = Electron magnetic moment, Magnetization, Ferrite shape factor

m_0 = Electron mass = 9.11×10^{-31} kg

n = Number of heat sink fins, Number of transformers, Intermediate variable in network synthesis, Number of abstract layers in transient thermal analysis

p = Intermediate variable in network synthesis, Air pressure

q = Intermediate variable

r = Radius, Circulator input VSWR, Intermediate variable in network synthesis

s = Resonator spacing

s_0 = Eigenvalue

s_- = Eigenvalue

s_+ = Eigenvalue

t = Time, Stripline thickness, Dielectric thickness

t_1 = Intermediate variable in network synthesis

t_2 = Intermediate variable in network synthesis

t^*_2 = Intermediate variable in network synthesis

w = Heat sink fin spacing, Fractional bandwidth

x = Position of ferrite slab in waveguide, Coordinate axis

\hat{x} = Unit vector in x direction

y = Coordinate axis

\hat{y} = Unit vector in y direction

z = Heat sink fin height, Coordinate axis

\hat{z} = Unit vector in z direction

A = Area, Ferrite triangle altitude, Altitude derating factor, Intermediate variable, Altitude, Directional coupler directivity

A_{eff} = Effective ferrite triangle altitude

A_g = Area of air gap

A_i = Area of iron or steel

A_m = Magnet area

A' = Intermediate variable

B = Magnetic induction, Susceptance, Intermediate variable

B_d = Magnet induction at operating point

B_g = Magnetic induction in air gap

B_i = Magnetic induction in iron or steel

BW = Bandwidth

B' = Circulator junction susceptance slope parameter, Intermediate variable

C = Capacitance, Intermediate variable, Specific heat capacity, Flow rate
(vent-hole pumping conductance), Source match term

C_a = Disk capacitance term

C_r = Disk capacitance term

$CVCM$ = Collected Volatile Condensable Materials

C_2 = Disk capacitance term

C_{2s} = Disk capacitance term

C_f' = Fringing capacitance

D = Inductor coil diameter, Determinant, Vent-hole diameter

D_D = Dielectric diameter

D_{disk} = Diameter of ferrite disk

D_{ring} = Diameter of ferrite ring

D' = Intermediate variable

F = Applied force, Frequency, Flow rate of water or air, Fourier number,
Magnetic leakage factor

G_r = Circulator junction conductance

H = Magnetic field intensity

H_a = Anisotropy magnetic field intensity

H_C = Critical microwave magnetic field intensity, Magnetic coercivity

H_d = Magnet field strength at operating point

H_{dc} = Internal dc magnetic field intensity

H_{ext} = Applied external dc magnetic field intensity

H_{RF} = RF magnetic field intensity

H_{dc}' = Scaled dc magnetic field intensity

I = Isolation

I_{RF} = RF current

IM_3 = Third-order intermodulation

IP_3 = Third-order intercept point

K = Intermediate variable in network synthesis

L = Angular momentum, Length, Inductance

L_g = Length of air gap

L_m = Magnet length

L_p = Pole piece thickness

L_0 = Inductance of lumped-element circulator coil in air

L_{\pm} = Inductance of lumped-element circulator coil for two modes

M = Total ferrite magnetization, Integer, Mass, Magnetic moment

$MTBF$ = Mean Time Between Failures

M_0 = Ferrite magnetization

M'_0 = Scaled ferrite magnetization

N = External torque, Integer, Number of turns of wire in a coil,
Demagnetizing factors

P = Power, Intermediate variable

P_g = Permeance of working gap

P_{in} = Average input power

$P_{leakage}$ = Permeance due to leakage flux

P_{output} = Output power

P_t = Total Permeance

Q = Dissipated power, Outgassing rate

Q_L = Loaded Q of circulator junction

Q_u = Unloaded Q of circulator junction

R = Ferrite radius, Resonator radius, Electromagnet winding resistance,
Resistance, Radial distance

R_C = Cavity radius

R_{eff} = Effective resonator radius

R_g = Reluctance of air gap

R_i = Reluctance of iron or steel path

R_{in} = Circulator input resistance

RL = Return Loss

R_0 = Characteristic plane radius

R_1 = Resistance

R_2 = Resistance

R' = Scaled disk radius

S_{\min} = Minimum VSWR

S_{\max} = Maximum VSWR

$\mathbf{S}_{11}, \mathbf{S}_{12}, \mathbf{S}_{21}, \mathbf{S}_{22} \dots$ = Scattering- (S-) parameters

$\mathbf{S}'_{11}, \mathbf{S}'_{12}, \mathbf{S}'_{21}, \mathbf{S}'_{22} \dots$ = Scattering- (S-) parameters of cascaded segments

T = Temperature rise or drop, Layer temperature in transient thermal analysis, Air temperature

\mathbf{T} = Scattering- (S-) parameters of a cascaded device (\mathbf{T})

\mathbf{T} = Generalized tensor

T_C = Curie temperature

TML = Total Mass Loss

TOI = Third-Order Intercept

U = Perimeter (or circumference) of pole piece

V = Voltage

V_{dw} = Dielectric withstanding voltage

$VSWR$ = Voltage Standing Wave Ratio

$VSWR_C$ = Circulator Voltage Standing Wave Ratio

$VSWR_L$ = Load Voltage Standing Wave Ratio

$VSWR_S$ = Source Voltage Standing Wave Ratio

W = Stripline width, Energy required to magnetize ferrite

X = Phase compensation for waveguide step discontinuity

X_{in} = Circulator input reactance

X_1 = Intermediate variable in network synthesis

X_2 = Intermediate variable in network synthesis

X_3 = Intermediate variable in network synthesis

Y_{eff} = Effective circulator junction admittance

Y_r = Circulator junction admittance

Y_s = Characteristic admittance of short-circuited stub of resonator equivalent circuit

Y_0 = Characteristic admittance

Z = Impedance

Z_d = Diode impedance (in one-port negative-resistance amplifier)

Z_n = Eigenvalue term

Z_t = Transformer impedance

Z_ψ = Stripline characteristic impedance

Z_0 = Characteristic impedance

Z_{0S} = Static microstrip characteristic impedance

Z^0 = Eigenvalue

Z^+ = Eigenvalue

Z^- = Eigenvalue

α = Damping factor, Attenuation constant, Thermal diffusivity, Ratio of waveguide heights

β = Phase constant, Wave number, Intermediate variable in network synthesis

β_\pm = Phase constants for two modes

γ = Gyromagnetic ratio = 2.80 MHz/Oe

γ_{eff} = Effective gyromagnetic ratio

δ = Dielectric loss angle, Air density

ϵ = Permittivity (relative or absolute, depending on context), Intermediate variable in network synthesis

ϵ_D = Dielectric disk permittivity

ϵ_{eff} = Effective microstrip permittivity

ϵ_0 = Free-space permittivity = 8.85×10^{-12} F/m

θ = Angle

θ_0 = Angle

κ = Component of susceptibility and permeability tensors

κ' = Real component of κ

κ'' = Imaginary component of κ

λ = Wavelength, Mean free path

λ_C = Cutoff wavelength

λ_D = Wavelength in dielectric ring

λ_g = Guide wavelength

λ_0 = Wavelength at f_0

μ = Permeability (scalar)

$\boldsymbol{\mu}$ = Permeability (complex)

$\boldsymbol{\mu}$ = Permeability (tensor)

μ_e = Effective microstrip permeability

- μ_{eff} = Effective permeability
 μ_z = Permeability in direction of applied dc magnetic field
 μ_0 = Free-space permeability = $4\pi \times 10^{-7}$ H/m
 μ' = Real component of μ , Permeability of partially-magnetized ferrite
 μ'' = Imaginary component of μ
 μ_{eff}' = Real component of effective permeability
 μ_{eff}'' = Imaginary component of effective permeability
 μ_z' = Permeability of partially-magnetized ferrite in direction of applied dc magnetic field
 μ_0' = Permeability of demagnetized ferrite
 π = Archimedes' constant = 3.1415927
 ρ = Voltage reflection coefficient, Ferrite density
 ρ_C = Circulator voltage reflection coefficient
 ρ_D = Directional coupler voltage reflection coefficient
 ρ_L = Load voltage reflection coefficient
 ρ_S = Source voltage reflection coefficient
 σ = Electrical conductivity
 τ = Group delay
 τ_D = Directional coupler transmission coefficient
 ϕ = Angle, Faraday rotation, Magnetic flux
 χ = Susceptibility (complex)
 χ = Susceptibility (tensor)
 χ' = Real component of χ
 χ'' = Imaginary component of χ
 ψ = Stripline angle
 ω = Precession radian frequency, Microwave radian frequency
 ω_0 = Ferrimagnetic resonance radian frequency
 ω_{\pm} = Resonant radian frequencies of two modes
 Γ = Propagation constant
 Γ_L = Complex load reflection coefficient
 Γ_3 = Complex reflection coefficient of device connected to port 3
 Γ_{\pm} = Propagation constants for two modes

Δd = Ferrite thickness correction factor, Ferrite layer thickness in transient thermal analysis

Δt = Time step in transient thermal analysis

ΔH = Resonance line width

ΔH_{eff} = Effective resonance line width

ΔH_k = Spin-wave line width

ΔL = Length compensation for waveguide step discontinuity

ΔT = Temperature drop or rise

$\Delta \rho$ = Uncertainty in measured voltage reflection coefficient

$\Delta \tau$ = Uncertainty in measured voltage transmission coefficient

$4\pi M$ = Ferrite magnetization

$4\pi M_S$ = Ferrite saturation magnetization

$4\pi M_{S\ disk}$ = Ferrite disk saturation magnetization

$4\pi M_{S\ ring}$ = Ferrite ring saturation magnetization

Frequently Used Equations

$$\omega_0 = \gamma H_{dc} \quad (1.7)$$

$$VSWR = \frac{1 + \rho}{1 - \rho} \quad (2.4)$$

$$RL = -20 \cdot \log_{10} \rho \quad (2.5)$$

$$MismatchLoss = -20 \log_{10} \left(1 - |\rho|^2 \right) \quad (5.131)$$

$$InsertionLoss(dB) = 10 \log_{10} \left(1 - \frac{Q_L}{Q_u} \right) \quad (5.23)$$

$$P = \frac{V_{dw}^2}{Z_0(1 + \rho)^2 \sqrt{F_A}} \quad (2.9)$$

$$I = -20 \cdot \log_{10} \left(\frac{\rho_S - \rho_C}{\rho_L + \rho_C} \right) \quad (2.13)$$

$$\mathbf{S}_{11}' = \mathbf{S}_{11} + \frac{\mathbf{S}_{12}\mathbf{S}_{21}\boldsymbol{\Gamma}_L}{1 - \mathbf{S}_{22}\boldsymbol{\Gamma}_L} \quad (2.16)$$

$$4\pi M_S < \frac{\omega}{\gamma} - H_a \quad (4.4)$$

$$R = \frac{1.84\lambda}{2\pi\sqrt{\mu_{\text{eff}}\epsilon}} \quad (5.9)$$

$$k_0 R = \frac{1}{\sqrt{\epsilon}} \sqrt{\left(\frac{\pi R}{2d}\right)^2 + (1.84)^2} \quad (5.39)$$

Below resonance:

$$\kappa' = \frac{\kappa}{\mu} = \frac{\gamma M_0}{\omega} \quad (5.183)$$

$$\mu' \approx 1$$

$$\mu_{\text{eff}} = 1 - \kappa^2 = 1 - \frac{\gamma^2 M_0^2}{\omega^2} \quad (5.28)$$

Above resonance operating point:

$$\kappa' = \frac{\gamma M_0 \omega}{\omega_0^2 - \omega^2} \approx \frac{M_0 \omega}{\gamma H_{\text{dc}}^2} \quad (5.174)$$

$$\mu' = \mu_{\text{eff}} = 1 + \frac{\gamma M_0 \omega_0}{\omega_0^2 - \omega^2} \approx 1 + \frac{M_0}{H_{\text{dc}}} \quad (5.173)$$

$$\frac{\kappa}{\mu} = \frac{M_0 \omega}{\gamma H_{\text{dc}} (H_{\text{dc}} + M_0)} \quad (5.48)$$

$$B' = \frac{\omega \Delta B}{2 \Delta \omega} \quad (5.124)$$

$$Q_L = \frac{B'}{G} \quad (5.125)$$

$$\frac{\kappa}{\mu} = \frac{0.71}{Q_L} \quad (5.27)$$

$$Q_u = \frac{1}{\left| \frac{\mu_{eff}''}{\mu_{eff}'} \right| + \tan \delta} \quad (5.111)$$

$$Z = Z_0 \frac{(Z_{in}/Z_0) + j \tan \beta L}{1 + j(Z_{in}/Z_0) \tan \beta L} \quad (5.127)$$

$$\lambda_g = -\frac{1}{\sqrt{\frac{1}{\lambda_0^2} - \frac{1}{\lambda_c^2}}} \quad (5.160)$$

$$P \propto \frac{\omega^2 \Delta H_k^2}{\gamma_{eff}^2 4 p M_S^2} \quad (5.202)$$

$$H_{dc} = \sqrt{[H_{ext} + (N_x - N_z)M_0][H_{ext} + (N_y - N_z)M_0]} \quad (6.12)$$

$$N_x - N_z = N_y - N_z = \frac{c - a}{a + 2c} \quad (6.22)$$

$$L_m = \frac{H_{ext} A_g (R_g + R_i)}{H_d} \quad (6.39)$$

$$\Delta T = \frac{Qd}{kA} \quad (7.1)$$

$$\lambda = 2.61 R_C \sqrt{\mu_{eff} \epsilon} \quad (7.12)$$

$$C = \frac{0.225 \epsilon A}{t} \quad (\text{pF}) \quad (7.26)$$

$$M = 5 \times 10^6 \cdot B \cdot R^3 \quad (8.2)$$

About the Author

Douglas Linkhart is originally from New Jersey. He is a graduate of Thomas Edison State College in New Jersey, with a BS in computer science, and earned BS/BA and MBA degrees from the University of South Florida. He has completed additional degrees in computer science, physics, drafting and design, and automotive technology. He was a physics major at Trenton State College in New Jersey, and studied engineering management at the University of Evansville in Indiana. Mr. Linkhart is a Microsoft Certified Systems Engineer (MCSE), a Certified Master Electronics Technician (CETma), and holds an FCC General Radiotelephone (commercial) License with a Radar Endorsement. He authored the first edition of *Microwave Circulator Design* in 1989. He is also an author of “Unequal Splitter Design” (presented at RF Expo East, 1988), “Disk-Rod Filter Design” (presented at RF Expo East, 1989), software on RF Design Software Service disk RFD-0490 (April 1990), and “Twisted-Wire Transmission Line Design” (*RF Design* magazine, June 1990).

Mr. Linkhart has nearly 35 years of professional experience in the microwave industry, mostly in the design and engineering of microwave circulators and other components. He has worked for Micon and Triangle Microwave in New Jersey, MPD in Kentucky, and TRAK Microwave, Diversitronix, and Group Technologies in Florida. He currently works in Florida as a senior engineer, designing and engineering microwave circulators for military and space applications. He is a senior member of the IEEE and has served on the editorial board of the *IEEE Transactions on Microwave Theory and Techniques*.

His interest in microwave circulators started with bicycle racing as a teenager. At that time he met another cyclist whose father manufactured circulators in a garage shop. He was later hired as a machinist, and learned that an isolator does for RF what a diode does for dc. This early introduction to circulators ultimately led to a career devoted primarily to circulators.

Index

- Above resonance
 - circulator design procedure, 125
 - definition, 44
- Absorption method of matching, 290
- Absorptive
 - elements in dummy loads, 179
 - waveguide elements, 181
- Accuracy of measurement system, 271
- Active circulator, 32
- Alloy, temperature compensation, 102
- Altitude, 37, 47
 - derating factor, 42
- Aluminum substitution, 88
- Amplifier
 - buffer, 70
 - negative resistance, 79
 - stability, 70
- Amplitude
 - matching, 37, 40
 - tracking, 37, 40
- Analysis of variance (ANOVA), 278
- Andradite, 5, 87
- Angle units, 1
- Angular momentum, 6
- Anisotropy, 97
 - field, 97
- Antenna array performance, 40
- Antiferromagnetism, 8
- Area units, 1
- Assumptions, circulator design, 111
- Attenuation constant, 24, 27
- Auld, B. A., 122
- Average power
 - capacity
 - cables, 43
- connectors, 43
- junction circulators, 55, 188
- failure mode, 41
- Bandwidth
 - circulator, 37–38, 114, 126
 - differential phase shift, 60
 - equation, 114
 - junction, 55
 - lumped-element, 57
 - waveguide junction, 162
- effect of decoupling on, 189–190
- expression for, 114
- isolator,
 - field-displacement, 61
 - resonance, 65, 177
- maximum mode-free, 247
- relation to magnetic field, 282
- Bell Labs, 5
- Bessel function, 112
- B-H characteristics of metals, 215
- Bicycle wheel analogy, 11
- Bode, H. W., 286
- Bohr magneton, 14
- Bonds, ionic, 5
- Bosma, H., 111
- Breakdown power, calculation of, 193
- Calibration of test equipment, 271
- Capacitors
 - lumped-element circulator, 170
 - procedure for design, 255–256
- Cation size, 10
- Cavity modes, 244
 - excitation, 244

- Center cavity size, 244
Center conductor, 111–112
 circulator, 54
geometries, 123, 143
 apex-coupled triangle, 143
 characterization, 143
 disk, 143
 hexagon, 143
 side-coupled triangle, 144
 wye, 145
 wye with stubs, 145
resonator evaluation, 146–147
- Ceramic dielectrics, 103
Ceramic magnets, 9
CGS system of units, 1
Channel widths, 248–249
- Characteristic impedance
 microstrip, 158
 stripline, 129
 transformer, 132
 waveguide, 163
- Characteristic plane, 121
 location, 121
- Characteristics
 garnets, 93
 spinels, 93
- Circular polarization, waveguide, 174
- Circulation
 directions of, 114
 perfect, 108
- Circulator
 active, 32
 below-resonance, 123
 cascading with another device, 51
 composite-ferrite, 56, 165
 definition, 36
 failures, 35
 faraday-rotation, 16
 frequency range, 37
 general requirements for space
 applications, 48
 nanotechnology, 30
 octave-bandwidth, 123
 Okada, 61
 parameters, 37
 self-biased, 99–100
- semiconductor, 29
 experimental results, 29
 frequency limitation, 30
- short circuit at one port, 52
- stripline, 111, 123
 computation of performance metrics, 156
 effective disk radius, 157
 performance analysis, 156
 synthesis, 153
- switching, 60
- synthesis procedure, 153
- tracking, 313
- waveguide junction, 117, 120, 161
- Clarricoats, P. J. B., 172
- Cleaning
 circulator parts, 263
 ferrites, 89
- Coaxial circulator construction, 54
- Coercive force, magnet, 101
- Compression of ferrites, 242
- Comstock, R. L., 114
- Concurrent engineering (CE), 262
- Conductance, circulator junction, 127, 131
 Graphs, 128, 134, 150–152
- Conduction cooling, 234
- Conductivity, ferrite, 10
- Connectors, coaxial, 266
 center pin captivation, 266
 gauge, 267
 pin depth, 267
- Construction, isolator
 field-displacement, 61
 resonance, 64–65
- Contact, ferrite-ground plane, 242
- Controlling variation, 311
- Conversion
 factors, 1
 VSWR-reflection coefficient, 38
- Cooling
 circulator, 55–56
 junction, 56
 methods, 37, 47, 234
 conduction, 234
 forced-air, 235
 natural-convection, 234

- water, 235
- Coordination, ion site, 7
- Critical power, circulator, 44
- Crystal
- ionic, 5
 - lattice matching, 31
 - plane, 7
 - structure, 5
- Curie temperature, 46, 93
- measurement of, 92
- Cut-off wavelength, stripline, 129
- Cyclotron resonance, 29
- Damping factor, 18
- Data, recording of, 271
- Davies, J. B., 122
- De-embedding
- circulator junction, 287
 - lumped-element procedure, 291
- Decoupling, 189–190
- Degenerate PARAMP, 77
- Demagnetization curve, 216
- Demagnetizing factors, 15, 207, 210
- Design examples
- above-resonance stripline junction, 302
 - below-resonance stripline junction
 - circulator, 311
 - differential phase shift circulator, 329
 - lumped-constant, 333
 - microstrip, 324
 - waveguide junction, 319
- Design for manufacturing (DFM), 262
- Development of ferrite, 5
- Deviation from linear phase (DLP), 40
- Dielectric
- ceramic, 103
 - classification, 103
 - constant, 103
 - ferrite, 93
 - transformer, 132
 - measurement, 93
 - gases, 103
 - loss, ferrite, 11
 - loss tangent, ferrite, 93
 - material, resonance isolator, 177–178
 - silicone, 103
- sleeves, 162
- withstanding voltage, 42
- Differential phase shifts
- calculation of, 175
 - implementation of, 171
- Dimensional tolerances, ferrite, 90
- Dimensions
- importance of, 263
 - stripline center conductor, 111–112
- Diode
- avalanche, 79
 - BARITT, 80
 - IMPATT, 79
 - performance, 80
 - TRAPATT, 79–80
- Diplexer, 76
- Disk radius, ferrite, 162
- Dissimilar metals, 253
- Doping, rare-earth, 99
- Dunn, V. E., 169
- Duplexer, ferrite, 71
- Dyad, vector, 17
- Eddy-current losses, ferrite, 10
- Effective
- g-factor, 14, 15
 - gyromagnetic ratio, 15, 92
 - line width, 92
 - permeability, 112
 - above-resonance, 113, 125
 - below-resonance, 117, 131
 - microstrip structure, 158–159
 - transverse field, 25
 - graphs, 25, 26
- Eigenvalues, 295
- from two-port S-parameters, 296
 - phasor diagrams, 296–299
- Eigenvalue test sets, 295
- Electromagnet, 225
- Electromagnetic shielding, 37
- Electron,
- collision frequency, 30
 - mobility, 30
 - seeding, 275
 - spin, 13
- Ellipsoid model, 209

- Elliptical polarization, 26–28
EMI shielding, 46
Energy
 product of magnet, 101
 required to magnetize ferrite, 226
English system of units, 1
Environmental factors, 37, 47
Equivalent circuit, circulator, 116, 132, 139, 155, 286
- Face-centered-cubic (FCC) lattice, 7
Factors, conversion, 1
Fano, R. M., 286
Faraday effect, 15
Faraday, M., 15
Faraday rotation, 16, 27
Fay, C. E., 114
FCC lattice, 7
Ferrimagnetic
 materials, 4
 resonance, 11
 curve, shape of, 98
 resonance absorption, 28
Ferrimagnetism, 4, 88
Ferrite, 4
 cation size, 10
 classes of, 5
 crystal structure, 5
 Curie temperature comparison, 264
 demagnetization factors, 207
 density measurement, 264
 development, 5
 dielectric loss, 11
 disk conversion to triangle, 132, 162
 disk
 diameter, 123, 124, 170
 dimensions, 121
 radius, 113, 121, 127, 131, 162
 thickness, 121, 127, 131, 170
 garnet, 5
 grain size effects, 10
 hexagonal, 5, 9
 composition, 10
 composition variation, 9
 magnetic anisotropy, 9
 planar and uniaxial, 9
- S, R, and T blocks, 9
 types (M, Y, W, and Z), 9
hysteresis loop, 226
magnetization, symbol for, 4
magnetostrictive effects, 89
manufacturing, 88–89
material, 16
microstructure, 10
mounting, 264
polycrystalline, 5
positioning, 265
relaxation theory, 11
retentivity, 226
shape, 108
slab
 dimensions, 175
 position, 175–176
sphere as test sample, 91
spinel, 6
temperature compensating, 102
tests, to discriminate, 264
thermal annealing, 89
thickness, 145, 162
thin films, 31
triangle correction factor, 122
- Ferromagnetism, 8
Field-displacement isolator pictures, 63
Field patterns, triangular, 109
Filling factor, 190
Finishing, 37, 253
Firing of ferrites, 89
Flux density in shield material, 217
Forced-air cooling, 235
Forming of ferrite shapes, 89
Free magnetic poles, 208
Frequency
 dispersion, microstrip, 158–159
 limits
 field-displacement isolator, 63
 junction circulator, 55
 lumped-element circulator, 56–57
 range, 37
 resonance, triangular resonator, 122
 sensitivity,
 phase shifter, 81
 transmission lines, 290

- splitting, 110, 115
above-resonance approximation, 127
below resonance, approximation, 131
graph, 27
variation with saturation
magnetization, 115
- G-effective value, 14, 15, 92
G factor, 14
Gadolinium, 88, 99
Gadolinium gallium garnet (GGG), 31
Gain
negative resistance amplifier, 80
pole piece, 224
- Galvanic
corrosion, 105, 253
series, 105, 253
- Garnets, 5, 9, 87
Geometry, circulator, 172
Gilbert equation of motion, 18
Grain size, ferrite, 10, 90
Green, J. J., 124
Green's function, 112
Griffiths, 14
Ground-plane spacing, 123, 193–194
Ground planes, circulator, 54
Group delay, 37, 40
flatness, 40
- Guide wavelength, 162
- Gyromagnetic ratio, 4, 15
effective, 15, 92
- Gyroscope system, 12
- Gyroscopic effect, 12
- Harmonic generation, 44, 58
- HCP lattice, 7
- Heat conduction formula, 231
- Helszajn, J., 118, 120, 122, 160
- Hexaferrites, 5, 88
- Hexagonal close-packed (HCP) lattice, 7
- Hexagonal ferrite, 5, 9, 88
availability, 93
composition, 10
composition variation, 9
magnetic anisotropy, 9, 93
planar and uniaxial, 9
- resonance line width, 93
S, R, and T blocks, 9
types (M, Y, W, and Z), 9
- Hilpert, 4
- Holmium, 88
- Homogeneity of ferrites, 88
- Hoshino, N., 168
- Humidity, 47
- Hund's rule, 6
- Hysteresis loop, ferrite, 226
- Image plane, 121
- Impedance,
circulator input, 114, 155
matching,
best possible, 286
circuit design, 287
effects of lumped components, 294
empirical, 294
limitations on, 285
techniques, lumped-element, 132, 171
- Indium Antimonide (InSb), 30
- Inductance
coil, 255
stripline, 170
- Inductor design procedure, 255
- Insertion loss, 37
approximation of, 116, 126
calculation of, 126
differential-phase-shift circulator, 175
field-displacement isolator, 63
junction circulator, 55
lumped-element circulator, 57
monitoring, 269
multiplexer, 77
resonance isolator, 65
- Insertion phase, 37
- Insulation, strip, 171
- Intermodulation
distortion, 37, 186
products, 58
third-order, 44–45
- International system of units, 1
- Ion
metallic, 6
oxygen, 6

- Isolation, 37, 69
 - differential-phase-shift circulator, 176
 - multiplexer, 76
 - PARAMP, 80
 - required, 39, 49
 - resonance isolator, 65
 - transmit-receive, 72
- Isolator,
 - definition of, 36
 - field-displacement, pictures, 63
 - resonance, pictures, 64–65
- James, D. S., 122
- Jet casting, 100
- Junction
 - circulator, composite-ferrite, 56
 - circulator pictures, 52–53
 - circulator propagation constant, 26
 - radius, microstrip circulator, 157
 - unit, 163
- Kato, Y., 5
- Kittel, 14
- Kittel's equation, 209
- Konishi, Y., 168
- Laminates, printed circuit, 103
- Landau and Lifshitz precession, 14
- Landé splitting factor, 14
- Lattice,
 - crystal, 7
 - difference between FCC and HCP, 7
 - face-centered cubic (FCC), 7
 - hexagonal close-packed (HCP), 7
- Leakage flux, 213
- Length units, 1
- Light, plane-polarized, 15
- Limiter
 - cavity, 73–74
 - comb, 73–74
 - ferrite, 72–75
 - orthogonal stripline, 72–73
 - subsidiary resonance, 73, 75
- Line width, resonance, 92, 98
 - effective, 92
- Linear vector operator, 17
- Linearity, 37
- Load, stub-resistor (stub-R), 133
- Loaded Q
 - approximation of, 117, 118, 120
 - calculation of, 116, 127, 131
 - graph
 - one-transformer network, 128
 - two-transformer network, 134
 - waveguide junction, 150–152
- Local oscillator, 70
- Lodestone, 4
- Longitudinal field
 - propagation constant, 26
- Low-field loss, 96
- Low-noise amplifiers, 70
- Lumped components
 - effects on bandwidth, 294
- Lumped-constant construction, 56–57
- Lumped-element
 - circulator
 - design procedure, 167
 - picture, 57
 - symmetry, 171
 - matching techniques, 132, 171
- Lyon, R. W., 160
- Machining
 - ferrite, 89
 - quality, waveguide circulators, 257
- Magnet
 - alnico, 100, 284
 - calibration, 284
 - ceramic, 9, 100
 - chargers, 267, 284
 - coercive force, 101
 - dimensions, calculation of, 216
 - energy product, 101
 - NdFeB, 100
 - operating temperature, 102
 - oxidation (rusting), 102
 - operating point, 216
 - permanent, 205
 - size, 215
 - stabilization, 285
 - thermal stabilization, 267
 - wells, 242
- Magnetic
 - bias, 111

- circuit, typical, 205
dipole moment, net, 46
field,
 adjustment, 268–271
 critical microwave, 28
dc, 14–15
effect on insertion loss, 282
external, 15, 211
intensity, units, 1
internal to external relationship, 209
polarity, 269
requirements, lumped-element
 circulators, 170
RF, 14
 in ferrite of lumped circulator,
 168–169
selection, 126
uniformity, microstrip circulator, 228
flux density, shield material, 217
induction, units, 1
leakage factor approximation, 214
losses
 estimation of, 99
 ferrite, 99
moment, 5
 atomic, 6
 electron, 14
 ferrite ion, 5
 net, 6
operating point, 96–97
 junction circulator, 55
 lumped-element circulator, 58, 170
 microstrip circulator, 158
 resonance isolator, 64, 177
operating regions, 44
 below-resonance, 118
poles, free, 208
returns, 205–206, 284
shielding, 46, 207
shunts, 205–206, 284
temperature compensating material, 222
 data for, 222
Magnetite, 4
Magnetization, ferrite, symbol for, 4
Magnetizer, capacitive-discharge, 267, 284
Magnetostrictive effects, 89
Masers, 80–81
Matching, impedance
 circuit design, 287
 limitations on, 285
 structures, 123, 133
Materials, 37, 47
 ferrimagnetic, 4
 outgassing properties, 47
Matrix form of tensor, 18
Measurement system
 accuracy, 271
 precision, 271
 qualities of, 271
 uncertainty, 271
Measurement tools, precision, 263
Metals,
 compatibility, 105
 divalent, 6
Microstrip
 circulator construction, 54
 circulator design procedure, 157
 effective permeability, 158–159
 effective permittivity, 159
 electrical length, 159
 frequency dispersion, 158–159
 line impedance, 158
 static characteristic impedance, 158
Microstructure of ferrite, 10
Mismatch loss, 282
MKS system of units, 1
Mode
 dominant, triangular resonator, 122
 matching, analysis technique, 122
 splitting
 definition, 115
 variation with frequency, 115
 suppression, circular modes, 244
 suppressors, 245, 247
Modes
 counter-rotating, 129
 higher-order, 129,
 of operation, 96–97
 rotating, analysis, 107
Monte Carlo analysis, 310–311
Multipaction, 41, 196, 273–275
Nanotechnology, 30
NASA Earth Atmosphere Model, 194

- National Institute of Standards and Technology (NIST), 271
Natural-convection cooling, 234
Néel, L., 5
Network parameters,
 calculation, 135
 single transformer ($n = 2$), 135
 two transformers ($n = 3$), 136
empirical determination, 133
optimization using software, 133
synthesis, 161
table lookup, 133
Nickel-steel alloy temperature
 compensation material, 102
Noise figure,
 degradation, 70
 PARAMPs, 79
Nondegenerate PARAMP, 77
Nonlinearity, circulator, 44
Nonreciprocal properties, ferrite, 15
Notebooks, 271
- Octants, 7
Okada circulator, 61, 163
 power handling, 164
Operating point, magnet, 216
Operation of differential phase shift
 circulators, 58
Orbital
 atomic, 5
 interactions, 5
 motion, electron, 6
Outer conductor, coax termination, 180
- Packaging schemes, stripline, 237
Paramagnetism, 5
Parameters, circulator, 37
Particle size, ferrite, 88
Peak power capacity, 90
 coaxial connector, 42
 junction circulator, 55
 lumped-element circulator, 57, 171
Peak power mechanism for breakdown,
 41
Percentage bandwidth, circulator, 38
Performance
 differential-phase-shift circulator, 60
 field-displacement isolator, 63
junction circulator, 55
lumped-element circulator, 57
resonance isolator, 65–66, 177
waveguide junction circulator, 54
Permanent magnets, 205
Permeability
 effective, 112
 above-resonance, 113, 125
 below-resonance, 117
 simplified expression for, 113
 transverse field, 25
 graphs, 25, 26
 magnetized ferrite, 17
measurements, 124
partly magnetized ferrite, 124
tensor, 18
unmagnetized ferrite, 124
z-axis, 125
Permittivity,
 symbol for, 4
 tensor, 29
Phase
 constant, 27
 matching, 37, 40
 shifter,
 dual-mode, 82–83
 Fox, 83–84
 reflective, 81
 Reggia-Spencer, 82–83
 TEM, 83–84
 toroidal waveguide, 82
 term, of propagation constant, 24
 tracking, 37, 40
Phillips Gloeilampenfabriken Labs, 5
Polder, 17
 tensor, 21
 derivation of, 18
 graphs, 22
Pole piece, 205
 designs, good and bad, 225
 discussion about, 223
 material for, 223
Polycrystal, 5
Polycrystalline ferrite, 89
Polyiron, 179–181
Power dissipation
 circulator junction, 233
 in ferrites, 188

- Power handling (capacity), 37
average, concerns, 187
CW, waveguide, 41
differential-phase-shift circulator, 60
field-displacement isolator, 63
junction circulator, 55
lumped-element circulator, 57
resonance isolator, 66
stripline, 231
Power level, PARAMPs, 79
Power limit
average power, 43
peak power, 41
Power threshold, ferrite, 44, 90, 99, 199
Precession, 12–14
Precision
measurement system, 271
measuring tools, 263
Presintering, 88
Pressure, atmospheric, 37, 47
Printed circuit laminates, 103
Probing, empirical matching method, 295
Process temperature, 46
Propagation
constant, 23
in circulator junction, 107
in resonance isolators, 64–65
Pulling, oscillator, 69
Pulse
repetition rate, effect on waveguide power handling, 41
width, effect on waveguide power handling, 41
Pump source, PARAMP, 78
- Q, loaded
approximation of, 117, 118, 120
calculation of, 116, 127, 131
circulator junction, 116
graph
one-transformer network, 128
two-transformer network, 134
waveguide junction, 150–152
Q, unloaded, circulator junction, 116
Quantum numbers, 6
Quarter-wavelength impedance
transformers, 117, 119–120, 123, 131–132
- Rare earth, 9
Rare-earth doping, 99
of ferrites, 99
Ratio, gyromagnetic, 4
Raw materials, ferrite, 88
Receiver applications of isolators, 70
Reflection coefficient, 38
Relaxation theory, ferrite, 11
Reliability, circulator, 37, 47
Reluctance, 215
Repeatability and reproducibility (R & R), 277
Resistive elements, field-displacement isolator, 61–63
Resistors, thin-film, 179
Resonance
absorption, 28, 65
cyclotron, 29
ferrimagnetic, 11
curve, shape, 98
frequency, triangular resonator, 122
isolators, pictures, 64–65
linewidth, 19
test for, 91
operating region, 44
subsidiary, 28
Resonator
PARAMP, 78
radius, 125, 127
effective, 157, 160
Retentivity, ferrite, 226
Return loss, 38
Returns, magnetic, 205–206
Rexolite, 103
RF leakage test methods, 46
RF load parameters, 180
RF radiation, 253
RFI shielding, 46
Roberts, R. W., 169
- Sandy, F., 124
Saturation magnetization
measurement of, 91
selection of, 96
above-resonance, 97
below-resonance, 96–97
symbol for, 4
Scaling, frequency, 130

- Scattering matrix, 111, 122
Schloemann, 124
Sealing,
 hermetic, 253
Segmentation, 51
 analysis, 51
Self-biased circulators, 99–100
Semiconductor circulators, 29
 experimental results, 29
 frequency limitation, 30
Separation of ports, PARAMP, 79
Series-resonant circuit
 lumped-element circulator, 168
Shape, resonance isolator, 64
Shells, atomic, 6
Shield
 design procedure, 219
 magnetic, 205, 207
Shielding
 connectors, 46
 electromagnetic, 37
 magnetic, 37
 purposes of, 219
Shock, 37
 effect on lumped-element circulators, 58
Shunts, magnetic, 205–206
SI system of units, 1
Silicone dielectric materials, 103
Simon, J. W., 123
Single-crystal ferrite, 89
Sites
 dodecahedral, 9
 garnet, 9
 ion, 7
 octahedral, 7
 tetrahedral, 7
Size
 circulators, 37
 differential-phase-shift circulators, 60
 junction circulators, 56
Smith chart, 287
Snoek, J. L., 5
Solid-state,
 devices, 69
 plasma, 29
Spin
 axes, electron, 13
 wave instability, 198
 waves, 28, 44
Spin-wave line width, 90
 measurement of, 92
Spinel, 5, 87
 ferrimagnetic properties of, 7
Stability
 amplifier, 70
 temperature, of ferrite, 93
Standards, primary and secondary, 271
Standing-wave pattern, 109
 ferrite, 109
 rotation of, 109
Strip width, lumped-element circulator, 170
Stripline,
 characteristic impedance of, 129
 circuit construction
 bonded-stripline, 240
 bonded-substrate, 237
 box-and-cover, 239
 channeled-plate, 238
 flat-plate, 237
 circuit packaging techniques, 237
 circulator construction, 54
 circulator synthesis, 153
 construction techniques, 237
 power-handling capacity, 187, 193, 231
width
 calculation of, 129, 131
 determination of, 129
 effect on coupling, 129
 restrictions on, 113, 129
Stub-resistor (Stub-R) load, 133
Subshell, atomic, 6
Subsidiary resonance, 28
Substrate thickness, microstrip circulator, 157
Surface finish, ferrite, 90
Susceptance slope
 computation, 155
 parameter, 119
Susceptibility tensor, 20
Switch
 ferrite, 60, 73, 75
 reciprocal, 75
Symbol
 ferrite magnetization, 4

- permittivity, 4
saturation magnetization, 4
Symmetry, electrical, 249
- Takei, T., 5
Tan, F. C., 120
Taper length, dummy load, 180–181
TDK Corporation, 5
Teflon (PTFE), 103
- Temperature
Curie, 93
ferrite material, 46
measurement of, 92
- drop, across ferrite, 233
effects
above resonance, 181
below resonance, 183
graphs, 182–185
on magnets, reversible, 102
- ferrite surface, reduction of, 189
compensation material
data for, 222
magnetic, 222
- operating
circulator, 37
lumped-element circulator, 58
magnet, 102
- process, 46
stability of ferrite, 102
storage, circulator, 46
- Temperature compensation
using capacitors, 223
- Tensor
definition, 17
permeability, significance of, 18
permittivity, 29
polder permeability, 21
- Test
data, recording of, 272
methods, RF leakage, 46
set-up, typical, 39
- Thermal
annealing of ferrites, 89
conductivity
of selected materials, 232
units, 1
performance, 188
- stabilization of magnets, 267
transient analysis, 191
- Thin ferrite films, 31
- Thin-film techniques, 158
- Third-order intercept point, circulator, 44
Third-order intermodulation, 44–45
Tokyo Institute of Technology, 5
Tracking solution, 313
Transformer,
quarter-wavelength, 117, 119–120, 123, 131–132
waveguide, design, 163
- Transition
coaxial to stripline, 148
compensation method
contour, 249
triangular, 249
equivalent circuits, 250
models, 250
step, stripline, 249–250
- Transverse field propagation constant, 24
- Triangular resonator field patterns, 122
- Tubes, microwave, 69
- Uncertainty of measurements, 276
voltage reflection coefficient, 276
voltage transmission coefficient, 277
- Unit junction, 163
- Units
angle, 1
area, 1
CGS system of, 1
English system of, 1
International system of, 1
length, 1
magnetic field intensity, 1
magnetic induction, 1
MKS system of, 1
propagation constant, 24
SI system of, 1
thermal conductivity, 1
used in this book, 1
- Unloaded Q, circulator junction, 116
- Vacuum, high, operation in, 47
Vacuum tubes, microwave, 69

- Variation, controlling, 311
Venting, 37, 47, 235
Vent hole
 gas flow, 236
 RF radiation, 236
Vernier scale, 263
Vibrating sample method, saturation
 magnetization measurement, 91
Vibration, 47
 effect on lumped-constant circulators, 58
Voltage breakdown, 193
 arcing, 194
 calculation of, 193
 corona, 194
 creep path, 196
VSWR, 37, 70
 circulator, 116
 junction circulator, 54–55
 lumped-element circulator, 57

Water cooling, 235
Water-pipe analogy of circulator, 36

Wave
 admittance, 115
 components, counter-rotating, 107
 number, 112, 121, 162
Waveguide
 characteristic impedance, 163
 height, 162
 height transitions, 250
 junction circulators, 54, 117, 120
 geometries, 149
 synthesis algorithm, 161
 transformer design, 163
Wavelength, guide, 162
Web thickness, 233, 242, 243
Weight
 circulator, 46
 differential-phase-shift circulator, 60
 junction circulator, 56
Wheeler, H. A., 157

YIG (yttrium iron garnet), 87
Yttrium, 9
Yttrium iron garnet (YIG), 87

Recent Titles in the Artech House Microwave Library

Chipless RFID Reader Architecture, Nemai Chandra Karmakar,
Prasanna Kalansuriya, Randika Koswatta, and Rubayet E-Azim

Design of Linear RF Outphasing Power Amplifiers, Xuejun Zhang,
Lawrence E. Larson, and Peter M. Asbeck

Design Methodology for RF CMOS Phase Locked Loops,
Carlos Quemada, Guillermo Bistué, and Iñigo Adin

Design of CMOS Operational Amplifiers, Rasoul Dehghani

Design of RF and Microwave Amplifiers and Oscillators, Second Edition, Pieter L. D. Abrie

Digital Filter Design Solutions, Jolyon M. De Freitas

Discrete Oscillator Design Linear, Nonlinear, Transient, and Noise Domains, Randall W. Rhea

Distortion in RF Power Amplifiers, Joel Vuolevi and Timo Rahkonen

EMPLAN: Electromagnetic Analysis of Printed Structures in Planarly Layered Media, Software and User's Manual, Noyan Kinayman and M. I. Aksun

An Engineer's Guide to Automated Testing of High-Speed Interfaces, José Moreira and Hubert Werkmann

Essentials of RF and Microwave Grounding, Eric Holzman

FAST: Fast Amplifier Synthesis Tool—Software and User's Guide, Dale D. Henkes

Feedforward Linear Power Amplifiers, Nick Pothecary

Foundations of Oscillator Circuit Design, Guillermo Gonzalez

Frequency Synthesizers: Concept to Product, Alexander Chenakin

Fundamentals of Nonlinear Behavioral Modeling for RF and Microwave Design, John Wood and David E. Root, editors

Generalized Filter Design by Computer Optimization, Djuradj Budimir

Handbook of Dielectric and Thermal Properties of Materials at Microwave Frequencies, Vyacheslav V. Komarov

Handbook of RF, Microwave, and Millimeter-Wave Components, Leonid A. Belov, Sergey M. Smolskiy, and Victor N. Kochemasov

High-Linearity RF Amplifier Design, Peter B. Kenington

High-Speed Circuit Board Signal Integrity, Stephen C. Thierauf

Integrated Microwave Front-Ends with Avionics Applications, Leo G. Maloratsky

Intermodulation Distortion in Microwave and Wireless Circuits, José Carlos Pedro and Nuno Borges Carvalho

Introduction to Modeling HBTs, Matthias Rudolph

Introduction to RF Design Using EM Simulators, Hiroaki Kogure, Yoshie Kogure, and James C. Rautio

Klystrons, Traveling Wave Tubes, Magnetrons, Crossed-Field Amplifiers, and Gyrotrons, A. S. Gilmour, Jr.

Lumped Elements for RF and Microwave Circuits, Inder Bahl

Lumped Element Quadrature Hybrids, David Andrews

Microstrip Lines and Slotlines, Third Edition, Ramesh Garg, Inder Bahl, and Maurizio Bozzi

Microwave Circulator Design, Second Edition, Douglas K. Linkhart

Microwave Circuit Modeling Using Electromagnetic Field Simulation, Daniel G. Swanson, Jr. and Wolfgang J. R. Hoefer

Microwave Component Mechanics, Harri Eskelinen and Pekka Eskelinen

Microwave Differential Circuit Design Using Mixed-Mode S-Parameters, William R. Eisenstadt, Robert Stengel, and Bruce M. Thompson

Microwave Engineers' Handbook, Two Volumes, Theodore Saad, editor

Microwave Filters, Impedance-Matching Networks, and Coupling Structures, George L. Matthaei, Leo Young, and E. M. T. Jones

Microwave Materials and Fabrication Techniques, Second Edition,
Thomas S. Laverghetta

Microwave Materials for Wireless Applications, David B. Cruickshank

Microwave and Millimeter-Wave Electronic Packaging,
Rick Sturdivant

Microwave Mixer Technology and Applications, Bert Henderson and
Edmar Camargo

Microwave Mixers, Second Edition, Stephen A. Maas

Microwave Network Design Using the Scattering Matrix,
Janusz A. Dobrowolski

Microwave Radio Transmission Design Guide, Second Edition,
Trevor Manning

Microwave Transmission Line Circuits, William T. Joines,
W. Devereux Palmer, and Jennifer T. Bernhard

Microwaves and Wireless Simplified, Third Edition,
Thomas S. Laverghetta

Modern Microwave Circuits, Noyan Kinayman and M. I. Aksun

Modern Microwave Measurements and Techniques, Second Edition,
Thomas S. Laverghetta

Neural Networks for RF and Microwave Design, Q. J. Zhang and
K. C. Gupta

Noise in Linear and Nonlinear Circuits, Stephen A. Maas

Nonlinear Microwave and RF Circuits, Second Edition,
Stephen A. Maas

Q Factor Measurements Using MATLAB®, Darko Kajfez

*QMATCH: Lumped-Element Impedance Matching, Software and
User's Guide,* Pieter L. D. Abrie

*Passive RF Component Technology: Materials, Techniques, and
Applications,* Guoan Wang and Bo Pan, editors

Practical Analog and Digital Filter Design, Les Thede

Practical Microstrip Design and Applications, Günter Kompa

Practical RF Circuit Design for Modern Wireless Systems, Volume I: Passive Circuits and Systems, Les Besser and Rowan Gilmore

Practical RF Circuit Design for Modern Wireless Systems, Volume II: Active Circuits and Systems, Rowan Gilmore and Les Besser

Production Testing of RF and System-on-a-Chip Devices for Wireless Communications, Keith B. Schaub and Joe Kelly

Radio Frequency Integrated Circuit Design, Second Edition,
John W. M. Rogers and Calvin Plett

Radio Frequency System Architecture and Design,
John W. M. Rogers, Calvin Plett, and Ian Marsland

RF Bulk Acoustic Wave Filters for Communications,
Ken-ya Hashimoto

RF Design Guide: Systems, Circuits, and Equations, Peter Vizmuller

RF Linear Accelerators for Medical and Industrial Applications,
Samy Hanna

RF Measurements of Die and Packages, Scott A. Wartenberg

The RF and Microwave Circuit Design Handbook, Stephen A. Maas

RF and Microwave Coupled-Line Circuits, Rajesh Mongia, Inder Bahl,
and Prakash Bhartia

RF and Microwave Oscillator Design, Michal Odyneic, editor

RF Power Amplifiers for Wireless Communications, Second Edition,
Steve C. Cripps

RF Systems, Components, and Circuits Handbook, Ferril A. Losee

The Six-Port Technique with Microwave and Wireless Applications,
Fadhel M. Ghannouchi and Abbas Mohammadi

Solid-State Microwave High-Power Amplifiers, Franco Sechi and
Marina Bjattini

Stability Analysis of Nonlinear Microwave Circuits, Almudena Suárez
and Raymond Quéré

Substrate Noise Coupling in Analog/RF Circuits, Stephane Bronckers,
Geert Van der Plas, Gerd Vandersteen, and Yves Rolain

System-in-Package RF Design and Applications, Michael P. Gaynor

*TRAVIS 2.0: Transmission Line Visualization Software and User's
Guide, Version 2.0*, Robert G. Kaires and Barton T. Hickman

Understanding Microwave Heating Cavities, Tse V. Chow Ting Chan
and Howard C. Reader

For further information on these and other Artech House titles, including previously considered out-of-print books now available through our In-Print-Forever® (IPF®) program, contact:

Artech House Publishers

685 Canton Street

Norwood, MA 02062

Phone: 781-769-9750

Fax: 781-769-6334

e-mail: artech@artechhouse.com

Artech House Books

16 Sussex Street

London SW1V 4RW UK

Phone: +44 (0)20 7596 8750

Fax: +44 (0)20 7630 0166

e-mail: artech-uk@artechhouse.com

Find us on the World Wide Web at: www.artechhouse.com
